KU LEUVEN

ARENBERG DOCTORAL SCHOOL
FACULTY OF ENGINEERING SCIENCE

SHM system for composite aeronautic structures using combination of different methods: A contribution for residual strength prediction

Ricardo De Medeiros

Supervisors:
Prof dr. ir Dirk Vandepitte
(KU Leuven)

Prof dr. ir Volnei Tita
(USP)

Dissertation presented in partial fulfilment of the requirements for the degree of PhD in Mechanical engineering.

January 2016

UNIVERSITY OF SÃO PAULO – USP
SÃO CARLOS SCHOOL OF ENGINEERING
DEPARTMENT OF AERONAUTICAL ENGINEERING
GRADUATE PROGRAM IN MECHANICAL ENGINEERING

AND

KATHOLIEKE UNIVERSITEIT LEUVEN
FACULTY OF ENGINEERING SCIENCE
DEPARTMENT OF MECHANICAL ENGINEERING
GRADUATE PROGRAM IN MECHANICAL ENGINEERING

Ricardo De Medeiros

SHM system for composite aeronautic structures using combination of different methods: A contribution for residual strength prediction

São Carlos
2016

Ricardo De Medeiros

SHM system for composite aeronautic structures using combination of different methods: A contribution for residual strength prediction

A thesis presented to the *São Carlos School of Engineering, University of São Paulo* in fulfillment of the requirements for the degree of *Doctor in Mechanical Engineering*.

Concentration area: Aircraft

A thesis presented to *Faculty of Engineering Science, Katholieke Universiteit Leuven* in fulfillment of the requirements for the degree of *Doctor in Engineering Science*.

Co-tutorship Thesis:

Brazil Supervisor: Associate Professor Volnei Tita (USP)

Belgium Supervisor: Full Professor Dirk Vandepitte (KU Leuven)

São Carlos

2016

Medeiros, Ricardo de
M488d Development of a criterion for predicting residual strength of composite structures damaged by impact loading / Ricardo de Medeiros; orientador Volnei Tita; coorientador Dirk Vandepitte. São Carlos, 2015.

Tese (Doutorado) - Programa de Pós-Graduação em Engenharia Mecânica e Área de Concentração em Aeronaves -- Escola de Engenharia de São Carlos da Universidade de São Paulo, 2015.

1. Monitoramento da integridade estrutural. 2. Estruturas inteligentes. 3. Impacto em materiais compósitos. 4. Análise via elementos finitos. 5. Ensaios experimentais. I. Título.

FOLHA DE JULGAMENTO

Candidato: Engenheiro **RICARDO DE MEDEIROS.**

Título da tese: "Desenvolvimento de um critério para previsão da resistência residual de estruturas em material compósito danificados por impacto".

Data da defesa: 20/01/2016.

Comissão Julgadora:	**Resultado:**
Prof. Associado **Volnei Tita (Orientador)** (Escola de Engenharia de São Carlos/EESC)	Aprovado
Prof. Dr. **Dirk Vandepitte** (Katholieke Universiteit Leuven/KU Leuven)	Aprovado
Prof. Associado **Flávio Donizeti Marques** (Escola de Engenharia de São Carlos/EESC)	APROVADO
Prof. Associado **José Ricardo Tarpani** (Escola de Engenharia de São Carlos/EESC)	Aprovado
Prof. Dr. **Antonio Marcos Gonçalves de Lima** (Universidade Federal de Uberlândia/UFU)	Aprovado
Prof. Dr. **Paul Sas** (Katholieke Universiteit Leuven/KU Leuven)	Aprovado

Coordenador do Programa de Pós-Graduação em Engenheira Mecânica:
Prof. Associado **Gherhardt Ribatski**

Presidente da Comissão de Pós-Graduação:
Prof. Associado **Paulo César Lima Segantine**

To my family,

especially my wife, mother, father, and brother,

for their continual support, encouragement, inspiration, and patience.

Acknowledgment

Completion of the research presented in this work was the result of efforts by many people to whom I owe much appreciation. First, I would like to express my heartfelt appreciation and gratitude to my advisor Professor Volnei Tita (São Carlos School of Engineering, University of São Paulo) for providing me with endless encouragement and guide me through multitude of challenges. I am sincerely grateful for his supervision and support throughout my doctoral studies. I would like to thank you Prof. Dirk Vandepitte (Katholieke Universiteit Leuven) for accepting the proposed work to be carried out at the KU Leuven and for his supervision and support during the Belgium time. I would like to thank you Prof. Rui Guedes, Prof. Mario Vaz (Faculty of Engineering of University of Porto) and Prof. Hernani Lopes (Instituto Politécnico do Porto) for helping with the shearography tests.

I would like to thank you Prof. Marcelo Leite Ribeiro (São Carlos School of Engineering, University of São Paulo) for your friendship and help, as well as for the ABAQUS™ license. Also, I would like to thank you Prof. Elmer Gennaro (São Paulo State University) and Prof. Romeu Rony (Federal University of Technology – Paraná). I also would like to thank my colleagues in our research group for their friendship and hours of useful discussions. They are André, Andres, Daniel, David, Douglas, Felipe Eloy, Felipe Rendeiro, Gregório, Jonathan, José Augusto, Marcel, Murilo, Tarcísio, Vagner, Wander, Willian from Brazil, and Andy, Frederik, Roland, Ruben from Belgium.

I would like to thank my family, especially my wife Ângela, for putting up with me during this process and giving me valuable critics that helped immensely.

Finally, I gratefully acknowledge the partial support in Brazil by the Sao Paulo Research Foundation (FAPESP process number: 2012/01047-8) and in Belgium by the Coordination for the Improvement of the Higher Level Personnel (CAPES process number: 011214/2013-09). I also would like to thank Navy Technological Centre (CTM – Brazil) for manufacturing specimens.

“You will never find time for anything.
If you want time, you must make it.”
(Charles Buxton)

Abstract

MEDEIROS, R. *SHM system for composite aeronautic structures using combination of different methods: A contribution for residual strength prediction*. 2016, 246p. Thesis (Doctorate) – São Carlos School of Engineering, University of São Paulo, São Carlos, SP, Brazil, 2016.

Advanced aerospace materials, including fibre reinforced polymer and ceramic matrix composites, are increasingly being used in critical and demanding applications, challenging not only the current damage prediction, detection, and quantification methodologies, but also the residual life of the structure. The main objective of this work consists of developing theoretical and experimental studies about residual strength for composite structures, which are damaged by impact loading, aided by a SHM system, which combines different methods. For this, it is necessary: to identify, and to localize damage, as well as to calculate the severity of the damage and to predict the residual strength of the composite structure. To achieve these goals, the research methodology should consider three methods: (1) Vibration Based Method (VBM); (2) Shearography Speckle (SS) and (3) Flexural After Impact (FAI). Composite plates, made of epoxy resin reinforced by carbon or glass fibre, are evaluated. Firstly, VBM provide Frequency Response Functions to be analysed by suitable metrics (including a new metric), which are compared in terms of their capability for damage identification and global location. Afterwards, the extension of impact damage is determined by using shearography speckle. This technique has demonstrated great potential for damage detection in composite laminated structures. The identification of the damage from the measurements performed with the SS technique is based on the analysis of disturbances in the speed field caused because of the different properties of the material. These abnormal deformations can be verified as typical strains in damaged structures. SS is a laser interferometry method sensitive to displacement gradient in a surface direction out of the plane. Under the action of a smaller load, the structure is deformed and the presence of damage is shown through local peculiarities of surface deformation observed field. Finally, a flexure after impact (FAI) test is used to evaluate its limitations and potentialities as a damage tolerance technique. The residual flexural strength of damaged specimens is evaluated by quasi-static four-point bending test. A new criterion based on a relationship between damage metric from VBM and FAI analysis is presented and discussed. Thus, these results are normalized by using the maximum load and the metrics for damage analyses, *i.e.* if there is no damage in the structure, then the metric returns zero value. If the structure is partially damaged then the metric returns a number between one and zero. In addition, if the structure is totally damaged (*i.e.* residual strength is lower than specified in design), then the metric returns a value equal one. Finally, it is discussed the advantages and limitations of this combination into the context of SHM system (Structural Health Monitoring System).

Keywords: Composite structures. Residual strength. Structural Health Monitoring. Smart structures. Impact on composite structures. Finite element analysis. Experimental analysis.

Resumo

MEDEIROS, R., *Sistema SHM para estruturas aeronáuticas em material compósito usando a combinação de diferentes métodos: Uma contribuição para a previsão da resistência residual*. 2016. 246p. Tese (Doutorado) – Escola de Engenharia de São Carlos, Universidade de São Paulo, São Paulo, 2016.

Materiais compósitos estão cada vez mais sendo usados em aplicações críticas e exigentes, desafiando não apenas as metodologias atuais de previsão de dano, detecção, quantificação, mas também da vida residual da estrutura. O principal objetivo deste trabalho consiste no desenvolvimento de estudos teóricos e experimentais sobre a resistência residual de estruturas de compósito, que são danificadas pelo carregamento de impacto, auxiliado por um sistema SHM, que combina diferentes métodos. Para isso, é necessário: identificar, localizar danos, bem como determinar a severidade dos danos e estimar a resistência residual da estrutura. Para atingir esses objetivos, a metodologia de pesquisa considerou três métodos: (1) Método baseado em vibração; (2) Shearography Speckle (SS) e (3) Flexão após Impacto (FAI). Placas de compósito, fabricadas em resina epóxi reforçada por fibra de carbono ou de vidro, são avaliadas. Em primeiro lugar, o método baseado em vibração produz Funções de Resposta em Frequência, que são analisadas através de métricas adequadas (incluindo uma nova métrica), que são comparadas em termos de sua capacidade de identificação de danos e de localização global. Depois disso, a extensão de danos causados pelo impacto é determinada empregando SS. Esta técnica tem demonstrado grande potencial na detecção de dano em estruturas laminadas compósito. A identificação do dano a partir das medidas realizadas com a técnica SS tem por base a análise das perturbações no campo de curvaturas causada devido à heterogeneidade das propriedades do material. Estas deformações anormais podem ser verificadas como deformações típicas de estruturas danificadas. A SS é um método de interferometria laser sensível ao gradiente de deslocamento de uma superfície na direção fora do plano. Sob a ação de um pequeno carregamento, a estrutura é deformada e a presença de danos é revelada através de singularidades locais do campo de deformação observado na superfície. Finalmente, teste de flexão após o impacto (FAI) é usado para avaliar suas limitações e potencialidades como uma técnica de tolerância ao dano. A resistência à flexão das amostras intactas e danificadas é avaliada por ensaio de flexão em quatro-pontos quase-estático. Um novo critério baseado em uma relação entre a métrica de dano prevista pelos métodos de vibração e a análise via FAI é apresentado e discutido. Assim, estes resultados são normalizados utilizando a carga máxima e as métricas de dano, ou seja, se não houver nenhum dano na estrutura, a métrica retorna valor igual a zero. Se a estrutura é parcialmente danificada, a métrica retorna um valor entre um e zero. Além disso, se a estrutura está totalmente danificada (ou seja, a resistência residual está abaixo do especificado em projeto), a métrica retorna um valor igual a um. Por fim, discutem-se as vantagens e limitações desta combinação para o contexto de sistema SHM (Sistema de Monitoramento da Integridade Estrutural).

Palavras-chave: Estruturas em material compósito. Resistência residual. Monitoramento da integridade estrutural. Estruturas inteligentes. Impacto em estruturas em compósitos. Análise via elementos finitos. Ensaios experimentais.

Nederlandse samenvatting

MEDEIROS, R. *SHM system for composite aeronautic structures using combination of different methods: A contribution for residual strength prediction*. 2016, 246p. Thesis (Doctorate) – São Carlos School of Engineering, University of São Paulo, São Carlos, SP, Brazil, 2016.

Geavanceerde luchtvaartmaterialen, zoals vezelversterkte composieten met polymeer- en keramiekmatrix, worden steeds vaker aangewend voor kritische en hoog-performante toepassingen. Deze vormen een uitdaging voor het schatten, inspecteren en kwantificeren van schade, maar vooral voor het bepalen van de overblijvende levensduur van een betreffende structuur. De doelstelling van dit doctoraatsonderzoek is de voorspelling van de reststerkte van composietstructuren via theoretische en experimentele benaderingen, welke schade hebben ondervonden door impact, door middel van een SHM systeem die verschillende methodes combineert. Het is hierbij van essentieel belang om de schade te identificeren, te lokaliseren, alsook berekeningen te doen over de ernst van de schade en finaal de reststerkte van de composietstructuur te voorspellen. Om deze doelstellingen te behalen maakt de methodologie gebruik van volgende drie methodes: (1) Vibratie Gebaseerde methode (VBM); (2) Shearography Spikkelpatroon (SS); (3) Buigtest na Impact (FAI). Composietplaten, bestaande uit epoxy hars versterkt met koolstof- of glasvezel, zijn geëvalueerd. VBM resulteert in frequentierespons functies die geanalyseerd moeten worden met geschikte meetstaven (ook nieuwe meetstaven), welke op zich vergeleken worden op basis van hun geschiktheid om schade te identificeren en te lokaliseren in de ruimte. Vervolgens, wordt de schade door impact in meer detail bepaald via SS. Deze techniek heeft een groot potentieel aangetoond voor schade detectie in composiet gelamineerde structuren. De identificatie van schade uit meetexperimenten met de SS techniek is gebaseerd op de analyse van verstoringen in het snelheidsveld veroorzaakt door verschillen in materiaaleigenschappen. Abnormale afwijkingen worden vergeleken met typische rek die aanwezig is in beschadigde structuren. SS is een laser interferometrie methode die sensitief is aan de gradiënt van de verplaatsing in een oppervlak volgens de uit-het-vlak oriëntatie. Wanneer een kleinere belasting aangelegd wordt, vervormt de structuur en wordt schade opgemerkt door lokale typische afwijkingen van de oppervlaktevervorming in het waargenomen veld. In een laatste stap, wordt een buigtest na impact (FAI) uitgevoerd ter evaluatie van de beperkingen en mogelijkheden als techniek voor schade tolerantie. De restbuigsterkte van de beschadigde specimen wordt bepaald via een quasi-statische vierpuntsbuigproef. Een nieuw criterium gebaseerd op de relatie tussen de schade meetstaaf van de VBM en FAI analyse is uitgewerkt en besproken. De resultaten zijn genormaliseerd met de maximale belasting en de meetstaven voor schade analyse: als er geen schade in de structuur aanwezig is dan moet de meetstaaf nul aangeven; als de structuur deels beschadigd is, dan zal de meetstaaf een waarde aannemen tussen één en nul; als de structuur volledig beschadigd is (de reststerkte is lager dan gespecifieerd in het ontwerp) moet de meetstaaf gelijk zijn aan één. Verder worden ook de voordelen en beperkingen van deze combinatie van methodes bediscussieerd in de context van SHM systemen (Structural Health Monitoring System)

Sleutelwoorden: Composietstructuren, Reststerkte, Structural Health Monitoring, Smart structures, Impact op Composietstructuren, Eindige Elementen Analyse, Experimentele analyse.

List of Figures

List of Tables

List of Acronyms and Abbreviations

AFC	Active Fibre Composite
ASTM	American Society for Testing and Materials
BD	Bidirectional Fibres
BVID	Barely Visible Impact Damage
CAI	Compression After Impact
CCD	Charge Coupled Device
CDM	Continuum Damage Mechanics
CFRP	Carbon Fibre Reinforced Polymer
CMOS	Complementary Metal-Oxide-Semiconductor
CTM	Brazilian Navy Research Centre
DCT	Discrete Cosine Transform
DIA	Dynamic Implicit Analyses
DOF	Degree of Freedom
DME	Dynamic Materials Evaluation
DSPI	Digital Speckle Pattern Interferometer
ESPI	Electronic Speckle Pattern Interferometry
FAA	Federal Aviation Administration
FEA	Finite Element Analysis
FAI	Flexure After Impact
FEM	Finite Element Model
FFT	Fast Fourier Transform

FRF	Frequency Response Function
GRP	Glass-Fibre Reinforced Polyester
LASER	Light Amplification by Stimulated Emission Experimental
LED	Light Emitting Diode
MFC	Macro Fibre Composite
NDE	Non-Destructive Evaluation
NDE	Non-Destructive Examination
NDI	Non-Destructive Inspection
NDT	Non-Destructive Testing
PCG	Weighted Regularized Preconditioned Conjugate Gradient
PZT	Lead Zirconium Titanate
RI	Resin Infusion
RVE	Representative Volume Element
SHM	Structural Health Monitoring
SI	Speckle Interferometry
SS	Shearography Speckle
UD	Unidirectional Fibres
VBM	Vibration Based Method
VIP	Vacuum Infusion Process
WFT	Windowed Fourier Transform

List of Symbols

δ	Rotation angle of the mirror	^{o}
ε_0	Dielectric constant of space	F/m
ε_{ij}	Dielectric tensor	F/m
ε_{11}	Strain in fibre direction	m/m
ε_{22}	Strain in transverse direction	m/m
Δ	Relative difference	
Δx	Step in the x-direction	
$\Delta\phi(x,y)$	Phase map	
$\Delta\phi'(x,y)$	Phase map filtrate	
ϕ	Phase angle of the wave front	
$\psi(x,y)$	Phase difference between two wavefronts	
ρ	Density	kg/m^3
τ	Time	s
ν_{12}	Poisson ration in ply plane 1-2	
ν_{13}	Poisson ration in ply plane 1-3	
ν_{23}	Poisson ration in ply plane 2-3	
λ	Wavelength of light	
ω	Frequency	Hz
ζ	Damping	
θ	Damage angle	^{o}

σ	Standard deviation	
σ_{11}	Stress in fibre direction	Pa
σ_{22}	Stress in transverse direction	Pa
σ_{220}	Transverse linear elastic limit from experimental analyses	Pa
σ_{22y}	Linear to non-linear limit in σ_{22} *vs.* ε_{22} curve for off-axis lamina	Pa
τ_{12}	Shear stress	Pa
A_0	Wave amplitude	
$A(\theta)$	Linear function	
$B(\theta)$	Threshold values when $f > 0$	
$C(\theta)$	Linear function	
c	Speed of light	m/s
C	Stiffness	Pa
C_1	Distance between the plane until the plate	mm
C_2	Distance between the plane until the plate	mm
d	Piezoelectric constant	m/V or C/N
$D(\theta)$	Threshold values when $f > 0$	
d_1	Damage variable related with σ_{11}	
d_2	Damage variable related with σ_{22}	
d_{33}	Piezoelectric electrode configuration	
d_6	Damage variable related with τ_{12}	
e	Thickness	m
E_{11}	Elastic modulus in fibre direction	Pa
E_{110}	Initial value of elastic modulus in fibre direction	Pa
E_{22}	Elastic modulus in transverse direction	Pa
E_{220}	Initial value of elastic modulus in transverse direction	Pa
E_{33}	Elastic modulus in transverse direction	Pa

$E(r,t)$	Electromagnetic wave	
E_{DC}	Strain energy	
F	Force	N
f	Elastic domain function	
$f(\varepsilon_{11})$	Strain dependence function under compression in fibre direction for secant modulus	
$f(\varepsilon_{22})$	Strain dependence function under compression in transverse direction for secant modulus	
fr	Resonant frequency	Hz
G_{12}	Shear modulus in ply plane 1-2	Pa
G_{120}	Initial value of shear modulus in ply plane 1-2	Pa
G_{13}	Shear modulus in ply plane 1-3	Pa
G_{23}	Shear modulus in ply plane 2-3	Pa
h	Height	m
I	Light intensity	
j	Complex constant	$\sqrt{-1}$
l	Length	m
[M]	Mass matrix	kg
P_I	Intensity statistical distribution of the speckle pattern	
P_ϕ	Phase statistical distribution of the speckle pattern	
r	Wave space vector	
S_{12}	Shear strength in ply plane 1-2	Pa
S_{12y}	Shear strength surface in ply plane 1-2	Pa
S_{13}	Shear strength in ply plane 1-3	Pa
S_{23}	Shear strength in ply plane 2-3	Pa
t	Time	s
V	Voltage	V
V_f	Fibre volumetric fraction	%

w	Width	m
w(x,y)	Transverse displacement on a plate	m
x	Spatial coordinate	m
X_T	Tensile strength limit in fibre direction	Pa
X_C	Compression limit in fibre direction	Pa
X_{C0}	Fibre linear behaviour limit value under compression	Pa
Y_T	Tensile strength limit in transverse direction	Pa
Y_C	Compression limit in transverse direction	Pa
y	Signal response	-
y	Spatial coordinate	m

Table of Contents

CHAPTER 1

Introduction

The sudden failure of an engineering structure usually constitutes a major economical loss and in some cases might constitute a danger to human life. As a result, the majority of engineering disciplines have interest in Non Destructive Damage Detection Methods. All available damage detection methods require prior knowledge of the possible damage vicinity. Additionally, in some applications such as aerospace structures or off shore oil structure visual inspection may be cumbersome or even impossible. On the other hand, during the last decades, composite materials are gaining acceptance and demand in several commercial markets, including transportation, sporting goods and construction. For many of these applications, such as aircraft, the total maintenance cost of ownership may become a limiting factor for the usage of composite structure due to the lack of a reliable damage detection approach. Thus, the main Non-Destructive Techniques (NDTs) have become a good alternative to overcome this challenge. Then, some of NDTs procedures have been presented, considering their strengths and weaknesses for in-service testing of composite materials. In recent years, there have been a range of new damage detection techniques and sensing technologies. These methods allow for global, online monitoring of large structures and fall into the area of Structural Health Monitoring (SHM). They are capable of achieving continuous monitoring for damage involving the application of new sensors. Damage monitoring systems, which often use advanced sensor technologies, are concerned with a new design philosophy. Actuators, sensors, and signal processing are integrated to offer progress in this area. Structural Health Monitoring (SHM) can play a significant role in improving the safety of structures as well as extending their life time. Greater complexity, aging, higher operational loads, and severe environmental effects result in more attention to this field. However, after more than 30 years of research, SHM has not been vastly applied in real world structures. This chapter presents a survey of Structural Health Monitoring (SHM) systems for composite materials. An overview for the techniques used for composite components in aircraft industry is also presented. In addition, this chapter lists the motivations to implement SHM systems for composite aeronautic structures and the scope of the Thesis, which is focused on using a combination of different methods and proposing a new residual strength criterion for impact damaged composite structures.

1.1. Background and Motivation

All structures degrade with the passage of time due to various reasons like environmental conditions, operational variations, accidental events, and probably imperfect design. Whatever is the reason for degradation, there is a need to assess the useful remaining life of the structure. Visual inspection of structural parts has been the first and most common procedure. Depending on the type of the structure, its cost of maintenance, and the cost of changing worn-out parts, various methods have been developed over time.

Qualitative and non-continuous methods of SHM have long been used to evaluate structures and equipment for their capacity to serve the intended purpose. For instance, since the beginning of the 19th century, the sound of a hammer striking on the train wheel was a useful tool to detect damage (Ferdinand, 2014). In the last half a century, the development of quantifiable SHM approaches has been closely coupled with the evolution of digital computing hardware and inexpensive, fast networking technologies. Significant developments in the field have originated from major construction projects, such as offshore gas/oil production installations, large dams and highway bridges.

During the 1970s and 1980s, the oil industry received the greatest attention and research effort to develop damage identification methods for offshore platforms (Farrar *et al.*, 2001). Applications of vibration based methods (VBM) of SHM in the aerospace community started during the late 1970s and early 1980s in conjunction with the development of the space shuttle (Farrar *et al.*, 2001). The development of a composite fuel tank for a reusable launch vehicle in mid-1990s motivated studies of damage identification for composite materials (Farrar *et al.*, 2001).

The aeronautic industry always requires innovations like new materials (*e.g.* composite materials) and new technologies (*e.g.* smart structures), but before these innovations can be implemented for operations in aircraft, they must overcome requirements for aeronautic certification in order to guarantee airworthiness. The design becomes challenging, because on the one hand, weight and maintenance costs must be kept low, and on the other hand, both structure and systems must overcome rigorous requirements.

Each structure has (small) defects. As long as these defects are limited in size and if no heavy overload occurs, this is no problem. Structural damage can continue to grow for a long time (cumulative damage), but the final failure is usually a sudden event and the consequences

can be catastrophic (*e.g.* an aircraft crash, collapse of a structure). Such disasters can be predicted and ultimately avoiding such events is an important motivation for SHM.

On the other hand, safe-life, damage tolerance and fail-safe are normally used to design aeronautical structures. All philosophies, mainly the damage tolerance, predict inspection periods for critical regions of the airplane. However, based on the literature and on the experience of the operators, the maintenance cost can be reduced with suitable inspection periods, which are very complicated to be determined, mainly for composite structures (*cf.* Fig. 1-1). In other words, it is necessary to avoid putting a properly functioning structure out of service. Even during extreme events (*e.g.* a storm, earthquake, collision, explosion, etc.) an SHM system can be used to determine what the damage is and whether it is still safe to continue using the mechanical structure.

(a) Aircraft structure inspection (*photo from Sandia National Laboratories, USA*)

(b) Wind turbine inspection (*photo from power-technology.com*)

(c) Bridge inspection (*photo from facelift.co.uk*)

Figure 1-1. An overview of potential application fields for SHM techniques.

In this scenario, SHM is an acceptable way not only for minimising the number of inspections, but also for maintaining the structural stability, integrity and for maximising the life span of the structure as much as possible. SHM can replace the traditional maintenance plan, reducing the operational costs of the airplane and preventing needless maintenance activities. In the specific case of composite structures, the laminate can be manufactured using not only structural fibres, but also piezoelectric sensors. These sensors are an essential part of the SHM system, they can detect the occurrence and the position of damage, and they may predict the damage extension. Therefore, the SHM system should inform, all the time

throughout the entire structure life, a diagnostic of the material state as well as the structure condition. It should further match the specifications of the initial structural project. However, the material state and the structure condition change as a function of the time due to aging, environment effects and in service load cycles, occasional events and others. Based on the complete history, the SHM system can also perform a prognostic of the structure status, for example, a prediction of residual strength.

Therefore, it is possible to conceptualise SHM as a continuous or an intermittent observation of a mechanical structure or system. In addition, parameters are measured with a direct or indirect causal relationship with the current "*state of health*" of the structure.

SHM can be basically used in a passive and an active way. The passive SHM consists of the operational parameters measurement and the verification of the influence of each parameter on the structural integrity. For example, first, the SHM system monitors some flight parameters like air speed, load factors, vibration levels and strains in critical regions. Based on the collected information and reference data of the initial project, later, the SHM system compiles all information using numerical algorithms, which can estimate the lifetime of the structure. Passive SHM is useful, but it does not directly address the crux of the problem, *i.e.*, it does not directly examine if the structure has been damaged or not (Giurgiutiu, 2014). In a passive SHM system only sensors are needed and "natural" sources like impact, ambient vibrations or acoustic emission (AE) caused by crack generation and growth are detected (Fig. 1-2a).

On the other hand, the active SHM is concerned with directly assessing the state of structural health by trying to detect the presence and extension of structural damage. Therefore, the active SHM is similar to NDT, but the SHM system is usually more efficient. In fact, active SHM attempts to develop damage detection sensors/actuators net, which can be permanently installed on the structure and monitoring methods that can provide on demand a structural health bulletin in real-time (Giurgiutiu, 2014). In an active SHM system the transducers are acting as both, sensors and actuators (Fig. 1-2b). By using pulse-echo or acoustic signature techniques, scattered waves from inside the structure or changes in acoustic signature response can be detected and used as damage indicator. A set of transducers spans a so-called "synthetic aperture". By temporally delayed excitation and detection by individual actuators and sensors, elastodynamic wave fields can be focused to specific control volumes of the structure serving as basis for powerful SHM imaging techniques.

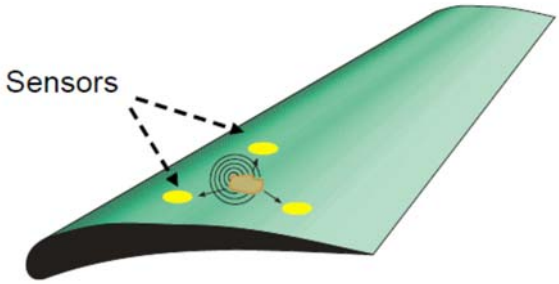

(a) Passive SHM approach: The sensors are used for detection of acoustic emission events caused by impacts or crack generation and growth. Also ambient vibrations can be monitored in principle.

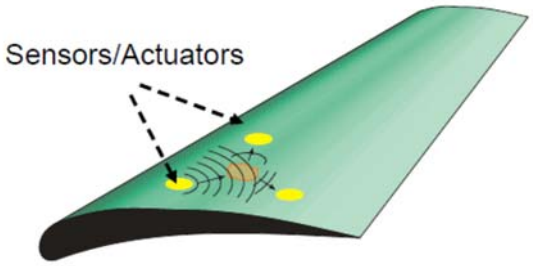

(b) Active SHM approach: The transducers are used as both, actuators and sensors in pulse-echo or transmission mode. Changes in acoustic signature response due to defect generation and growth serve as damage indicator during lifetime of the structure.

Figure 1-2. SHM systems (a) Passive and (b) active (Lehmann *et al.*, 2006)

There is a wide variety of NDT methods and visual inspection techniques, which are being used offline. In time, a number of these techniques may be replaced by an on-line SHM system. In a SHM-monitoring system, sensors are permanently mounted on or in the structure. Figure 1-3 shows in detail the principles of a SHM system. The software interprets the sensor information and is responsible for the processing and management of the signals. The major difference between a traditional NDT and SHM system lies mainly in the integrated system approach and autonomous inspection, which is confirmed by the latter results in the development of intelligent structures.

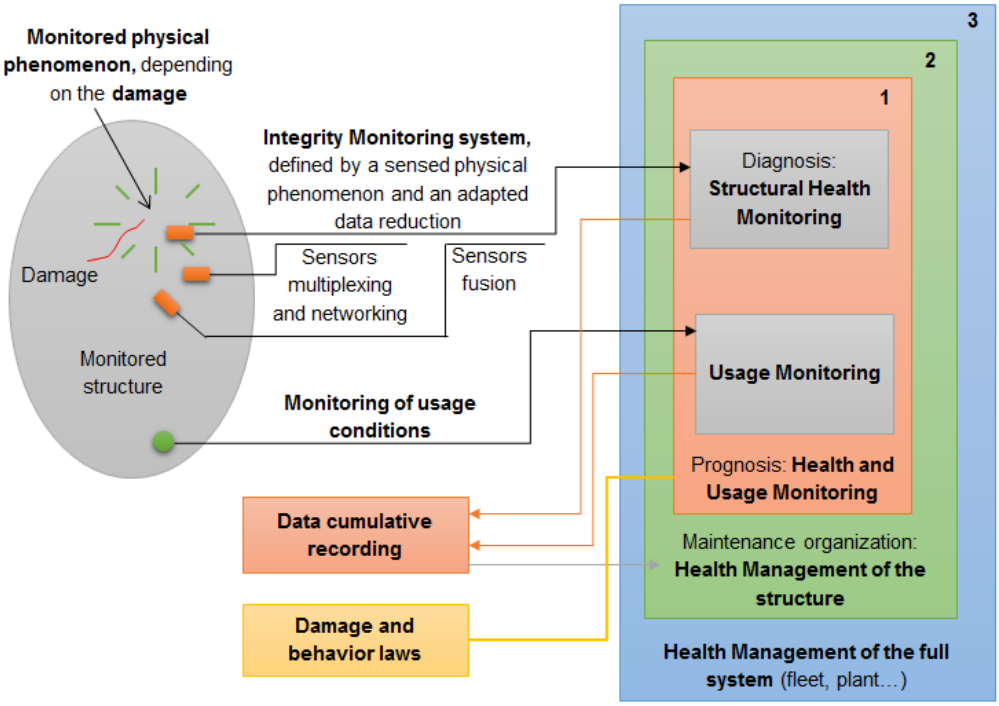

Figure 1-3. Principles and organization of SHM system (Balageas, 2006)

At the level of the methodology for SHM (and detection), there are basically two options. The first methodology is the load (*e.g.* temperature, vibrations, strains, etc.) monitoring and damage prediction using a numerical model and calculation method. In the second methodology, damage is monitored directly through the structural behaviour or the physical phenomenon (*e.g.* crack propagation). It is important to detect with a high level of certainty in order to ensure that there is no negative influence of the sensor network on the properties of the structure. This assembly should result in intelligent, autonomous structures. SHM systems are analogues to human nervous system with built-in sensors and diagnostic capabilities (*cf.* Fig. 1-4).

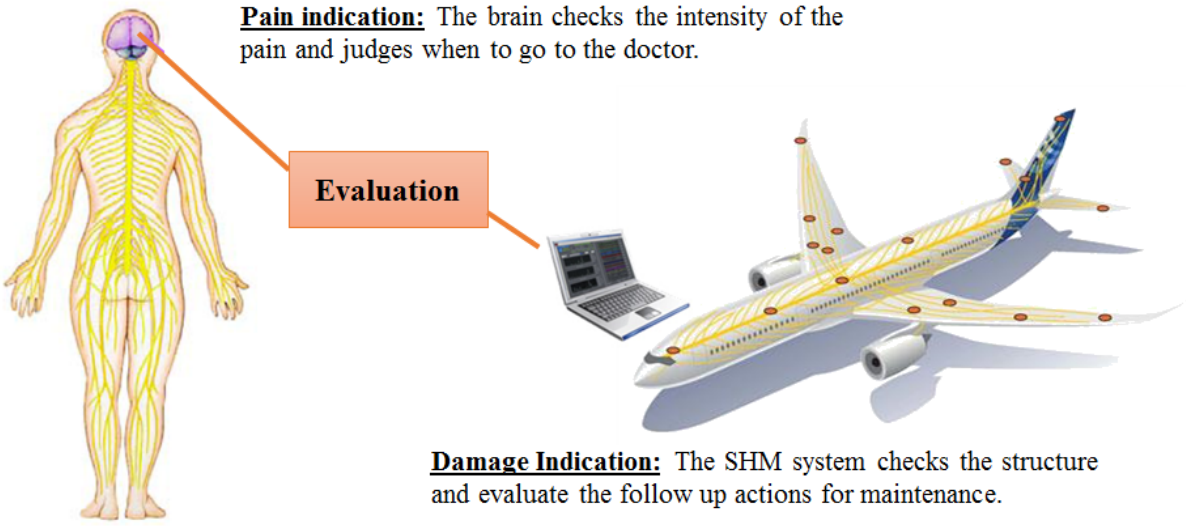

Figure 1-4. Analogy between the operation of the human nervous system and of a structure SHM (*photo from OWI application lab http://www.owi-lab.be*)

As previously mentioned, the prediction of structural integrity in real-time through the SHM system is a very important goal to be reached by manufacturers and operators of airplanes. For composite structures, this issue is strategic, because the prediction of damage and failure mechanisms during the design is very complicated due to the anisotropy and heterogeneity of the material.

The development of new SHM systems for composite structures can contribute for different aspects, such as:

⇒ Maximise the lifetime of the structure and minimise the out-of-service time due to inspection periods, which are inadequately programmed.

⇒ Prevent catastrophic failures.

⇒ Improve the quality of the products.

⇒ Improve the organisation of the maintenance tasks.

In view of the benefits provided by an SHM system, the development of research projects in this issue is totally justified, mainly for composite structures, which can suffer damage in service due to cyclic, static or impact loadings. However, in the present work, it will be focus the damage caused by impact loadings. Therefore, the present work consists on developing a new SHM system for composite aeronautic structures, which is a combination of different methods to identify, locate, estimate the extension (severity) of impact damage and provide information about the residual strength of flat and curved composite structures. For this, vibration based methods (VBM) will be chosen for identification and global localization of the impact damage using few piezoelectric sensors, which almost do not interfere in the weight of the monitored aeronautic structures. In addition, a new damage metric will be developed, which takes in to account the effects of amplitude and phase of the Frequency Response Function (FRF) obtained from VBM. Moreover, shearography speckle (SS) will be chosen for local localization and provide the extent of damage. This choice is based on program maintenance of airplanes. In fact, during the operation of airplanes, it is necessary to perform maintenance of aeronautic structures. Thus, there are checks of structures during the life of the airplane, which can be performed by shearography speckle on ground in the region of the aircraft structure that is previously indicated by the VBM. Also, SS is well known and certified by the regulatory agencies. Finally, a residual strength criterion will be developed based on Flexure After Impact (FAI) instead of Compression After Impact (CAI) due to buckling problems in the compression tests. And, a correlation between damage metric from VBM and other damage metric from FAI will be developed in order to provide information about residual strength of the impact damaged composite structure. This work will show that comparisons between experimental and computational tests can be used to extrapolate the correlation between the damage metrics to obtain the response of the structure for a determined range of interest. Thus, the scientific contribution of the present work can affect the development of smart aircraft structures, which offer significant improvements in the aircraft's life cycle and total weight, as well as in manufacturing and operational/maintenance cost.

1.2. State of Art of SHM Systems

In the most general terms, damage can be defined as changes appearing in a structure that may affect its current or future performance (Cuc, 2002). From this definition of damage, it is possible to observe two different states of the structure, *i.e.* the initial state, which is assumed to represent the intact (undamaged or healthy structure), and the other, which corresponds to the damaged state. Farrar and Worden (2007) defined SHM as the process of implementing a damage detection and characterisation strategy for engineering structures. In this definition, damage is identified as changes to the material and/ or geometric properties of a structure, including changes to the boundary conditions and system connectivity, which adversely affect the structure's performance. The interest in structural health monitoring, aiming at early damage detection, has been motivated by, amongst other factors, the risk of losing human lives, due to unpredictable structural failures, such as airplane crashes and bridges or buildings collapses (Lopes *et al.*, 2011). Damage detection and localisation aim to prevent the structures failure by repairing or replacing the damaged part.

The need of global methods for damage detection has been essentially motivated by aeronautical and aerospace applications. Currently 27% of an average aircraft (both for commercial and military vehicles) life cycle cost is spent on inspections and repairs (Kessler, 2002). In these applications, the less critical components have been progressively replaced by components manufactured from composite materials. Although their high specific stiffness and strength compared to those of metals, composite materials are more sensitive to certain type of damages and present different kinds of failure or damage mechanisms. There are different damage types in laminated composites, such as interlaminar debonding, micro-cracks and micro buckling, besides inclusions. Internal defects usually result from manufacturing and assembling processes or in service loadings. Moreover, delamination or interlaminar debonding is undetected by visual means and, therefore, one of the most critical types of damage, being also the most common in aeronautical components (Lopes *et al.*, 2011).

Currently, the main inspection techniques can be classified into global and local methods. Non-destructive testing (NDT), developed over 30 years, have been used in science and industry to evaluate the properties of material, structure or system without damage (Zhu *et al.*, 2011). The terms Non-destructive examination (NDE), Non-destructive inspection (NDI), and Non-destructive evaluation (NDE) are also commonly used to describe this technology. NDT is defined as the process of measuring and characterising the damage performed off-line

with portable sensors and it is used to detect and determine the size of damage in localized areas. Many NDT techniques are well developed and successfully instrumented for a variety of applications, such as acoustic emission, ultrasonic inspection, magnetic fields testing, eddy current testing, thermal testing, X-radiography testing and optical methods. A condition for applicability of these methods is that the damage localisation must be known a priori, and the portion of the structure, which is being inspected, must be accessible. Thus, traditional NDT methods cannot nor satisfy the increasing needs of on-line inspection and continuous assessment of structures health condition while the structures are in service, neither predict the remaining life once some damage is detected.

A wide range of NDT techniques can be employed for damage identification purposes. An overview of the most commonly used NDT techniques and their characteristics is presented in Table 1-1. The majority of these techniques can only be applied when the structure is not in operation ("off-line"), and readily accessible. Consequently, only a few of these techniques can be applied in a SHM environment.

Table 1-1. An overview of the most commonly used non-destructive testing – NDT (Ooijevaar, 2014)

Technique	Inspection area	Inspection mode	Structure accessibility
Electric/magnetic/ electromagnetic			
Electrical conductivity testing	Local/Global	Off-/on-line	Not required
Magnetic particle testing	Local	Off-line	Required
Eddy current testing	Local	Off-line	Required
Radiography (X-ray)	Local	Off-line	Required
Infrared thermography	Local/Global	Off-/on-line	Required
Mechanic/dynamic			
(Quasi-) static	Local	Off-/on-line	Not required
Structural vibrations and acoustics	Local/Global	Off-/on-line	Not required
Electro-mechanical impedance	Local/Global	Off-/on-line	Not required
Acoustic emission	Local/Global	On-line	Not required
Acoustic-ultrasonic	Local/Global	Off-/on-line	Not required
Ultrasonic testing	Local	Off-line	Required
Optical			
Shearography Speckle (SS)	Local	Off-line	Required
Visual inspection	Local/Global	Off-line	Required

Considering the technological advances in smart materials, such as in sensors, data and signal processing, computational power as well as needs on real time assessment of structural health status, it is not surprising that SHM has emerged as a natural evolution from traditional

NDE technologies to meet those requirements. Although SHM may be literally categorised under the framework of NDE in terms of terminology, it does deviate from traditional concepts of NDE in the sense that the ultimate goal of SHM is the real time, automatic and continuous assessment of structures in service with minimum human intervention involved.

According to Housner *et al.* (1997), SHM is a non-destructive in-situ structural sensing and evaluation method, which uses a variety of sensors to monitor the structural response, to analyse the structural characteristics for the purpose of estimating the severity of damage/deterioration and to evaluate the consequences on the structure in terms of response, capacity, and service-life. SHM may also include the use of many devices, techniques and systems, which are traditionally designated as Non-Destructive Testing (NDT) and Non-Destructive Evaluation (NDE) tools. There is no formal delineation between each approach, but there is a difference between NDT/NDE and SHM. NDT/NDE normally refers to a one-time assessment of the condition of materials and the effect or extent of the deterioration in the structure using equipment external to the structure. The SHM approach normally refers to activities focused on a continuous/periodic assessment of the structure state. Most importantly, SHM also involves the interpretation of the recorded data in order to quantify the changes of the structural state and assess capacity and remaining service-life (Benzoni *et al.*, 2013). Structural health monitoring is the multidisciplinary process of implementing a strategy for damage identification in a way that non-destructive testing becomes an integral part of the structure (Ooijevaar, 2014). Figure 1-5 shows a simplified process, which consists of a diagnostic and a prognostic part. Diagnostic analysis is used to estimate the current state of the structure. Prognostic analysis evaluates the damage evolution and estimates the residual service life.

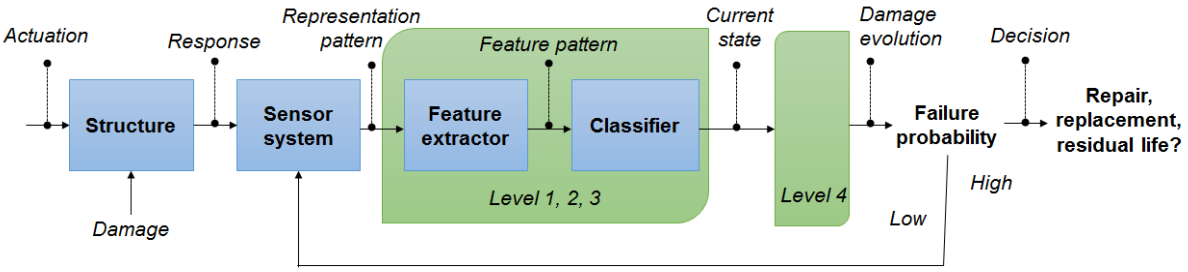

Figure 1-5. The multidisciplinary structural health monitoring process (Ooijevaar, 2014)

A brief comparison of differences between traditional NDT methods and current SHM techniques is given in the Table 1-2. It is noted that apparent distinction between the two approaches is difficult, since many ideas and techniques are certainly applicable for both NDT and SHM.

Table 1-2. Comparison between traditional NDT and SHM (Wang, 2004)

	Traditional NDT	**SHM**
Objectives	Detection of a local structural damage.	Continuous assessment of structural health conditions, including damage detection and lifetime prediction
Data history	No historical data required	Data history needed for continuous monitoring.
Maintenance approach	Schedule-based; fixed-time overhauls	Condition-based
Typical techniques	Visual inspection; liquid penetrant; eddy current; ultrasonic wave; magnetic particles; acoustic emission; radiography; etc.	Variety such as vibration-based (global or local), wave propagation, strain; etc.
Physics	Capillary action; electrical/magnetic properties; wave propagation; X-ray.	Static or dynamic changes in physical properties due to presence of damage.
Damage format	Cracks (internal and surface); voids; pores; surface corrosion; etc.	Any kind of structural damage.
Instrumentation	Well instrumented.	To be instrumented.
Sensor	Single type of sensor; isolation from host structures.	Sensor array; fusion of different kinds of sensors; integration of sensors to host structures.
On-line or off-line	Off-line inspection.	Both, with on-line targeted.
Accessibility	Direct access to damage locations.	Direct access not necessary.
Cost	High maintenance cost.	Low labour and maintenance costs.
Operational guidance	No guidance with damage removed during downtime.	On-line guidance while damage is developing.

In the extensive literature about damage characterisation in composite materials, several methodologies are referenced. These have been typically created from experimental techniques for measuring parameters in a localized (local variable) and/or distributed way (global variable) on the structure. These methodologies are based on the structural response, which supports the development of vibration based techniques by using piezoelectric sensors and interferometry techniques. According to Rytter (1993), a system of classification for damage-identification methods can be classified into four levels:

⇒ Level 1: Determination of the *presence* of the damage in the structure;

⇒ Level 2: Determination of the geometric *location* of the damage;

⇒ Level 3: Quantification of the *extent /severity* of the damage;

⇒ Level 4: Prediction of the *remaining service life* of the structure.

Thus, SHM has been defined in the literature as the acquisition, validation and analysis of technical data to facilitate life-cycle management decisions (Kessler, 2002). More generally, SHM denotes a system with the ability to detect and interpret adverse changes in a structure in order to improve reliability and reduce costs. According to Kessler (2002), the most fundamental challenge in designing a SHM system is knowing what changes to look for and how to identify them. The resulting changes, or damage signature, dictate the type of sensors, which are required, which in-turn determines the requirements for the rest of the elements in the SHM system. Table 1-3 presents the state of art in SHM for composite structures, there is a list of the most important publications and their contributions for the state of art.

After an extensive literature review, the author suggests a new question about the SHM systems, the kind of damage present in the structure. Thus, the standard SHM systems compose of four levels as defined by Rytter (1993) can be evaluated by using five questions:

1. Is there damage in the structure (*Identification*)?
2. Where is the damage in the structure (*Location*)?
3. What kind of damage is present (*Type*)?
4. How severe is the damage (*Extension*)?
5. How long is the *residual life* of the structure? Or, is there still enough *Residual Strength*, considering design requirements?

The questions 1, 2, 4 and 5 will be addressed in the present work. However, the question 3 is outside the proposed objectives for this work. In fact, only preliminary predictions will be performed, considering the damage model used, which provides the type of intralaminar failure (fibre or matrix failure).

Table 1-3. State of art in SHM systems for composite structures.

Authors	Main Contribution
Pardoen, 1989	Effect of delamination on the natural frequencies of composite laminates.
Islam and Craig, 1994	Damage detection in composite structures using piezoelectric materials and neural net.
Giurgiutiu and Rogers, 1998	Recent advancements in the Electro-Mechanical (E/M) Impedance method for structural health monitoring and NDE.
Zou *et al.*, 2000	Review of vibration-based model-dependent damage (delamination) identification and health monitoring for composite structures.
Kessler *et al.*, 2002a	Attempts to fill some of the gaps remaining in SHM technologies.
Yam *et al.*, 2004	Non-destructive detection of internal delamination by vibration-based method for composite plates.
Fritzen, 2005	Discuss the basic physical ideas of different vibration-based methods.
Giurgiutiu and Cuc, 2005	Embedded non-destructive evaluation for structural health monitoring, damage detection, and failure prevention.
Nilsson, 2005	Residual strength prediction of composite laminates containing impact damage.
Montalvão *et al.*, 2006	Review the vibration-based structural health monitoring with special emphasis on composite materials.
Su *et al.*, 2006	Review the state of the art of Lamb wave-based damage identification approaches for composite structures.
Lopes, 2007	Development of interferometric, continuous and pulsed techniques pplied to damage analysis of composite structures
Raghavan and Cesnik, 2007	Review the Guided-wave structural health monitoring.
Ciang *et al.*, 2008	Review the damage detection methods for a wind turbine system.
Moaveni *et al*., 2008	Damage identification of a composite beam using finite element model updating.
Worden *et al.*, 2008	Review the nonlinear dynamics applications to structural health monitoring.
Shahdin *et al.*,2009	Preliminary study on composite beams to correlate low-energy impact damage with changes in modal parameters.
Sinou, 2009	Review the damage detection and health monitoring of mechanical systems from changes in the measurement of linear and non-linear vibrations.
Staszewski *et al.*, 2009	Active and passive approach for health monitoring of aerospace composite structures.
Maio and Trindade, 2011	Evaluation of metrics and techniques for the detection of delamination in composite structures using piezoelectric sensors.
Ullah, 2011	Vibration-based structural health monitoring of composite structures
Liu and Nayab, 2012	State of the art and perspectives of the structural health monitoring.
Sundaram *et al.*, 2012	Issues and challenges of structural heath monitoring of composite structures.
Slatte and Javanov, 2012	Investigation of the potential using the finite element method for structural health monitoring for aerospace composite structures.
Subramanian, 2013	Damage detection and characterization of fibre reinforced composites using ultrasonic technique.
Ooijevaar, 2014	Presents the relations between the characteristics of the structure, the potential damage scenarios and the damage identification method together define the performance of the vibration based damage identification strategy.
Zhu *et al.*, 2014	Debonding detection of honeycomb sandwich structures using frequency response functions.
Trendafilova *et al.*, 2015	Application of damage assessment based on general signal correlation for delamination diagnosis in composite structures.
Zhong *et al.*, 2015	Multi-impact source localisation on aircraft composite structure using uniform linear PZT sensors array.

1.3. Objective and Scope

Regarding the challenges in order to maximise the inspection periods and minimise the cost and maintenance, it is necessary to develop efficient SHM systems for composite aeronautic structures. These systems need to have accuracy in damage identification (detection), using reduced numbers of sensors. In aeronautical structures, the major indicator of structural design "quality" is weight (Bordegoni and Rizzi, 2011). It can be demonstrated by Solid Mechanics, but it is also common sense that lighter structures provide aircrafts with better performances in flight. Another challenge is related to the residual strength criterion for impacted structures. Damage tolerance in laminates is usually studied by determining the effect of different impact energies on their residual strength, and then Compression After Impact (CAI) tests are carried out for composite structures damaged by low energy impact. However, these tests are complex and involve higher costs, because the laminated specimens must have large dimensions, and the compression load cannot cause global or total buckling on the tested specimen. The expected result considers micro-buckling mechanisms followed by fibre breakage, cracks, etc. (Paiva *et al*., 2005).

Based on the scenario pointed above, as commented earlier, the main objective of this work consists on developing a new SHM system based on the combination of different methods. This new SHM system should be able to identify, locate, estimate the extension (severity) of damage and provide information about the residual strength of composite structures damaged by impact loading. Thus, the main objective can be divided in different steps, which will become clear in the next chapters:

- ⇒ Perform a literature review in order to understand the most relevant scientific papers, as well as the most recent publications, which have been developed in the areas of SHM used in composite structures;
- ⇒ Carry out experimental and computational analyses of composite plates without damage in order to evaluate the dynamic behaviour using piezoelectric sensors;
- ⇒ Simulate impact tests on plates through material models previously developed by GEA (Aeronautical Structures Group – EESC/USP);
- ⇒ Perform impact tests (under low velocity) on composite structures using (or not) piezoelectric sensors/actuators for monitoring the test in real-time;

⇒ Perform experimental and computational analyses of composite structures damaged by impact in order to evaluate the dynamic behaviour using piezoelectric sensors/actuators;

⇒ Propose a method to identify and globally localise the damage using vibration based methods, and develop a new metric for damage identification;

⇒ Propose a method to locate and evaluate the extension (severity) of the damage using optical methods (*e.g.* speckle shearography);

⇒ Develop a criterion to predict the residual strength of damaged specimens by impact loading;

⇒ Correlate the metric provide by the vibration based method with the damage metric provide by bending test;

⇒ Evaluate the potentialities and limitations of the numerical models, comparing the results of the experimental tests and computational simulations, as well as the proposed approach for predicting residual strength.

Therefore, considering the presented goals, the present work will contribute to the development of a design tool for research engineers, to assist the implementation of SHM systems in safety critical composite structures, and a new approach to predict residual strength of impact damaged composite structures (such as, plates and cylinders made of epoxy resin reinforced by carbon or glass fibre).

1.4. Outline

This PhD thesis consists of eight chapters organised as shown by Figure 1-6.

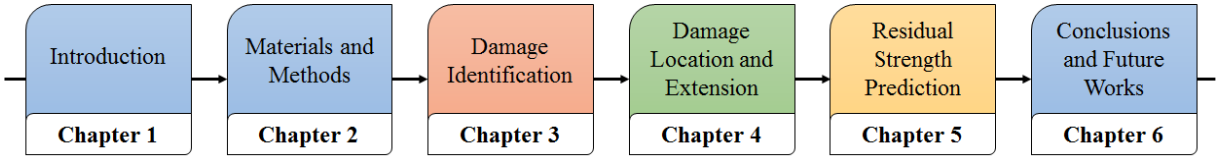

Figure 1-6. Schematic overview of the thesis outline

⇒ **Chapter 1 – Introduction:** Serves as an introduction to the SHM topics and to give concise background information on the motivation behind SHM system and NDE/NDT methods. The research objectives, main tasks and scientific issues are also addressed.

⇒ **Chapter 2 – Material and Methods:** Describes the methodology used in this work, provides the description of the materials and methods used to manufacture and test the composite structures. In addition, synthetises the material damage model. Also, gives a description of the piezoelectric sensor and the procedure to determine the mechanical, electrical and dielectric properties.

⇒ **Chapter 3 – Damage Identification:** Provides a literature search and an overview of existing vibration-based method (VBM). Presents modal testing and experimental modal analysis of composite structures. Describes the finite element models of the test structures. Gives the theory, background and methodology of the damage identification and global localisation method. Presents damage metric results applied to the composite structures, considering a new one. Discusses the results of the FRF-based damage identification and global localisation methods using numerical and experimental data.

⇒ **Chapter 4 –Damage Location and Extension:** This chapter presents a general explanation of the fundamentals of Shearography Speckle measurements. The principle and procedure of this technique, phase stepping algorithm and phase map unwrapping are presented. Contains the experiments with damage composite structures. Thermoelastic deformations are considered for their use with the shear system in order to local localisation and quantify the extension (severity) of the damage. Discusses the results to locate and provide the extent of damage.

⇒ **Chapter 5 – Residual Strength Prediction:** Presents a discussion of residual strength calculations. Provides the detailed descriptions of experiments and results, considering the used setup. Describes the finite element models of the test. A criterion is proposed to predict the residual strength of the composite structures based on flexural tests. Finally, it is present a correlation between the damage metric provide by vibration based method and the damage metric provide by flexural test.

⇒ **Chapter 6 – Conclusions and Future Works:** This chapter begins by summarising the work performed. Final conclusions are then presented along with the recommendations on future's research needs.

CHAPTER 2

Materials and Methods

Composite materials constitute a new challenge for several sectors of the scientific community, and their introduction in engineering and society generally represents an even greater challenge for researchers and academics. The use of composites in several sectors of industry seems inevitable, although in practice engineers are still hesitant when confronted with composites. The main reasons for this reluctance are the unawareness on the part of engineers concerning the advantages of composite materials, the complexity of classifying the behaviour of composites in terms of rules and regulations, and the difficulty of developing a commonly accepted accurate method for the life prediction of these materials. Despite this lack of enthusiasm, fibre-reinforced composites are seeing widespread usage in the military, aviation, and automotive industries. A fibre-reinforced composite laminate is typically comprised of several layers, or plies, within which there are two constituents: the fibre and matrix. Common fibre/matrix combinations include carbon/epoxy and fiberglass/epoxy composites. These composites boast superior strength-to-weight ratios and the ability to tailor the structure's material properties by using arbitrary fibre directions and ply stacking sequences. During the last decades, composite materials are gaining acceptance and demand in several commercial markets, including transportation, sporting goods and construction. Traditional manufacturing and mechanical testing techniques have been developed by the aerospace industry to address the feasibility of composite material systems as structural components in high performance applications. New applications are continually emerging, however, so these standardised methods are being modified to accommodate the specific engineering requirements. Thus, this chapter introduces the techniques, materials, and methods used to manufacture and test composite structures. Firstly, the global methodology used in this work is presented. After that, the manuscript addresses composite materials, properties and specimens used in the present work. Then, a summary of the damage model applied in the computational simulations is discussed. Finally, the homogenised piezoelectric sensors properties are presented and discussed.

2.1. Methodology

The usage of piezoelectric sensors is investigated to detect and to provide an estimation of residual strength of composite structures damaged by impact loading. Experimental and numerical tests are performed and compared. The detection and global localisation of damage are based on dynamic response of the structure using damage identification methods via piezoelectric sensors. Vibration based methods can identify stiffness changes in the structure, which causes or not a noticeable shift in the natural frequencies and changes in the respective mode shapes. In addition, these methods are easily applied and fairly sensitive to damage, but they are often more practical in detecting global loss of stiffness than localising the degraded region and they are not able to provide the extension of the damage, using only few sensors. Consequently, optical methods, such as Shearography Speckle (SS), can be used to locate damaged regions by measuring full fields. Hence, SS, which requires non-contact and provides high-resolution measurements, is applied in order not only to give the location of the damage with more accuracy, but also to obtain the extent of damage. In fact, SS is an optical method, which uses speckle shearing interferometry to measure displacement gradients at the surface of the structure. Therefore, the used research methodology (Figure 2-1) combines VBM and SS techniques to detect, to locate and to provide the extension of the damage.

In the research methodology, there are 3 main stages (Fig. 2-1): (I) Before Impact Test; (II) During Impact Test (real-time) and (III) After Impact Test. In each stage, there is a comparison between numerical analyses and experiments, which is based on modal properties (resonance frequencies, mode shapes and FRFs). In case of bad correlation between Finite Element models and experiments, model updating procedures are used to improve the finite element model.

1. Step 1 of the stage I consists on a updated review about SHM systems and techniques for it.
2. The step 2 of the stage I covers the use of computational models for composite structures without damage in order to evaluate the dynamic behaviour (FRF, modal shapes, natural frequencies) using piezoelectric sensors/actuators. The models are developed by using the finite element software code Abaqus^{TM}, complemented with Fortran and Python subroutines.

3. Step 3 of stage I consists of the preparation of composite specimens, which are manufactured by CTM-SP (Brazilian Navy Research Centre) or in the Aeronautic Structure Laboratory (University of Sao Paulo).
4. Also, in the Step 3 of stage I, the piezoelectric sensors/actuators are attached on the surface of the composite specimens, which is analysed by dynamic test (*e.g.* vibration tests, *cf.* Fig. 2-1) in step 4. Therefore, the composite structures are analysed before the impact test, *i.e.* the specimens do not have damage.
5. In the step 5 (Check I) of the stage I, the numerical results are compared to the experimental analyses (*cf.* Figure 2-1). If there is an agreement between both results, then the next stage is initiated, otherwise, it is necessary to improve the computational model. In order to improve the computational model, different updating parameters can be used, such as: finite element type; mesh convergence analysis (more refined mesh); boundary conditions, material properties and geometry. It is important to highlight that the experimental and computational results are obtained from a modal survey test with the structure suspended by soft cords to simulate "free-free" boundary conditions. As it is known, it is possible to represent more accurately the "free-free" conditions in the computational model by using spring elements.
6. Step 6 of stage II is the simulation of impact tests (under low velocity) on composite structures using computational models developed previously by Aeronautic Structure Group at University of São Paulo (Brazil). However, others computational models can be used, as well.
7. Step 7 consists of experimental impact tests (under low velocity) on composite structures by using piezoelectric sensors/actuators for monitoring the test in real-time (*cf.* Fig. 2-1). This data can assist in the evaluation and validation of the computational model. As well known, the piezoelectric effect is the ability of certain materials to generate an electric charge in response to applied mechanical stress. They also have the opposite effect, i.e. the application of electric voltage produces mechanical strain in the materials. During the experimental testing, it is measured the response of the piezoelectric sensors to obtain the deformation values at specific positions and after, compare these results with the computational analysis. However, in the present thesis, these data will not be explored.
8. Step 8 of stage III is the use of computational models (similar models of step 2) in order to simulate damaged composite structures by using piezoelectric sensors. The models

are developed by using the finite element software Abaqus™, complemented with Fortran and Python subroutines.

9. Step 9 of the stage III is the preparation of composite specimens with damage caused by impact. The piezoelectric sensors are verified and replaced if necessary. In addition, the damage is quantified in order to verify if it is small and local. In that case, its effect may remain undistinguishable and then a threshold value must be exceeded before damage is noticeable.
10. In step 10 of the stage III, the damaged composite specimens are analysed by dynamic tests (*e.g.* vibration tests, *cf.* Fig. 2-1).
11. In step 11 (Check II) of stage III, the numerical results are compared to the experimental analyses. If required, the computational model is improved for adequate correlation with the experimental results. In order to improve the computational model, different approaches can be used, for example: finite element type, mesh convergence analysis (refined mesh), boundary conditions, material properties, geometry, total thickness, thickness of each layer, and more consistent representation of the damage region (material damage model).

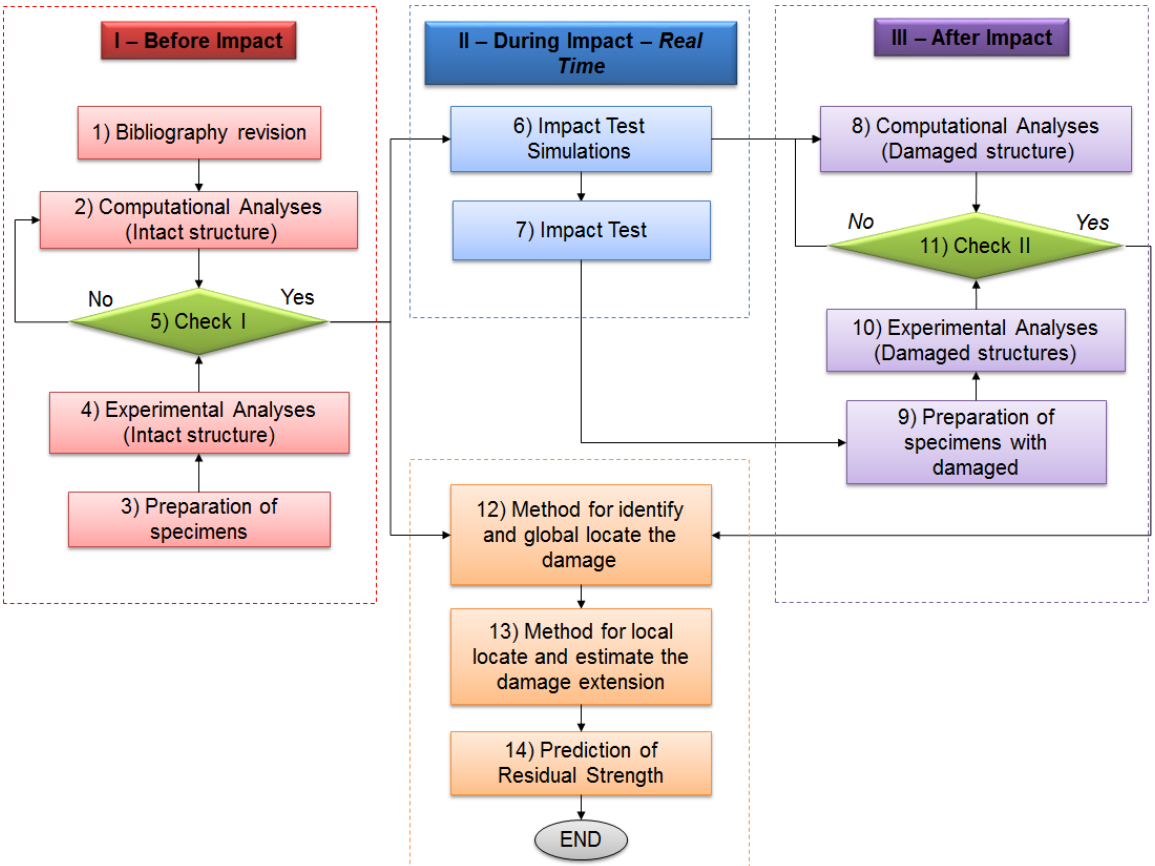

Figure 2-1. Research methodology

Finally, there are 3 more steps, which consist in the development of proposed SHM system:

12. In the Step 12, a method is proposed to identify and localise the damage using deterministic methods, such as a vibration based method. Thus, the main goal consists on obtaining modal properties (in this work: mode shapes, natural frequencies and frequency response function) from the structural dynamic output response. The limitation and advantages of this method is investigated through intact (undamaged) and damaged composite specimens. The dynamic tests aim to assess the behaviour of the damaged composite structure by impact, *i.e.* through the analysis of the signals. The natural frequencies, damping, mode shapes, and frequency response function (FRF) can be determined. A new damage metric is developed in order to use FRF (amplitude and phase) data. Based on this metric is possible to identify the damage in the composite structure.
13. In the Step 13, a method is proposed to localise damage (with more accuracy) and evaluate its severity using deterministic methods, such as Shearography Speckle. Shearography is an optical method, which uses speckle shearing interferometry to measure displacement gradients at the surface of a structure. The speckle patterns produced by a structure in stressed and unstressed states are subtracted, revealing changes in displacement gradient. The method is generally faster in damaged regions. Laser speckles are produced whenever a surface, whose roughness is of the order of one wavelength of light or greater, is illuminated with highly coherent light. These parameters are used for local locate and determine the extent of damage in impact damaged composite structure.
14. In the Step 14, a criterion is proposed to predict the residual strength of the structures. A new damage metric is proposed based on the flexural tests. Finally, a correlation between the damage metrics provide by vibration based method and the damage metrics provide by flexural test is presented and discussed.

Figure 2-2 shows the main parameters and tests used for the methodology and the residual strength criterion. The data of intact and damaged structure are input parameters for damage metrics. It is important to notice that computational models are evaluated in Steps 5 and 11 (*cf.* Figure 2-1), where is investigated the limitations and potentialities of numerical models to predict dynamics parameters. Hence, it is possible to have an estimative of the residual strength supported by numerical simulations, as well.

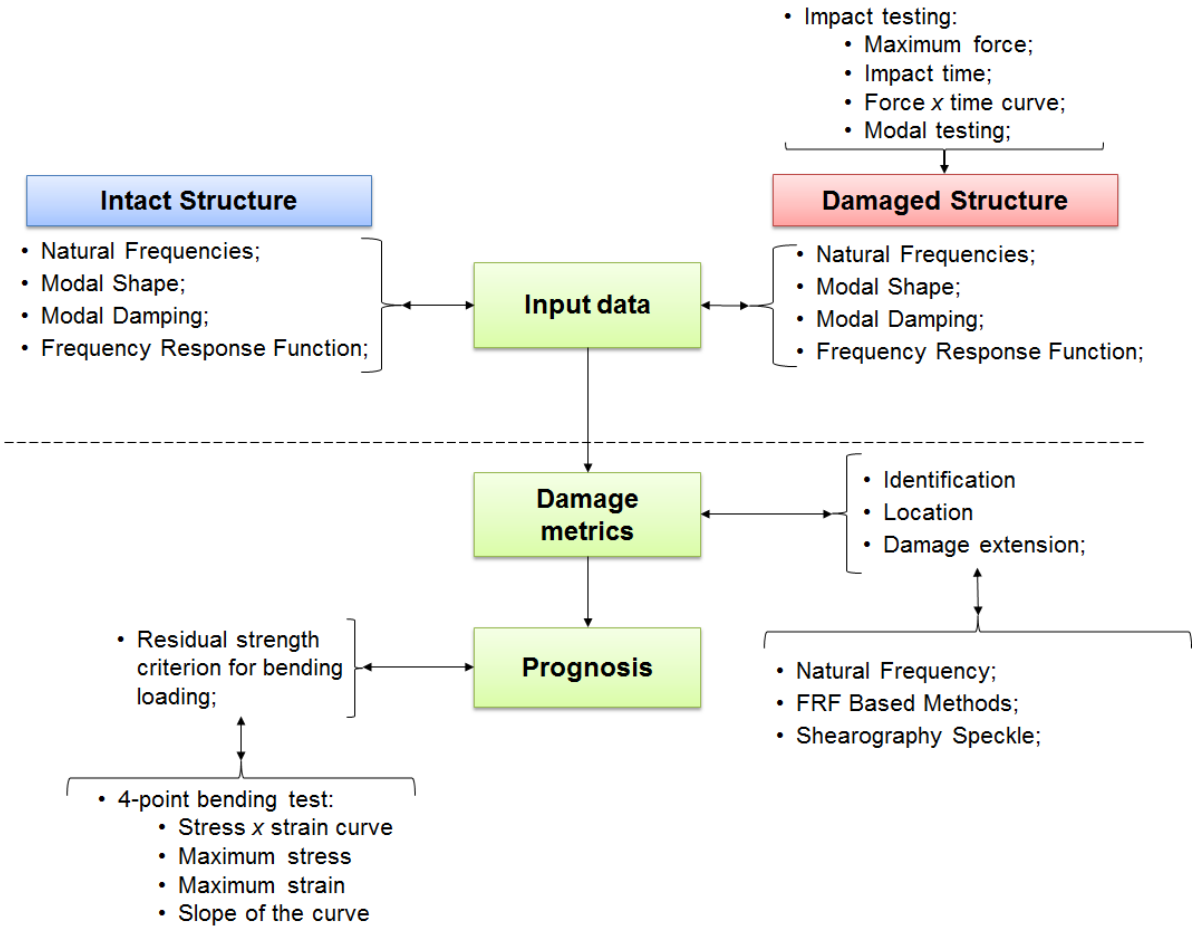

Figure 2-2. Main parameters and tests used for the methodology and the residual strength criterion

After that, a speckle technique is used to localise with more accuracy and estimate the damage extent. Figure 2-3 presents the experimental methodology used for this optical method. It is important to highlight that shearography is a full-field speckle interferometric technique used to determine surface displacement derivatives. For an interferometric technique, shearography is particularly resilient to environmental disturbances and has hence become an invaluable measurement tool outside of the optics laboratory. Furthermore, the inclusion of additional measurement channels has turned shearography from a qualitative inspection tool into a system suitable for quantitative surface strain measurement (Francis *et al.*, 2010). Shearography systems are used for wide range of applications, in laboratories, in industrial environments, as well as in the field. The most import application at present is undoubtedly in the field of NDT, but strain measurements and vibration analysis are also possible (Rastogi and Hack, 2013).

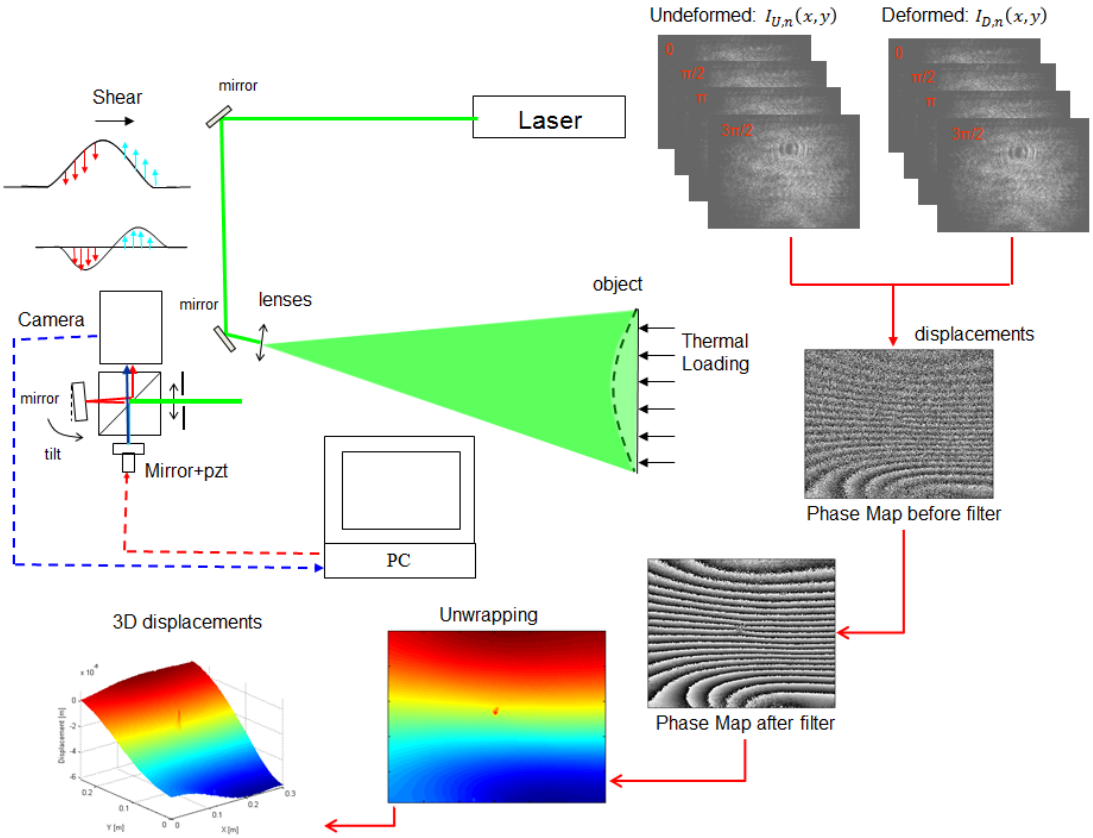

Figure 2-3. Methodology for damage locate and quantification via SS

The shearography technique consists of combining the laser speckle pattern with another coherent laser beam, which has a speckle pattern or a smooth wave front, the image obtained from the interference also has a random speckle appearance known as a "speckle interference pattern". The resulting speckle interferogram is imaged on a CCD (Charge Coupled Device) camera. When the surface moves, the speckle interferogram is changed due to the change in path length difference between the object and the reference. Thus, this second interferogram is subtracted from the first one, pixel by pixel. The result is processed and displayed as a set of bright and dark fringes, known as correlation fringes, which depicts a contour map of the displacement of the object surface. The shear interferometry measures the displacement based on the principle of Michelson Interferometer. The Michelson interferometer is a popular choice of shearing device since it is simple to set up, offers easy adjustment of the image shear. And, phase analysis through the temporal phase stepping technique can be easily implemented by mounting one of the mirrors on a piezoelectric transducer (PZT). The applications of SS can be divided into two classes: static and dynamic. Depending on the type, namely static or dynamic, different loading and processing methods are used. For static

applications, mechanical loading or thermal loading or pressure differences are used; for dynamic applications, loading can be implemented by mechanical means such as electromagnetic or piezo-driven devices. Alternatively, sound is also used as loading. In this work, it was used static method with thermal loading. This method is capable of accentuating the impact damage area in composite laminate specimens, because the delamination can take place in the impact damage area.

Finally, flexural testing is used instead of Compression After Impact (CAI) due to the buckling effects, as mentioned previously. Four point bending test is chosen. This test is very similar to the three point bending test. The major difference consists on having in 4-point bending only constant bending moment in the middle span of the specimen, instead of the combination of bending moments and transverse shear loading in the middle span of 3-point bending specimen.

Figure 2-4 shows a schema of the methodology applied during the present work.

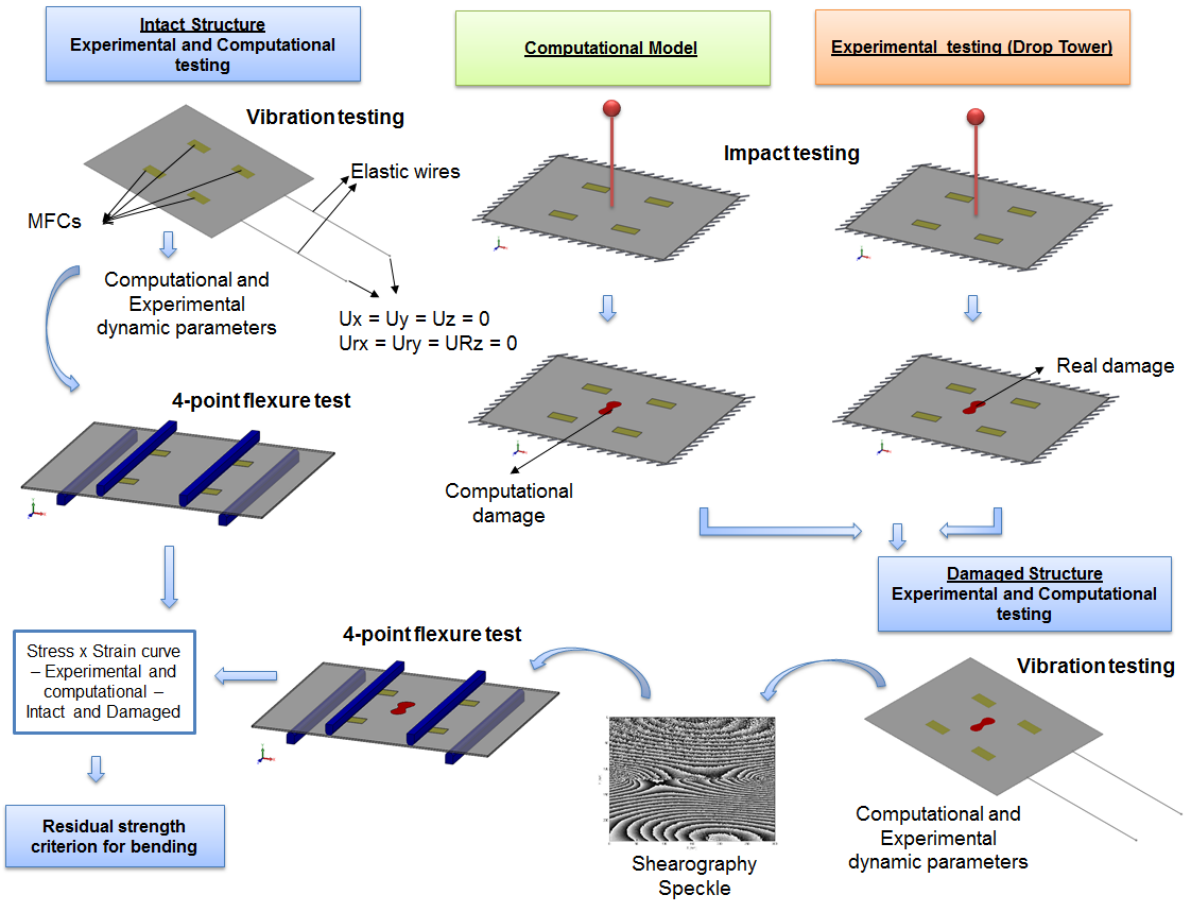

Figure 2-4. Schematic methodology: Experimental tests and computational analyses

2.2. Composite Material: Manufacturing and testing

A composite material can be defined as a combination of a matrix and a reinforcement, which when combined gives properties superior to the properties of the individual components. In fact, the primary advantages of composite materials are their high strength, relatively low weight, and corrosion resistance (FAA, 2012). Thus, as commented earlier, composite materials are becoming more important in the construction of aerospace structures. Aircraft parts made from composite materials, such as fairings, spoilers, and flight controls, were developed during the 1960s for their weight savings over aluminium parts. New generation large aircraft are designed with all composite fuselages and wings, and the repair of these advanced composite materials requires an in-depth knowledge of composite structures, materials, and tooling. For example, knowledge about residual strength of impact damaged composite structures is very strategic for manufacturers and operators.

Hence, in this work, in order to investigate this issue and considering the methodology shown in the Figure 2-4, a matrix of experimental tests is proposed. Table 2-1 shows the matrix of experimental tests required for the development of the present work. The type of structure, ply orientations, and the types of tests to be performed are listed.

Regarding the type of structures, there are two main reasons for the focus on simple ones: (1) most structures or their major structural elements in aeronautical and mechanical engineering can be simplified as a beam or plate or cylinders, and (2) the problem of identifying a specific damage in a beam/plate provides an important benchmark for effectiveness and accuracy of identification techniques. Regarding the stacking orientation of the ID 01 and 02 (Table 2-1), the main reasons for this is due to the limitations of the manufacturing process used to obtain carbon fibre reinforced plastic specimens (filament winding), which were produced by CTM-SP (Brazilian Navy Research Centre). It is important to highlight that there is a confidential agreement for scientific cooperation between Aeronautic Structure Group (USP) and CTM-SP. Therefore, it is not possible to provide details about the manufacturing process of the carbon fibre composite specimens.

Regarding the type of testing, dynamic test was chosen, because for real structures, dynamic loads in flight combined to measurements from piezoelectric sensors can be used to monitor the structural health. The impact testing was chosen, because different types of impact events can cause damage in composite structures, such as small debris impact, bird strikes, hail

impact and stone impact in service and dropping of hand tools during maintenance process. Figure 2-5 shows the typical local loads on an aircraft.

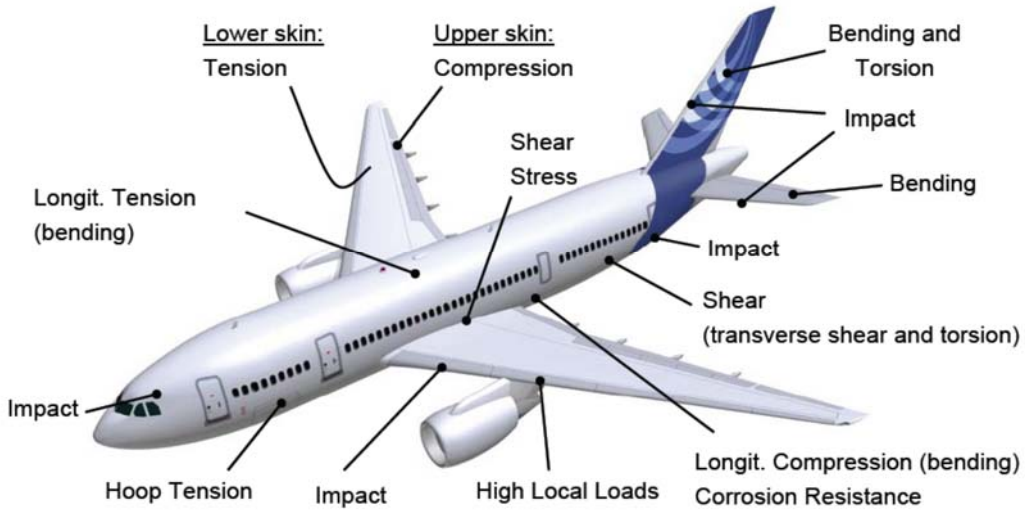

Figure 2-5. Typical local loads on an airliner (Kaufmann, 2008)

Shearography speckle was chosen because it is used for wide range of applications, in laboratories, in industrial environments, as well as in the aeronautic field. The full-field nature of the results allows an accurate and easy determination of material parameters and the identification of highly stressed areas. In contrast to conventional methods *e.g.* strain gauge, scanning vibrometer, ESPI systems combine an unsurpassed density of measuring points with very high sensitivity. Bending test was chosen instead of Compression After Impact (CAI) due to the buckling problems. During the CAI test the compression load cannot cause global or total buckling on the tested specimen. The expected result considers micro-buckling mechanisms followed by fibre breakage, cracks, etc. Also, CAI tests are not very simple to carry out and require more material than the conventional mechanical tests, as tensile, compressive, and flexural.

Regarding the material type, carbon or glass fibre and epoxy resin were chosen, because they are very common in aeronautic composite structures. In fact, composite materials are used more and more for primary structures in aeronautic, because they have higher performance then metals due to excellent strength-to-weight and stiffness-to-weight ratios. This is usually expressed as strength divided by density and stiffness (modulus) divided by density. These are so-called "specific" strength and "specific" modulus characteristics. Laminate patterns and ply build-up in a part can be tailored to give the required mechanical properties in various

directions. It is easier to achieve smooth aerodynamic profiles for drag reduction. Complex double-curvature parts with a smooth surface finish can be made in one manufacturing operation.

Table 2-1. Matrix of experimental tests

ID	Type	Orientation	Type of testing
01	Plate	$[0]_8$	✓ Dynamic testing (Intact structure) ✓ Impact loading (Drop test) ✓ Dynamic testing (Damaged structure) ✓ Shearography speckle testing (Damaged structure) ✓ 4-point flexure test
02	Plate	$[0/15/-15/0/15/-15]_s$	✓ Dynamic testing (Intact structure) ✓ Impact loading (Drop test) ✓ Dynamic testing (Damaged structure) ✓ Shearography speckle testing (Damaged structure) ✓ 4-point flexure test
03	Plate	$[45/-45/0/90/45/-45/0/90]_s$	✓ Dynamic testing (Intact structure) ✓ Impact loading (Drop test) ✓ Dynamic testing (Damaged structure) ✓ 4-point flexure test
04	Cylinder	$[90/60/-60/90/60/-60/90]_S$	✓ Dynamic testing (Intact structure) ✓ Impact loading (Drop test) ✓ Dynamic testing (Damaged structure) ✓ Shearography speckle testing (Damaged structure)
05	Cylinder	$[90/30/-30/90/30/-30/90]_S$	✓ Dynamic testing (Intact structure) ✓ Impact loading (Drop test) ✓ Dynamic testing (Damaged structure) ✓ Shearography speckle testing (Damaged structure)
06	Cylinder	$[90/30/-60/60/-60/30/-30]_S$	✓ Dynamic testing (Intact structure) ✓ Impact loading (Drop test) ✓ Dynamic testing (Damaged structure) ✓ Shearography speckle testing (Damaged structure)

It is import to notice that the composite specimens, ID 03, were made of glass fibre and epoxy resin. Two different types of glass fibre were used, a bidirectional textile (BD) [WR-83] of 83 gr/m^2, and unidirectional textile (UD) [WRU-140] of 140 gr/m^2 supplied by Texiglass. The polymeric matrix used to produce both composites was an epoxy resin supplied by ARALDITE composed of resin [1564 BR (85% m/m)] and hardener [REN HY 150 BR (15% m/m)]. The use of this material is because there are aircraft regions/structures manufactured by

unidirectional and bidirectional fibres. The glass fibre reinforced plastic specimens were manufactured and mechanically tested in the Aeronautical Structure Laboratory (LEA) at São Carlos School of Engineering of University of São Paulo (EESC-USP). Both glass fibre composites (UD and BD) were produced by resin infusion (RI). Firstly, dry fibres were laid-up over a flat glass mould, according to the stacking sequence. After careful mixture of both resin components, according to the referred proportions, this was poured and spread over the fibres. Then, the vacuum bag was closed with the aid of a tape. The specimen for the impact/bending tests were cut from the produced laminate plates. Their dimensions (width of 100 mm and length of 150 mm) are according to ASTM D 7136 Standard. Figure 2-6 shows the resin infusion process under vacuum.

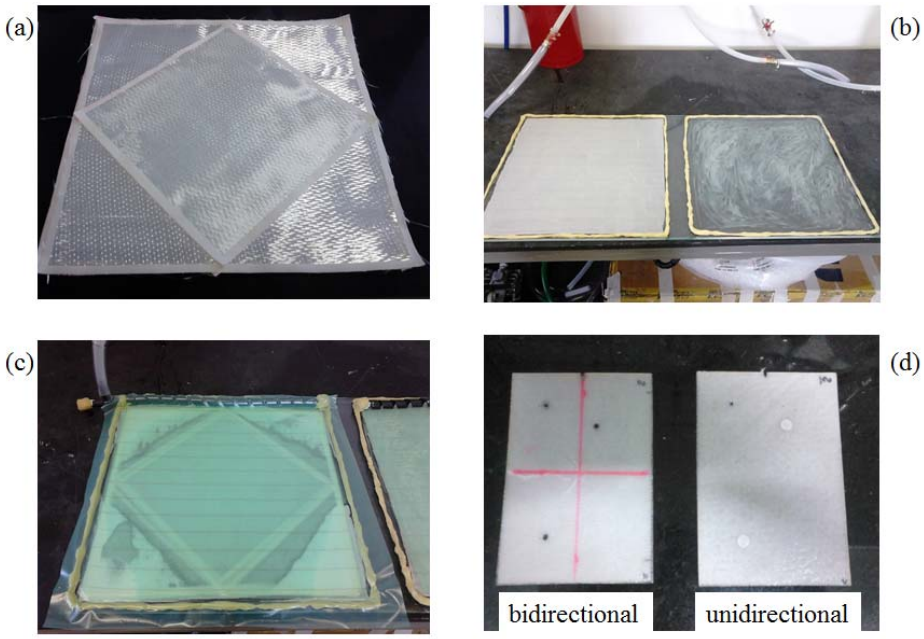

Figure 2-6. Vacuum Infusion Processing (a) Cut and preparation of the composite layup, (b) Vacuum bag, (c) Vacuum bag and resin drive, (d) Composite specimens

On the other hand, the specimens ID (01, 02, 04, 05 and 06) were made of carbon fibre and epoxy resin and they have been manufactured by using a filament winding process with a parallelepiped shape mandrel, which allows the plate winding due to two larger faces. In fact, laminate plates and cylinders can be obtained by this process. After that, the laminates are cured in a controlled oven. Depending on the stacking sequence of the laminate, it is possible to obtain almost flat plates with a single curvature. As commented previously, the manufacturing processes described above have been carried out by the Brazilian Navy Technology Centre in

São Paulo (CTM-SP). Due to an agreement between Brazilian Navy Technology Centre in São Paulo (CTM-SP) and Aeronautic Structural Group (University of Sao Paulo), all information about the manufacturing processes and material is classified. Therefore, the elastic properties and strength values cannot be shown in this work. In order to aid the readers for understanding the mechanical behaviour of composite material manufactured by CTM-SP (see Tab. 2-1), it is possible to mention that the CTM's material is similar (elastic and strength values) to the composite material investigated by Ribeiro (2013a) and Tita (2003) during their PhD Thesis. The specimens manufactured and studied by Tita (2003) were made from prepreg M10 from Hexcel^{TM}, which are pre-impregnated unidirectional carbon fibres by epoxy resin, and the fibre volume ratio of the laminates was equal to 63%. The elastic properties and strength values are shown either in Table 2-2 or can be found in Tita (2003) and Tita *et al.* (2008).

Table 2-2. Elastic properties and strength values (Tita, 2003)

Elastic Properties	
E_{11}	127 GPa
$E_{22} = E_{33}$	10 GPa
$G_{12} = G_{13}$	5.44 GPa
G_{23}	3.05 GPa
$\upsilon_{12} = \upsilon_{13}$	0.34
υ_{23}	0.306
ρ	1580 kg/m^3
Strength Values	
X_T	1400 MPa
X_C	930 MPa
Y_T	47 MPa
Y_C	130 MPa
$S_{12} = S_{13}$	53 MPa
S_{23}	89 MPa
Fibre Volume Fraction	
V_f	60%

2.3. Composite Specimens

The methodology is carried out by using data from experiments and numerical simulations performed in different types of specimens. The analyses were performed on composite plates made of carbon-epoxy (Tab. 2-3 and Fig. 2-7) and glass-epoxy (Tab. 2-4 and Fig. 2-8) as well as composite cylinders made of carbon-epoxy (Tab. 2-5 and Fig. 2-9). The Tab. 2-3 is related to the ID 01 and ID 02 of the Tab. 2-1. The Tab. 2-4 is related to the ID 03 of the Tab. 2-1. And, the Tab. 2-5 is related to the ID 04 (Type A), ID 05 (Type B) and ID 06 (Type C) of the Tab. 2-1. The carbon fibre composite plates are made of eight layers, plates 1-8, and twelve layers, plates 9-16 (*cf.,* Tab. 2.3). The glass fibre composite plates are made of sixteen layers with two different types of textile: unidirectional (UD) and bidirectional (BD) (*cf.,* Tab 2-4). The carbon fibre composite cylinders are made of fourteen layers with three different stacking sequences: A, B and C (*cf.,* Tab. 2-5). The tables list the identification code, damage type, dimensions, as well as the stacking sequence of the specimens.

Table 2-3. Plate specimens made of carbon fibre and epoxy resin

Plate	*Damage*	*Length [mm]*	*Width [mm]*	*Thickness [mm]*	*Stacking sequence*
P01$_{CF}$	Impact	305.00	245	2.247	$[0]_8$
P02$_{CF}$	Hole	305.39	244.86	2.245	
P03$_{CF}$	Impact	305.39	244.71	2.257	
P04$_{CF}$	Impact	305.00	245	2.246	
P05$_{CF}$	Impact	304.9	245.67	2.207	
P06$_{CF}$	Impact	304.94	246.12	2.218	
P07$_{CF}$	-	305.30	245.79	2.208	
P08$_{CF}$	-	303.84	245.88	2.212	
P09$_{CF}$	Impact	306.64	247.45	3.331	$[0/15/-15/0/15/-15]_s$
P10$_{CF}$	Impact	305.52	246.19	3.336	
P11$_{CF}$	Impact	305.45	245.21	3.493	
P12$_{CF}$	Impact	305.82	243.55	3.468	
P13$_{CF}$	-	306.62	247.13	3.370	
P14$_{CF}$	-	304.14	245.21	3.333	

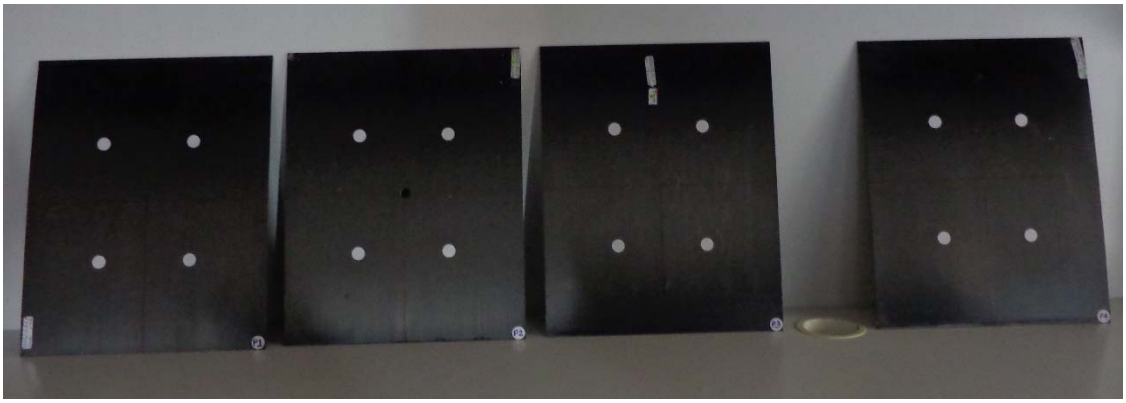

Figure 2-7. Carbon fibre composite plate specimens

Table 2-4. Plate specimens made of glass fibre and epoxy resin

Plate	*Damage*	*Length [mm]*	*Width [mm]*	*Thickness [mm]*	*Stacking sequence*
P01$_{GF}$-UD	Impact	155.0	102.5	1.7	
P02$_{GF}$-UD	Impact	151.0	100.0	1.7	
P03$_{GF}$-UD	Impact	152.0	99.0	1.7	
P04$_{GF}$-UD	-	152.0	103.5	1.7	
P05$_{GF}$-UD		153.0	101.0	1.7	$[45/-45/0/90/45/-45/0/90]_s$
P06$_{GF}$-BD	Impact	150.0	101.6	1.6	
P07$_{GF}$-BD	Impact	149.0	101.9	1.6	
P08$_{GF}$-BD	Impact	149.0	98.8	1.6	
P09$_{GF}$-BD	-	149.0	99.0	1.6	
P10$_{GF}$-BD		150.0	101.5	1.6	

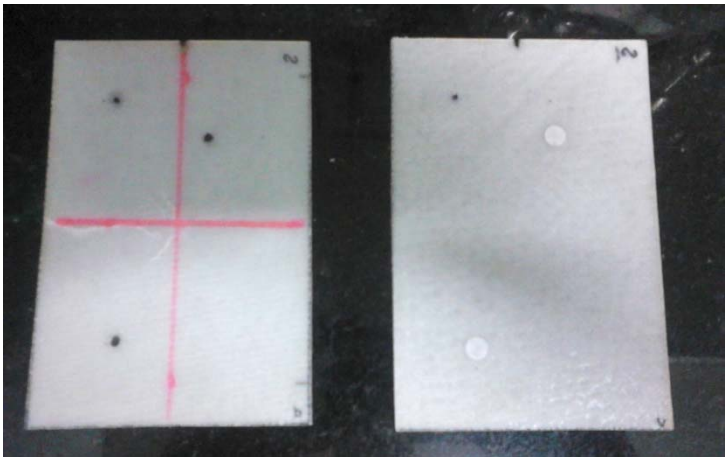

Figure 2-8. Glass fibre composite plate specimens

Table 2-5. Cylinder specimens made of carbon fibre and epoxy resin

Cylinder	*Damage*	*Length [mm]*	*Diameter [mm]*	*Thickness [mm]*	*Stacking sequence*
C01$_{CF}$-A	-	145.00	163.7	3.49	$[90/60/-60/90/60/-60/90]_s$
C02$_{CF}$-A	Impact	145.00	163.7	3.49	
C03$_{CF}$-A	Impact	145.00	163.7	3.49	
C04$_{CF}$-A	Impact	145.00	163.7	3.49	
C05$_{CF}$-A	Impact	145.00	163.7	3.49	
C06$_{CF}$-B	-	145.00	163.7	3.25	$[90/30/-30/90/30/-30/90]_s$
C07$_{CF}$-B	Impact	145.00	163.7	3.25	
C08$_{CF}$-B	Impact	145.00	163.7	3.25	
C09$_{CF}$-B	Impact	145.00	163.7	3.25	
C10$_{CF}$-B	Impact	145.00	163.7	3.25	
C11$_{CF}$-C	-	145.00	163.7	3.54	$[90/30/-60/60/-60/30/-30]_s$
C12$_{CF}$-C	Impact	145.00	163.7	3.54	
C13$_{CF}$-C	Impact	145.00	163.7	3.54	
C14$_{CF}$-C	Impact	145.00	163.7	3.54	
C15$_{CF}$-C	Impact	145.00	163.7	3.54	

Figure 2-9. Carbon fibre composite cylinder specimen

Due to the fact that the carbon fibre composite plates are made by filament winding process with stacking sequence $[0]_8$, it can be observed a small curvature in the plates. In order

to simulate better the experimental analyses, it was developed computational models with geometry obtained from 3D Coordinate Measurement System applied on real plates. For this purpose, ATOS Compact Scan machine was used. This machine guarantees rapid evaluation of complete and complex surfaces of components, and provides 3-D coordinates of surface points, full surface deviations to CAD data, inspection sections and complete measurement reports by using optical measurements. In Fig. 2-10 and Tab. 2.6, it is possible to observe the geometry determined by using this technique. Hence, there is slight evidence that C_1 and C_2 (*cf.* Table 3.2) will be different in the computational models, and they influence a lot in the modal analyses as it will be shown in the next chapters.

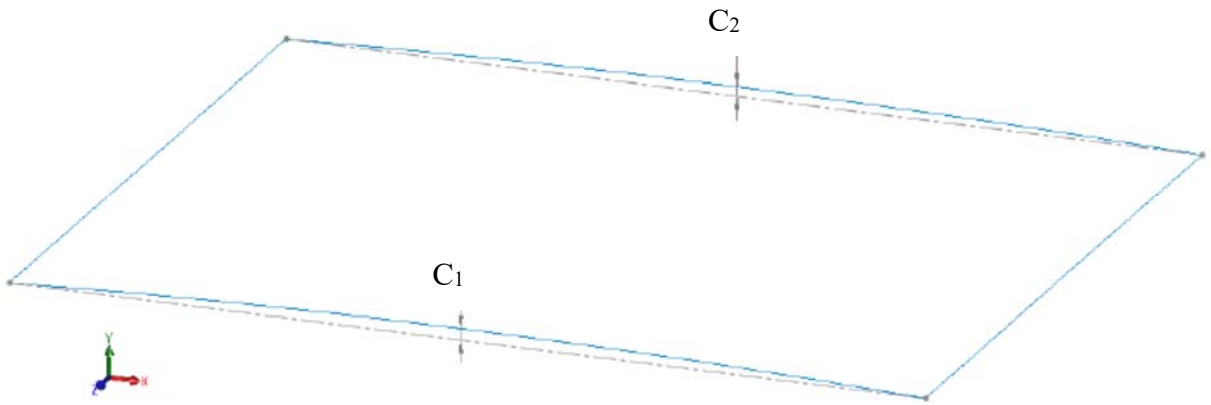

Figure 2-10. Geometry with curvature effects

Table 2-6. Values of C_1 and C_2 given by ATOS compact scan machine used in the computational models

Plate	C_1 [mm]	C_2 [mm]
P01$_{CF}$	3.825	3.182
P02$_{CF}$	4.269	4.008
P03$_{CF}$	4.557	4.180
P04$_{CF}$	3.937	3.705
P05$_{CF}$	3.940	3.721
P06$_{CF}$	4.165	3.200
P07$_{CF}$	4.060	4.225
P08$_{CF}$	4.385	4.643

2.4. Damage Model

The damage model is used to predict the failure/damage caused by the impact loading on the composite specimens, which is quantified on a meso-scale. The equations of the model were written for a homogenised lamina, which is considered to be an orthotropic material. Three material directions are specified: direction 1 (aligned the fibres); direction 2 (normal to the fibres and in the ply plane) and direction 3 (normal to the ply plane 1-2). The behaviour of the composite laminated structures depends on the behaviour of each homogenized lamina, including the damage mechanisms of the fibres and the matrix (epoxy resin). These damage mechanisms are represented by mathematical equations based on experimental observations performed by Ribeiro *et al.* (2012a, 2013b). The fundamentals of the damage model can be found at Ribeiro's PhD thesis (Ribeiro, 2013a). The equations of the damage model shown in the Table 2-6 were implemented as a user material subroutine for implicit simulations (UMAT) in FORTRAN language. The subroutine was then linked to the commercial FE code (ABAQUS^{TM}). The same symbols and notations shown at Ribeiro *et al.* (2013b) will be used in this work. For example, the parameter *d* is the damage variable related to stress.

Table 2-7. Material model summary (Ribeiro *et al*., 2013b)

Failure Criteria	Type of Failure	Degradation Law
$\frac{\sigma_{11}}{X_T} \geq 1$	Fibre Tension	$E_{11} = 0$
$\frac{\lvert\sigma_{11}\rvert}{X_{C_0}} \geq 1$	Fibre Compression	$E_{11} = \frac{X_{C_0}}{\lvert\varepsilon_{11}\rvert}\left(1 - f\left(\varepsilon_{11}\right)\right) + f\left(\varepsilon_{11}\right) E_{11_0}$
$f \geq 0$	Matrix Tension	$d_2 = A(\theta) Y_2 + B(\theta)$
$f \geq 0$	Matrix Compression	$E_{22} = \frac{\sigma_{22y}}{\lvert\varepsilon_{22}\rvert}\left(1 - f\left(\varepsilon_{22}\right)\right) + f\left(\varepsilon_{22}\right) E_{22_0}$
$f \geq 0$	Shear	$d_6 = C(\theta) Y_6 + D(\theta)$

The damage onset of composite laminates can be identified as the deterioration of material properties (Kachanov, 1986). The elastic properties deterioration can be evaluated by quasi-static cyclic tensile and/or compressive tests. In this work, the damage onset surface f (in Table 2-6) is described by Eq. (2.1), where S_{12y} is the shear stress linear elastic limit and σ_{220} is the transverse linear elastic limit obtained from experimental analyses.

$$f = \sqrt{\sigma_{22}^2 + \tau_{12}^2} - \left[-S_{12y} + \frac{2S_{12y}}{1 + \left(\frac{|\sigma_{22}|}{\sigma_{22_0}} \right)^3} \right] \tag{2.1}$$

Ply brittle fracture is expressed by the critical value of the strain energy, E_{DC}, obtained by experimental tests, then d_2 is equal to 1 (one) and, d_6 is equal to 1 (one), also. Another important aspect of the applied damage model consists of the adjustments for the Poisson coefficients to take into account the damage effect. Using the Continuum Damage Mechanics (CDM) formulation (Matzenmiller *et al.*, 1995), the compliance tensor is given by Eq. (2.2), where $K = (1 - (1 - d_1)(1 - d_2)\nu_{12}\nu_{21})$.

$$D = \frac{1}{K} \begin{bmatrix} (1-d_1)E_{11} & (1-d_1)(1-d_2)\nu_{21}E_{22} & 0 \\ (1-d_1)(1-d_2)\nu_{12}E_{11} & (1-d_2)E_{22} & 0 \\ 0 & 0 & K(1-d_6)G_{12} \end{bmatrix} \tag{2.2}$$

The material model does not include material self-healing behaviour as the damage parameters d_1, d_2 and d_6 never decrease from their maximum values obtained during the calculation process. More details about the damage model can be found in Ribeiro *et al.* (2012a, 2013a, 2013b).

2.5. Piezoelectric Sensor

SHM systems can be developed using different types of sensors. Based on the knowledge of the present authors, smart composite materials present great potential for applications in aerospace industry as sensors and/or actuators for noise (Fuller and Von Flotow, 1995), vibration (Giurgiutiu, 2000), precision position control (Main *et al.*, 1995), energy harvesting (Erturk *et al.*, 2010), and Structural Health Monitoring (Raghavan and Cesnik, 2007). Regarding these applications, there are different types of smart composites, such as Active Fibre Composite – AFC (Hagood and Bent, 1993) and Macro Fibre Composite – MFC^{TM} (Wilkie *et al.*, 2000). These smart composites are made of piezoelectric materials (also denoted as PZT), which have the property of converting electrical energy into mechanical energy, and vice-versa. Either AFC or MFC consist on fibres of piezoelectric materials, which are embedded in a

polymer matrix (conductive or not) polarised by electrodes. Therefore, these smart composite materials show a high potential for application in engineering problems involving structural composite laminates, because they can be integrated in the structure as a single ply or reinforcements. However, this work only considers external applications of piezoelectric sensors (*i.e.* on the composite structure), not embedded. This strategy was used because outer plies exhibit the highest strain values under flexural loads created during impact or vibration tests, and it is very complicated to manufacture composite specimens with embedded active fibres. A detailed description of PZT sensors and the identification of their properties are necessary, because the manufactures data sheet do not provide all the information and some values are not accurate.

2.5.1. Macro Fibre Composite (MFC) Sensor

The composite structures considered in this work employ M2814-P1 type MFC manufactured by Smart Material Inc., which use the 33 mode of piezoelectricity (Fig. 2-11(a)). This sensor was chosen, because offer high performance, flexibility (mainly for structures under flexural loads like aircraft panels) and reliability in a cost competitive device. Moreover, because MFC is more sensitive than AFC sensors, they are easy to assembly on the structure and easy to use ("plug and play"). In order to obtain more accurate computational models, mainly in terms of piezoelectric transducer properties, a similar MFC (M8507-P1) observed by Bilgen (2010) was used. Fig. 2-11 shows the piezoelectric fibres and the interdigitated electrodes by using a microscope.

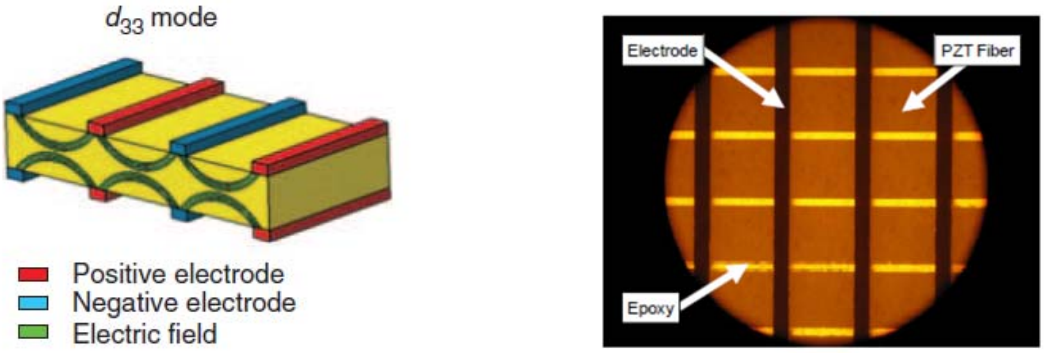

(a) (b)

Figure 2-11. (a) Electric field distribution for d_{33} mode electrode configurations (Deraemaeker *et al.*, 2009), (b) Digital photograph of the planar view of a MFC M8507-P1 by using a microscope (Bilgen, 2010)

2.5.2. Geometric Properties of MFC M2814-P1

Figure 2-12 shows the MFC with zoom for critical areas (Bilgen, 2010). Figure 2-12(a) presents the top view of the whole transducer. Figure 2-12(b) is a microscope image of the area where the piezoceramic fibres (running horizontal to the page) end. Figure 2-12(c) shows the area with uniform fibre and electrode (running vertical to the page) distribution. Finally, Figure 2-12(d) presents the side transition area where electrode bus connects to (every other) interdigitated electrodes.

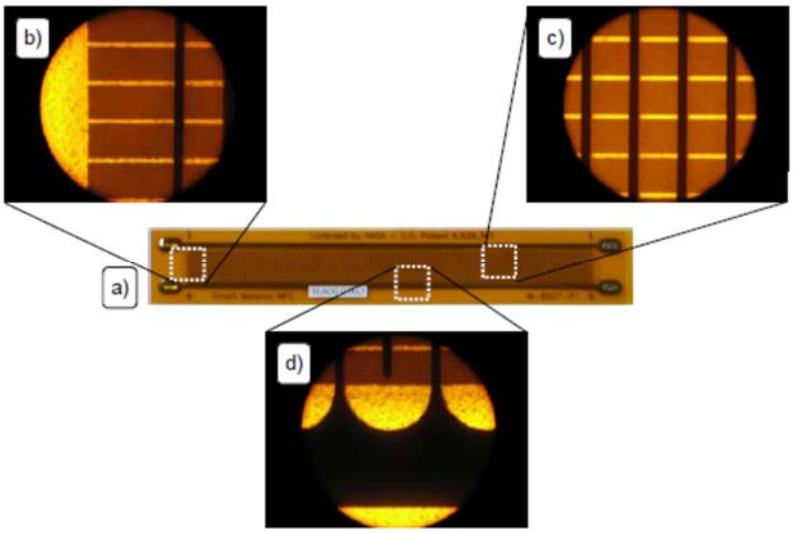

Figure 2-12. Digital photograph of the MFC M8507-P1 type device (a) top view, (b) piezoceramic fibre ends, (c) uniform active area and (d) electrode bus connection to the interdigitated electrodes (Bilgen, 2010)

According to Bilgen (2010), the thickness and width of each piezoceramic fibre are approximately 180 μm and 355 μm respectively, and each epoxy layer between the fibres has a width of 51.25 μm. The total thickness of the active region is around 305 μm, and therefore, each of the top and bottom Kapton layers in the active region is about 60 μm thick.

Based on the data obtained by Bilgen (2010) and the measured values of the MFC M2814-P1 type, Tab. 2-8 presents the geometric properties of the piezoelectric device. Considering the total active width is approximately 14.45 mm, each sample has approximately 35 piezoceramic fibres, resulting in a total piezoceramic width (b_{pt}) of 12.425 mm. The width of each electrode in the direction of length (u_e) is 97 μm and the spacing between the electrodes (u_0) is 410 μm. Therefore, the number of electrode pairs over the beam length is Ne ≅ 24 (~ 48 electrode fingers). The specific MFC model, used throughout this thesis, has a total length of

37.65 mm and a total width of 19.95 mm. The active area is 0.305 mm thick. The inactive area (sides) is 0.142 mm thick. Table 2-8 presents the geometric properties of the MFC device. Some values could not be measured; hence reported values from the manufacturer and Bilgen (2010) are used. Figure 2-13 shows the carbon fibre composite plate with the mounted sensors and orientations.

Table 2-8. Geometric properties of MFC M2814-P1 type piezoelectric device (adapted from Bilgen, 2010)

Property	Value	Unit	Local Axis
Overall			
Length	37.65	mm	3
Width	20.05	mm	2
Thickness, active**	305.00	µm	1
Thickness, inactive**	142.00	µm	y
Active Area			
Length*	28.00	mm	3
Width	14.45	mm	1
Piezoceramic Fibre			
Length*	28.00	mm	3
Width*	355.00	µm	1
Thickness*	180.00	µm	2
Spacing**	51.25	µm	1
Epoxy			
Length*	28.00	mm	3
Width**	51.25	µm	1
Thickness*	180.00	µm	2
Spacing**	355.00	µm	1
Electrodes			
Length**	7.30	mm	1
Width**	97.00	µm	3
Thickness	n/a	n/a	2
Spacing**	410.00	µm	3
Others			
Kapton Thickness**	60.00	µm	2
Number of Electrodes	48	n/a	n/a
Number of Piezo Fibbers	35	n/a	n/a

* Values reported by the manufacturer
** Values reported by Bilgen (2010)

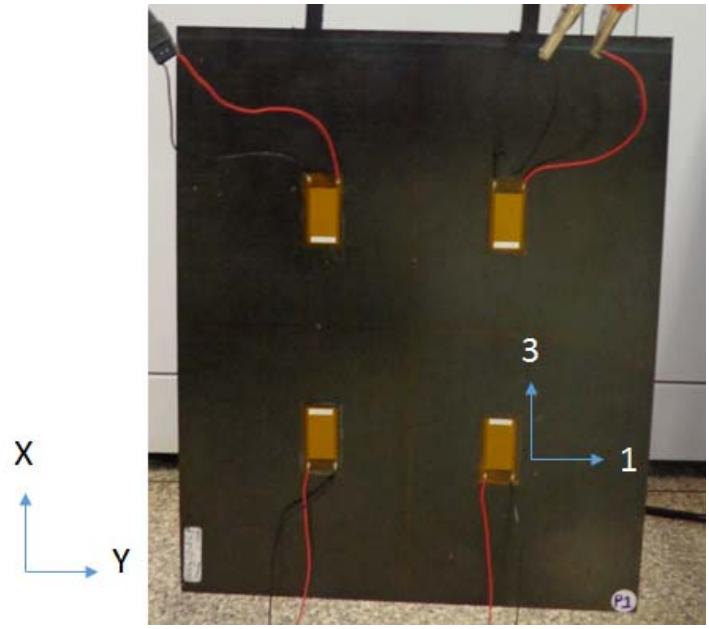

Figure 2-13. Carbon fibre composite specimen with the mounted sensors and configurations

2.5.3. Mechanical, Electrical and Piezoelectric Properties

The elastic and the dielectric behaviours are coupled in piezoelectric materials, where the mechanical stress and strain variables are related to the electric field and displacement variables. The coupling between mechanical and electric fields is obtained by piezoelectric coefficients. The constitutive equations of piezoelectric materials are assumed to be linear and can be written in the following form (adopting the Einstein summation convention):

$$\begin{aligned} T_{ij} &= c^{E}_{ijkl}\ S_{kl} - e_{kij}\ E_{k,} \\ D_{i} &= e_{ikl}\ S_{kl} + \varepsilon^{S}_{ik}\ E_{k,} \end{aligned} \tag{2.3}$$

where T_{ij} and S_{ij} denotes the second rank stress and strain tensors, respectively, E_k and D_i are, respectively, the electric potential field and the electrical displacement vectors, c^{E}_{ijkl} denotes fourth-order elasticity tensor at constant electric field, e_{kij} is the third-order piezoelectric coupling tensor, and ε^{S}_{ik} is the second-order dielectric tensor at constant strain field. Equation (2.3) can be written as a constitutive effective matrix format by Voigt's notation as:

$$\begin{Bmatrix} \{T\} \\ \{D\} \end{Bmatrix} = \begin{bmatrix} [c]^{E} & -[e] \\ [e]^{t} & [\varepsilon]^{S} \end{bmatrix} \begin{Bmatrix} \{S\} \\ \{E\} \end{Bmatrix}, \tag{2.4}$$

where the superscript *t* indicates transpose matrix, *E* constant electric field and *S* constant strain field. For an orthotropic (direction 3 aligned to the piezoelectric fibres) and transversely isotropic piezoelectric solid, the stiffness, the piezoelectric, and the dielectric matrices present 11 (eleven) independent coefficients. Consequently, the constitutive relations in equation (2.4) can be written in terms of the following expanded matrix form:

$$\begin{Bmatrix} T_{11} \\ T_{22} \\ T_{33} \\ T_{12} \\ T_{23} \\ T_{31} \\ D_1 \\ D_2 \\ D_3 \end{Bmatrix} = \begin{bmatrix} c_{11}^{E} & c_{12}^{E} & c_{13}^{E} & 0 & 0 & 0 & 0 & 0 & -e_{13} \\ c_{13}^{E} & c_{11}^{E} & c_{13}^{E} & 0 & 0 & 0 & 0 & 0 & -e_{13} \\ c_{13}^{E} & c_{13}^{E} & c_{33}^{E} & 0 & 0 & 0 & 0 & 0 & -e_{33} \\ 0 & 0 & 0 & c_{66}^{E} & 0 & 0 & 0 & 0 & 0 \\ 0 & 0 & 0 & 0 & c_{44}^{E} & 0 & 0 & -e_{15} & 0 \\ 0 & 0 & 0 & 0 & 0 & c_{44}^{E} & -e_{15} & 0 & 0 \\ 0 & 0 & 0 & 0 & 0 & e_{15} & \varepsilon_{11}^{S} & 0 & 0 \\ 0 & 0 & 0 & 0 & e_{15} & 0 & 0 & \varepsilon_{11}^{S} & 0 \\ e_{13} & e_{13} & e_{33} & 0 & 0 & 0 & 0 & 0 & \varepsilon_{33}^{S} \end{bmatrix} \begin{Bmatrix} S_{11} \\ S_{22} \\ S_{33} \\ S_{12} \\ S_{23} \\ S_{31} \\ E_1 \\ E_2 \\ E_3 \end{Bmatrix} \tag{2.5}$$

The smart composites effective properties can be defined by the average fields in the same form as equation (2.5), which can be written in a compact matrix form:

$$\begin{Bmatrix} \{\bar{T}\} \\ \{\bar{D}\} \end{Bmatrix} = \begin{bmatrix} [c]_{eff}^{E} & -[e]_{eff} \\ [e]_{eff}^{T} & [\varepsilon]_{eff}^{S} \end{bmatrix} \begin{Bmatrix} \{\bar{S}\} \\ \{\bar{E}\} \end{Bmatrix} \tag{2.6}$$

where the subscript *eff* denotes effective property.

Considering the procedure developed by Medeiros *et al*. (2012, 2015a), Rodríguez-Ramos *et al.* (2013) and Tita *et al.* (2015) and knowing the material properties of each constituent and through combinations of loads and appropriate boundary conditions, it is possible to obtain the constitutive matrix parameters. Thus, a Finite Element model of the periodic structure with perfect fibre–matrix interface, which have fibres aligned to the axis 3

(direction z), is developed. Hence, the RVE of three-dimensional (3D) piezoelectric unit cell with suitable BCs and loads is solved using Finite Element Analysis (FEA). After that, the Theorem of Average has been applied to calculate the effective properties of the piezoelectric composite, where the properties of the homogenized model are calculated from the average properties of each constituent of the piezoelectric composite material. Thus, in this approach, it is assumed that the average mechanical properties of a unit cell is equal to the average properties of the particular composite. Figure 2-14 shows the representative volume element (RVE) used in this work, which consists of fibre, epoxy, kapton and electrodes (copper). It is very important to highlight that this particular 3D FE model is developed in an isolate way in order only to determine the effective properties of the piezoelectric sensor used in this work. Once the effective properties are determined, those ones will be used in the 2D FE models dedicated for the modal analyses of the undamaged and damaged composite laminates, which are monitored by PZT sensors.

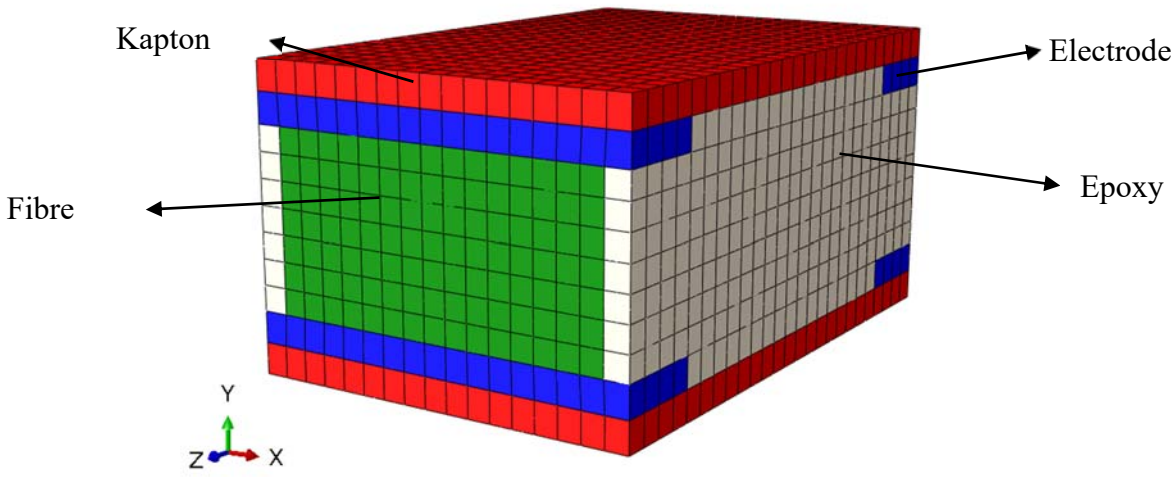

Figure 2-14. Representative volume element (RVE) used for homogenisation of the piezoelectric properties of the sensors.

For meshing the unit cell, three-dimensional multi-field 20-node elements are used. These quadratic piezoelectric brick elements (C3D20E – Abaqus^{TM} nomenclature) have three mechanical displacements and an additional electric potential degrees of freedom (DOFs). It is thus possible to perform fully coupled electromechanical analyses. The simplified set of constitutive equations (*cf.,* Eq. (2.5)) with prescribed boundary conditions allows for the evaluation of the effective material properties. Therefore, to evaluate all eleven effective coefficients, only six analyses are necessary. Table 2-9 summarizes boundary conditions and loads used in this work (Tita *et al.*, 2015).

Table 2-9. Loads and boundary conditions (BCs). (Tita *et al.*, 2015).

	Equation[(a)]	Prescribed displacement field [m]	Prescribed force field [N]	Prescribed electric potential field [V]	Displacement BCs [m]	Electric Potential BCs [V]
1st line	$c_{13}^{eff} = \frac{\bar{T}_{11}}{\bar{S}_{33}}$	positive u_Z surface Z^+	-	-	Zero normal displacements surfaces X^+, X^-, Y^+, Y^-, Z^-	Zero all surfaces
3rd line	$c_{33}^{eff} = \frac{\bar{T}_{33}}{\bar{S}_{33}}$				$S_{11} = S_{22} = S_{12} = S_{23} = S_{31} = 0$	$E_1 = E_2 = E_3 = 0$
1st line	$e_{13}^{eff} = \frac{\bar{T}_{11}}{\bar{E}_3}$	-	-	positive voltage surface Z^+	Zero normal displacements all surfaces	Zero surface Z^-
3rd line	$e_{33}^{eff} = -\frac{\bar{T}_{33}}{\bar{E}_3}$				$S_{11} = S_{22} = S_{33} = S_{12} = S_{23} = S_{31} = 0$	
9th line	$\varepsilon_{33}^{eff} = \frac{\bar{D}_3}{\bar{E}_3}$					
1st line	$c_{11}^{eff} = \frac{\bar{T}_{11}}{\bar{S}_{11}}$	positive u_X surface X^+	-	-	Zero normal displacements surfaces X^-, Y^+, Y^-, Z^+, Z^-	Zero all surfaces
2nd line	$c_{12}^{eff} = \frac{\bar{T}_{22}}{\bar{S}_{11}}$				$S_{22} = S_{33} = S_{12} = S_{23} = S_{31} = 0$	$E_1 = E_2 = E_3 = 0$
7th line	$\varepsilon_{11}^{eff} = \frac{\bar{D}_1}{\bar{E}_1}$	-	-	positive voltage surface X^+	Zero normal displacements all surfaces	Zero surface X^-
					$S_{11} = S_{22} = S_{33} = S_{12} = S_{23} = S_{31} = 0$	
4th line	$c_{66}^{eff} = \frac{\bar{T}_{12}}{\bar{S}_{12}}$	-	$+F_y$ and $-F_y$ surfaces X^+ and X^- $+F_x$ and $-F_x$ surfaces Y^+ and Y^-	-	Zero y-displacements faces X^+, X^- Zero x-displacements surface Y^- Uniform x-displacements surface Y^+	Zero all surfaces
5th line	$e_{15}^{eff} = \frac{\left(-\bar{E}_2 \cdot \varepsilon_{11} + \bar{D}_2\right)}{\bar{S}_{23}}$	-	$+F_y$ and $-F_y$ surfaces Z^+ and Z^- $+F_z$ and $-F_z$ surfaces Y^+ and Y^-	-	Zero y-displacements surfaces Z^+, Z^- Zero z-displacements surface Y^- Uniform z-displacements surface Y^+	Zero surfaces X^+, X^-, Y^+, Y^-
8th line	$c_{44}^{eff} = \frac{\left(\bar{T}_{23} + \bar{E}_2 \cdot e_{15}^{eff}\right)}{\bar{S}_{23}}$					

[(a)]: Lines number refer to equation (2.5).

More accurate results are obtained when the load is applied in fibre longitudinal direction, denoted here as *z*-direction (or direction 3), as well as *x*-direction and *y*-direction, which are aligned to the directions 1 and 2, respectively. Table 2-10 shows the effective materials properties calculated by using the procedure developed by Medeiros *et al*. (2012, 2015a), Rodríguez-Ramos *et al.* (2013) and Tita *et al.* (2015).

Table 2-10. Effective material properties used in this work for PZT sensors.

Effective coefficient	Value	Unit
c_{11}^{eff}	14.40	[GPa]
c_{12}^{eff}	2.09	[GPa]
c_{13}^{eff}	4.32	[GPa]
c_{33}^{eff}	33.90	[GPa]
c_{44}^{eff}	1.58	[GPa]
c_{66}^{eff}	1.61	[GPa]
e_{13}^{eff}	-0.1768	[C/m^2]
e_{15}^{eff}	0.0044	[C/m^2]
e_{33}^{eff}	12.3696	[C/m^2]
ε_{11}^{eff}	0.455	[nF/m]
ε_{33}^{eff}	9.08	[nF/m]
ρ	5440	[kg/m^3]
FVF - Fibre	51.52	%
FVE - Epoxy	15.50	%
FVK - Kapton	20.49	%
FVC - Copper	6.58	%
*** considering c^E and ε^S**		

2.6. Partial Conclusions

This chapter presents the research methodology to be applied in this work with all steps, and mainly the explanation why each step is used and/or required. First, vibration based method is used to identify and global locate the damage. Shearography speckle is used to local locate and provide the extent of damage. Flexure after impact is used instead of the compression after impact to determine the residual strength of the structures. The matrix of test was presented for all structures and materials used. Epoxy resin reinforced by carbon and glass fibre was employed due to broad application in aeronautic structures. Carbon fibre-epoxy plates and cylinders were manufactured by filament wound process, and glass fibre-epoxy plates were manufactured by resin infusion. The damage model was presented, which is implemented as a user material subroutine for implicit simulations (UMAT/Abaqus). Finally, it was presented the procedure for determining the effective properties of the MFC sensors.

CHAPTER 3

Damage Identification and Global Location

The basic concept of the vibration based damage identification methods is that the dynamic behaviour of a structure can change if damage occurs. Damage in a structure can alter the structural integrity, and therefore, the physical properties like stiffness, mass and/or damping may change. The dynamic behaviour of a structure is a function of these physical properties and will, therefore, directly be affected by the damage. The dynamic behaviour can be described in terms of time, frequency and modal domain parameters. The changes in these parameters (or properties derived from these parameters) are used as indicators of damage. Hence, this chapter has two main objectives. The first one is to provide an overview of the structural vibration based damage identification methods. For this purpose, a fundamental description of the structural vibration based damage identification problem is given, followed by a short literature overview of the damage features, which are commonly addressed. The second objective is to create a damage identification method for detection and global location of the damage in composite structures. To aid in this process, two basic principles are discussed, namely the effect of the potential damage case on the dynamic behaviour, and the consequences involved with the information reduction in the signal processing. Modal properties (in this work: mode shapes and natural frequencies) from the structural dynamic output response are obtained. Also, in this chapter, experimental and computational results are presented for the application of modal analysis techniques applied to composite specimens with and without damage. The excitation of the structures is performed using an impact hammer and, for measuring the output data, accelerometers as well as piezoelectric sensors. Finite element models are developed by shell elements, and numerical results are compared to experimental data, showing good correlation for the response of the specimens in some specific frequency range. Finally, FRFs are analysed using suitable metrics, including a new one, which are compared in terms of their capability for damage identification. The experimental and numerical results show that the vibration-based damage methods combined to the metrics can be used in Structural Health Monitoring (SHM) systems to identify the damage in the structure.

3.1. Review of Vibration Based Methods

Structural damage can be defined as a permanent change in the mechanical state of a material medium and it may affect the structural performance. Common sources of damage in structural components include micro-structural defects (dislocations, voids, inclusions), corrosion (loss of material), residual stress, cracking (fatigue, matrix, ply), fastening fault (weld crack, bold preload, broken rivet), adhesive fault (de-bonding, delamination, separation) and instabilities (*e.g.* buckling) (Adams, 2007). This set of damage induces different behaviours of the material, thereby increasing the risk of unpredicted structural failure causing catastrophic, economic, and human life loss. Hence, in order to maintain the safety and reliability of the product, it is necessary to inspect periodically the structure. This is the reason why it is possible to find several non-destructive techniques (NDT) for the identification of damage in a structure (Fan and Qiao, 2011).

Successful damage detection and localisation in structures is essential for structural health monitoring and maintenance. As commented earlier, NDE/NDT, which can identify damage, may be used for this purpose. However, most of the non-destructive methods, such as ultrasonic methods, require the location of the damage and that location must be accessible. The methods, which are based on vibration responses, usually do not show these limitations. The basis of vibration response methods is that damage changes the dynamic behaviour of the structure. Damage in a structure can alter the structural integrity, and therefore, the physical properties like stiffness, mass and/or damping may change. The dynamic behaviour of a structure is a function of these physical properties and will, therefore, directly be affected by the damage. The dynamic behaviour can be described by time, frequency and modal domain parameters. The changes in these parameters (or properties derived from these parameters) are used as damage indicators.

Table 3-1 provides a more detailed comparison about the NDT techniques performances. The low frequency structural vibration and electromechanical impedance techniques primarily rely on standing wave patterns, while the higher frequency acoustic emission, acoustic-ultrasonic and ultrasonic testing utilise travelling wave characteristics. Methods of the former group provide data, which are relatively easy to interpret. More complex structures can be analysed via these methods, and a relatively large area can be explored in a single operation.

Table 3-1. An overview of the dynamics based non-destructive testing (NDT) technologies (Ooijevaar, 2014).

Technology	Frequency range [Hz]	Actuation approach	Sensitivity to damage	Ease of data interpretation	Applicability for SHM
Structural vibration and acoustics	10^0 - 10^4	Active / passive	■■□□□	■■■□□	■■■■□
Electro-mechanical impedance	10^3 - 10^5	Active	■■■□□	■■■□□	■■■■□
Acoustic emission	10^4 - 10^6	Passive	■■■■□	■■□□□	■■■□□
Acoustic-ultrasonic	10^4 - 10^6	Active	■■■■□	■□□□□	■■■■□
Ultrasonic testing	10^5 - 10^7	Active	■■■■■	■■□□□	■□□□□

Vibration-based structural health monitoring (SHM) and damage detection techniques have received much attention recently in the aeronautic engineering field (Liu and Nayak, 2012). A good SHM system can greatly increase the efficiency of structural maintenance, reduce maintenance cost and enhance the reliability of structures, as well. In addition, experimental methods for establishing dynamic characteristics of linear vibrating structures, such as matrix of impulse response functions, complex frequency response functions or modal characteristics (natural frequencies, modal damping, and mode shapes) are currently well established (McConnell and Varoto, 1995; Ewins, 2000). These characteristics depend upon some parameters: elastic constants; mass density; boundary conditions and geometric dimensions. Any change related to these parameters modifies the structural dynamic properties, such as natural frequencies, modal damping and/or mode shapes, i.e. these modifications may produce global changes in the structure response. Therefore, the approaches for structural health monitoring (SHM) can be classified as local and global monitoring. For example, non-destructive techniques are the most widely used methods for local SHM and, normally, methods, which are vibration-based schemes, are used for global SHM.

Due to the simple instrumentation and development of new powerful system identification techniques, SHM systems based on the changes in the vibration characteristics of the structure have gained an increasing worldwide attention in the last years. Important advances in this field have been discussed by Doebling *et al.* (1996); Salawu (1997); Doebling *et al.* (1998); Zou *et al.* (2000); Carden and Fanning (2004); Montalvão *et al.* (2006); Worden *et al.* (2008); Fan and Qiao (2011); Liu and Nayak (2012), who have shown comprehensive reviews on SHM systems.

Ooijevaar (2014) has categorised the vibration based methods according to their damage sensitive feature and statistical classifier, as schematically shown in Figure 3-1. The earliest studies on this subject report on the relation between natural frequency shift or modal damping

changes and structural damage. In addition, Ooijevaar (2014) has presented a comprehensive list of the damage features that are used in the literature and they are presented in Table 3-2. This work, uses the green boxes of Figure 3-1, *i.e.* the structural vibration technique, frequency response functions, natural frequencies and mode shapes damage feature, and frequency response function damage index as statistical classifier.

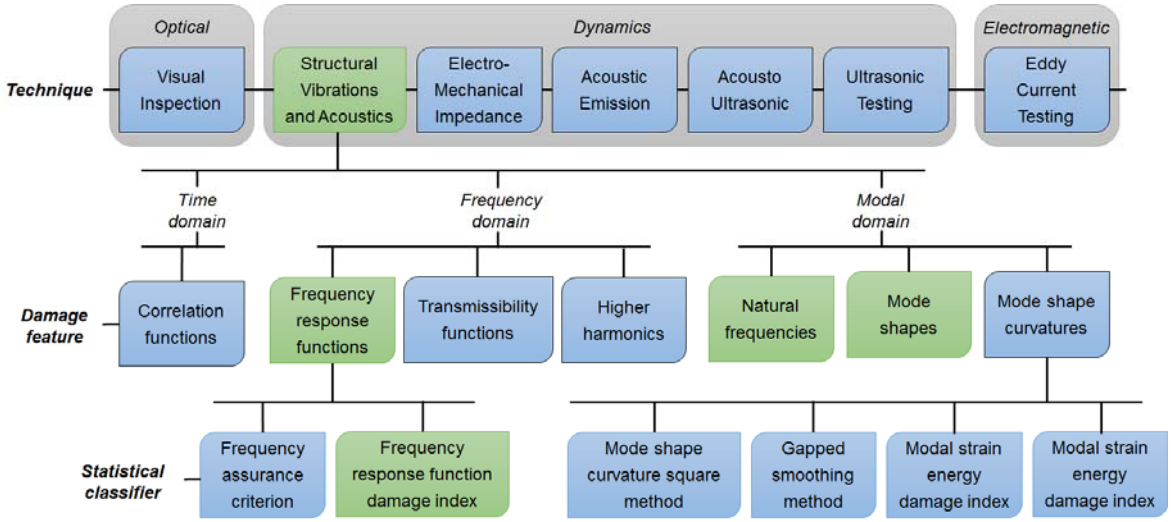

Figure 3-1. Schematic overview of the wide range of damage identification approaches (adapted from Ooijevaar, 2014)

Table 3-2. An overview of the vibration based damage features categorized according to the time, frequency and modal domain (Ooijevaar, 2014).

Time domain	Frequency domain	Modal domain

• Time response / waveform
• Statistical time series analysis:
  o Correlation functions (non-parametric)
  o Autoregressive models (parametric)
• Time-frequency response
	• Fourier / Power spectra
	• Frequency response function
	• Frequency response function curvature
	• Mechanical impedance
	• Transmissibility functions
	• Antiresonances
	• High harmonics (nonlinear)
	• Modulations (nonlinear)
		• Natural frequencies
		• Mode shape
		• Mode shape curvature
		• Modal damping
		• Dynamic stiffness
		• Dynamic flexibility
		• Updating methods

The first papers published in damage detection were based on natural frequencies variations between the undamaged and damaged structures (Adams *et al.*, 1975; Vandiver, 1977). Natural frequency-based methods use the FRF (Frequency Response Function) change as the basic feature for damage identification. However, as the natural frequencies and damping factors are global parameters, these methods were not capable of locating the damage. After

that, Pandey *et al.* (1991) investigated a parameter defined as curvature mode shapes, which consists on determining a possible candidate for identifying and locating damage in a structure. Other researchers, such as Sampaio *et al.* (1999) and Maia *et al.* (2003) also investigated the curvature mode shapes. Juneja *et al.* (1997) developed a damage detection measurement by using a limited instrumentation and by using the contrast maximisation to calculate the excitation forces, which create maximum differences in the response of the intact and damaged structure. To increase the reliability of the approach under modelling and measurement errors, the contrast maximisation approach is combined to an approach based on changes in frequency signature. The detectability of any particular damage with the proposed technique depends on the ratio of the magnitude of damage and the magnitude of errors in the measurements, as well as on how much the damage influences the measurements. Wang *et al.* (1997) formulated a new damage detection algorithm to use an original analytical model and FRF data measured before and after to damage for structural damage detection. Based on nonlinear perturbation equations of FRF data, an algorithm has been derived, which can be used to determine a damage vector, indicating both location and magnitude of damage. Thyagarajan *et al.* (1998) investigated the optimisation of Frequency Response Functions (FRFs) in order to diagnose damage using a minimum number of sensors.

Monaco *et al.* (2000) presented a formulation based on an experimental procedure to employ in problems of damage analysis of structural elements. The proposed method depends on the acquisition and comparison of Frequency Response Functions (FRFs) of the monitored structure before and after damage occurrence. Structural damages modify the dynamic behaviour of the structure and, consequently, using the FRFs, it is possible the calculation of a representative Damage Index (DI). Kessler *et al.* (2002) investigated the feasibility of modal evaluation techniques in detecting damage of composite structures by using SHM systems. The studied characteristics showed that these methods can detect various types of damage. Also, the authors discussed the precision in determining the damage location and the sensitivity to the damage density. Mickens *et al.* (2003) developed a vibration-based method of damage detection for monitoring ageing structures. The method intended to detect damage during operation of the vehicle before the occurrence of catastrophic failure. Furukawa *et al.* (2006) presented a statistical damage detection method, which takes in to account uncertainty in the FRFs, and which considers the effects of the measurement errors and does not assume any distribution functions. Kurata *et al.* (2010) proposed two types of error functions in order to estimate the error intrinsic to a hypothetical damage state. The first error function compares the modal

properties (*e.g.* modal frequency and mode shape) of the true and trial models. The second error function is based on the flexibility of the structure. The proposed model was verified numerically and, after that, through experimentation using an aluminium plate with a crack intentionally introduced near a welded stiffener element.

Ooijevaar *et al.* (2010) investigated experimentally 16-layer unidirectional carbon fibre PEEK reinforced plate structure with two stiffener sections. The authors investigated the dynamic response of an intact and a damaged plate using the Modal Strain Energy Damage Index algorithm in order to detect and localise impact defects. Salehi *et al.* (2010) presented a technique of damage detection based on real and imaginary parts of measured FRFs. The method uses intact and damaged state information of the structure. Hence, the need for an analytical model is eliminated. In addition, the authors used real and imaginary residual FRF shape signals in order to detect damage. Bandara *et al.* (2011) introduced a new damage index using principal component analysis (PCA). This index can detect damage of structures even if noise pollutes frequency response functions (FRFs). Elshafey *et al.* (2011) discussed the experimental applicability of the modified mode shape difference technique in damage identification and localisation. Lin *et al.* (2012) presented a damage location index (SubFRFDI) in order to detect the damage locations for civil structures under earthquake excitations using a novel substructure-based FRF approach. Reddy and Swarnamani (2012) showed the effectiveness using the frequency response function (FRF) curvature energy damage index. Also, the authors established the capability of the method to detect and to localise damage.

Medeiros *et al.* (2012) presented a case study about the usage of SHM metrics and techniques for detecting damage using numerical simulations (Finite Element Analysis) and experimental data (vibration tests) of an aluminium cantilever beam with piezoelectric sensors/actuators attached on the structure. The approach based on Frequency Response Function (FRF) was used. In addition, Ribeiro *et al.* (2012) and Medeiros *et al.* (2014a) presented an investigation about the damage effects on the structural response, considering filament wound composite tubes damaged by impact loading. The computational analyses were carried out using an impulse load, which excited the structure, and piezoelectric sensors, which measured the output data. The results showed that the application of vibration-based methods for detecting damage is feasible. Medeiros *et al.* (2013), Medeiros *et al.* (2014b) and Flor *et al.* (2015) investigated experimentally and numerically through the vibration-based method the changes of mechanical behaviour of a metal-composite bonded joint using piezoelectric sensor and accelerometers in order to monitor the damage in the joint.

Many non-destructive fault detection techniques have been developed over the past several years. Most are "local", requiring access to the vicinity of the suspected fault location, and are, furthermore, typically time consuming and costly. They are usually based upon radiography, eddy-current, acoustic, ultrasound, magnetic, and thermal field principles. In recent years, significant attention has been paid to fault detection via vibration based methods (Fassois and Sakellariou, 2006). These appear as particularly promising and offer a number of potential advantages, such as no requirement for visual inspection, "automation" capability, "global" coverage (in the sense of covering large areas of the structure), and capability of working at a "system level". Furthermore, they tend to be time effective and less expensive than the most alternatives. In addition, aeronautical structure in flight under loads suffer vibrations and this vibrations can be monitored by piezoelectric sensors, *i.e.* the fact that for some of these vibration based damage identification methods no artificial excitation is needed, but only the response at certain degrees of freedom (DOFs) of the structure. This is another important advantage, because the structure can remain in operation. As a consequence, these methods can be used for permanent health monitoring. The use of few PZT sensors can avoid the increment of the weight of the aeronautic structures. In some cases, the sensor can be embedded in the laminate structure (*e.g.* piezoelectric fibre sensors) and has the potential for damage detection in flight with appropriate structural modelling. The fundamental principle upon which vibration based methods are founded is that small changes (faults) in a structures cause behavioural discrepancies in its vibration responses.

3.2. Structural Dynamics in Frequency Domain

The governing equation of structural dynamics in the time domain can be developed by applying Newton's 2nd law of motion for the analytical model of a structure undergoing small deformations, by equating the internal resisting forces (inertia, damping and elasticity) with the external excitation forces:

$$[m]\{\ddot{u}(t)\} + [c]\{\dot{u}(t)\} + [k]\{u(t)\} = \{f(t)\} \tag{3.1}$$

where *[m]*, *[c]* and *[k]* are the mass, damping and stiffness matrices of the structures, *f(t)* is the external excitation and $\{\ddot{u}(t)\}$, $\{\dot{u}(t)\}$ and $\{u(t)\}$ are the acceleration, velocity and displacement vectors.

Mathematically Eq. (3.1) represents a system of 2nd order linear differential equations whose solutions can be obtained, in principle, by standard procedures for solving linear differential equations with constants coefficients, assuming mass, stiffness and damping matrices of the structure are independent of time. Different procedures can be applied in order to solve Eq. (3.1) and they can be divided into two classes: the direct integration methods and the mode superposition method. A more manageable form for Eq. (3.1) can be obtained by transforming it into frequency domain.

$$\{\ddot{u}\} + (c/m)\{\dot{u}\} + (k/m)\{u\} = f(t)/m \tag{3.2}$$

using,

$$c/m = 2\xi\omega_n \tag{3.3}$$

$$k/m = \omega_n^2 \tag{3.4}$$

where, ω_n is the natural frequency (radian/sec) and ξ is the damping ratio.

Substituting Eq. (3.3) and Eq. (3.4) into Eq. (3.2),

$$\{\ddot{u}\} + 2\xi\omega_n\{\dot{u}\} + \omega_n^2\{u\} = \omega_n^2 f(t)/k \tag{3.5}$$

The Fourier transform may be taken for each side of Eq. (3.5) to derive the steady-state transfer function for the displacement response, which after many steps of simplification is given in terms of mass, stiffness and damping coefficients of the structure and as a function of forcing frequency (ω), as

$$H(\omega) = \frac{1}{-\omega^2 m + j\omega c + k} \tag{3.6}$$

$$H(\omega) = \frac{1}{k}\left[\frac{\omega_n^2}{\omega_n^2 - \omega^2 + j(2\xi\omega\omega_n)}\right] \tag{3.7}$$

where, $j = \sqrt{-1}$.

Thus, for a linear system the frequency response function (FRF), $H(\omega)$ can be defined as,

$$[X(\omega)] = [\mathrm{H}(\omega)] \cdot [\mathrm{F}(\omega)] \tag{3.8}$$

$$[H(\omega)] = \frac{[X(\omega)]}{[F(\omega)]} \tag{3.9}$$

where, $X(\omega)$ is the output response spectra and $F(\omega)$ is the input forcing spectra.

In this case, this ratio is called the compliance (displacement/force) and it is given by the ratio of the output/input spectra. The response of a structure can be described by displacement, velocity or acceleration. The corresponding FRF is termed as compliance, mobility and acceleration, respectively. They are algebraically related to each other:

$$Compliance: \quad \mathrm{H}(\omega) = \frac{X(\omega)}{F(\omega)}\left[\frac{m}{N}\right] \tag{3.10}$$

$$Mobility: \quad M(\omega) = \frac{\dot{X}(\omega)}{F(\omega)}\left[\frac{ms^{-1}}{N}\right] = j\omega \cdot H(\omega) \tag{3.11}$$

$$Acceleration: \quad A(\omega) = \frac{\ddot{X}(\omega)}{F(\omega)}\left[\frac{ms^{-2}}{N}\right] = -\omega^2 \cdot H(\omega) \tag{3.12}$$

According to Chandra and Barai (2014), the modal parameters of all the modes within the frequency range of interest constitute a complete dynamic description of a structure. Hence, modal parameters represent the inherent dynamic properties of a structure and any changes in the mass, stiffness or damping properties, such as in the case of damage, are reflected in the modal parameters. Modal analysis is the process of determining the modal parameters of a structure for all modes in the frequency range of interest and may be carried out either through analytical or experimental techniques.

3.3. Vibration Based Method for SHM

Vibration based methods have been recognised as important approaches for developing SHM systems. As commented earlier, they are based on the observation of changes in the structural vibration responses, which result from damage occurrence. Some of them use model-based diagnostics defined in the following way: the undamaged model of a particular structure is evaluated, and this model is compared to the model identified from the measured data of the structure in the current state. Differences between these two models indicate the structure modification (*e.g.* stiffness or strength), which may be caused by damage. In order to help in the identification of this modification, different types of metrics have been developed for the detection and monitoring of damage in structures, and they are shown by the literature. Normally, a frequency response function (FRF), which relates the structural response to an

applied force, is used by the metrics. The FRF response may be written in displacement, velocity or acceleration. Theoretically, the FRF can be expressed in terms of the structural properties such as mass, stiffness, damping, and modal properties. Measured FRF data, provide clear benefits as they provide much more damage information in a desired broadband frequency range than the modal data. In fact, the modal data are identified mainly from a very limited number of FRF data around the resonance frequency, and changes in mode shapes are more difficult to measure than FRF data. For this reason, FRF data are considered to be more useful for detecting the structural damage.

Figure 3-2 shows the sequence of analyses used in the present work. Firstly, modal analyses are carried out in the intact structure in order to determine the natural frequencies and modal shapes. Then, vibration analyses are carried out on an intact structure in order to determine the undamaged behaviour. Impact tests are performed using a material model in order to predict the damage extension. Therefore, vibration analyses in damaged plates are carried out to determine the behaviour of the damaged plates. Finally, the intact and damaged behaviour are using different metrics.

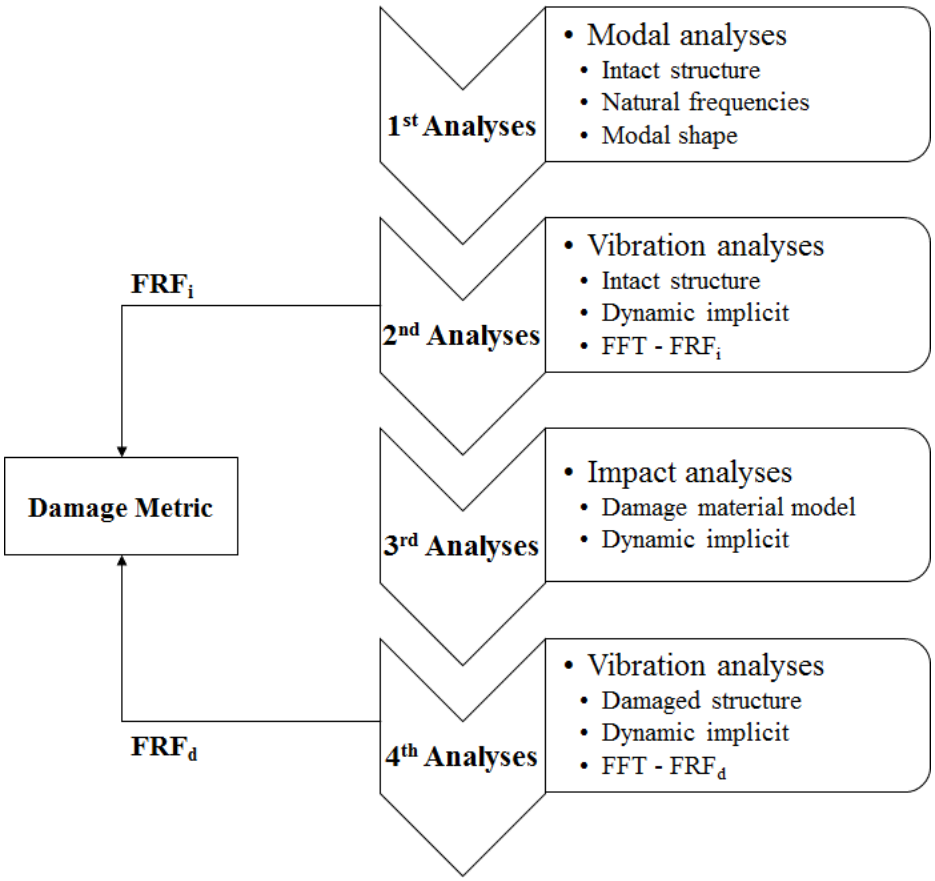

Figure 3-2 – Vibration based method: sequence of experimental and numerical implicit analyses

Different modal parameters can be used to calculate those metrics such as resonance frequencies, amplitudes, phases and vibration modes. These parameters must be chosen regarding several factors, such as the type of analysis used, previously known experimental data of the structure, the type of sensors attached to the structure, as well as their location and the type of damage, which should be detected. Hence, in the present work, different metrics are compared by using the FRFs magnitude and frequency.

3.3.1. Vibration Damage Index

Several different approaches can be identified in the literature, some of them have concentrated on the use of FRF measurements directly, as opposed to the modal data extracted from the FRF measurements.

⇒ Sampaio *et al.* (1999) presented a method that is an extension of the Pandey *et al.* (1991) method to all frequencies in the measurement range and not just the modal frequencies; *i.e.*, it uses FRF data rather than just mode shape data. In fact, the method uses something like an "operational mode shape" defined, for each frequency, by the frequency response at the different locations of the structure. The frequency response curvature can be estimated by using a central difference approximation and is defined by:

$$H_{jk}(\omega)'' = \frac{H_{i+1,k}(\omega) - 2H_{i,k}(\omega) + H_{i-1,k}(\omega)}{h^2} \tag{3.13}$$

where H_{jk} is the receptance or individual Frequency Response Function measured at the j^{th} location with a single excitation applied at the k^{th} coordinate for a given frequency ω, h is the frequency increment between the measurement FRF $i + 1$ and $i - 1$.

One of the main advantages of this method is the simplicity of use due to the fact that the receptance is known, and the calculation of the frequency response curvature approximation can be easily done. The absolute difference between the FRF curvatures of the damaged and intact structure at location j is calculated, in the chosen frequency range, for an applied force at point k. The changes in intact and damaged measured FRFs is used to determine the Damage Index (*DI*).

$$DI_{\Delta H''_{jk}}(\omega) = \sum_{\omega} \left| H^{d}_{jk}(\omega)'' - H^{i}_{jk}(\omega)'' \right| \tag{3.14}$$

Finally, one can sum up for several fore location cases:

$$DI_{\Delta H} = \frac{1}{N} \sum_{k} \Delta H''(\omega) \tag{3.15}$$

where N is the number of frequency lines, *i.e.* it depends on the chosen sampling frequency and frequency bandwidth of acquisition. The $DI_{\Delta H}$ expression returns values greater than zero, if any change in the structural dynamic behaviour occurs, and $DI_{\Delta H}$ returns zero, if there is not any damage in the structure.

⇒ Monaco *et al.* (2000) used the changes in measured FRFs in order to determine the Damage Index (*DI*). This method is based on the acquisition and comparison of FRFs from the monitored structure before and after damage occurrence. As commented previously, structural damages modify the dynamic behaviour of the structure and, consequently, its FRFs, this makes possible the calculation of a representative *DI*. In this approach, the calculated *DIs* are the averages of the differences between intact and damaged structures. Two *DI* expressions are considered:

$$DI_{ABS_{jk}} = \frac{\sum_{m=1}^{N} \left| H^{i}_{jk}(\omega) - H^{d}_{jk}(\omega) \right|}{\sum_{m=1}^{N} \left| H^{i}_{jk}(\omega) \right|}, \tag{3.16}$$

$$DI_{ABSF_{jk}} = \sum_{m=1}^{N} \frac{\left(\frac{\left| H^{i}_{jk}(\omega) - H^{d}_{jk}(\omega) \right|}{\left| H^{i}_{jk}(\omega) \right|} \right)}{N}, \tag{3.17}$$

where N is the number of frequency lines. Both *DI* expressions return values greater than zero, if any variation in the structural dynamic behaviour occurs, and they return zero, if there is no damage in the structure.

⇒ Johnson and Adams (2002) discussed the use of frequency domain transmissibility functions for detecting, locating, and quantifying damage in linear and nonlinear structures. The feature used to detect, locate, and quantify damage is derived from

the quotient of transmissibility ratios, $H_{jk}^{i}(\omega)/H_{jk}^{d}(\omega)$, where $H_{jk}^{i}(\omega)=X_j(\omega)/X_k(\omega)$, is the first, or reference, transmissibility function for the baseline (intact) system, and $H_{jk}^{d}(\omega)$ is the second function for comparison from a later time at a (potentially) damaged state. Although the entire frequency domain function, $H_{jk}^{i}(\omega)/H_{jk}^{d}(\omega)$, can be used as an indicator of damage, most of the discussion to follow used a condensed damage index. The damage index was calculated using a linear sum along all spectral lines of the function, $H_{jk}^{i}(\omega)/H_{jk}^{d}(\omega)$, for each j^{th} pair of DOFs and adapted from a frequency range:

$$\mathrm{DI}_{\mathrm{T_{jk}}}=\frac{1}{\mathrm{N}}\left|\sum_{\omega}1-\frac{\left|\mathrm{H_{jk}^{i}}(\omega)\right|}{\left|\mathrm{H_{jk}^{d}}(\omega)\right|}\right|, \tag{3.18}$$

where H is the transmissibility and the superscripts i and d denote the intact and damage structures, respectively. The DI_T expression returns values greater than zero, if any variation in the structural dynamic behaviour occurs, and DI_T return zero, if there is not any damage in the structure.

⇒ Mickens *et al.* (2003) presented a metric which is based on the fact that FRFs are sensitive to small changes and damage in a structure. To quantify this sensitivity, a damage indicator was calculated to determine the difference in the FRF responses between intact (undamaged) and damaged structures. The damage indicator for the structure is calculated considering firstly the percent difference between the magnitude of the FRFs of the undamaged and damaged structures. Any physics quantity can be used to compute the FRF, such as acceleration/force, velocity/force, displacement/force, strain/force or PZT (piezoelectric) sensor voltage/PZT excitation voltage. The damage indicator D is obtained by computing the mean value of $y(\omega)$ for the frequency range of interest.

$$\mathrm{y}(\omega)=\mathrm{abs}\left(\frac{\left|\mathrm{H_{jk}^{i}}(\omega)\right|-\left|\mathrm{H_{jk}^{d}}(\omega)\right|}{\left|\mathrm{H_{jk}^{i}}(\omega)\right|}\right), \tag{3.19}$$

$$\mathrm{DI_A}=\frac{\Delta\omega}{\omega_2-\omega_1}\sum_{\omega_1}^{\omega_2}\mathrm{y}(\omega), \tag{3.20}$$

where the superscripts *i* and *d* denote the intact and damaged structures, respectively, and the vertical bars represent the magnitude of the function. Also, ω_1 is the lower frequency and ω_2 is the upper frequency of the range of interest and $\Delta\omega$ is the frequency increment between measurement points. In addition, Eq. (3.19) and (3.20) provide a damage indicator, which gives a normalised measurement of damage in the structure. These values once collected for different sensor/actuator pairs can roughly quantify the amount of damage in a structure. The *DI* expression returns values greater than zero if any variation in the structural dynamic behaviour occurs, and *DI* returns zero, if there is not any damage in the structure.

⇒ Maia *et al.* (2003) presented a metric that uses the FRF curves differences between two FRFs, which are measured at specific positions. This metric is used to determine the influence of the damage in the free-free vibration analysis. This method can be defined as:

$$\Delta H_{jk}(\omega) = \left| H_{jk}^{d}(\omega) - H_{jk}^{i}(\omega) \right| \tag{3.21}$$

where the superscripts *i* and *d* represent the intact and damaged structures, respectively, the subscripts *j* and *k* denote the location of measure and force, respectively. $H(\omega)$ denotes the frequency response function, and ω denotes the frequency range.

If more than one frequency and force are considered, the index is the sum of the damage indices from each frequency and force. This method can be defined as:

$$DI_{MS_j} = \frac{1}{N} \sum_{\omega} \sum_{k} \Delta H_{jk}(\omega) \tag{3.22}$$

Another DI presented by Maia et al. (2003) can be defined as:

$$\left(\Delta \mathrm{H}_{\mathrm{jk}}^{''}(\omega)\right)^2 = \left| \left(\mathrm{H}_{\mathrm{jk}}^{\mathrm{d}}(\omega)^{''}\right)^2 - \left(\mathrm{H}_{\mathrm{jk}}^{\mathrm{i}}(\omega)^{''}\right)^2 \right| \tag{3.23}$$

If more than one frequency and force are considered,

$$\mathrm{DI}_{\mathrm{MSCS}_{\mathrm{jk}}} = \frac{1}{\mathrm{N}} \sum_{\omega} \sum_{\mathrm{k}} \left(\mathrm{H}_{\mathrm{jk}}^{''}(\omega)\right)^2 \tag{3.24}$$

The third one DI presented by Maia *et al.* (2003) can be defined as:

$$\beta_{jk}(\omega)=\frac{\left(\left(H_{jk}^{d}(\omega)^{"}\right)^{2}+\sum_{m=1}^{N}\left(H_{jk}^{d}(\omega)^{"}\right)^{2}\right)\sum_{m=1}^{N}\left(H_{jk}^{i}(\omega)^{"}\right)^{2}}{\left(\left(H_{jk}^{i}(\omega)^{"}\right)^{2}+\sum_{m=1}^{N}\left(H_{jk}^{i}(\omega)^{"}\right)^{2}\right)\sum_{m=1}^{N}\left(H_{jk}^{d}(\omega)^{"}\right)^{2}} \tag{3.25}$$

and, once again, if more than one frequency and force are considered, the index is the sum of damage indices from each frequency and force:

$$DI_{\beta_{jk}}=\frac{1}{N}\sum_{\omega}\sum_{k}\beta_{jk}(\omega) \tag{3.26}$$

All these *DI* expression returns value zero, if there is no variation in the structural dynamic behaviour.

⇒ Zang *et al.* (2003) presented the global shape correlation function (*GSC*) and global amplitude correlation function (*GAC*) for structural health monitoring. Similar to the definitions in Zang *et al.* (2003), it can be defined as:

$$GSC_j=\frac{\left|\left[H_{jk}^{i}(\omega)\right]^{T}\cdot\left[H_{jk}^{d}(\omega)\right]\right|^{2}}{\left(\left[H_{jk}^{i}(\omega)\right]^{T}\cdot\left[H_{jk}^{i}(\omega)\right]\right)\cdot\left(\left[H_{jk}^{d}(\omega)\right]^{T}\cdot\left[H_{jk}^{d}(\omega)\right]\right)}, \tag{3.27}$$

$$DI_{GSC_j}=\frac{1}{N}\sum_{\omega}GSC_j, \tag{3.28}$$

$$GAC_j=\frac{2\cdot\left|\left[H_{jk}^{i}(\omega)\right]^{T}\cdot\left[H_{jk}^{d}(\omega)\right]\right|}{\left(\left[H_{jk}^{i}(\omega)\right]^{T}\cdot\left[H_{jk}^{i}(\omega)\right]\right)+\left(\left[H_{jk}^{d}(\omega)\right]^{T}\cdot\left[H_{jk}^{d}(\omega)\right]\right)}, \tag{3.29}$$

$$DI_{GAC_j}=\frac{1}{N}\sum_{\omega}GAC_j, \tag{3.30}$$

where the superscript *T* is a transpose column vector, and N is the number of frequencies chosen in the frequency range of interest. Based on Eq. (3.28) and Eq. (3.30), it can be seen that GSC_j and GAC_j are real-valued functions of frequency between zero and unity. Also, the shape correlation coefficient is sensitive to mode shape differences, but not to relative scales. On the other hand, the amplitude correlation coefficient uses damaged response amplitudes. Moreover, DI_{GSC} and

DI_{GAC} provide real constant values between zero and unity to indicate total/zero change of structural responses Zang *et al.* (2003).

⇒ Silva *et al.* (2008) showed a damage metric chart obtained by frequency response from input-output data. The damage metric is an index based on the root-mean-square deviation (RMSD). This feature is computed with data in the frequency domain. This damage index is originally proposed for the electrical impedance signal, but in the present work, it is adapted to be used in vibration analysis and investigated range of frequency. Thus, this metric can be defined as:

$$DI_{M_j} = \frac{1}{N}\sum_{\omega}\sqrt{\frac{\left[H_{jk}^{i}(\omega) - H_{jk}^{d}(\omega)\right]^2}{\left[H_{jk}^{i}(\omega)\right]^2}} \tag{3.31}$$

These values can be collected for different sensors, such as accelerometers and piezoelectric transducers, in order to quantify the amount of damage in a structure. *DI* expression returns values greater than zero if any change in the structural response occurs, and *DI* returns zero, if there is no damage in the structure.

⇒ Medeiros *et al.* (2015a; 2015b) proposed a new damage metric used to determine the influence of the damage in the free-free vibration response. Different measurements can be used to compute the FRF, such as acceleration/force, velocity/force, displacement/force, strain/force or piezoelectric (PZT) sensor voltage/PZT excitation voltage. DI_{GAP} indicator (Global Amplitude Phase Damage Indicator) is obtained by computing the value for the frequency range of interest.

$$\mathrm{DI}_{\mathrm{GAP_j}} = \left| 1 - \frac{\sum_{\omega}\left(\mathrm{H}_{\mathrm{jk}}^{\mathrm{d}}(\omega)\cdot\mathrm{P}_{\mathrm{jk}}^{\mathrm{d}}(\omega)\right)}{\sum_{\omega}\left(\mathrm{H}_{\mathrm{jk}}^{\mathrm{i}}(\omega)\cdot\mathrm{P}_{\mathrm{jk}}^{\mathrm{i}}(\omega)\right)} \right| \tag{3.32}$$

where the superscripts *i* and *d* represent the undamaged and damaged structures, respectively. And, the subscripts *j* and *k* denote the location of measure and force, respectively. $H(\omega)$ denotes the amplitude, $P(\omega)$ denotes the phase, and ω denotes the frequency range. DI_{GAP} expression returns value equal zero, if there is no changes in the structural dynamic behaviour, *i.e.* there is no damage in the structure.

3.4. Experimental Setup and Testing Procedures

3.4.1. Vibration Test – Carbon Fibre Composite Plates

The experimental analyses were carried out via vibration tests on composite plates hanged by elastomeric wires in order to simulate "free-free" boundary conditions. Firstly, the modal analyses were performed using only two accelerometers (for measuring the output signals) and Maxwell's reciprocity theorem, where an impact hammer was used for providing the impulse input signal in 63 different points (markers) in z-direction (Figure 3-3). In fact, a grid of 9 (lines) *vs.* 7 (columns) measurement points (markers) was printed on the face of each vibration test plate as verified in Fig. 3-3, which were selected after evaluated the first eight mode shapes of the composite plate via FE model. Each signal consists of 2048 points and sampling occurred at 512Hz. The number of averaging individual time records was selected to be five in order to reduce the variation effects. This analysis can be evaluated comparing not only the FRFs, but also the coherence values.

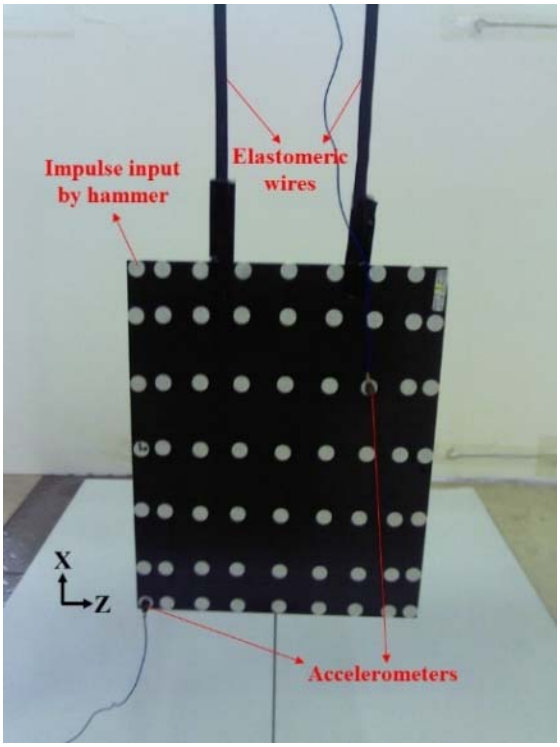

Figure 3-3 – Experimental setup of the modal analysis in carbon fibre composite plates.

When all 63 measurements through the grid markers were obtained and stored, the FRFs were calculated, where resonant frequencies could be identified using the signal processing software Test.Lab with PolyMAX non-iterative frequency domain parameter estimation method (Peeters *et al.*, 2004). It is based on a (weighted) least-squares approach and uses multiple-input/multiple-output frequency response functions as primary data. The PolyMAX or poly reference least-squares complex frequency-domain method can be implemented in a very similar way as the industry standard poly reference (time-domain) least-squares complex exponential method. Thus, in a first step, a stabilisation diagram is built containing frequency, damping and participation information. Next, the mode shapes are found in a second least-squares step, based on the user selection of stable poles. One of the specific advantages of the technique lies in the very stable identification of the system poles and participation factors as a function of the specified system order, leading to easy-to-interpret stabilization diagrams. The modal coefficients are computed, and the mode shapes are obtained (Heylen *et al.*, 1997).

After the modal analyses using 63 different input points and only 2 accelerometers, FRFs for damage identification were obtained using, firstly, only 1 input point and four accelerometers output data (Fig. 3-4a). The accelerometers are model 352A24 lightweight structure. Accelerometer 1 (sensitivity 102.34mV/g) was set on the position 1, accelerometer 2 (sensitivity 104.59mV/g) was set on the position 2, accelerometer 3 (sensitivity 99.95mV/g) was set on position 3 and accelerometer 4 (sensitivity 104.35mV/g) was set on position 4, which can be seen in Fig. 3-4. And, the impulse input by impact hammer is given in back side of the position 1. It is important to highlight that the positions of the accelerometers were selected based on the previous modal analyses, avoiding the presence of sensors in nodal lines, considering the first five mode shapes.

Secondly, four piezoelectric transducers were glued in the same positions of the accelerometers (Fig. 3-4b). M2814-P1 type MFC (Macro Fibre Composite) is manufactured by Smart Material Inc., and it uses the d_{33} piezoelectricity mode. Since, the fibre layer is embedded into a polymer matrix; the piezoelectric sensors have an overall geometry of 38mm length, 20mm width and 0.305mm total thickness. However, due to the package, the active geometry has 28mm length, and 14mm width. The excitation for both sets of vibration tests was applied by using an impulse signal through an impact force hammer PCB Model 0860C3 (Piezotronics).The input was set on the position 1 in the back side of the plate (Fig. 3-4).

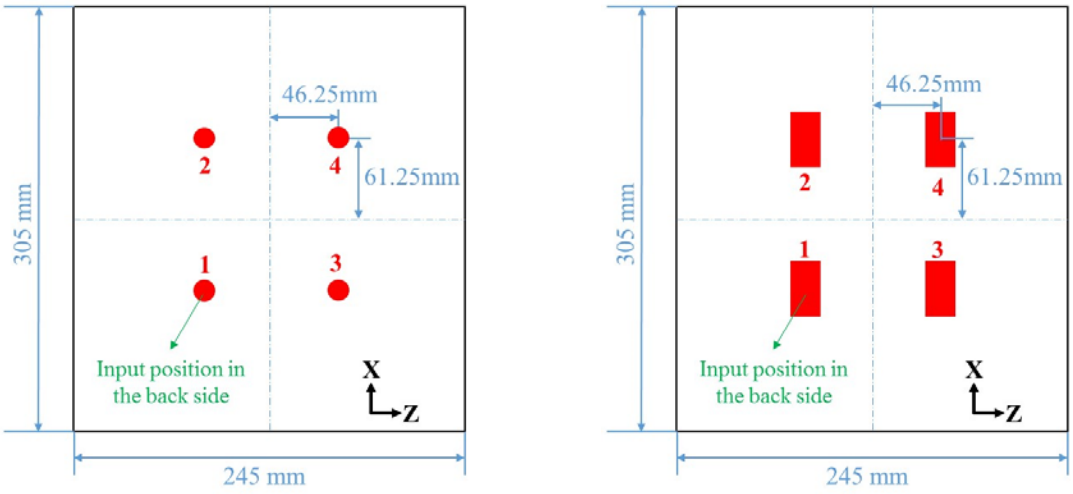

Figure 3-4 – Schematic experimental set for vibration based identification in carbon fibre composite plate (a) with accelerometers and (b) with MFCs

Figure 3-5 show all data acquisition set-ups used in the experiment for damage identification. Again, the specimen is suspended by elastomeric wires to simulate "free-free" boundary condition, the accelerometers (Fig. 3-5a) and MFCs transducer (Fig. 3-5b) and the hammer linked to an LMS SCADAS Mobile equipment, which was controlled by the Test.Lab software (LMS Test.Lab). The LMS SCADAS Mobile is plug and play equipment and it has multifunction analogy, digital and timing I/O board for USB bus computers.

Many times the number of frequency points, which can be used, is limited either by the testing conditions or by available computational power. Sometimes only a small number of points may be measured due to the large time per frequency point cost, as with as indwell test. Conversely, if a test where a large number of frequency points may be generated, such as a broad-band random test, it may be limited by the available computers. To determine how to choose which frequency points to use in the analysis, as commented earlier, the natural frequencies of the structure are analysed using a FE model. Each signal consists of 2048 points and sampling occurred from 0 Hz to 512Hz. It is selected the frequency band of 512Hz, because the aim of this work is to calculate the damage index (damage metric) by vibration based method for the first five natural frequencies of the structure. The number of averaging individual time records was selected to be five in order to reduce the variation effects. This analysis can be evaluated comparing not only the FRFs, but also the coherence values. The dataset contains mode shape and FRFs, which include information on natural frequencies and damping factor. Table 3-3 summarises all information about the experimental setup for the carbon fibre composite plates.

Table 3-3. Experimental setup used for damage identification in carbon fibre composite plates

Trigger	
Scope time	5s
Input range	35.1111N
Trigger level	1.0003N
Pre trigger	0.0063s
Bandwidth	
Bandwidth	512Hz
Spectral lines	2048
Acquisition time	4s
Resolution	0.25Hz
Averages	5
Windows input	Force – exponential – cut-off: 1.06%
Windows response	Exponential – decay: 100%
Test variance	2 days

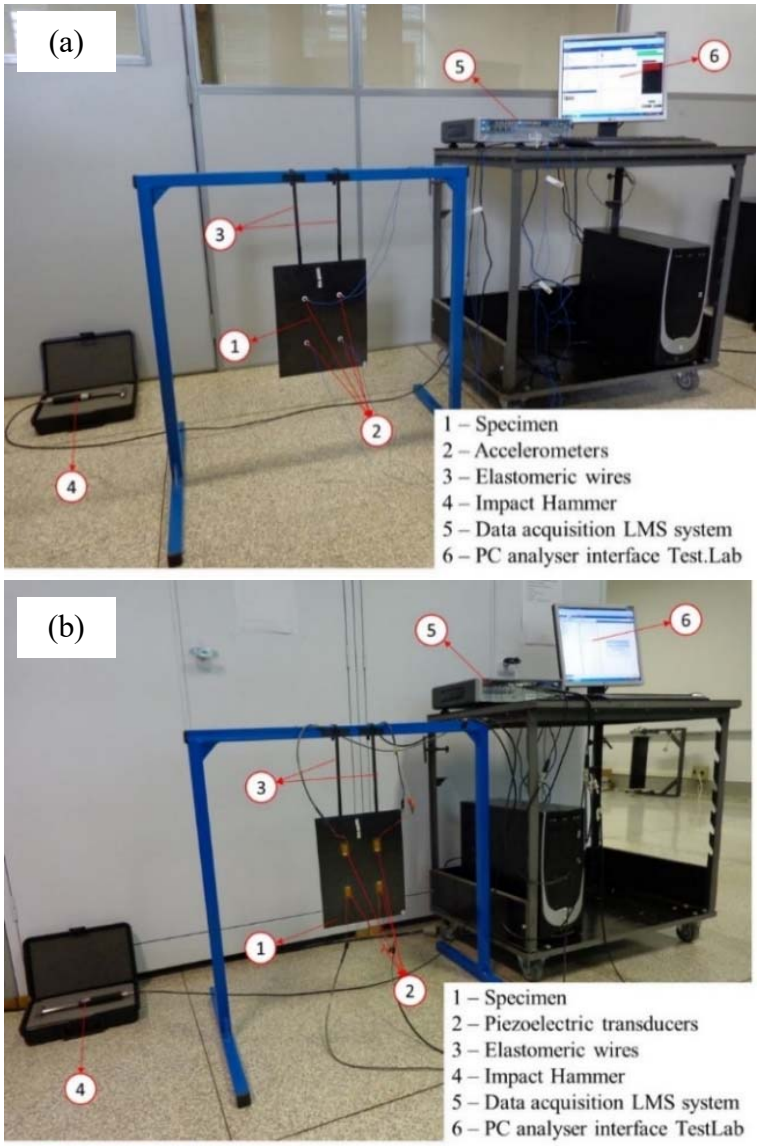

Figure 3-5 – Experimental layout for vibration identification in carbon fibre composite plate by using (a) accelerometers and (b) piezoelectric sensors

3.4.2. Vibration Test – Glass Fibre Composite Plates

The experimental analyses were carried out by vibration tests in glass fibre reinforced polymer (GFRP) plates using accelerometers attached to one of its faces and used as sensors. The natural frequencies and FRFs were obtained using accelerometers (Fig. 3-6). The accelerometers are model 352A24 and 352C22 lightweight structure. The accelerometer 1 (model 352A24 and sensitivity 99.6mV/g) was set on the position 2 and the accelerometer 2 (model 352C22 and sensitivity 9.94mV/g) set on the position 3, which can be seen in Fig. 3-6. Again, the positions of the accelerometers were selected based on previous modal analyses, avoiding the presence of sensors in nodal lines, considering the first five mode shapes. As observed, the positions are different than the last ones in carbon fibre composite plates. This occurs because the dimension of the plate is different as confirmed by the Tables 2-3 and 2-4.

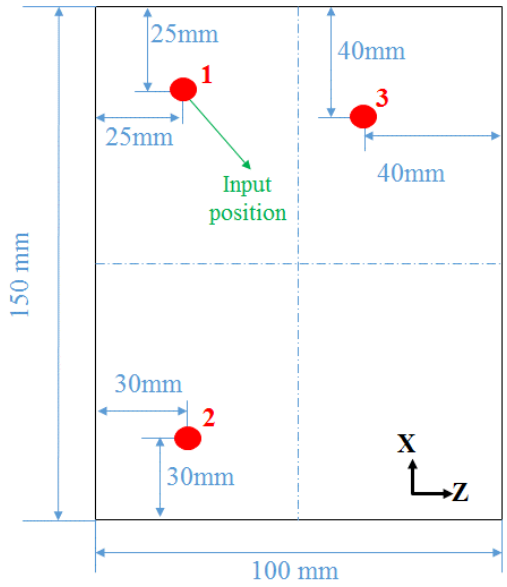

Figure 3-6 – Schematic experimental set with accelerometers for vibration based identification in glass fibre composite plate

The plates were also suspended in a frame using a wire to simulate "free-free" boundary condition. The applied input was a impulse signal through an impact force hammer to produce the excitation on the structure. Thus, firstly, FRFs for damage identification were obtained for two intact plates. After that, one plate was damaged by drilling a centre hole (controlled damage), and the other plate was damaged by impact loading (uncontrolled damage). Then, FRFs were obtained for the damaged plates. The experimental results were analysed for intact

and damaged using the metrics described earlier, which are compared in terms of their capability for damage detection, showing the limitations and advantages for each one.

More details about the experimental setup for the vibration test can be seen in Fig. 3-7. The figure shows the elastomeric wires attached to the specimen, the accelerometers and the hammer linked to the LMS equipment, which is connected to a personal computer equipped with data acquisition software and a PC analyser interface. All undamaged and damaged types were assessed by acquiring the FRF signatures for both the accelerometers and one impacted position as shown in Fig. 3-6.

Table 3-4. Experimental setup used for vibration based identification in glass fibre composite plates

Trigger	
Scope time	5s
Input range	17.3611N
Trigger level	1.0003N
Pre trigger	0.0063s
Bandwidth	
Bandwidth	1024Hz
Spectral lines	2048
Acquisition time	2s
Resolution	0.5Hz
Averages	5
Windows input	Force – exponential – cut-off: 1.32%
Windows response	Exponential – decay: 100%
Test variance	2 days

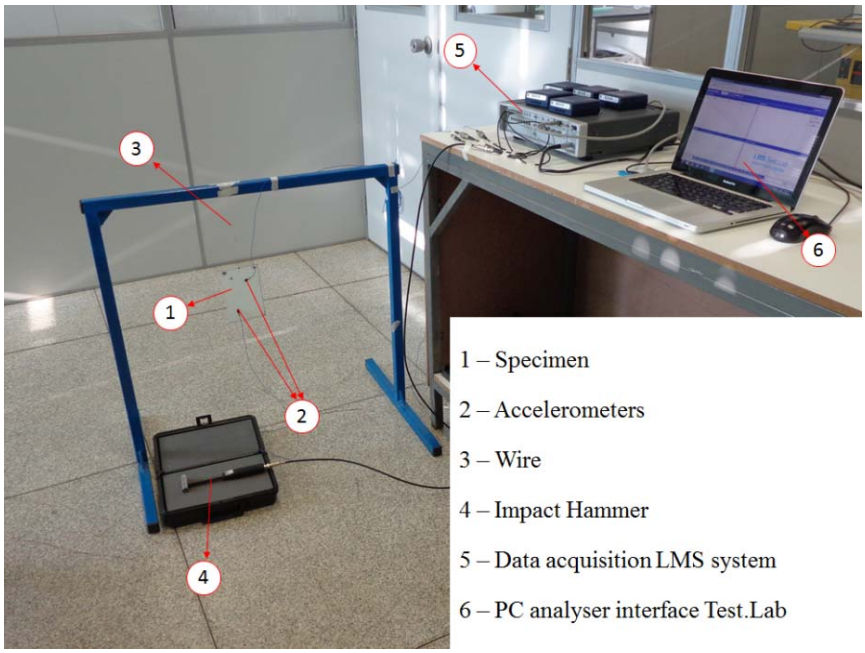

Figure 3-7 – Experimental layout for vibration based identification in GFRP plates using accelerometers

The output was measured using two accelerometers (PCB Piezotronix). Each time signal consisted of 2048 points and it was sampled until 1024 Hz. As commented earlier, the FRFs were calculated from both the measured force and response signals (accelerometers). The number of averaging individual time records was selected to be five to reduce the random fluctuation in the estimation of the FRFs. This analysis can be evaluated comparing not only the FRFs, but also the coherence values. This information can be used to identify the presence of damage at the structure. However, sometimes, it is necessary to use suitable metrics in order to identify the damage. Table 3-4 summarises all the information about the experimental setup for the glass fibre composite plates.

3.4.3. Vibration Test – Carbon Fibre Composite Cylinders

The experimental analyses were performed on 15 composite cylinders. The composite cylinders are made of fourteen layers of epoxy resin reinforced by carbon fibres with three different stacking sequences (*cf.*, Tab 2-5). Firstly, the natural frequencies and the Frequency Response Functions (FRFs) for undamaged and damaged cylinders were obtained using two accelerometers (A2 and A3). The accelerometers were the model 352A24 or 352C22 lightweight structure as shown in Fig. 3-8. The accelerometer 1 (model 352C22 and sensitivity 9.57mV/g) was set on the position 2 and the accelerometer 2 (model 352A24 and sensitivity 99.6mV/g) set on the position 3. The excitation was created by an impulse signal (F1) generated by an impact of a hammer PCB Model 0860C3 (Piezotronics). Dynamic excitation was performed at position 1 according to Fig. 3-8.

Figure 3-9 shows all the used equipment in the experiments. The specimen was suspended using elastomeric wire to simulate a “free-free” boundary condition. The accelerometers and the hammer were linked to LMS SCADAS Mobile equipment, which was controlled by the Test.Lab software (LMS Test.Lab). Each signal consisted of 3000 points with a sampling rate of 1500Hz. The number of averaging individual time records was selected to be five to reduce the variation effects. This analysis can be evaluated comparing not only the FRFs, but also the coherence values. Table 3-5 summarises all information about the experimental setup for the carbon fibre composite cylinders.

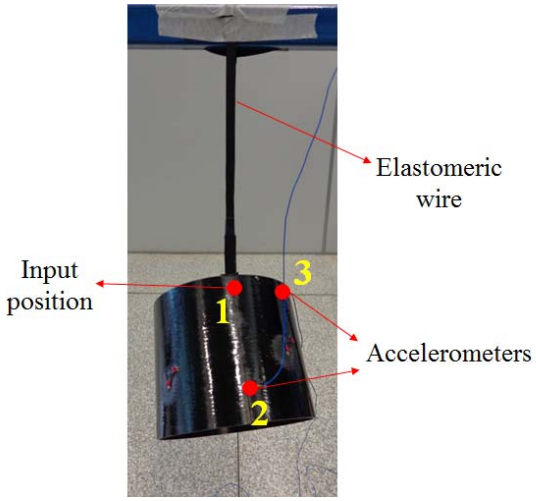

Figure 3-8 – Composite cylinder vibration analysis setup

Table 3-5. Experimental setup used for vibration based identification in carbon fibre composite cylinders

Trigger	
Scope time	5s
Input range	34.8018N
Trigger level	0.7781N
Pre trigger	0.0078s
Bandwidth	
Bandwidth	1500Hz
Spectral lines	3000
Acquisition time	2s
Resolution	0.5Hz
Averages	5
Windows input	Force – exponential – cut-off: 0.8178%
Windows response	Exponential – decay: 100%
Test variance	2 days

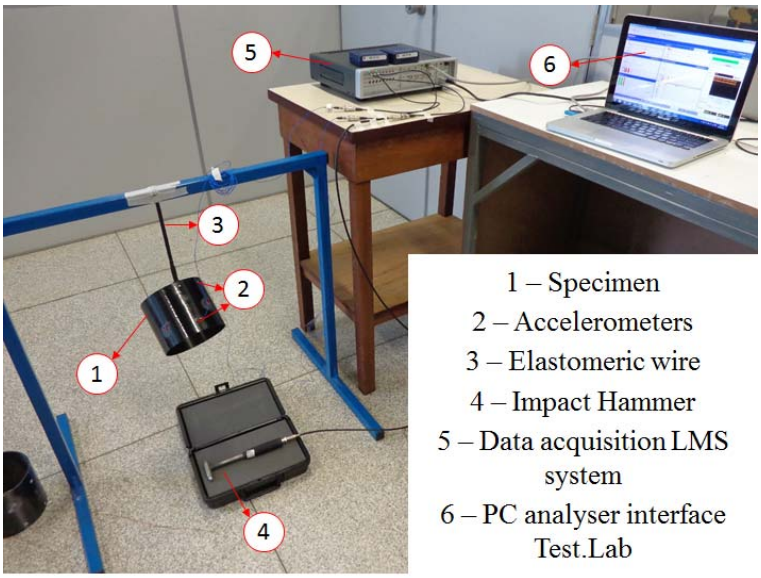

Figure 3-9 – Experimental layout used for vibration based identification in carbon fibre composite cylinders.

3.4.4. Low Velocity Impact Test

The aim of the impact test is to cause the damage in the composite structures. Therefore, it is not possible to define a frequency range to be used. In fact, two different setups were used. For the carbon fibre structures (plates and cylinders), the drop tests were performed at KU Leuven (Belgium). However, for the glass fibre composite structure (plates), the tests were performed at USP (Brazil).

The drop tower apparatus (Fig. 3-10a) consists of two vertical bars which guide the falling weight during the test. The test specimens are set at the base of the tower. The tests have been performed using an aluminium round impactor head with a diameter of 16mm (Fig. 3-10b).

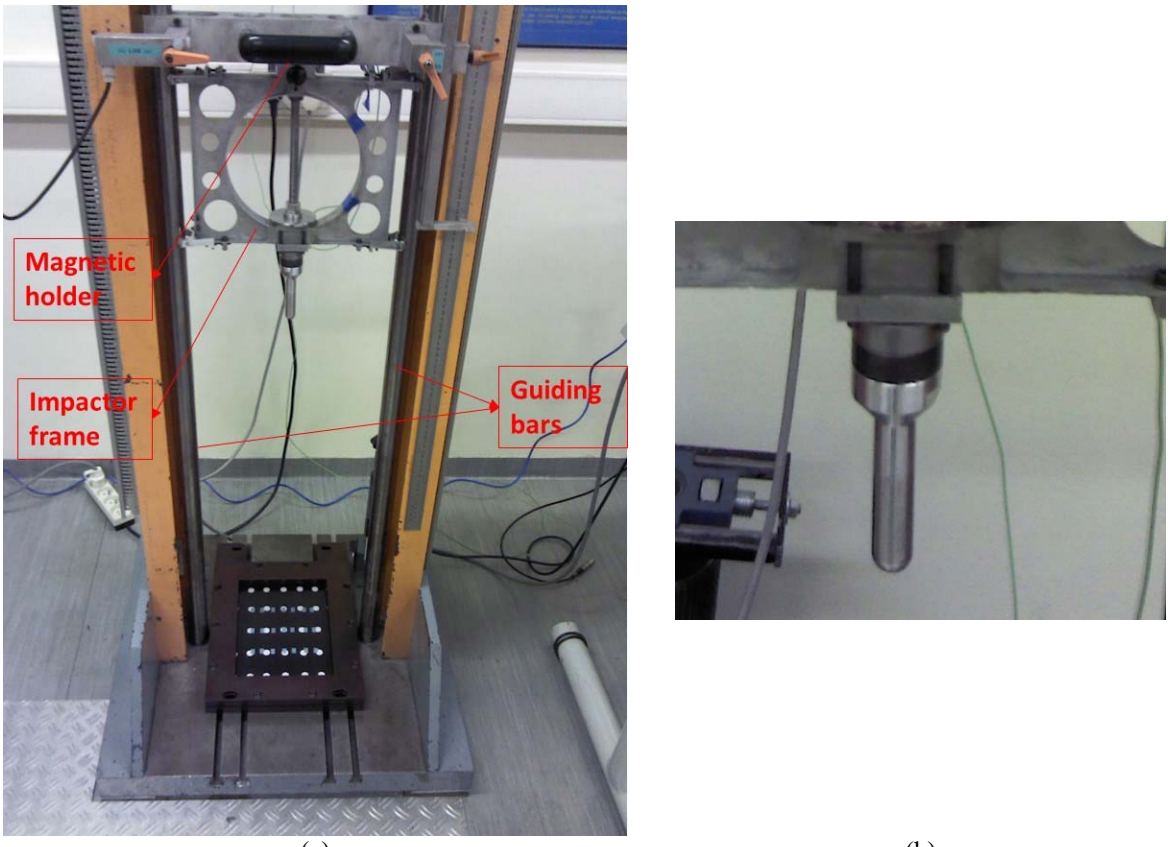

(a) (b)

Figure 3-10 – (a) Experimental set-up of the impact test for the carbon fibre composite structures (KU Leuven), (b) round impactor head

The round head avoids penetration of the coupon, which would occur if a sharp head were used. A piezoelectric crystal, set between the impactor head and the impactor frame, is used as a load cell for impact force acquisition. The displacement data have been acquired using

a light detector placed at the bottom of the drop tower apparatus, which measures the intensity of a Light Emitting Diode (LED) mounted on the impactor frame. The displacement is set "zero" at the point on the top of the plate, when the impactor touches the specimen for the first time. In this work, the plate specimens have been positioned in a special device (Fig. 3-11a), which clamps all edges of the plate, and the cylinders were put on the flat base of the drop tower (Fig. 3-11b) or supported by a "V-block" as discussed by Ribeiro (2013a) in his PhD Thesis.

The default set-up of the drop test machine consists of the load cell, which was plugged on a Kistler^{TM} amplifier (model 5007). This equipment was connected to an acquisition system, which had 11-bit data, with three channels for input and sampling frequency set to 20 kHz. The software was set to recorder samples at 20 kHz frequency and the sample size had 64000 points. Also, for the piezoelectric sensor, it was used the LMS system, however the LMS system is not able to capture the loading data, because the acquisition rate is very low.

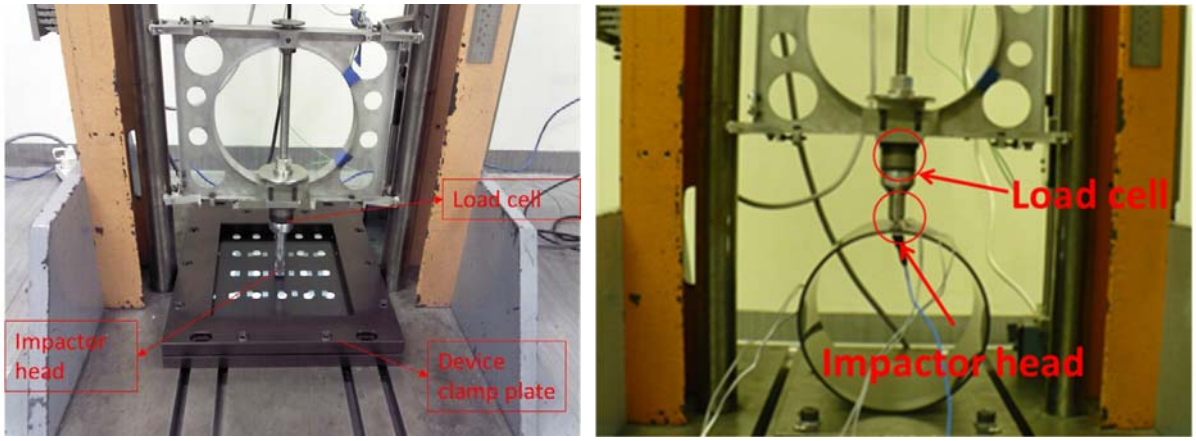

(a) (b)

Figure 3-11 – Test specimens positioned for the drop test (KU Leuven) (a) composite plate clamped by the device and (b) composite cylinder on the flat base.

For the glass fibre composite plates, the impact tests were performed at Aeronautic Structure Laboratory (University of São Paulo). Figure 3-12 shows the drop tower apparatus and the test specimen mounted in the device ASTM 7136M on the basis of the drop tower. This test method determines the damage resistance of multidirectional polymer matrix composite laminated plates subjected to a drop-weight impact event.

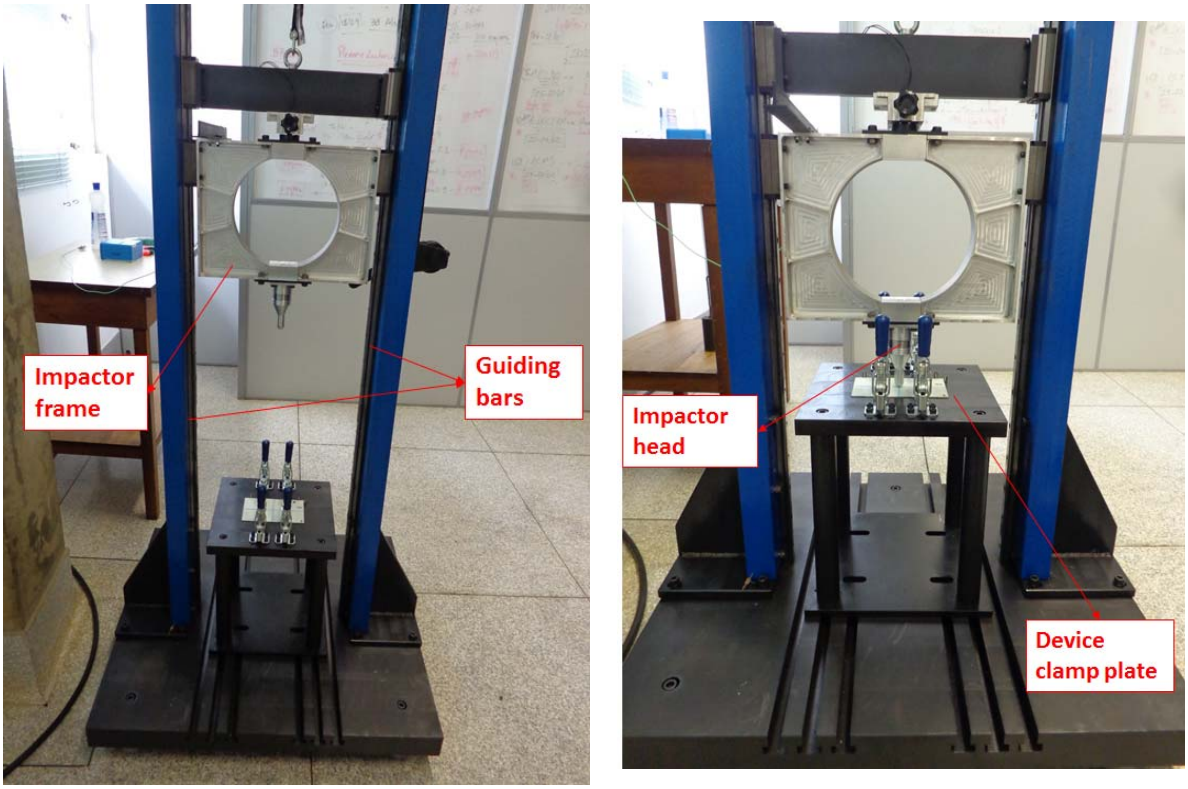

(a) (b)

Figure 3-12 – (a) Experimental setup of the impact test (USP) and (b) Test specimen clamped in the ASTM 7136M device on the basis of the drop tower.

A flat rectangular glass fibre composite plate is subjected to an out-of-plane, concentrated impact using a drop-weight device with a hemispherical impactor (diameter of 16mm). The potential energy of the drop-weight, as defined by the mass and drop height of the impactor, is specified prior to test (*cf.* Tab. 3-6). The damage resistance is quantified in terms of the resulting size and type of damage in the specimen. According the ASTM 7136M, the damage resistance properties generated by this test method are highly dependent upon several factors, which include specimen geometry, lay-up, impactor geometry, impactor mass, impact force, impact energy, and boundary conditions.

The experimental tests have been carried out in the composite specimens, allowing a critical investigation of the damage process in three different composite coupons. In addition, the influence of the anisotropy and boundary conditions was investigated as well as the impact energy on the impact response. Table 3-6 shows the number of tests and the energy level carried out for each composite specimen.

Table 3-6. Energy level for different test specimens

ID	Energy level [J]	Mass [kg]	Place
P01_CF	9.4	1.268	KU Leuven
P03_CF	12.4	1.268	
P04_CF	12.4	1.268	
P05_CF	9.4	1.268	
P06_CF	9.4	1.268	
P09_CF	19.3	1.268	
P10_CF	19.3	1.268	
P11_CF	19.3	1.268	
P12_CF	19.3	1.268	
P01_GF-U	8.9	4.422	USP
P02_GF-U	8.9	4.422	
P03_GF-U	8.9	4.422	
P05_GF-B	8.9	4.422	
P06_GF-B	8.9	4.422	
P07_GF-B	8.9	4.422	
C02_CF-A	31.0	3.24	KU Leuven
C03_CF-A	31.0	3.24	
C04_CF-A	31.0	3.24	
C05_CF-A	31.0	3.24	
C07_CF-B	31.0	3.24	
C08_CF-B	31.0	3.24	
C09_CF-B	31.0	3.24	
C10_CF-B	31.0	3.24	
C12_CF-C	31.0	3.24	
C12_CF-C	31.0	3.24	
C12_CF-C	31.0	3.24	
C12_CF-C	31.0	3.24	

3.5. Numerical Analyses

3.5.1. Vibration Test Simulations - Carbon Fibre Composite Plates

Two different conditions were considered in this work. In the first condition, accelerometers are used and, in the second one, piezoelectric (PZT) sensors are used. However, the accelerometer will not use in the SHM system designed to make measurements in flight. Using

the accelerometer is to compare the damage index (metric) DI_{accel} provided by the accelerometers to the damage index (metric) DI_{PZT} provided by the PZT sensors, *i.e.* to evaluate the methodology for damage identification. On the other hand, accelerometer and PZT numerical analysis can evaluate the computational model with or without the influence of PZTs sensors in the metrics.

A four node reduced integration shell element with six degrees of freedom (DOF) per node (defined as S8R - ABAQUS^{TM}) was used to model the composite plate. The plate was modelled with 2928 quadrilateral elements with 9003 nodes. As previously commented, the material properties are given by Ribeiro *et al.* (2012), similar to Tita (2003). The specimens manufactured and studied by Tita (2003) were made from prepreg M10 from Hexcel^{TM}. In fact, they were unidirectional carbon fibres with epoxy resin and the fibre volume ratio was around 63%. The elastic properties and strength values are shown either in Table 2-2 or in Tita (2003) and Tita *et al.* (2008).

Macro Fibre Composite (MFC) PZT sensor are used, which consist of a rectangular piezo ceramic rods sandwiched between layers of adhesive, electrodes and polyimide film. The electrodes are attached to the film in an interdigitated pattern, which transfers the applied voltage MFC-structure directly to and from the ribbon shaped rods. This assembly enables in-plane poling, actuation and sensing in a sealed and durable, ready to use package. As the type of sensor is thin, it can be applied (normally bonded) to various types of structures or embedded in a composite structure.

As commented earlier, the piezoelectric sensors (smart composite) are made of Lead-Zirkonate-Titanate (PZT) ceramic type by Smart Material^{TM} (M2814-P1), which had the effective properties determined by using a separated 3D FE model. For the vibration test simulations, the PZT sensors were modelled using 20-noded solid elements (defined as C3D20E – ABAQUS^{TM}) with parabolic interpolation attached to the shell model of the composite structure. The piezoelectric sensor was modelled using 760 hexahedron elements with 5613 nodes, using the effective properties previously determined. Each node gives displacements in x, y and z directions and electric voltage. Therefore, the electric potential was measured in a specific node of the model on the free surface, which corresponds to local information for an applied strain. In practice, the free surface of each PZT sensor is covered with an electrode, which ensures a uniform level of induced electric potential (equipotential) in the free surface of the sensor. In order to ensure perfect bonding between the PZT sensor and the composite plate, the nodes on the bottom surface of the PZT are coupled to the surface of

the plate using the "tie" contact (Abaqus, 2014). The grounding of nodes of the PZT surfaces attached to the plate is set as zero potential at any stage of strain. The purpose of grounding consists of defining a reference value. Thus, the PZT sensor in the FE model is simulated through solids elements with homogenised properties obtained from the procedure proposed by Medeiros et al (2012a, 2012b, 2012c), and arising from the detailed model of PZT (*cf.* Tab. 2-10).

Firstly, numerical simulations consist on performing modal analyses using the Finite Element Method (Fig. 3-13). The analyses were performed using a "quasi" free-free boundary conditions, because elastic wires are attached to the composite plate as used in the vibration experimental tests (Fig. 3-3). Modal analysis was carried out for undamaged plate to determine the natural frequencies and mode shapes of the intact structure. The frequency range of 0-512 Hz is considered like in the experimental tests. The numerical modal results are used to assist in the experimental tests, mainly for the determination of the markers positions when accelerometers are used. In fact, the marker positions are the points, which show null or maximum amplitude during vibration of the plate as commented earlier. It is noteworthy that the selected accelerometers have very small mass when compared to the mass of the plate. Thus, no additional mass was included in the simulated, *i.e.* the output results were obtained directly from the nodal values. Concerning the position of the posts, the first five vibration modes of the structure were observed, and the sensors are not positioned exactly on nodal lines. In addition, in some cases, the mode shape shows very distant nodal lines of the PZTs position, especially for the first bending mode.

As proposed by the research methodology, numerical simulation is done through a dynamic implicit analysis via Finite Element to obtain the FRF of the intact and damaged structure (Fig. 3-14). The same boundary conditions (described previously) are also applied on the model. In addition, an impulse loading is applied on the surface of the plate close to the piezoelectric transducer, simulating the excitation of a hammer at the "loading" point (Fig. 3-4). The input signal is a transverse force with amplitude equal 1N concentrated in one node of the FE model. The frequency of the force is applied in the range 0-512 Hz, considering size step of 0.5 Hz. Based on the input (impact of hammer) and output signals (accelerometer and piezoelectric measurements), a Fast Fourier Transform (FFT) is applied to obtain the Frequency Response Functions (FRFs) for intact structures.

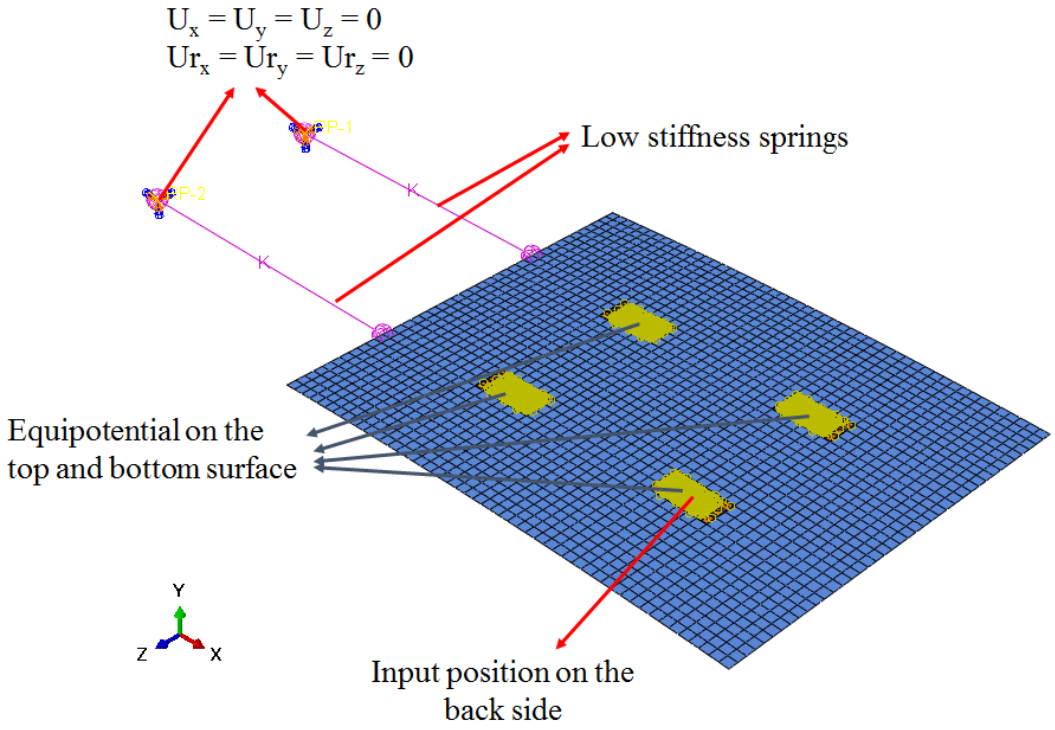

Figure 3-13 – FE model used in the modal numerical analyses for the composite plates using piezoelectric sensors

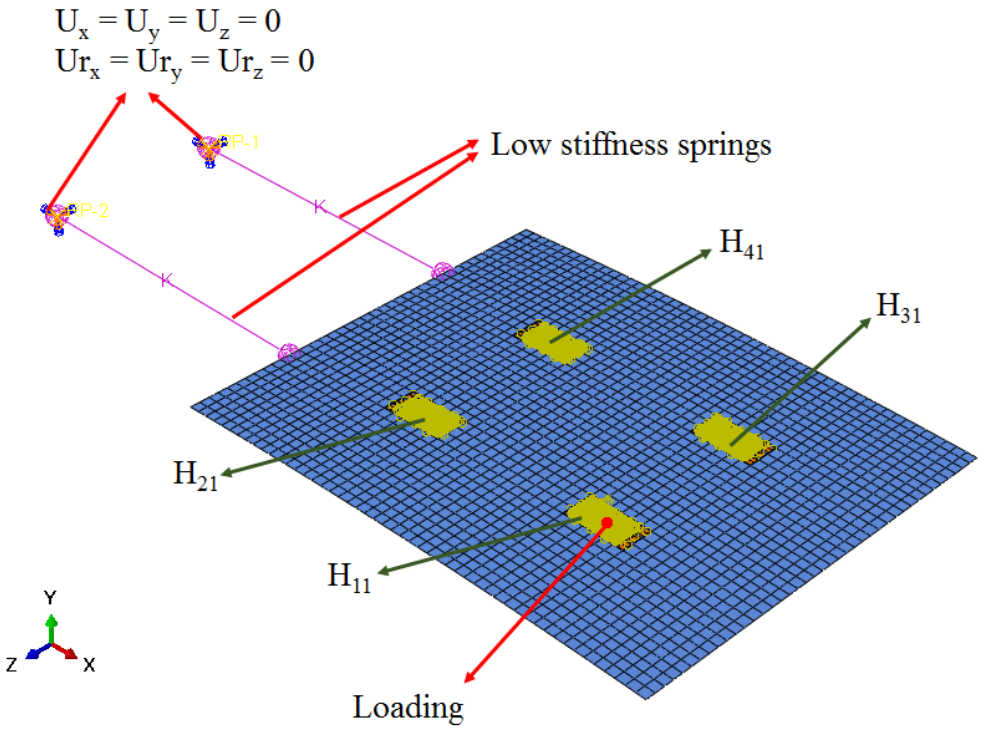

Figure 3-14 – FE model used in the dynamic implicit numerical analyses for the composite plates using piezoelectric sensors (before and after impact)

3.5.2. Vibration Test Simulations - Carbon Fibre Composite Cylinders

For the composite cylinders, FE models (Fig. 3-15) are developed using four node reduced integration shell elements with six degree of freedom (DOF) per node (defined as S4R - ABAQUS^{TM}) even in the impact analyses. In this case, the mesh is refined until eliminating severe element distortions, during the impact analysis, to avoid numerical convergence issues during damage analysis. The cylinder is modelled with 19200 quadrilateral elements and 19456 nodes. The piezoelectric sensor is modelled using eight node coupled 3D elements (defined as C3D8E - ABAQUS^{TM}) with four DOF per node, which are three linear displacements and one electric voltage. Therefore, measurement of the electric potential in a specific node on the free surface gives local information under an applied strain. In practice, the free surface of the PZT sensor is covered by an electrode, which ensures a uniform level of induced electric potential in this position (equipotential). The piezoelectric sensor is modelled using 325 hexahedron elements and 728 nodes attached to the shell elements. Another important issue of the FE model is to ensure the mechanical coupling between the composite cylinder and the PZT sensor. In order to have an ideal perfect bonding, the nodes on the bottom surface of the transducer are mechanically coupled to the ones on the top surface of the composite cylinder by using the "tie" tool in ABAQUS^{TM} like in the plate analyses (Fig. 3-15).

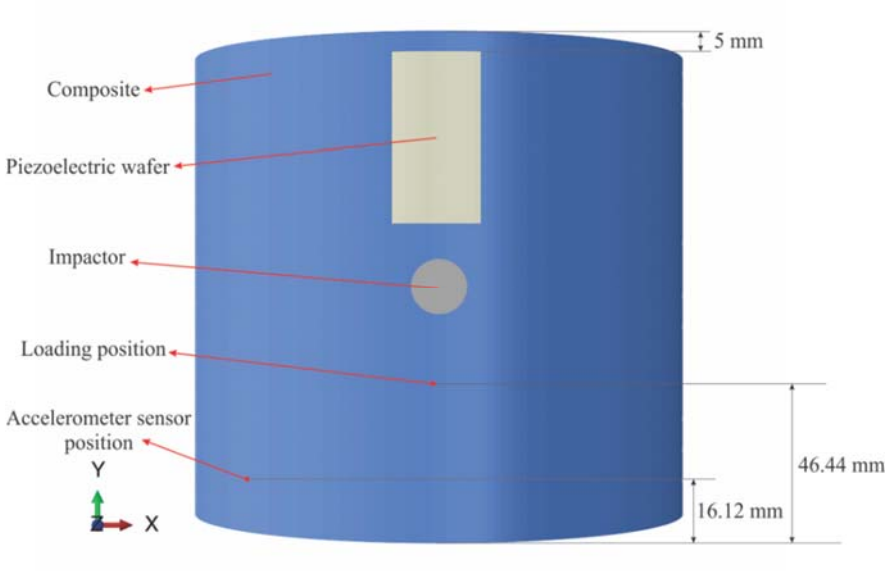

Figure 3-15 – Geometry of the FE model: composite cylinder with the MFC sensor attached on the outer surface

Once mechanical coupling is guaranteed, it is necessary to define suitable boundary conditions for obtaining the electric potential in the PZT sensor. In fact, the dielectric properties of the MFC transducer provide a homogeneous distribution of the induced electrical charges on the free surface of the transducer. Thus, all nodes of the piezoelectric transducer surface attached to the composite cylinder are considered to be electrically grounded. And the grounding nodes are assumed to have the potential equal to zero at any stage of strain. The purpose of grounding is to define a reference value for the induced voltages on the nodes of the free surface, which are measured. Thus, all nodes of the piezoelectric wafer free surface should respect to the equipotential condition.

Initial numerical analyses consist of modal analysis. Two lines of nodes in the cylinder FE model, which are in opposite position of the PZT sensor, have been restricted for all DOF ($U_x = U_y = U_z = UR_x = UR_y = UR_z = 0$ – Fig. 3-16) considering a future experimental setup. Modal analyses are performed using the eigenvalue solution in order to obtain the natural frequencies and the respective modal shapes of the intact structure. For these analyses, the frequency range from 0 to 1024 Hz is considered, and the results are used to evaluate the natural frequencies obtained via dynamic implicit analyses.

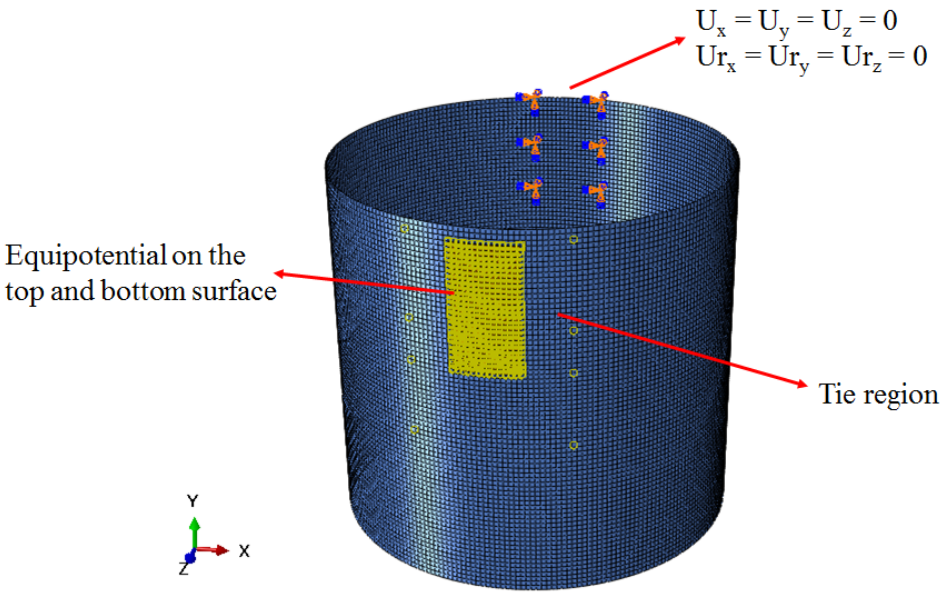

Figure 3-16 – FE model used in the modal numerical analyses for the composite cylinders

In a second stage, dynamic implicit analyses are done to obtain the FRFs for intact and damaged cylinder. The same boundary conditions (described previously for modal analyses)

are applied on the FE model. In addition, an impulse loading is applied on the surface of the cylinder close to the piezoelectric sensor (Fig. 3-17), simulating the excitation of a hammer at the "loading" point. Thus, for these analyses, the input signal is a transverse force of amplitude equal 1N localised in a specific node of the FE model. The frequency of the force is applied in a range from 0 to 1024 Hz, considering step size of 1.0 Hz for the numerical solution. Based on the input (impact of hammer) and output signals (acceleration of a specific node and PZT sensor measurement), Fast Fourier Transform (FFT) is applied to obtain the Frequency Response Functions (FRFs) for the PZT sensor (H_{12}) and for a specific node (H_{13} – simulating the position of an accelerometer) as shown in Fig. 3-17.

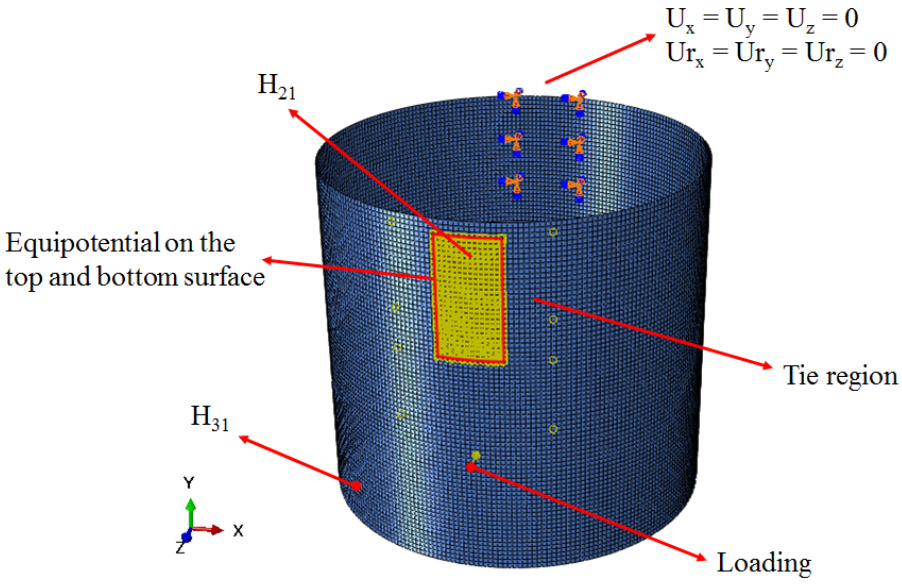

Figure 3-17 – FE model used in the dynamic implicit numerical analyses for the composite cylinders (before and after impact)

3.5.3. Low Velocity Impact Test Simulations

The impact numerical simulations are related to the investigation of how the damage evolves in the composite structure under impact loads using impact dynamic implicit analysis. Some composite specimens were damaged by impact loading, which was created via a drop tower apparatus. A certain mass is dropped from a certain height, hitting the test coupon. The nodes close to the border had all degrees of freedom restricted (Fig. 3-10 and Fig. 3-11). The damage model is used as proposed by Ribeiro *et al.* (2012a), which was implemented as a FORTRAN

Subroutine and linked to the finite element dynamic implicit algorithms (ABAQUS™ / Implicit). This material model is simple and it has a low computational cost. Also, the model parameters are easy to be obtained as shown by Ribeiro *et al.* (2012a).

The aluminium round impactor (diameter of 16 mm) was modelled using discrete rigid triangular elements (defined as R3D3 - ABAQUS™) and the mass, 1.268 Kg for the carbon plates and 3.24 Kg for the carbon cylinders, was applied in the mass point as shown by Fig. 3-18. The impactor was modelled using 1308 triangular elements with 656 nodes. Moreover, all rotations (Rx, Ry, Rz) as well as the Ux and Uy displacements were restricted in the impactor and initial velocity was applied in the impactor. The contact between the impactor and the plate was modelled by the Hard Contact algorithm for normal interactions and using the Penalty Method for tangential interactions. The friction coefficient was set at 0.3 for the tangential contact algorithm, which was provided by Ribeiro (2013a). Other important issue is the dissipation of impact energy. Part of the impact energy is dissipated by the irreversible process as damage (intra-ply failures and delamination) and another part is dissipated by damping effects. However, damping in composite materials depends on several factors, such as fibre volume fraction, composite lay-up, environmental factors, force magnitude, etc. (Zabaras and Pervez, 1990; Abrate, 1998). Also, the structure geometry has an important influence in the impact response. ABAQUS™ provides Rayleigh's model for direct integration dynamic analysis to simulate damping effects (Abaqus, 2014). The Rayleigh model was used to simulate the damping effects in the structure using a linear combination of mass and stiffness structure matrices, *i.e.* proportional damping.

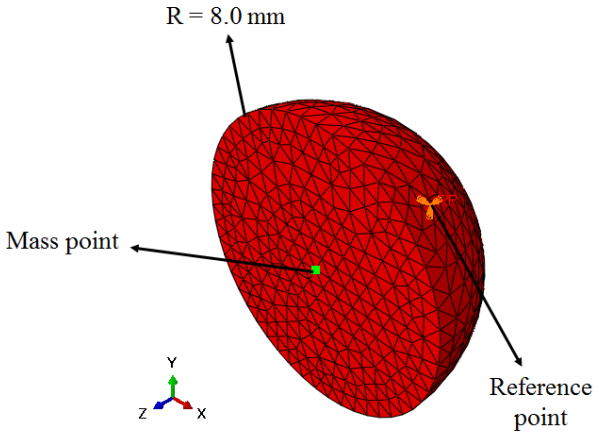

Figure 3-18 – Finite element model of the impactor.

All edges of the carbon fibre composite plates are clamped in the model ($U_x = U_y = U_z = UR_x = UR_y = UR_z = 0$ – Fig. 3-19(a)) to simulate the boundary conditions of the experimental setup. Two lines of nodes in the FE composite cylinder model, which are in opposite position of the impact point, as simply supported ($U_x = U_y = U_z = 0$ – Fig. 3-19(b)) to simulate the boundary conditions are constrained in the experimental setup as shown by Ribeiro (2013).

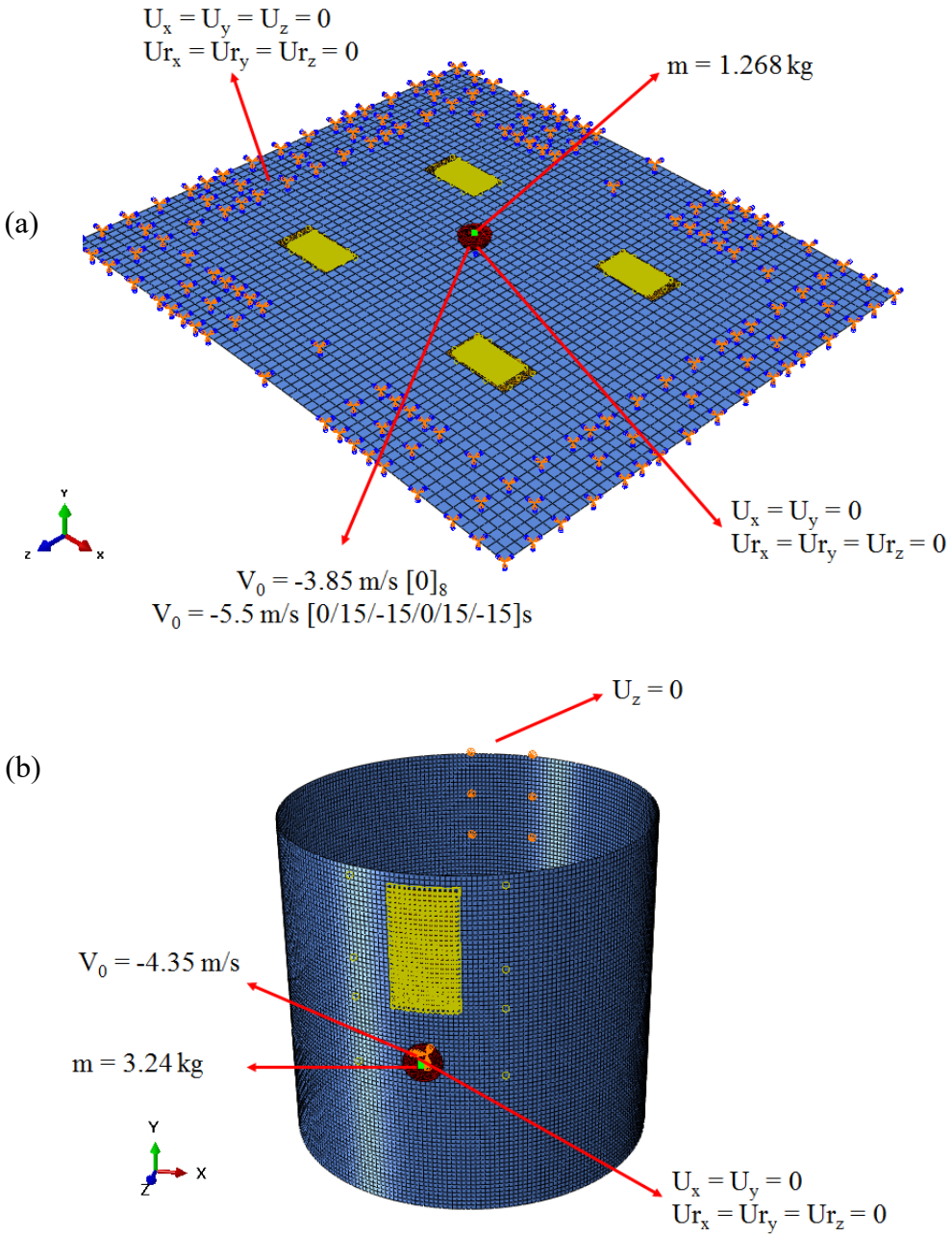

Figure 3-19 – Boundary conditions for impact dynamic implicit analysis (a) carbon plates with MFC sensor, and (b) carbon cylinders

3.6. Results and Discussion

This section presents the results for the dynamic response identified by numerical and experimental testing by using accelerometers and piezoelectric sensors. After that, damage metrics are presented to analyse the sensitivity of the vibration-based method for damage identification. The feasibility of using vibration-based NDT for damage identification in laminated composites is assessed by comparing the healthy (intact) and damaged structure for both experimental and computational results.

3.6.1. Carbon Fibre Composite Plates

First, all 63 measurements through the grid markers obtained and stored using the signal processing software Test.Lab via experimental tests were analysed. The markers are located at the points, which are hit by the hammer (Fig. 3-3). In addition, only 2 accelerometers are used, installed in the corner and close to the centre of the plate as shown in the Fig. 3-3. Figure 3-20 shows the FRF (magnitude and phase) and the coherence, for the positions H_{11}, H_{21}, H_{31}, and H_{41}, presented in the experimental tests (*cf.*, Fig. 3-4).

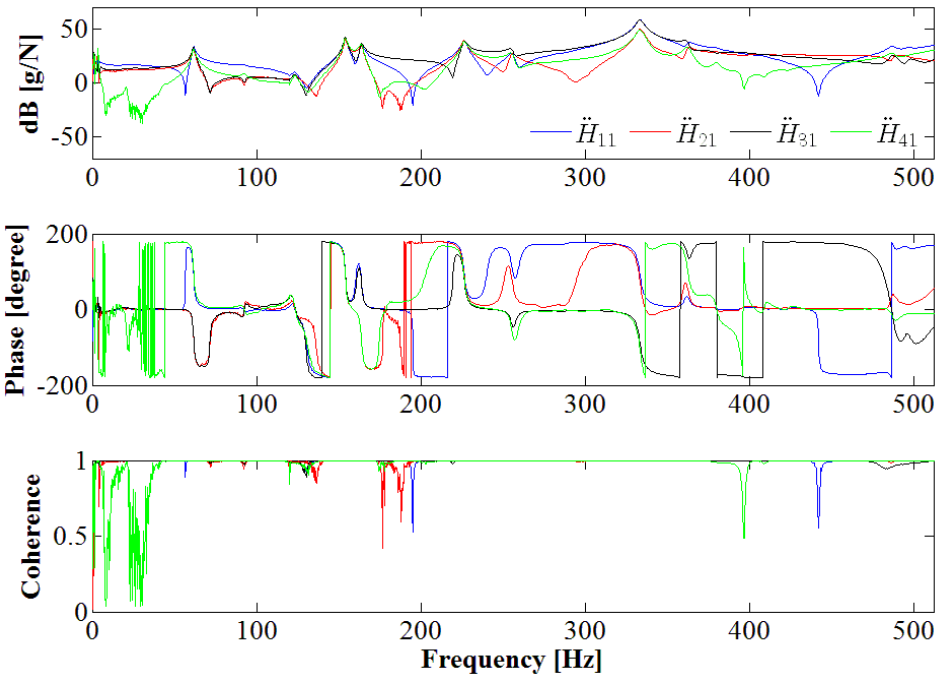

Figure 3-20 – FRF (magnitude and phase), and coherence for intact composite plate ($P01_{CF}^{E}$) using accelerometers.

Then, by using the Principle of the Reciprocity and the PolyMAX method, it was possible to obtain the natural frequencies and mode shape of the structures. The first five natural frequencies for the intact and damaged structure via experimental and numerical are shown in the Tab. 3-7 and Tab. 3-8. Figure 3-21 shows the first four mode shape of the carbon fibre composite plates.

Table 3-7. Experimental natural frequencies for intact and damaged (impact and hole) plates

Plate ID		Mode	ω_1 [Hz]	ω_2 [Hz]	ω_3 [Hz]	ω_4 [Hz]	ω_5 [Hz]
		Type	1st torsion	1st flexural	2nd torsion	2nd flexural	3rd torsion
$P01_{CF}^{E}$	*Intact*	*Freq.*	61.9	155.1	164.7	226.3	255.1
	Damaged	*Freq.*	64.2	158.4	126.3	225.5	255.8
	Relative difference		3.72%	2.13%	-23.32%	-0.35%	0.27%
$P02_{CF}^{E}$	*Intact*	*Freq.*	61.3	148.8	159.8	222.2	249.6
	Damaged	*Freq.*	60.3	150.0	159.6	221.5	251.4
	Relative difference		-1.63%	0.81%	-0.13%	-0.32%	0.72%
$P03_{CF}^{E}$	*Intact*	*Freq.*	60.2	153.1	158.5	224.8	250.4
	Damaged	*Freq.*	60.1	150.7	130.3	225.7	252.2
	Relative difference		-0.17%	-1.57%	-17.79%	0.40%	0.72%
$P05_{CF}^{E}$	*Intact*	*Freq.*	60.8	158.2	159.5	222.9	251.4
	Damaged	*Freq.*	62.1	153.3	136.1	222.5	251.3
	Relative difference		2.14%	-3.10%	-14.67%	-0.18%	-0.04%
$P06_{CF}^{E}$	*Intact*	*Freq.*	57.9	147.4	155.7	225.3	250.8
	Damaged	*Freq.*	57.9	147.9	119.3	222.7	249.9
	Relative difference		0.00%	0.34%	-23.38%	-1.15%	-0.36%
$P09_{CF}^{E}$	*Intact*	*Freq.*	95.4	132.9	250.6	316.2	349.4
	Damaged	*Freq.*	98.9	134.1	254.0	315.7	353.2
	Relative difference		3.67%	0.90%	1.36%	-0.16%	1.09%
$P10_{CF}^{E}$	*Intact*	*Freq.*	104.2	139.9	261.1	320.7	367.1
	Damaged	*Freq.*	106.4	140.3	263.4	320.1	369.0
	Relative difference		2.11%	0.29%	0.88%	-0.19%	0.52%
$P11_{CF}^{E}$	*Intact*	*Freq.*	106.1	145.6	266.0	332.9	379.7
	Damaged	*Freq.*	108.7	145.5	268.2	332.8	382.6
	Relative difference		2.45%	-0.07%	0.83%	-0.03%	0.76%
$P12_{CF}^{E}$	*Intact*	*Freq.*	107.4	147.4	269.0	333.0	382.8
	Damaged	*Freq.*	110.6	147.7	271.3	333.7	386.2
	Relative difference		2.98%	0.20%	0.86%	0.21%	0.89%

(*) Relative Difference = ($\omega_{damaged} - \omega_{intact}$) / ω_{intact}

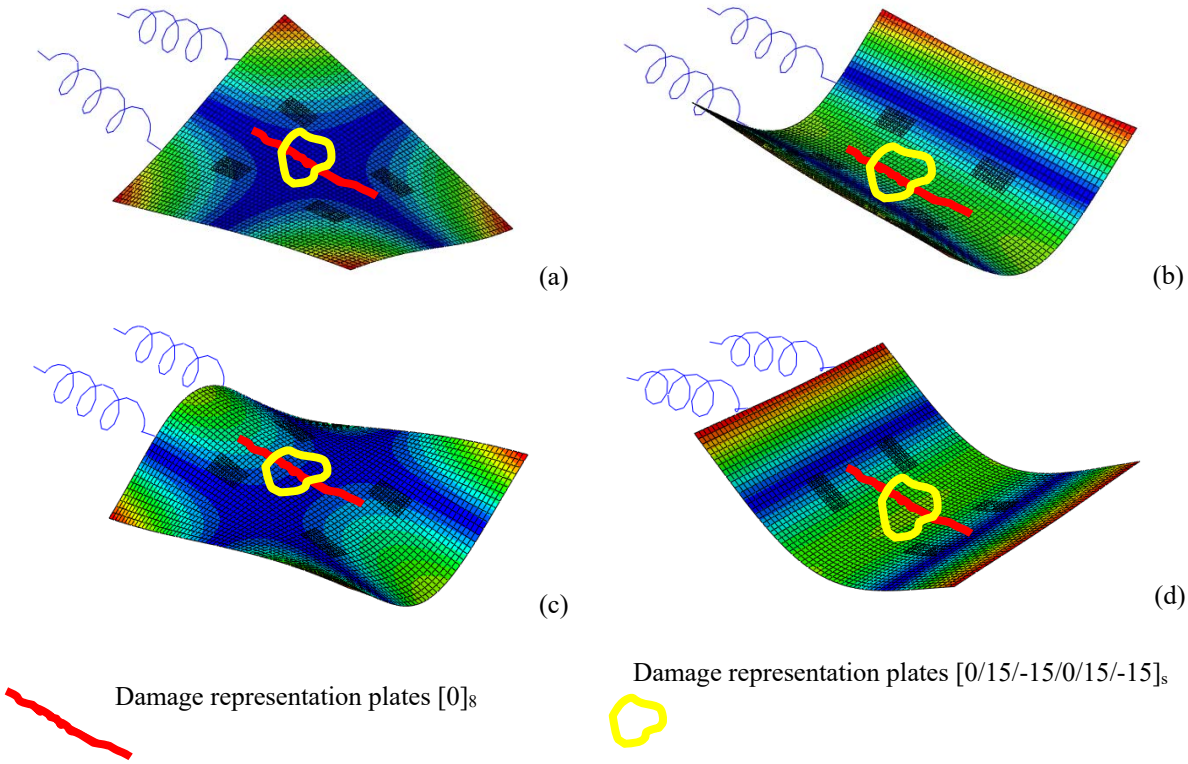

Figure 3-21 – Mode shape for the carbon fibre composite plates: (a) first torsion, (b) first flexure, (c) second torsion, (d) second flexure.

Table 3-7 demonstrated the differences between the intact and damaged data obtained from experimental analyses. It was possible to observe that as expected, some modes are more affected by damage. The largest difference is for 2nd mode (torsion), which is greater than 23.3%. This fact can be explained because the damage is not only in the nodal line region (blue). In addition, it can be also observed that the values obtained for the different types of damage in the plate do not exhibit high changes. However, for the Plates ($P01_{CF}^{E}$, $P03_{CF}^{E}$, $P05_{CF}^{E}$, $P06_{CF}^{E}$), the second and third modes are reversed due to the damage caused by impact event, *i.e.* the damage is not only in a nodal line region. Figure 3-21 shows the schematic representation of the damage in the two different stacking orientations. It is possible to conclude that for the first torsion mode both damage are in the nodal line, so there is no influence in the response of the plate. For second torsion mode, both damages are not only in the nodal line, so there is some influence in the global response. For first and second flexure mode.both damages are not in the nodal line. Table 3-7 shows that the resonance frequencies increase due to damage, this fact can be explained due to some factors, such as: uncertainties of modal parameters, uncertainties associated to the impact test, and this fact reinforces the need for a metric able to identify the damage not only using the natural frequencies. This explanation can be supported by the results present in the Tab. 3-8, for the computational analysis.

Figure 3-22 shows the FRF (magnitude and phase), and the coherence (position H_{11} of the plate $P11_{CF}^{E}$) for intact and damaged plate. Also, Figure 3-23 shows the FRF (magnitude and phase (position H_{11} of the plate $P11_{CF}^{C}$) for the intact and damaged plate. A free-free boundary condition is considered as presented in the experimental tests (*cf.*, Fig. 3-4).

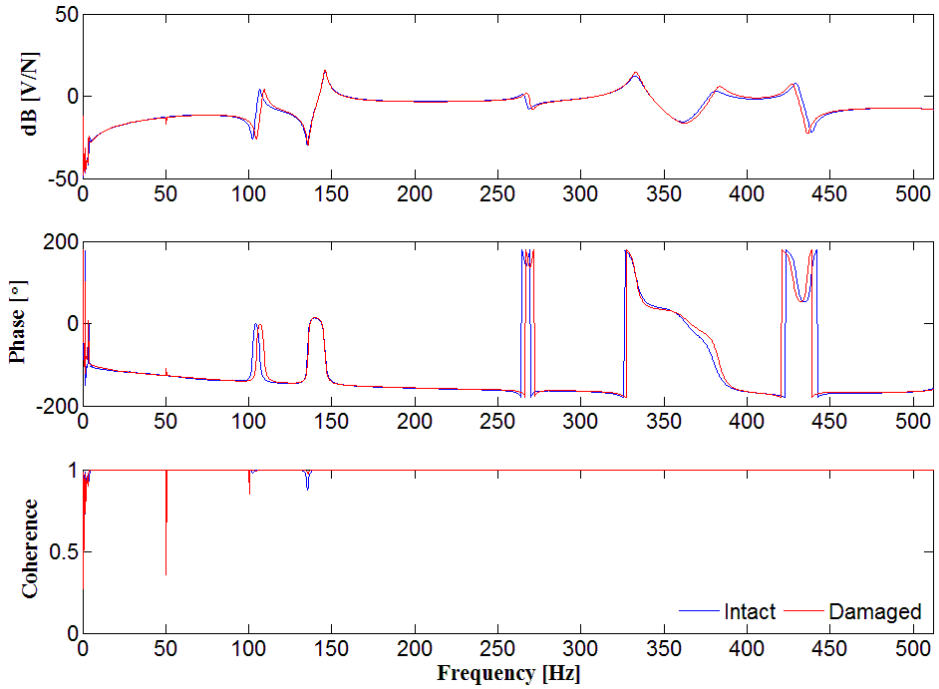

Figure 3-22 – FRF (magnitude and phase), and coherence for carbon fibre composite plate ($P11_{CF}^{E}$) using piezoelectric sensors (H_{11}).

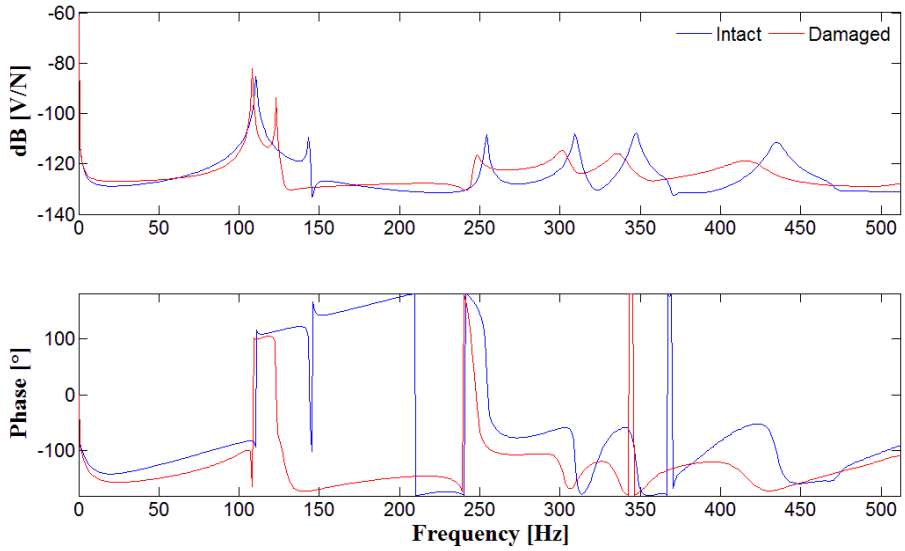

Figure 3-23 – FRF (magnitude and phase) for carbon fibre composite plate ($P11_{CF}^{C}$) using piezoelectric sensors (H_{11}).

The second mode presents significant difference. In this specific situation, this is due to the fact that the presence of the damage strongly changed the stiffness of the structure. However,

in the most of the cases, the damage is localized and the stiffness is almost unchanged. The small magnitude of the exciting pulse loading, keeps the structures could behaviour in a linear elastic regime, making the resonance frequencies remain practically unaltered. Therefore, an SHM metric, which accounts only for the variation in the resonance frequencies, may not be the best strategy for this type of damage.

Table 3-8. Numerical natural frequencies for intact and damaged (impact and hole) plates

		Mode	**ω_1 [Hz]**	**ω_2 [Hz]**	**ω_3 [Hz]**	**ω_4 [Hz]**	**ω_5 [Hz]**
		Type	1st torsion	1st flexural	2nd torsion	2nd flexural	3rd torsion
$P01_{CF}^{C}$	*Intact*	*Freq.*	59.0	149.1	156.2	224.2	248.2
	Damaged	*Freq.*	57.1	154.2	128.1	221.2	244.2
	Relative difference		-3.22%	3.42%	-17.99%	-1.34%	-1.61%
$P02_{CF}^{C}$	*Intact*	*Freq.*	58.4	144.5	157.4	231.5	258.8
	Damaged	*Freq.*	58.3	144.4	157.4	230.6	258.8
	Relative difference		-0.17%	-0.07%	0.00%	-0.39%	0.00%
$P05_{CF}^{C}$	*Intact*	*Freq.*	58.0	148.1	154.2	221.2	244.2
	Damaged	*Freq.*	55.1	149.1	127.1	218.2	240.2
	Relative difference		-5.0%	0.68%	-17.57%	-1.36%	-1.64%
$P09_{CF}^{C}$	*Intact*	*Freq.*	103.1	133.3	237.2	293.3	327.3
	Damaged	*Freq.*	100.1	114.1	231.2	287.3	317.3
	Relative difference		-2.91%	-14.40%	-2.53%	-2.05%	-3.06%
$P11_{CF}^{C}$	*Intact*	*Freq.*	110.1	143.1	254.2	309.3	347.3
	Damaged	*Freq.*	108.1	123.1	248.2	301.3	335.3
	Relative difference		-1.82%	-13.98%	-2.36%	-2.59%	-3.46%

(*) Relative Difference = ($\omega_{damaged} - \omega_{intact}$) / ω_{intact}

Table 3-8 shows the differences between the intact and damaged data obtained from numerical analyses. For the computational results the largest difference is for the 2nd torsion mode, which is greater than 17.55% for a plate with stacking sequence $[0]_8$, and for 1st flexural mode, which is greater than 14.40% for a plate with stacking sequence $[0/15/-15/0/15/-15]_s$. Thus, the structure presents the same behaviour of the experimental analysis between the intact and damaged plates. Figure 3-24 presents the first five mode shapes for the intact composite plate. Experimental and numerical data are compared.

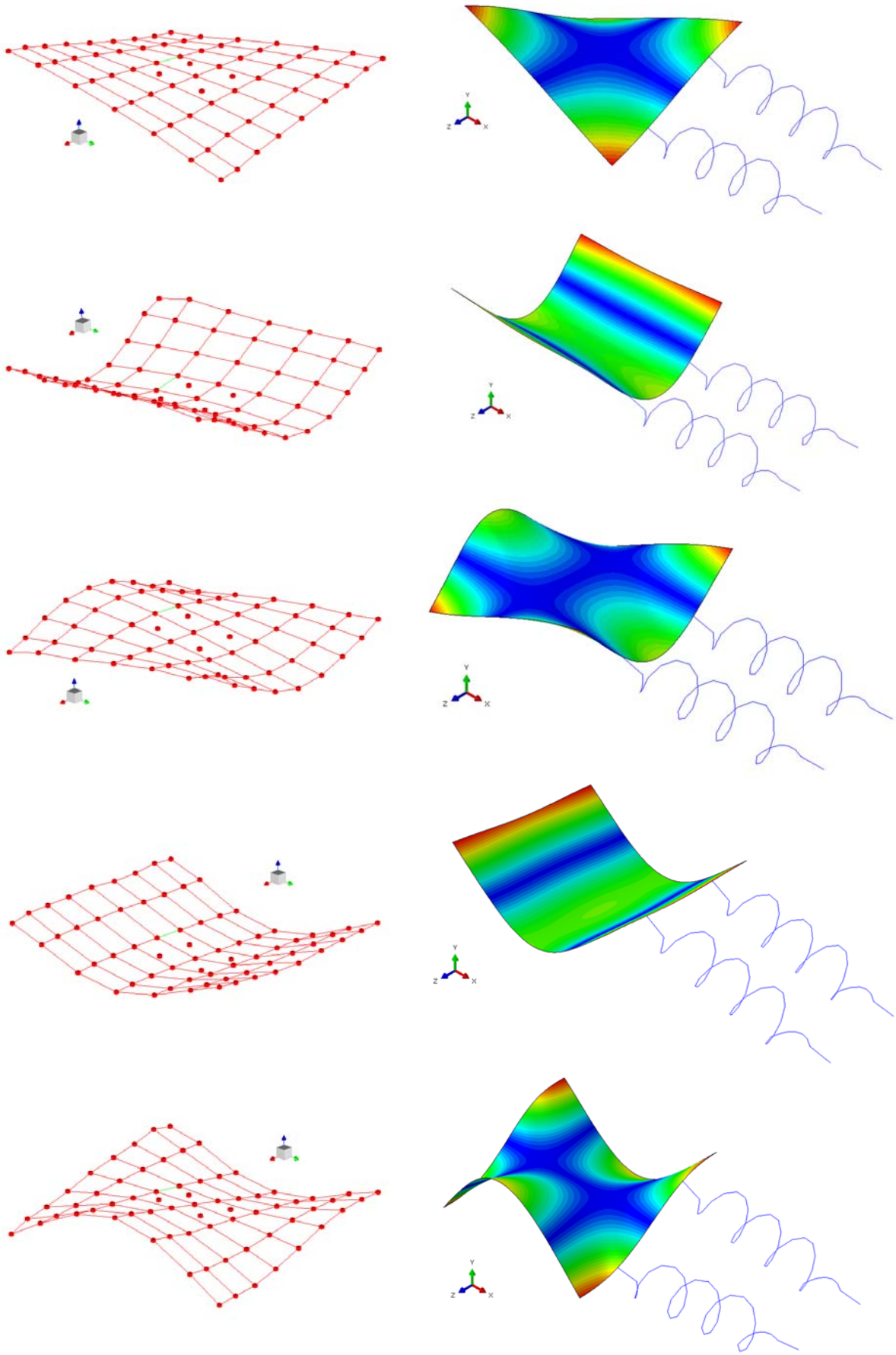

Figure 3-24 – First to fifth mode shape: Experimental and numerical for the intact composite plate

Figure 3-25 and 3-26 show the damaged area on the outer layer of the FE model for the composite plate via impact simulation (damaged area in red for outer layer) for the carbon fibre composite plate $P05_{CF}$ and $P09_{CF}$, respectively.

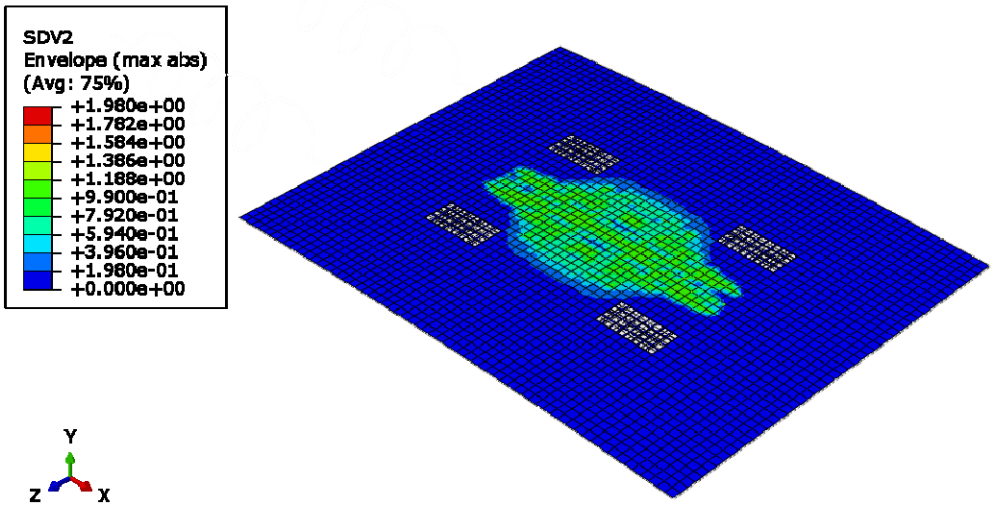

Figure 3-25 – Composite plate $P05_{CF}$ (after impact dynamic implicit analyses) with damaged zone in the outer layer for SDV2 (matrix damage).

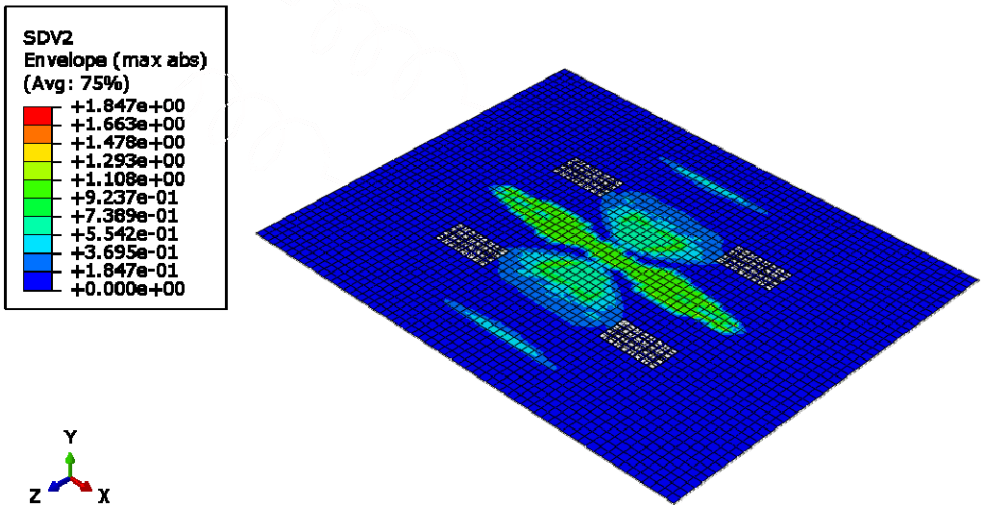

Figure 3-26 – Composite plate $P09_{CF}$ (after impact dynamic implicit analyses) with damaged zone in the outer layer for SDV2 (matrix damage).

Figure 3-25 and Figure 3-26 show the matrix damage zone provide by the damage model, it is possible to observe that, for the plates $[0]_8$, the damage is aligned with the fibre direction $[0]_8$. However, for the plates $[0/15/-15/0/15/-15]_s$, the damage exhibits 0°, 15° and -15° behaviour. To improve the computational model, a new damage model, which includes delamination effects need to be applied.

Figure 3-27 and Fig. 3-28, show the force *vs.* time and displacement *vs.* time for the experimental tests performed in the carbon fibre composite plates. The differences in the Force *vs* time graphics (Fig. 2-26) is because the different energy impact, (*cf.*, Tab. 3-3).

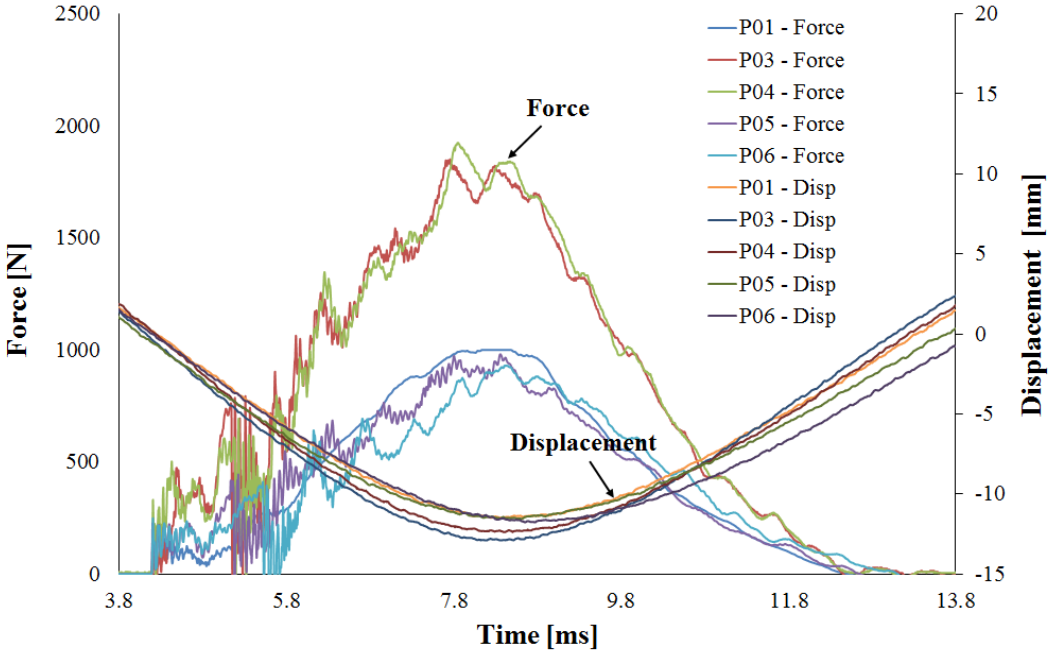

Figure 3-27 – Experimental results: force *vs.* time and displacement vs. time for the carbon fibre composite plates with stacking sequence $[0]_8$.

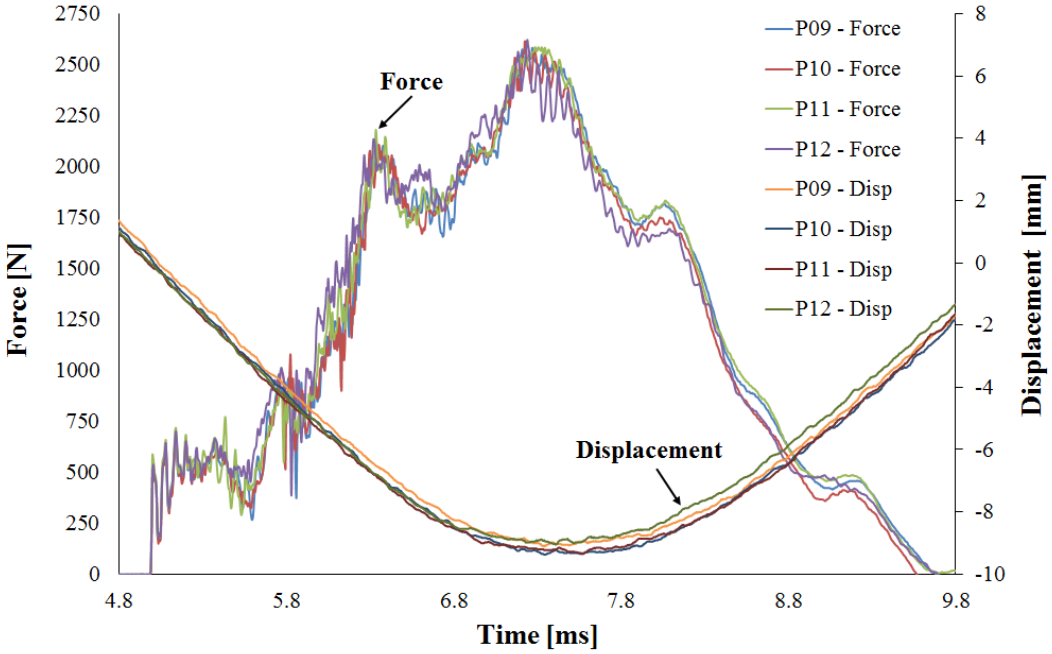

Figure 3-28 – Experimental results: force *vs.* time and displacement vs. time for the carbon fibre composite plates with stacking sequence $[0/15/-15/0/15/-15]_s$.

Table 3-9 shows the different damping factors by the experimental FRFs for the intact and damaged conditions of the plates. It can be observed that the damping values, for some modes, change when the resonance frequencies were modified by damage. When the values are compared to the data for different days, they remain almost unchanged. The energy dissipation and, hence, the damping increases with damage. This feature is stable and has a monotonic behaviour, therefore, damping can be confidently used as an alternative or complementary measure for damage assessment in spite of the accuracy of its identification. Modena *et al.* (1999) indicated that one of the advantages of using changes in damping is that undetectable cracks by using changes in natural frequencies (due to uncertainties or little decrease of frequencies) can cause important changes in the damping factor, allowing damage detection. In general, it is admitted that increasing the crack severity increases the damping factor. This occurs because the damping changes have the ability to detect the nonlinear behaviour, for example, dissipative effects caused by contact/friction between fracture surfaces.

Table 3-9. Damping factor obtained by experimental tests for the carbon fibre composite plates

Plate ID		**Mode**	**ζ_1 [Hz]**	**ζ_2 [Hz]**	**ζ_3 [Hz]**	**ζ_4 [Hz]**	**ζ_5 [Hz]**
		Type	1st torsion	1st flexural	2nd torsion	2nd flexural	3rd torsion
$P01_{CF}^{E}$	*Intact*	%	1.07	0.51	0.65	0.63	0.66
	Damaged	%	1.04	0.68	1.78	0.76	0.86
$P02_{CF}^{E}$	*Intact*	%	1.30	0.57	0.78	0.58	0.86
	Damaged	%	1.20	0.54	0.70	0.80	0.56
$P03_{CF}^{E}$	*Intact*	%	1.14	0.62	0.89	0.37	0.50
	Damaged	%	0.89	0.83	1.69	0.65	0.65
$P05_{CF}^{E}$	*Intact*	%	0.76	0.52	0.68	0.86	0.76
	Damaged	%	0.95	0.62	1.38	0.79	0.83
$P06_{CF}^{E}$	*Intact*	%	1.06	0.53	0.76	0.59	0.59
	Damaged	%	0.70	0.76	2.28	0.70	0.79
$P09_{CF}^{E}$	*Intact*	%	0.61	0.58	0.57	0.60	1.10
	Damaged	%	0.67	0.57	0.57	0.79	1.27
$P10_{CF}^{E}$	*Intact*	%	0.59	0.55	0.54	0.64	1.05
	Damaged	%	0.73	0.55	0.55	0.68	1.11
$P11_{CF}^{E}$	*Intact*	%	0.74	0.70	0.66	0.92	1.35
	Damaged	%	0.78	0.58	0.57	0.77	1.03
$P12_{CF}^{E}$	*Intact*	%	0.80	0.69	0.62	0.73	1.12
	Damaged	%	0.84	0.59	0.56	0.46	0.83

3.6.2. Glass Fibre Composite Plates

Two accelerometers are mounted on the plate as shown by the Fig. 3-6. Figure 3-29 and Figure 3-30 show the FRF (magnitude and phase), and the coherence (position H_{21}), for intact and damaged, unidirectional and bidirectional textile glass fibre composite plates, respectively. Free-free boundary conditions are applied in the experimental tests (*cf.*, Fig. 3-4).

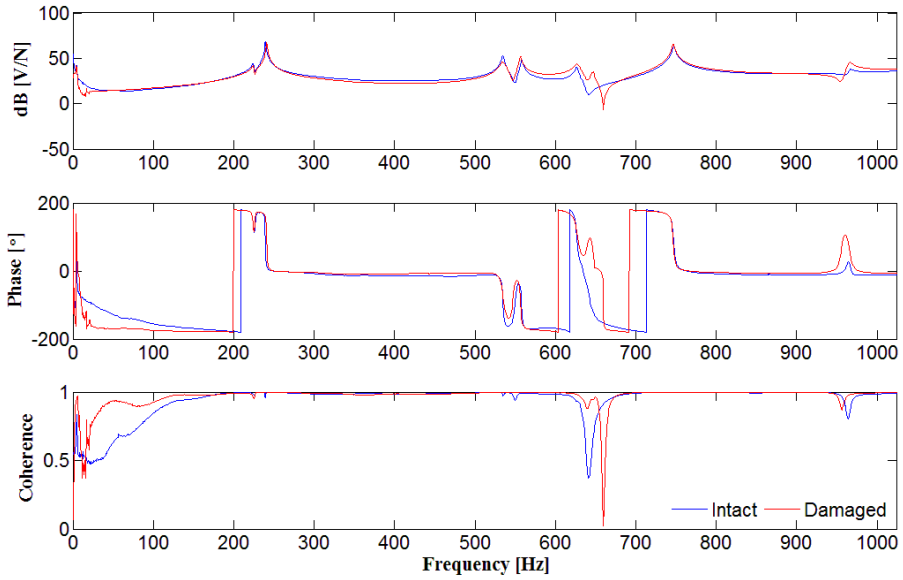

Figure 3-29 – FRF (magnitude and phase), and coherence for composite glass fibre unidirectional textile plate ($P02_{GF}$-UD^{E}) using accelerometers (H_{21}).

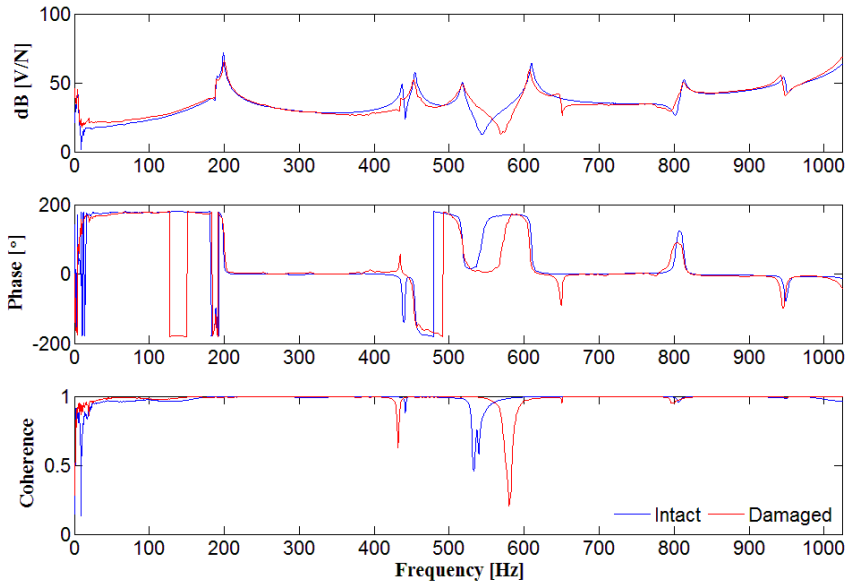

Figure 3-30 – FRF (magnitude and phase), and coherence for composite glass fibre bidirectional textile plate ($P06_{GF}$-BD^{E}) using accelerometers (H_{21}).

Based on the Figures 3-29 and 3-30, it is possible to observe some dips in the coherence values. This dips can be explained by the boundary conditions of the frame. The latter generates noise in these frequencies, causing the dips.

The PolyMAX method is used to estimate resonant frequencies of the structures. The first seven natural frequencies for the intact and damaged structure via experimental testing are shown in the Tab. 3-10. Small relative frequency differences are observed between intact and damaged FRFs. When the values are compared to the data for different days, they remain almost unchanged. The largest difference is 1.4% for the unidirectional textile glass fibre composite plates and 1.36% for the bidirectional textile glass fibre composite plates.

Table 3-10. Experimental natural frequencies for intact and damaged glass fibre plates.

Plate ID	Type		ω_1 [Hz]	ω_2 [Hz]	ω_3 [Hz]	ω_4 [Hz]	ω_5 [Hz]	ω_6 [Hz]	ω_7 [Hz]
	Intact	*Freq.*	226.3	229.6	527.2	535.3	619.5	734.0	959.7
P01_GF-UD^E	*Damaged*	*Freq.*	225.6	230.6	525.7	531.8	620.3	730.3	958.8
	Relative difference		-0.31%	0.44%	-0.28%	-0.65%	0.13%	-0.5%	-0.09%
	Intact	*Freq.*	224.4	238.9	534.2	557.4	626.4	756.7	965.5
P02_GF-UD^E	*Damaged*	*Freq.*	223.9	240.6	535.0	556.0	627.1	746.1	964.7
	Relative difference		-0.22%	0.71%	0.15	-0.25%	0.11%	-1.40%	-0.08%
	Intact	*Freq.*	230.5	244.6	550.0	576.1	636.1	770.4	988.6
P03_GF-UD^E	*Damaged*	*Freq.*	229.4	245.3	547.4	573.6	634.1	770.5	986.1
	Relative difference		-0.48%	0.29%	-0.47%	-0.43%	-0.31%	0.01%	-0.25%
	Intact	*Freq.*	189.3	198.3	436.8	453.9	517.1	609.1	811.1
P06_GF-B^E	*Damaged*	*Freq.*	188.8	199.8	434.4	452.3	517.1	606.3	812.0
	Relative difference		-0.26%	0.76%	-0.55%	-0.35%	0.00%	-0.46%	0.11%
	Intact	*Freq.*	188.3	196.4	429.1	448.2	513.0	598.5	804.3
P07_GF-B^E	*Damaged*	*Freq.*	188.2	196.2	425.6	445.8	515.2	593.3	802.9
	Relative difference		-0.05%	-0.10%	-0.82%	-0.54%	0.43%	-0.87%	-0.17%
	Intact	*Freq.*	191.6	203.8	451.2	463.8	523.6	621.6	826.9
P08_GF-B^E	*Damaged*	*Freq.*	189.7	202.7	448.1	457.5	523.3	618.3	822.3
	Relative difference		-0.99%	-0.54%	-0.69%	-1.36%	-0.06%	-0.53%	-0.56%

(*) Relative Difference = = ($\omega_{damaged} - \omega_{intact}$) / ω_{intact}

According to Hearn *et al.* (1991), mode shape, frequency and damping (parameters of the natural modes) are products of a structure (mass and stiffness). Deterioration of a structure can alter stiffness and change the modal parameters. The magnitude of change depends on both

the severity and the location of the deterioration, and a single deterioration event will affect each vibration mode differently, having a marginal differences on certain modes, depending on the location of damage. And, in case of the composite structures, it is possible to say that depends on the fibre orientations, as well.

Table 3-11 shows different damping factors obtained by the experimental FRFs for the intact and damaged settings of the plates. Damping values for some modes change when the resonance frequencies were modified by damage. Thus, damage detection in a structure based on damping is an alternative procedure. This occurs because the damping changes have the ability to detect the nonlinear behaviour, for example, dissipative effects caused by cracks. It appears natural to expect that an interesting indicator for damage detection would be the damping changes and dissipative effects due to the friction between crack surfaces.

Table 3-11. Damping factor obtained by experimental tests for glass fibre composite plates.

Plate ID		Mode	ζ_1 [Hz]	ζ_2 [Hz]	ζ_3 [Hz]	ζ_4 [Hz]	ζ_5 [Hz]	ζ_6 [Hz]	ζ_7 [Hz]
P01_CF^E	*Intact*	*%*	0.36	0.21	0.26	0.23	0.25	0.24	0.26
	Damaged	*%*	0.39	0.19	0.43	0.21	0.31	0.37	0.22
P02_CF^E	*Intact*	*%*	0.48	0.21	0.24	0.22	0.31	0.23	0.29
	Damaged	*%*	0.42	0.22	0.55	0.23	0.50	0.20	0.33
P03_GF-UD^E	*Intact*	*%*	0.32	0.21	0.20	0.24	0.30	0.27	0.33
	Damaged	*%*	0.32	0.19	0.68	0.25	0.45	0.27	0.34
P06_GF-B^E	*Intact*	*%*	0.65	0.28	0.24	0.27	0.33	0.23	0.27
	Damaged	*%*	0.48	0.56	0.25	0.49	0.65	0.26	0.55
P07_GF-B^E	*Intact*	*%*	0.43	0.44	0.27	0.28	0.32	0.23	0.29
	Damaged	*%*	0.46	0.81	0.37	0.28	0.46	0.52	0.51
P08_GF-B^E	*Intact*	*%*	0.50	0.36	0.25	0.25	0.39	0.25	0.25
	Damaged	*%*	0.52	0.75	0.29	0.43	0.38	0.72	0.46

3.6.3. Carbon Fibre Composite Cylinders

Numerical analysis modal is performed using the eigenvalue solution to obtain the natural frequencies (Tab. 3-12) and the respective mode shapes of the intact structure (Fig. 3-31). For these analyses, the frequency range from 0 to 1000 Hz was considered, and the results were used to evaluate the natural frequencies obtained via dynamic implicit analyses.

Table 3-12. Natural frequencies for intact composite cylinder with PZT sensor via numerical modal analysis (Medeiros *et al.*, 2014a).

Mode	**ω_1 [Hz]**	**ω_2 [Hz]**	**ω_3 [Hz]**	**ω_4 [Hz]**	**ω_5 [Hz]**	**ω_6 [Hz]**
Frequency [Hz]	105.66	194.31	293.02	526.50	616.86	949.17
Figure 3-31	(a)	(b)	(c)	(d)	(e)	(f)

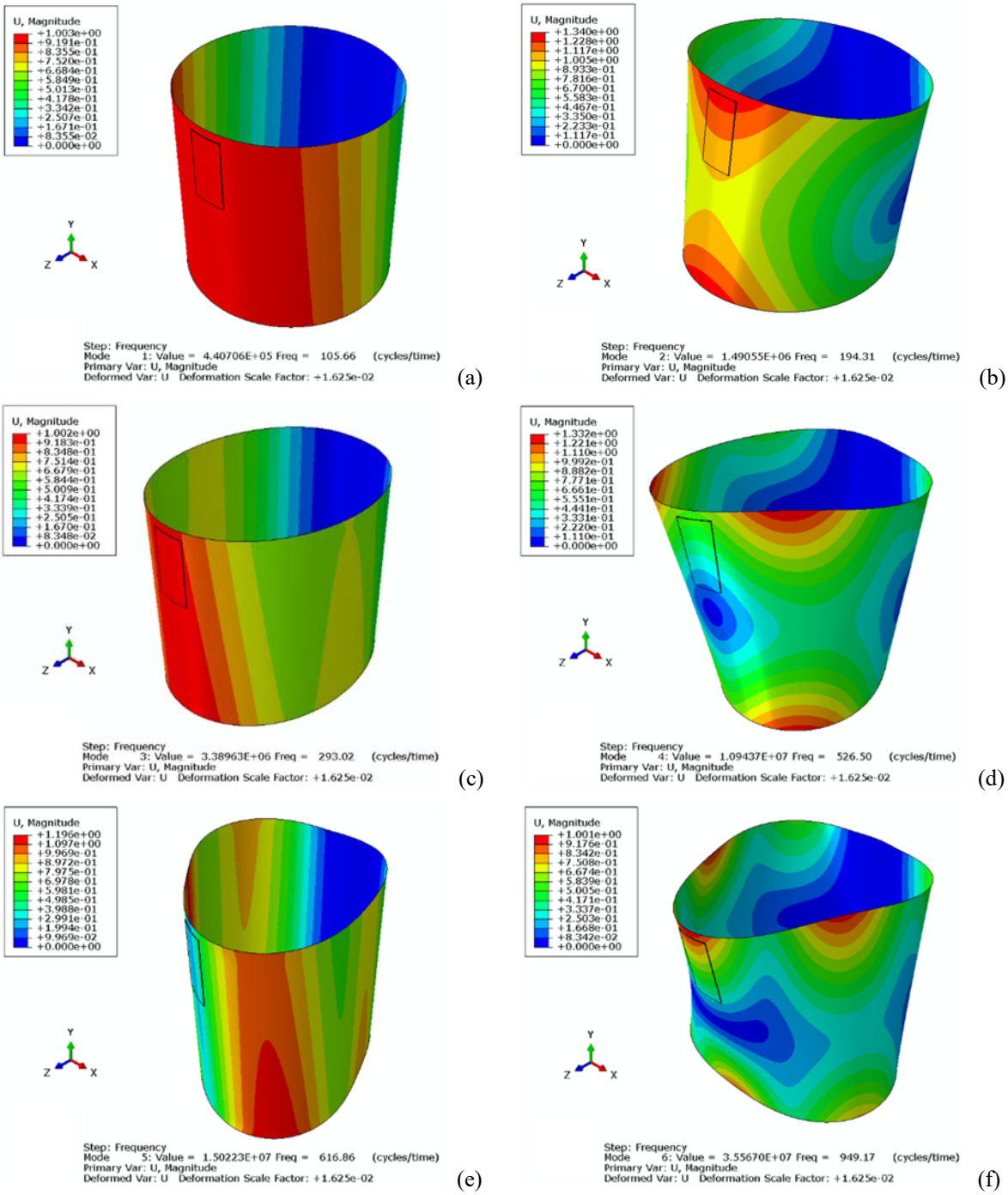

Figure 3-31 – Mode shapes for the first six natural frequencies via numerical modal analysis (Medeiros *et al.*, 2014a)

The second set of numerical simulations consists on carrying out dynamic implicit analyses via Finite Element Method in order to obtain the FRFs for undamaged cylinder. The same boundary conditions (described previously for modal analyses) are applied on the FE model. Based on the input (impact of hammer) and output signals (acceleration of a specific node and PZT sensor measurement), Fast Fourier Transform (FFT) was applied to obtain the Frequency Response Functions (FRFs) for the PZT sensor (H_{21}) and for a specific node (H_{31} – simulating the position of an accelerometer) as shown by the Fig. 3-16. Table 3-13 compares the natural frequency for the intact structure using modal analyses and dynamic implicit analyses. Relative differences are not greater than 2.21%. This difference can be explained by the solution type, while the modal analysis performed the simulation in the frequency domain, the dynamic implicit analysis performed the simulation in the time domain. After, a Fast Fourier Transform (FFT) is applied to obtain the data in the frequency domain.

Table 3-13. Natural frequencies for intact composite cylinder: Numerical Modal Analyses (MA) *vs.* Dynamic Implicit Analyses (DIA) (Medeiros *et al.*, 2014a).

	Mode	ω_1 [Hz]	ω_2 [Hz]	ω_3 [Hz]	ω_4 [Hz]	ω_5 [Hz]	ω_6 [Hz]
Modal Analyses (MA)	**Frequency [Hz]**	105.66	194.31	293.02	526.50	616.86	949.17
DIA – H_{12}	**Frequency [Hz]**	108.0	197.0	297.0	532.1	622.1	950.1
DIA – H_{13}	**Frequency [Hz]**	107.0	197.0	297.0	531.1	622.1	950.1
$\Delta^{(*)}$ – Modal *vs.* DIA-H_{12}		2.21%	1.38%	1.36%	1.06%	0.85%	0.10%
$\Delta^{(*)}$ – Modal *vs.* DIA-H_{13}		1.27%	1.38%	1.36%	0.87%	0.85%	0.10%

(*)Δ = (DIA – MA) / MA

The third set of numerical simulations is related to damage evolution in composite cylinders under impact loads (via dynamic implicit analyses). In this work, the composite cylinders are damaged by impact loading of a drop tower. The damage model evaluates fibre and matrix damage for normal and shear stresses. Considering the cylinder layup and impact energy level, all layers had matrix damaged due to shear and/or normal stresses. Only two internal layers exhibit the damage. Ribeiro *et al.* (2012a, 2013a, 2013b) gives more details about the damage model. Furthermore, Fig. 3-32 only shows the damage zone in the first layer (outer layer of the cylinder) in the final step of the numerical simulation for the cylinder Type A. It is very important to mention that this damaged model was used in the 4th analyses, *i.e.* vibration analyses of the damaged structure with the material properties reduced in the red zone.

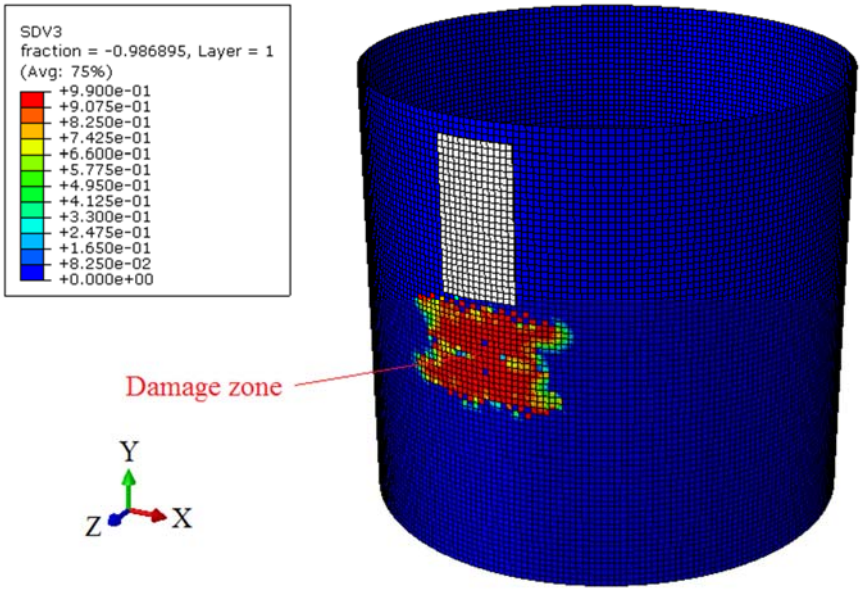

Figure 3-32 – Damaged zone in the outer layer for the dynamic implicit analyses carbon fibre cylinder Type A (Medeiros et al., 2014a).

Table 3-14 shows the comparison between the frequencies obtained via dynamic implicit analyses for intact and damaged structure using PZT sensor (H_{12}) or via a specific node of FE model (H_{13}), which represents the accelerometer in Fig 3-15.

Table 3-14. Natural frequencies for intact and damaged composite cylinder with PZT sensor (Medeiros *et al*, 2014a)

	Mode	ω_1 [Hz]	ω_2 [Hz]	ω_3 [Hz]	ω_4 [Hz]	ω_5 [Hz]	ω_6 [Hz]
Intact H_{12}	**Freq. [Hz]**	108.0	197.0	297.0	532.1	622.1	950.1
Intact H_{13}	**Freq. [Hz]**	107.0	197.0	297.0	531.1	622.1	950.1
Damaged H_{12}	**Freq. [Hz]**	107.0	197.0	296.0	531.1	621.1	946.1
Damaged H_{13}	**Freq. [Hz]**	108.0	197.0	297.0	531.1	621.1	946.1
$\Delta^{(*)}$: Intact *vs.* Damaged H_{12}		-0.93%	0.0%	-0.34%	-0.19%	-0.16%	-0.42%
$\Delta^{(*)}$: Intact *vs.* Damaged H_{13}		0.93%	0.0%	0.0%	0.0%	-0.16%	-0.42%

(*) $\Delta = (H_d - H_i) / H_i$

Figure 3-33 and 3-34 show the FRF (magnitude and phase) for the positions H_{21}, and H_{31}, presented in the computational model (*cf.*, Fig. 3-15). There are small frequency differences between intact and damaged FRFs.

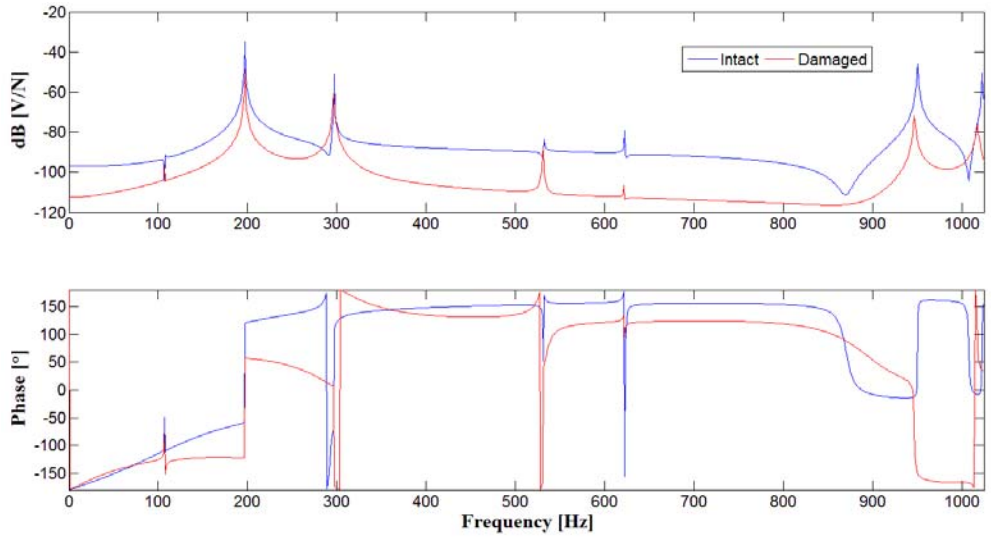

Figure 3-33 – FRF of the composite cylinder by using PZT sensor (H_{21}): undamaged *vs.* damaged.

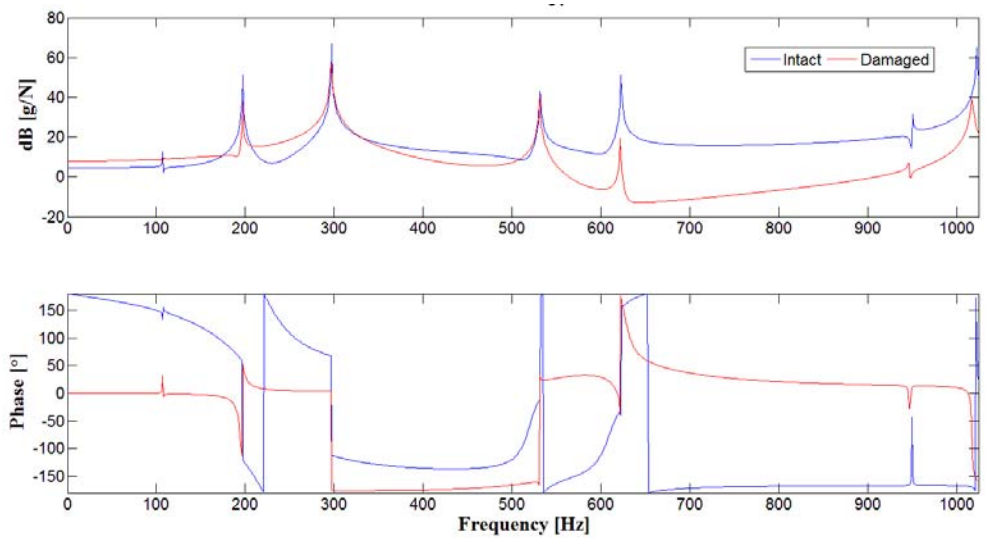

Figure 3-34 – FRF of the composite cylinder by using accelerometer sensor (H_{31}): undamaged *vs.* damaged.

Figure 3-35 to Fig. 3-37, show the force *vs.* time and displacement *vs.* time for the experimental impact tests performed on the carbon fibre composite cylinders. For type A cylinders under 31 J impact energy, the force *vs.* time and displacement *vs.* time results are shown in Fig. 3-34. The graphics show that the repetitions produce almost identical results. The 31 J impact tests on Type A cylinders (Fig. 3-34) show that the force increases quickly close to 5.2 ms and then a sudden force drop occurs. After that, the force increases again and a new sudden drop occurs. The maximum force peaks (around 2500 N) occur from 7 ms to 7.5 ms for all coupons. Just after this interval, the force drops again. The maximum force peak happens around 0.0078 s and the maximum displacement at 11.1 ms (response delay of 3.3 ms). This trend repeats close to 8.7 ms of the impact event.

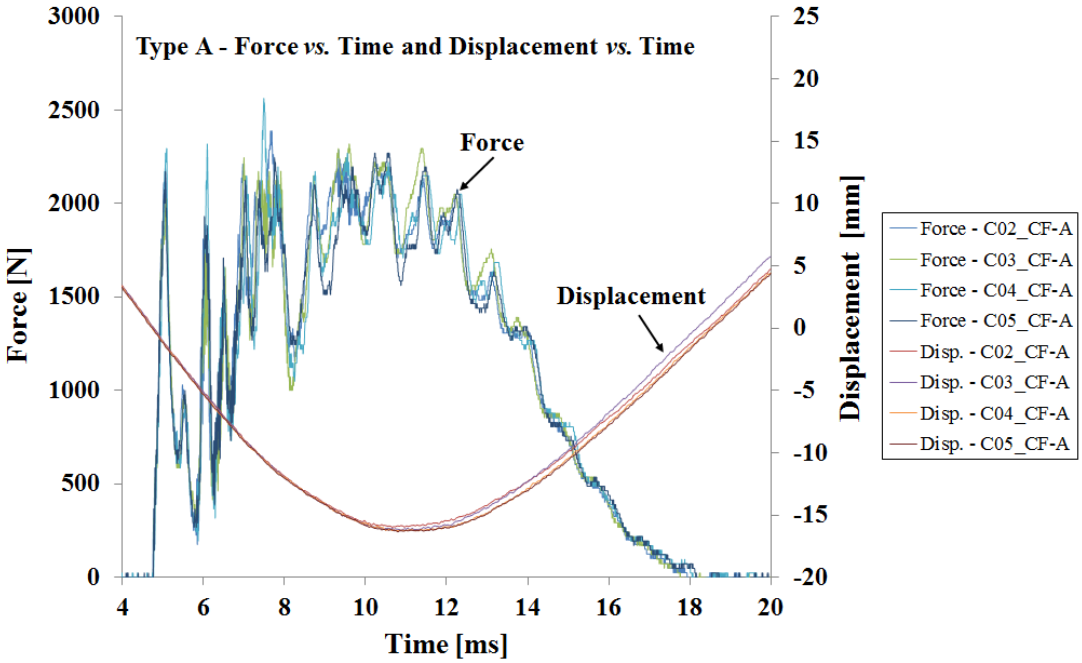

Figure 3-35 – Experimental results: force *vs.* time and displacement vs. time for the carbon fibre composite cylinders type A (Ribeiro *et al.*, 2015)

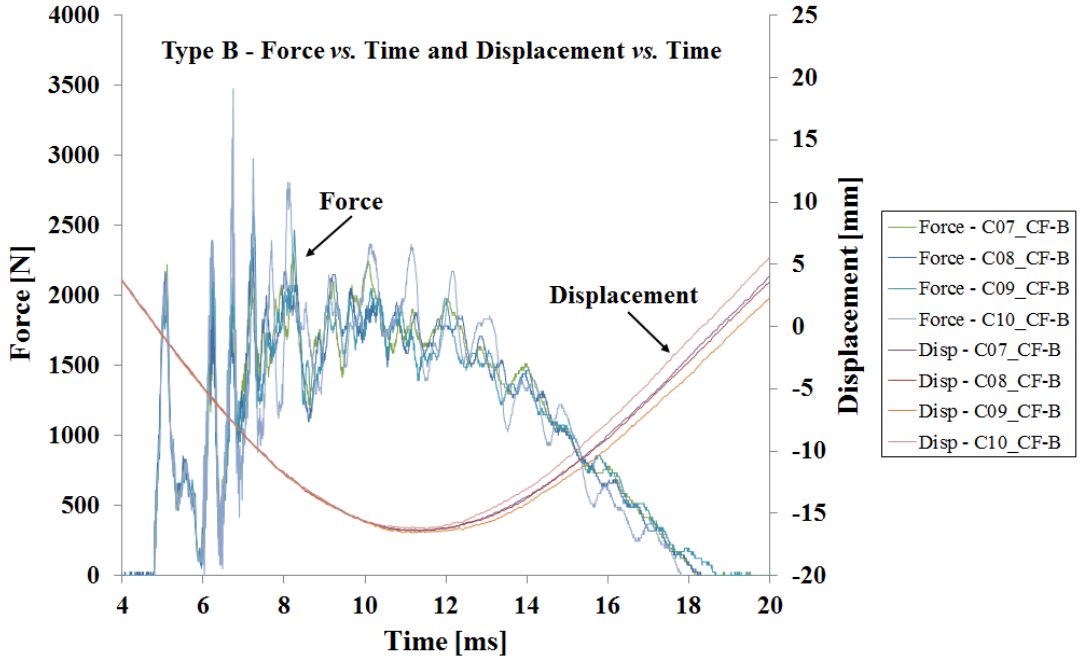

Figure 3-36 – Experimental results: force *vs.* time and displacement vs. time for the carbon fibre composite cylinders type B (Ribeiro *et al.*, 2015)

For type B cylinders, the results of 31 J impact tests (force vs. time and displacement vs. time) are shown in Fig. 3-36. All experimental data show a good repeatability of the tests. At a same high level of impact energy, type A cylinders and type B cylinders show a similar pattern of peaks and valleys. However, the force peak intensity is higher for cylinder type B,

due to the lay-up and the differences in the thickness of each layer. Delaminations, matrix damage and indentation marks (inelastic deformation) are detected for type B cylinders under 31 J impact tests, as well.

Figure 3-37 shows the force *vs.* time and displacement *vs.* time results for type C cylinders under 31 J impact test. The same evaluation for type A and B cylinders is applicable for those cylinders. Besides, this configuration reaches the highest value of force peak over all cylinders type. Delaminations, matrix damage and indentation marks (inelastic deformation) are also detected for type C cylinders.

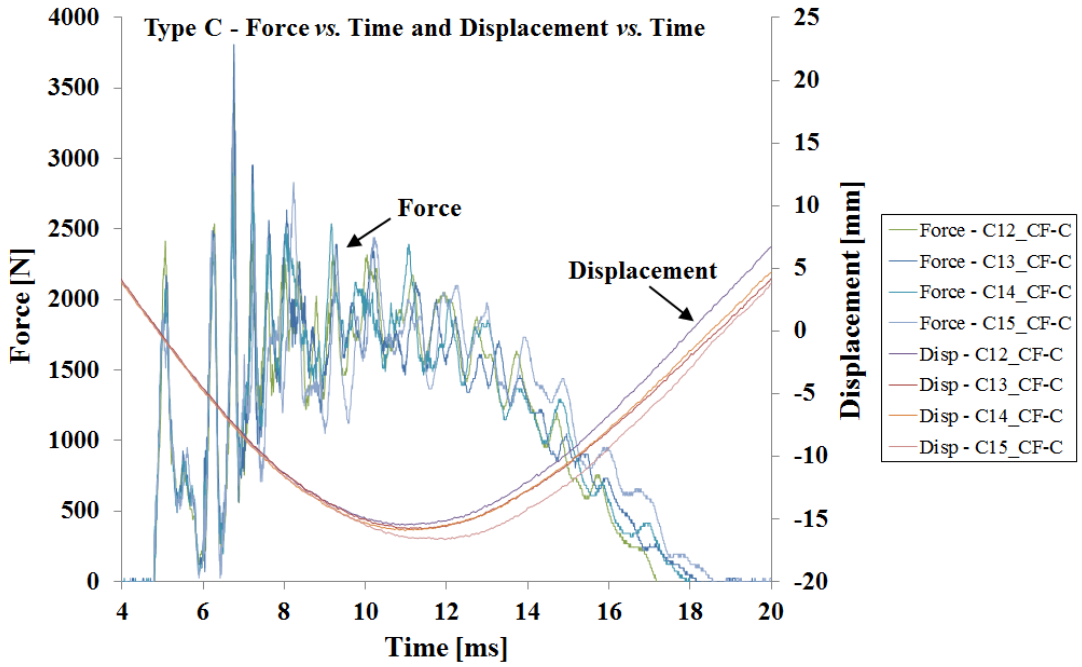

Figure 3-37 – Experimental results: force *vs.* time and displacement vs. time for the carbon fibre composite cylinders type C (Ribeiro *et al.*, 2015)

Changes in material properties such as reduced stiffness, increased damping or reduction in mass should in theory change the modal parameters of the structure. This change may be measured by dynamic testing and gives an indication of damage in the system. Then, in order to detect the damage using the vibration based method, the free-free boundary condition is considered as presented in the experimental tests (*cf.*, Fig. 3-8). Figures 3-38 to 3-40 show the FRF (magnitude and phase), and the coherence (position H_{21}) for intact and damaged carbon fibre composite cylinder, Type A, Type B, and Type C, respectively.

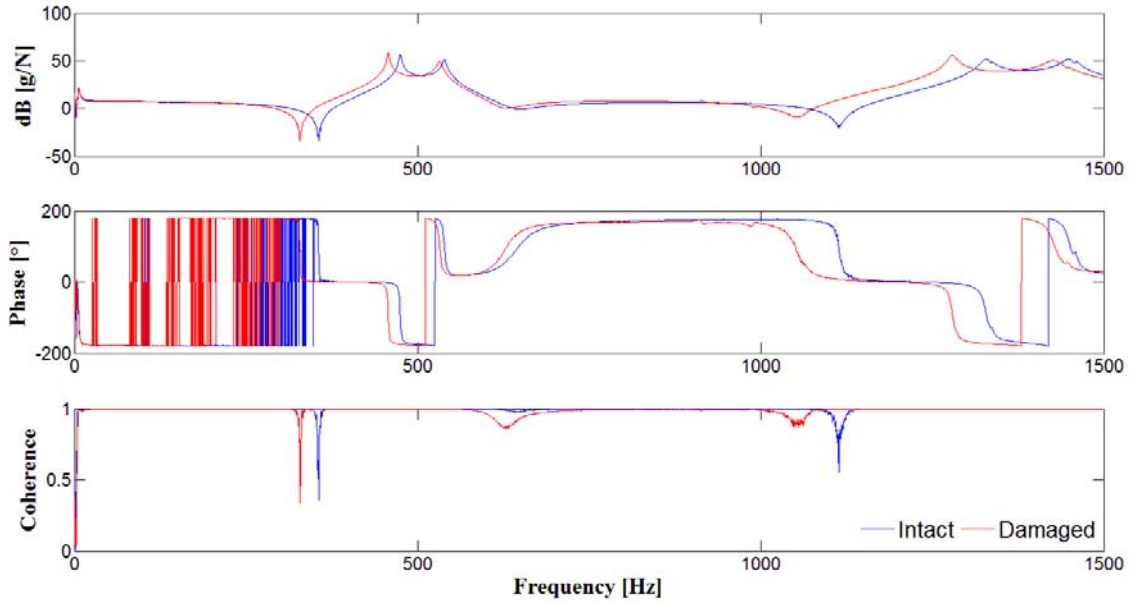

Figure 3-38 – FRF (magnitude and phase), and coherence for composite carbon fibre cylinder ($C02_{CF}$-A^{E}) using accelerometers (H_{21}).

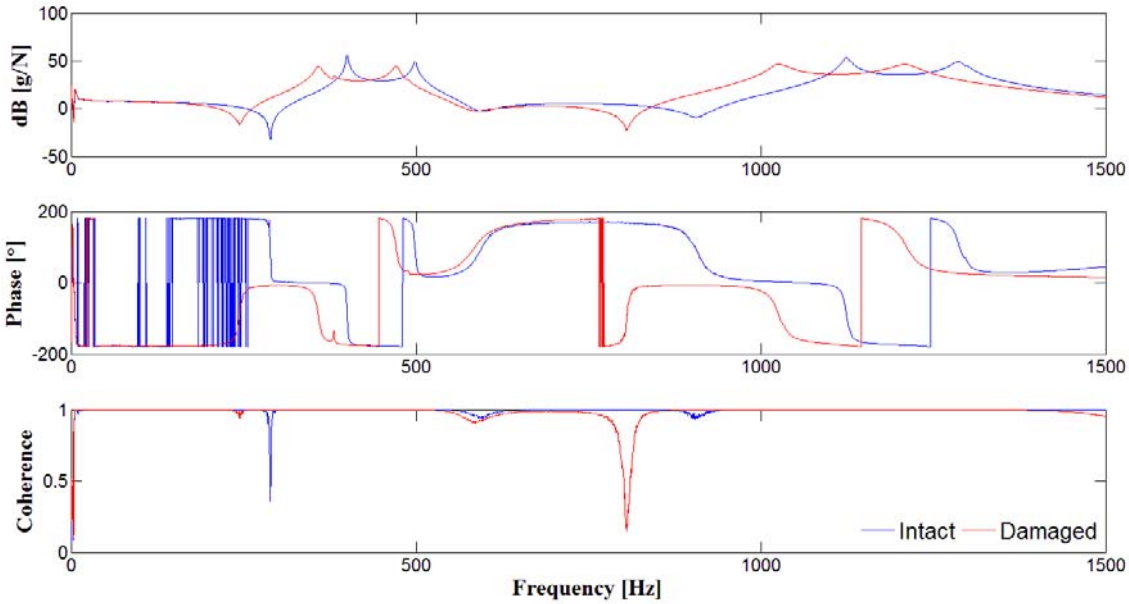

Figure 3-39 – FRF (magnitude and phase), and coherence for composite carbon fibre cylinder ($C07_{CF}$-B^{E}) using accelerometers (H_{21}).

Figures 3-38 to 3-40 show that the changes from the intact to damaged structure are significant. The stiffness of structure decreases due to the impact damage. This fact can be confirmed when the damage region is observed in more details (see section 4.4.2) by using shearography speckle technique. The cylinders present fibre, matrix and delamination damage.

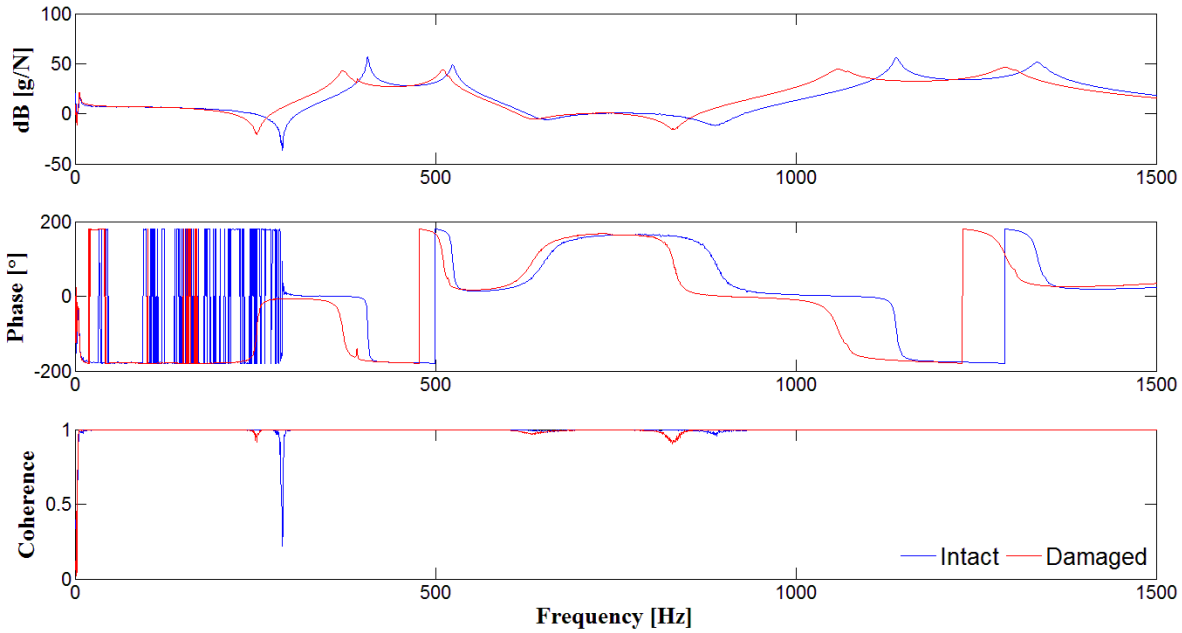

Figure 3-40 – FRF (magnitude and phase), and coherence for carbon fibre composite cylinder ($P12_{CF}$-C^{E}) using accelerometers (H_{21}).

Then, the PolyMAX method is used again to obtain the resonant frequencies of the structures. The first four natural frequencies (Hz) for the intact and for damage experimental scenarios have been computed separately for reference and are listed in the Tab. 3-15. Cylinders type A exhibit small variation in the resonant frequency, the largest difference is greater than 5.3%. However, for the cylinders type B and C the largest difference are greater than 14.1% and 14.0%, respectively (*cf.* Tab 3-15). The differences between the cylinders type A, B and C can be explained due the different stacking orientation, type A $[90/60/-60/90/60/-60/90]_s$, type B $[90/30/-30/90/30/-30/90]_s$, and type C $[90/30/-60/60/-60/30/-30]_s$.

Table 3-16 shows the different damping factors by the experimental FRFs for the intact and damaged conditions of the cylinders. It can be observed that the damping values, for some modes, changed when the resonance frequencies were modified by damage. This occurs because the damping changes have the ability to detect the nonlinear behaviour, for example, dissipative effects caused by cracks. It appears naturally as expected, and a good damage metric can be proposed for damage detection, considering damping changes and dissipative effects due to the friction between crack surfaces.

Table 3-15. Experimental natural frequencies for intact and damaged carbon fibre cylinders

Plate ID	Type		ω_1 [Hz]	ω_2 [Hz]	ω_3 [Hz]	ω_4 [Hz]
$C01_{CF}$-A^E	*Intact*	*Freq.*	474.18	538.73	1327.99	1450.16
$C02_{CF}$-A^E	*Damaged*	*Freq.*	456.96	531.93	1278.56	1426.97
	Relative difference		-3.63%	-1.26%	-3.72%	-1.60%
$C03_{CF}$-A^E	*Damaged*	*Freq.*	454.32	531.08	1269.78	1425.78
	Relative difference		-4.19%	-1.42%	-4.38%	-1.68%
$C04_{CF}$-A^E	*Damaged*	*Freq.*	449.04	524.07	1258.58	1403.39
	Relative difference		-5.30%	-2.72%	-5.23%	-3.23%
$C05_{CF}$-A^E	*Damaged*	*Freq.*	451.22	524.69	1261.84	1402.12
	Relative difference		-4.84%	-2.61%	-4.98%	-3.31%
$C06_{CF}$-B^E	*Intact*	*Freq.*	399.85	498.09	1123.43	1287.18
$C07_{CF}$-B^E	*Damaged*	*Freq.*	358.07	470.70	1025.22	1209.92
	Relative difference		-10.45%	-5.50%	-8.74%	-6.00%
$C08_{CF}$-B^E	*Damaged*	*Freq.*	352.51	470.07	1015.68	1202.18
	Relative difference		-11.84%	-5.63%	-9.59%	-6.60%
$C09_{CF}$-B^E	*Damaged*	*Freq.*	343.50	468.23	1008.09	1172.57
	Relative difference		-14.09%	-5.99%	-10.27%	-8.90%
$C10_{CF}$-B^E	*Damaged*	*Freq.*	369.59	488.80	1052.18	1252.03
	Relative difference		-7.57%	-1.87%	-6.34%	-2.73%
$C11_{CF}$-C^E	*Intact*	*Freq.*	405.70	523.56	1138.94	1335.34
$C12_{CF}$-C^E	*Damaged*	*Freq.*	371.15	510.17	1057.89	1291.21
	Relative difference		-8.52%	-2.56%	-7.12%	-3.30%
$C13_{CF}$-C^E	*Damaged*	*Freq.*	348.88	490.85	1016.74	1230.22
	Relative difference		-14.01%	-6.25%	-10.73%	-7.87%
$C14_{CF}$-C^E	*Damaged*	*Freq.*	354.92	468.53	1019.17	1219.88
	Relative difference		-12.52%	-10.51%	-10.52%	-8.65%
$C15_{CF}$-C^E	*Damaged*	*Freq.*	349.51	494.35	1016.36	1234.50
	Relative difference		-13.85%	-5.58%	-10.76%	-7.55%

(*) Relative Difference = ($\omega_{damaged} - \omega_{intact}$) / ω_{intact}

Table 3-16. Damping factor obtained by experimental tests for carbon fibre cylinders.

Plate ID	Type		ζ_1 [Hz]	ζ_2 [Hz]	ζ_3 [Hz]	ζ_4 [Hz]
$C01_{CF}$-A^E	*Intact*	*%*	0.24	040	0.46	0.53
$C02_{CF}$-A^E	*Damaged*	*%*	0.23	0.48	0.35	0.78
$C03_{CF}$-A^E	*Damaged*	*%*	0.30	0.41	0.46	0.60
$C04_{CF}$-A^E	*Damaged*	*%*	0.29	0.49	0.46	0.75
$C05_{CF}$-A^E	*Damaged*	*%*	0.45	0.48	0.41	0.73
$C06_{CF}$-B^E	*Intact*	*%*	0.24	0.41	0.37	0.68
$C07_{CF}$-B^E	*Damaged*	*%*	1.21	0.88	1.00	1.31
$C08_{CF}$-B^E	*Damaged*	*%*	1.19	0.95	1.00	0.37
$C09_{CF}$-B^E	*Damaged*	*%*	1.62	1.01	0.77	1.34
$C10_{CF}$-B^E	*Damaged*	*%*	0.83	0.63	0.77	1.12
$C11_{CF}$-C^E	*Intact*	*%*	0.22	0.46	0.27	0.51
$C12_{CF}$-C^E	*Damaged*	*%*	1.23	0.79	1.09	1.00
$C13_{CF}$-C^E	*Damaged*	*%*	1.68	1.06	1.15	1.31
$C14_{CF}$-C^E	*Damaged*	*%*	1.04	0.87	1.13	1.18
$C15_{CF}$-C^E	*Damaged*	*%*	1.25	0.85	1.20	1.30

3.6.4. Metrics for Damage Detection

According to Farrar and Worden (2007), the basic premise of SHM feature selection is that damage significantly alters the stiffness, mass or energy dissipation properties of a system, which, in turn, alter the measured dynamic response of that system as highlighted earlier. Although the basis for feature selection appears intuitive, its actual application poses many significant technical challenges. The most fundamental challenge is the fact that damage is typically a local phenomenon and may not significantly influence the lower-frequency global response of structures that is normally measured during system operation. Stated another way, this fundamental challenge is similar to that in many engineering fields where the ability to capture the system response on widely varying length- and time-scales.

Another fundamental challenge is that in many situations feature selection and damage identification must be performed in an unsupervised learning mode. For example, data from damaged systems are not available. Damage can accumulate over widely varying time-scales, which poses significant challenges for the SHM sensing system. This challenge is supplemented by many practical issues, which are associated to accurate and repeatable measurements over long periods of time for a limited number of locations on complex structures often operating in adverse environments.

After these first analyses, the conclusion is that the structure presents small difference between the intact and damaged behaviour. The next step consists in using another methodology to detect the damage. Indeed, it is difficult to identify the damage by visual inspection of the FRFs only; so it is necessary to introduce metrics to identify the presence or not of the damage. The following damage identification methods described in the section 3.3 are investigated here. These methods are all based on the measured frequency of the composite specimens.

Firstly, it is observed that the values obtained for the different types of sensor do not exhibit large changes between intact and damaged responses. Therefore, an SHM metric, which takes into account only the variation in the frequencies, may not be the best strategy for this type of damage. Furthermore, one of the first conclusions, which can be obtained from this data, is that the simulation of damage in the structure by drilling a hole cannot be representative for the case of stiffness degradation of the material (*cf.*, Tab 3-7 and 3-8 for the plate $P02_{CF}$). As observed from the FRFs, it is very complicated to identify the damage in the composite specimens, because it depends on the size and location of the damage, as well as on the frequency range of interest and the mode shape. On the other hand, use of the FRF is attractive

from the viewpoint of applications for SHM systems, because structural FRFs are sensitive to small changes and damage in a structure. To quantify this sensitivity, a damage indicator was used to calculate the difference in the FRF responses between healthy (intact) and damaged structures.

Using the data from the FRFs, both computational and experimental, Table 3-17 to 3-19 were obtained for different damage metrics shown previously. The metrics, which are based on the magnitude of the amplitude of the FRFs in specific frequencies, were calculated using relations between the responses obtained via different sets of sensors. Table 3-17 to 3-19 show the damage index/metrics ($DI_{\Delta H}$, DI_{ABS}, DI_{ABSF}, DI_{T}, DI_{A}, DI_{MS}, DI_{MSCS}, DI_{β}, DI_{GAC}, DI_{GSC}, and DI_{M}) for carbon fibre composite plates, carbon fibre composite cylinders and glass fibre composite plates, respectively. The mean values are listed. Also, it is observed that these DI are sensitive to different types of damage. In fact, values of DI are zero for the intact state while those for damaged states are not equal to zero. However, for the damage index DI_{GAC} and DI_{GSC}, values of DI are real constants between zero and unity to indicate total/zero change of structural responses, *i.e.* one for the intact state and zero for completely damage state.

Table 3-17. Experimental and Computational DI for the carbon fibre composite plates (impact and hole)

DI	ΔH Eq. 3.15	ABS Eq. 3.16	ABSF Eq. 3.17	T Eq. 3.18	A Eq. 3.20	MS Eq. 3.22	MSCS Eq. 3.24	β Eq. 3.26	GAC Eq. 3.28	GSC Eq. 3.30	M Eq. 3.31
$P01^{E}$	39.69	2.27	1.49	5.45	0.37	4.72	41.46	343.21	0.86	0.89	1.84
$P01^{C}$	59.97	5.98	1.26	4.71	1.26	12.37	31.05	25.32	0.78	0.77	0.86
$P02^{E}$	0.05	0.08	0.30	71.52	0.15	0.00	0.00	0.00	0.83	0.95	3.52
$P02^{C}$	30.03	4.08	1.14	4.01	0.57	39.04	3.10	0.00	0.94	0.85	2.15
$P03^{E}$	0.03	0.75	0.93	8.64	0.46	0.00	0.00	0.00	0.44	0.82	1.14
$P04^{E}$	0.05	0.61	0.82	12.97	0.41	0.00	0.00	0.00	0.66	0.85	1.36
$P05^{E}$	1.41	0.03	3.93	2.93	0.98	0.13	0.15	0.01	0.93	0.82	0.50
$P05^{C}$	0.14	0.06	0.85	0.79	0.85	0.03	0.00	0.00	0.73	0.75	1.41
$P06^{E}$	39.27	0.09	2.11	3.19	0.53	3.06	80.32	1.69E3	0.76	0.88	2.15
$P09^{E}$	1.34	0.01	0.25	27.93	0.06	0.16	0.13	0.00	0.86	0.95	3.99
$P09^{C}$	0.36	0.04	0.62	0.98	0.62	0.06	0.00	0.00	0.78	0.79	1.64
$P10^{E}$	1.42	0.01	0.15	22.23	0.04	0.22	0.13	0.00	0.91	0.98	6.81
$P11^{E}$	128.31	0.14	0.24	15.05	0.06	13.81	221.45	64.57	0.98	0.96	5.25
$P11^{C}$	5.15E3	1.22E5	0.62	1.78	0.62	1.17E6	1.8E11	5.0E19	0.89	0.80	1.63
$P12^{E}$	142.42	0.15	0.22	36.00	0.05	17.26	278.30	197.45	0.98	0.96	5.25

Table 3-18. Experimental and computational DI for the carbon fibre composite cylinders

DI	ΔH Eq. 3.15	ABS Eq. 3.16	ABSF Eq. 3.17	T Eq. 3.18	A Eq. 3.20	MS Eq. 3.22	MSCS Eq. 3.24	β Eq. 3.26	GAC Eq. 3.28	GSC Eq. 3.30	M Eq. 3.31
A^C	2.72E4	175.08	0.77	0.15	0.77	5.92E3	6.34E6	1.9E12	0.19	0.45	1.31
$A02^E$	2.48	0.04	1.28	5.82	0.64	0.04	0.14	0.19	0.24	0.84	0.12
$A03^E$	2.19	0.09	2.60	2.78	1.30	0.04	0.08	0.33	0.22	0.82	0.44
$A04^E$	2.80	0.06	1.87	2.22	0.94	0.03	0.16	0.23	0.15	0.81	0.55
$A05^E$	2.43	0.06	1.98	1.23	0.99	0.03	0.13	1.58	0.14	0.80	0.51
$B07^E$	3.88	0.16	3.69	1.05	1.85	0.04	0.21	0.22	0.14	0.74	0.29
$B08^E$	2.97	0.33	7.61	68.45	3.81	0.03	0.25	2.50	0.16	0.67	0.14
$B09^E$	3.66	0.30	7.33	5.75	3.67	0.03	0.21	4.39	0.16	0.65	0.14
$B10^E$	3.65	0.06	1.57	1.95	0.78	0.05	0.18	0.15	0.21	0.80	0.68
$C12^E$	2.69	0.09	2.26	1.74	1.13	0.04	0.06	0.82	0.17	0.77	0.49
$C13^E$	3.08	0.14	3.83	1.84	1.92	0.03	0.07	1.08	0.11	0.70	0.26
$C14^E$	3.07	0.14	3.70	1.04	1.85	0.03	0.07	1.29	0.10	0.69	0.27
$C15^E$	3.10	0.10	2.79	1.06	1.39	0.04	0.07	1.03	0.11	0.71	0.24

Table 3-19. Experimental DI for the glass fibre composite plates

DI	ΔH Eq. 3.15	ABS Eq. 3.16	ABSF Eq. 3.17	T Eq. 3.18	A Eq. 3.20	MS Eq. 3.22	MSCS Eq. 3.24	β Eq. 3.26	GAC Eq. 3.28	GSC Eq. 3.30	M Eq. 3.31
$P01^E$	0.23	3.7E-3	0.27	157.15	0.14	0.05	3.1E-4	1.3E-9	0.79	0.95	3.74
$P02^E$	0.28	4.3E-3	0.32	15.45	0.16	0.04	5.6E-4	2.1E-8	0.79	0.95	1.32
$P03^E$	0.30	5.1E-3	0.38	27.36	0.19	0.05	5.6E-4	1.6E-9	0.86	0.94	2.68
$P06^E$	0.24	4.6E-3	0.66	4.14	0.33	0.02	9.0E-4	4.2E-7	0.69	0.87	2.02
$P07^E$	0.38	5.1E-3	0.69	2.93	0.35	0.01	3.8E-4	1.2E-7	0.60	0.85	1.80
$P08^E$	0.24	1.1E-2	0.45	1.74	0.22	0.01	3.8E-3	2.1E-6	0.59	0.87	2.48

Damage metrics are clearly sensitive to damaged states and they can be used for damage identification purposes in structural health monitoring systems. It is observed that the numerical results given higher values than the experimental one. This behaviour can be explained because the uncertainty values in the numerical models such as damping factor, total and each layer thickness and curvature due to the manufacturing process of the plates. Also, due to the continuum damage mechanics formulation, which takes into account the damage in the fibre and in the matrix, however the damage provided by delamination is neglected. Therefore, the proof of concept of predicting the behaviour of SHM systems using the proposed numerical model was accomplished. Figures 3-41 to 4-43 present the damage index/metric in a graphic form.

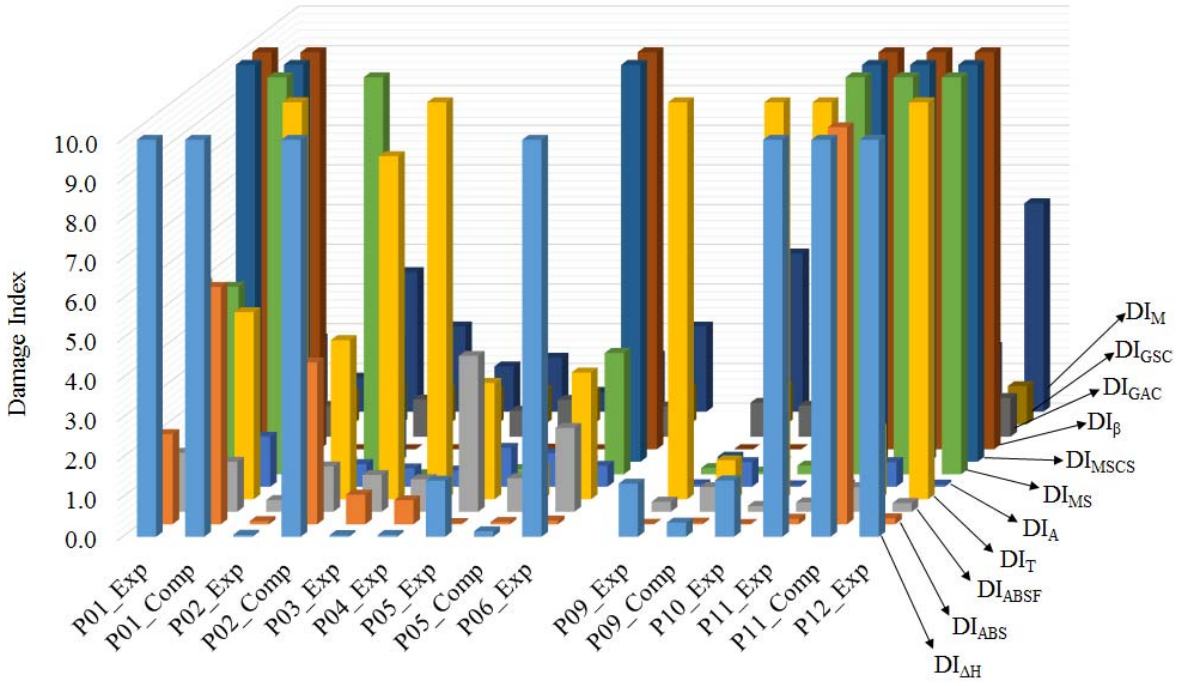

Figure 3-41 – Experimental and computational DI reported in the literature for carbon fibre composite plates.

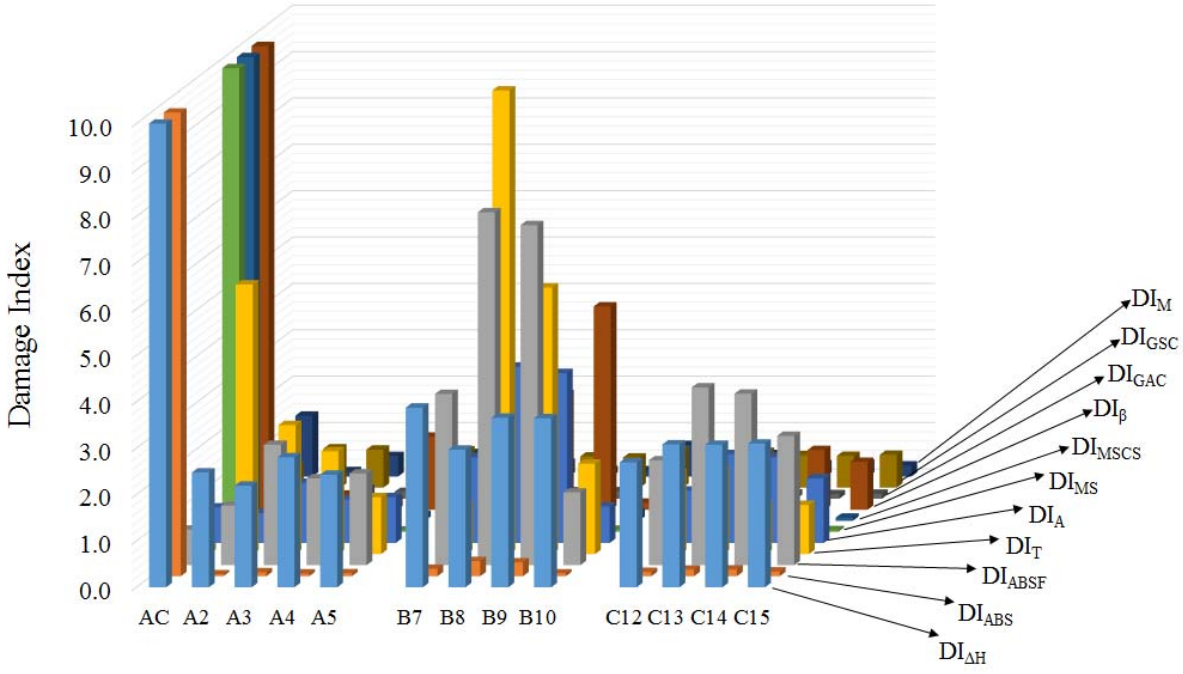

Figure 3-42 – Experimental and computational DI reported in the literature for carbon fibre composite cylinders.

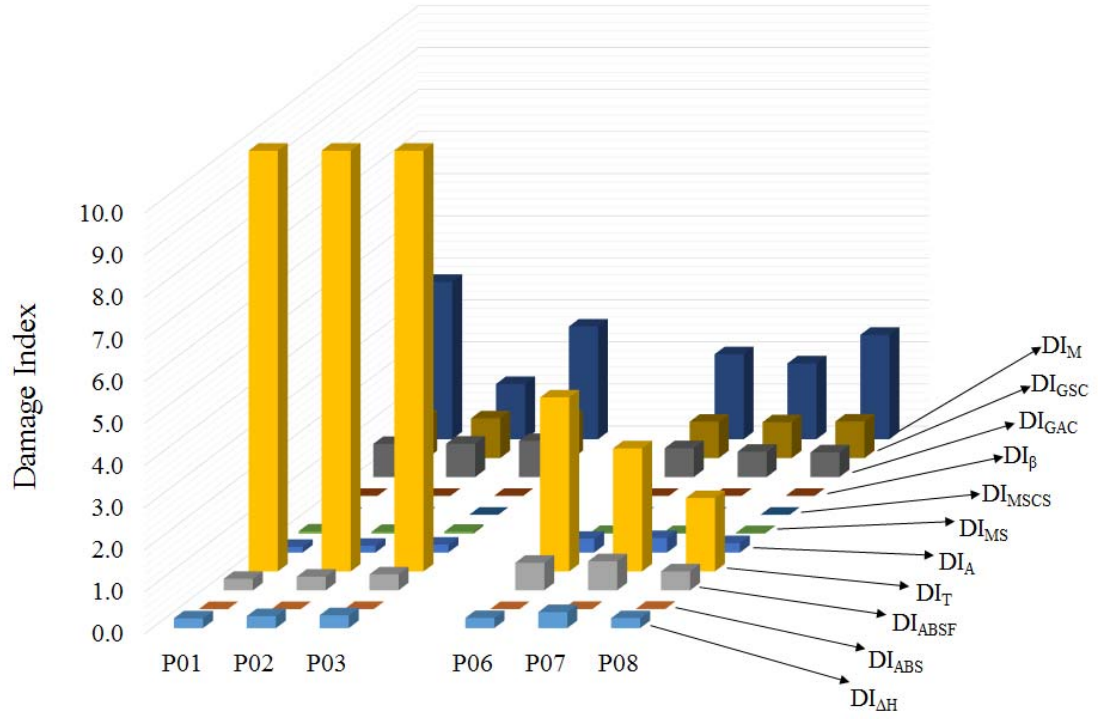

Figure 3-43 – Experimental DI reported in the literature for glass fibre composite plates.

Analysing the damage index provide by Tab. 3-17 to 319 and Fig. 3-41 to 3-43, it is possible to observe that some damage metrics highlight more the damage. For the carbon fibre composite plates, it is possible to observe that most of the metrics are efficient to detect the damage on the structure. For the carbon fibre composite cylinder is possible to observe that some metrics are more efficient to detect and some metrics are less efficient to detect the damage. For the glass fibre composite plate almost half of the damage metrics are not less efficient for detecting damage on the structure. It can be concluded that the efficiency of the damage metric depends on the type of damage, the frequency range of analysis (mode shape) and the orientation of the fibres. Thus, the metric can be more efficient for one situation, but not for another one. The important conclusion that can be made by looking at these results is that this damage detection method is working for composite plates. Because statistical distribution is not considered here, one can say that when the value of the damage indicator differs from the no damage value, damage is present in the plate.

The next step is to evaluate the new damage index proposed by Medeiros *et al.* (2015a, 2015b) .Using data from the FRFs, both experimental and numerical. Figs. 3-44 to 3-49 were constructed using damage metrics from Eq. (3.32).

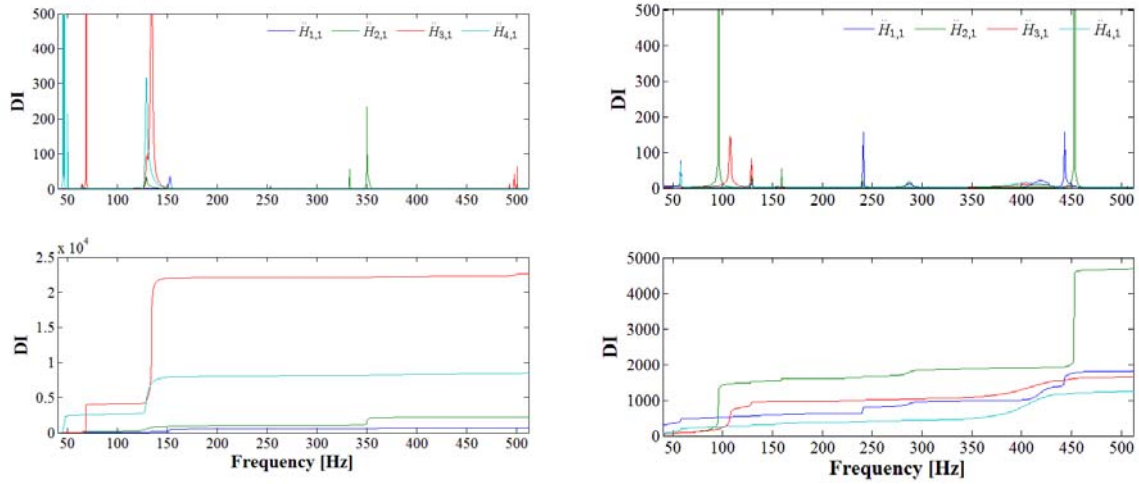

(a) (b)

Figure 3-44 – DI evolution of the carbon fibre composite plate ($P01_{CF}$) (a) experimental and (b) computational.

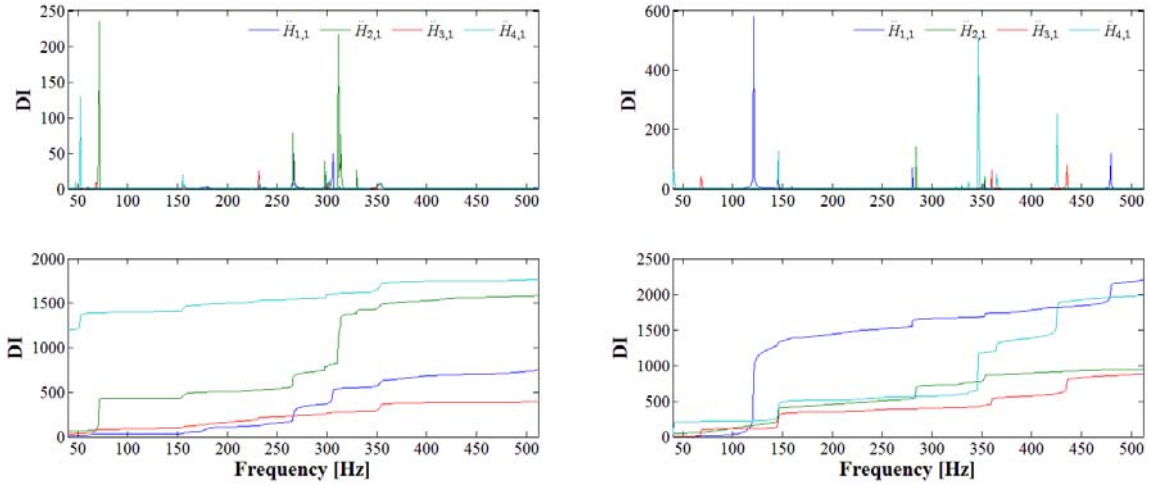

(a) (b)

Figure 3-45 – DI evolution of the carbon fibre composite plate ($P02_{CF}$) (a) experimental and (b) computational.

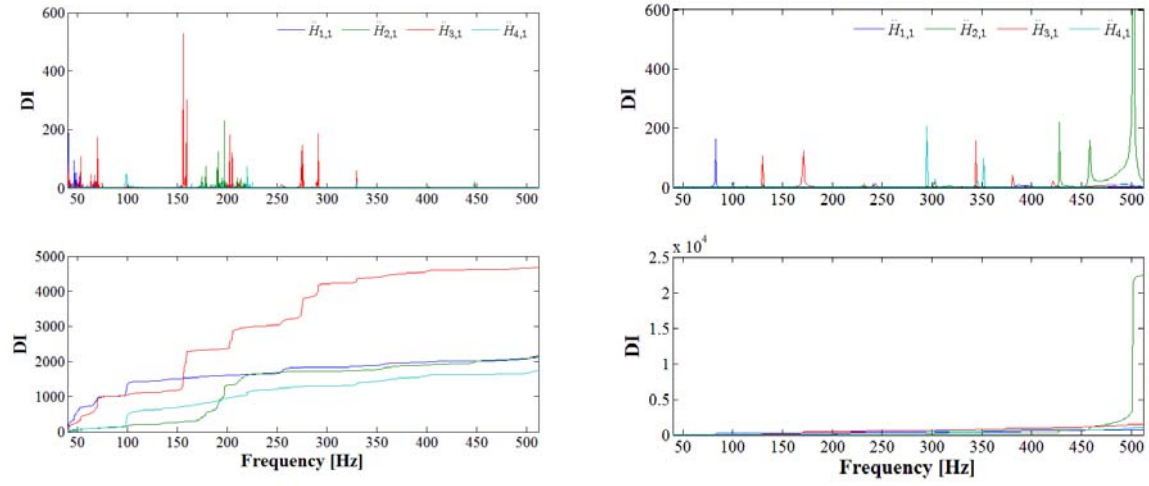

(a) (b)

Figure 3-46 – DI of the carbon fibre composite plate ($P09_{CF}$) (a) experimental and (b) computational.

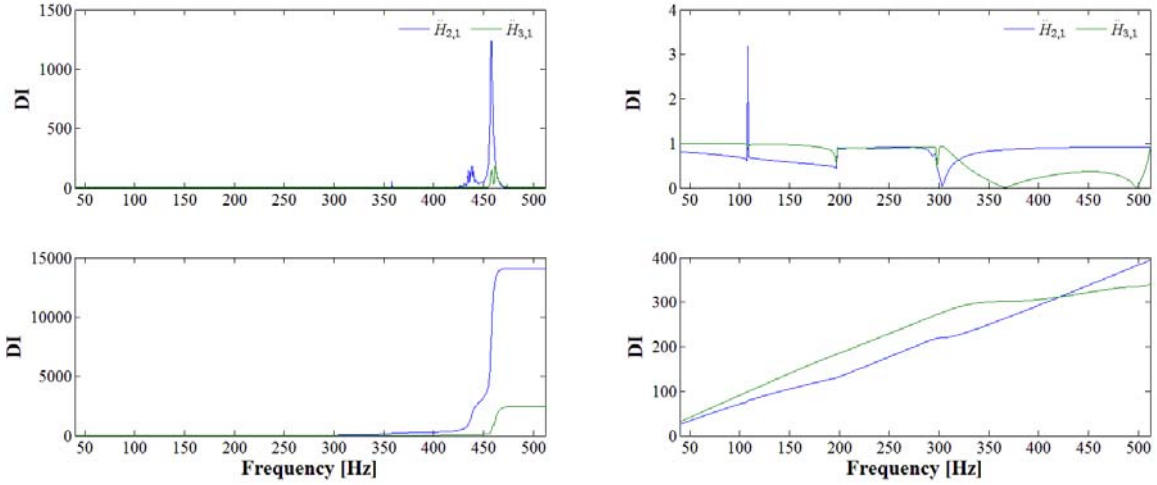

(a) (b)

Figure 3-47 – DI of the carbon fibre composite cylinder ($C02_{CF}$-A) (a) experimental and (b) computational.

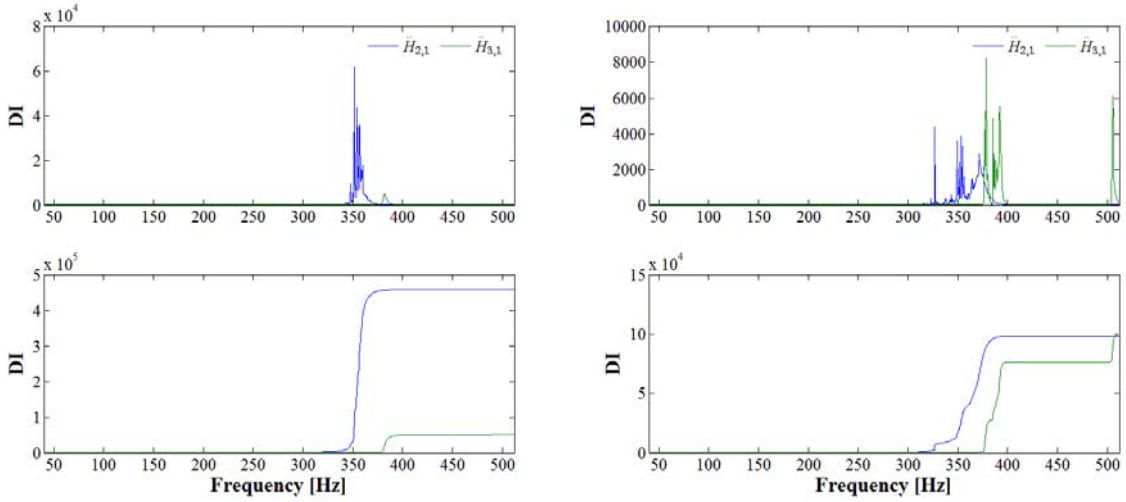

(a) (b)

Figure 3-48 – DI evolution of the carbon fibre composite cylinders (a) $C07_{CF}$-B and, (b) $C12_{CF}$-C.

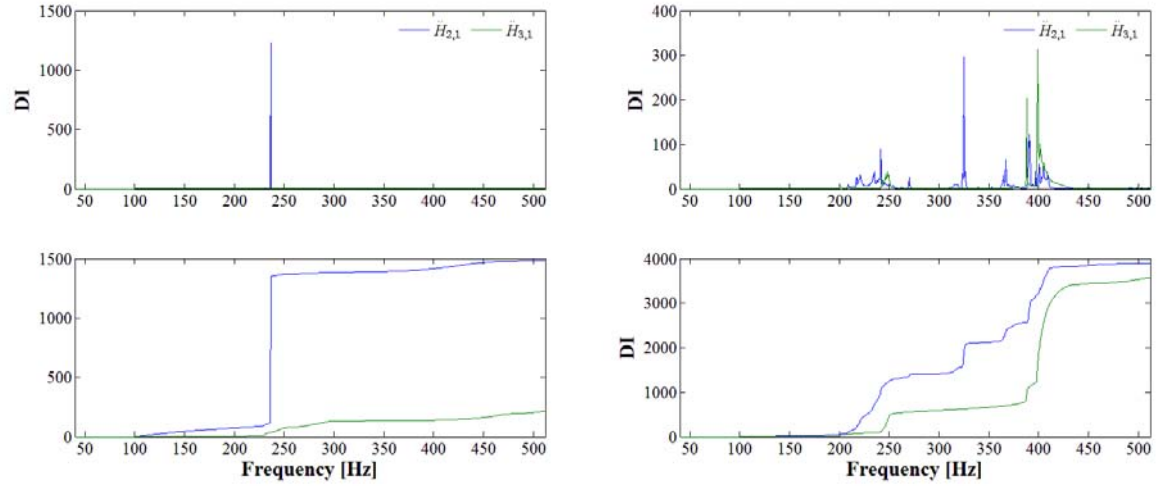

(a) (b)

Figure 3-49 – DI evolution of the glass fibre composite plate (a) $P01_{GF}$-UD and, (b) $P06_{GF}$-UD.

Based on Figs. 3-44 to 3-49, it is concluded that for these cases, the damage index/metric (DI_{GAP}) is sensitive to damaged states. In addition, the computational damage metric is more severe than the experimental one. As previously discussed, this behaviour can be explained, because the uncertainty values in the numerical models such as the damping factor, total and each layer thickness and curvature due to the manufacturing process of the plates. Also due to the continuum damage mechanics formulation, which takes into account the damage in the fibre and in the matrix, however the damage provided by delamination is neglected. Considering the DI evolution over the frequency range, Figs. 3-50 to 3.52 presented the DI values for the composite specimens, both experimental and computational.

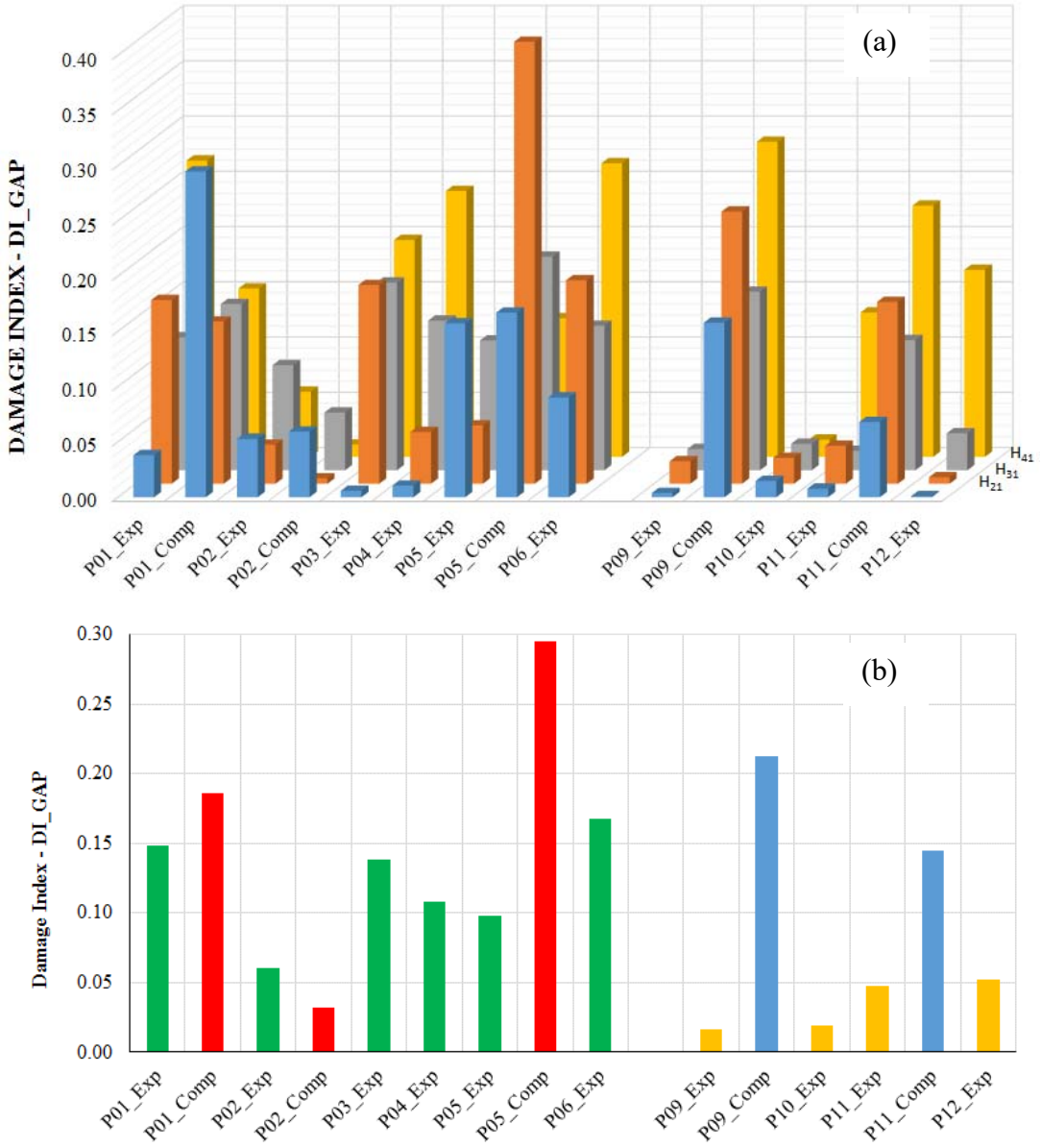

Figure 3-50 – Experimental and computational DI over the frequency range for the carbon fibre composite plates (a) all points and, (b) average values.

It is observed that the computational analysis given a higher value than the experimental tests. Also, it can be observed that the damage metric by impact is higher to damage by central hole for the plates with stacking sequence $[0]_8$. Comparing the different stacking sequence, the composites $[0]_8$ presented higher DI values compared to the composite plate $[0/15/-15/0/15/-15]_s$. Thus, it is concluded that the damage metric values also provide the severity of each damage.

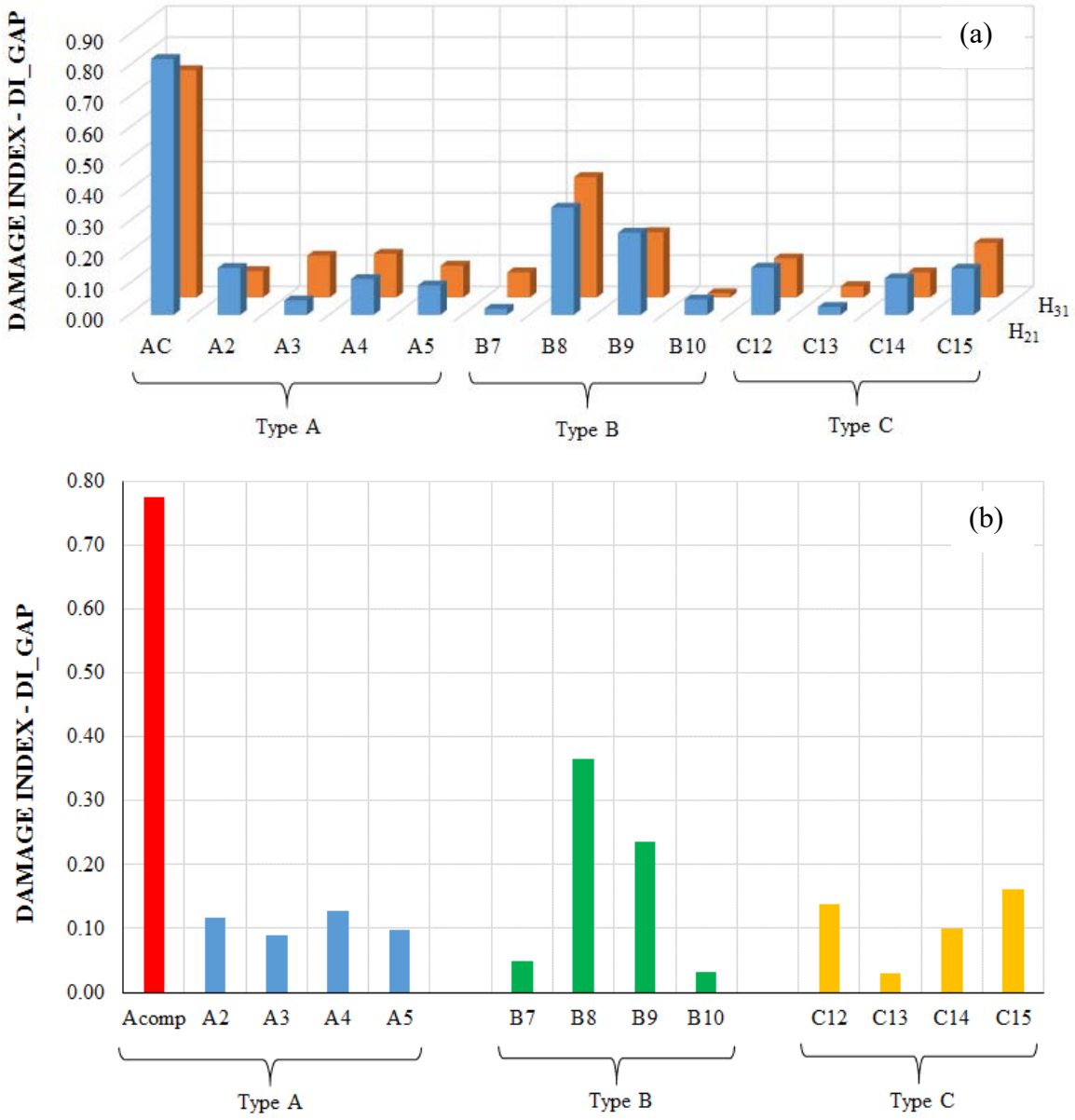

Figure 3-51 – Experimental and computational DI over the frequency range for the carbon fibre composite cylinders (a) all points and, (b) average values.

Again, it is observed that the computational analysis gives a higher value than the experimental tests. However, the boundary conditions were different for the computational and experimental analysis. Comparing the different stacking sequences, it is observed that the composite cylinder type B ($[90/30/-30/90/30/-30/90]_s$) presents higher values compared to composite cylinder type A ($[90/60/-60/90/60/-60/90]_s$) and type B ($[90/30/-60/60/-60/30/-30]_s$). This fact can be explained due the differences in the stacking orientation, *i.e.* composite cylinder type B is more susceptible to impact damage than other cylinders types.

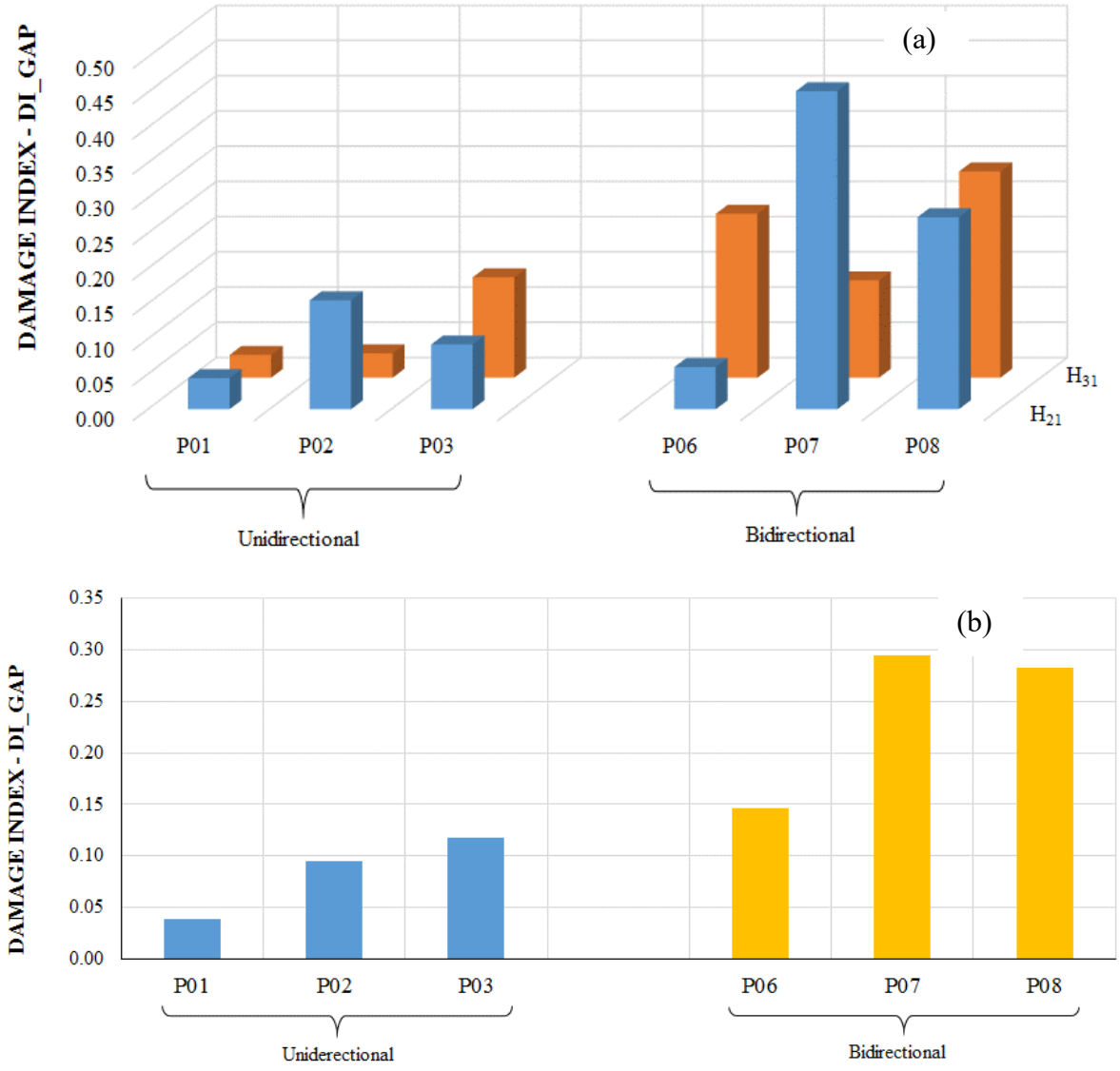

Figure 3-52 – Experimental DI over the frequency range for the glass fibre composite plates (a) all points and, (b) average values.

Based on Fig. 3-52, it is concluded that the glass fibre orthogonal configuration present higher values of damage when compared to the glass fibre unidirectional composite plate.

Comparing the numerical and experimental results, the differences in the damage metrics can be verified. This difference was already explained previously. However, it presents the same tendency for both the experimental and numerical results. In addition, the numerical damage metrics obtained are less than the experimental results. It is possible to observe a trend for the increase of damage in both the numerical and experimental calculations. As such, the proof of concept of predicting the behaviour of SHM systems using the proposed numerical model was accomplished.

Comparison of the different metrics used, leads to the conclusion that the use of a frequency based should be preferred over the use of a single frequency. The introduction of damage in a structure may affect the shape and frequency of close modes of vibration in unpredictable ways. However, the presence of damage can be seen in practically every single frequency, especially those near resonance frequencies. Moreover, after identifying the mode (or modes), which are most affected by a given type of damage, frequency specific metrics may be more accurate. Besides, this gives the necessity of identifying each type of damage signature and the mode, which is mostly affected. This kind of effect can be strategic for embedded systems, due to a single frequency comparison being faster calculated than a range of frequencies. Then future studies can be performed considering this issue.

3.7. Partial Conclusions

There are many advantages in using the vibration-based method for SHM systems. Among these advantages are the easy implementation and low cost. Also, it provides the global behaviour of the overall condition of the structure and may not require direct human accessibility. In some cases, the sensor can be embedded in the laminate structure (*e.g.* piezoelectric sensors) and has the potential for damage detection in flight with appropriate structural modelling. Therefore, experimental and computational investigations were conducted into the use of frequency response techniques for the detection of damage in composite specimens. The experimental and computational results showed that the vibration-based damage identification methods combined to the metrics can be an alternative to design and to

evaluate SHM systems. Furthermore, the results show the severe limitation of the applied methods to provide information about the location and the extension of damage. In fact, to these tasks, a net of sensors is recommended. And, sometimes, for aeronautic application, this is not convenient because the sensors increase strongly the weight of the structure.

Based on the natural frequencies and the mode shapes of the intact structure, it is possible to define the frequency range for the next analyses. The mechanical behaviour are determined using numerical and experimental modal analysis as a function of time, after that, it was applied the FFT to determine the FRF of the structure without damage. According to impact analyses, a material damage model was used to predict the damage evolution during an impact test performed by a drop tower apparatus. Using the damaged structure FE model, FRF are determined, again. The numerical results demonstrate the usefulness of vibration-based method using piezoelectric sensors in detection of impact damage. Comparing the computational results from PZT sensor and accelerometer, it is possible to observe that the PZT sensors return smaller values. This fact can be explained due the boundary conditions applied in the FE models. The PZT sensor was modelled as a solid element with mass and properties. On the other hand, the mass of the accelerometer was neglected, *i.e.* it was selected a nodal point to monitor the structural response. This method has the advantage of easy implementation and low cost. However, there are some limitations, as the method is a difference between the data of the intact and damaged structure, if the data having noise, this difference can wrong fully be considered as damage. For example, the comparison between FRFs from intact and damaged structure confirm that the localised damage has small influence on the lower frequencies. Therefore, it is concluded that the identification of the damage cannot solely be based on the difference of natural frequencies for intact and damaged structure. Thus, a suitable damage indicator is strongly recommended. It was shown that different damage metrics (including a new one) are a good option not only to identify the damage, but also to provide a prediction of the damage severity. However, even using damage metrics, SHM systems based on vibration methods provide little information about the location and extension of the damage, unless large quantities of sensors are employed. And, this will increase the cost and the weight of the component.

The final conclusion is that the application of vibration-based methods by using PZT sensors on SHM systems for composite structures is a good alternative for the aeronautic industry.

CHAPTER 4

Damage Location and Damage Extension

Optical non-destructive testing (NDT) has been investigated more and more in recent years due to its non-destructive imaging characteristics with high precision and sensitivity. Among these optical techniques, Shearography Speckle (SS) depends on the intensity distribution pattern formed from space interference, which is generated by illumination of coherent light onto rough object surfaces. Laser speckle interferometry is an effective NDT technology with advantages of non-contact. Even the illumination over the surface of the object not being uniform, it is possible to obtain high sensitivity and detection rate. This method combines the laser speckle pattern with another coherent laser beam, which has a speckle pattern or a smooth wavefront, the image obtained from the interference also has a random speckle appearance known as a "speckle interference pattern". The resulting speckle interferogram is imaged on a CCD camera, which is saved for comparison with other images. When the surface moves, the speckle interferogram is changed due to the change in path length difference between the object and reference. This second interferogram is subtracted from the first one, pixel by pixel. The result is rectified and displayed as a set of bright and dark fringes, known as correlation fringes, which depicts a contour map of the displacement of the object surface. The SS technique measures the displacement based on the principle of the Michelson Interferometer. To evaluate the limitations and potentialities of this technique, two types of damage and two types of geometry were studied. This chapter focusses on locating and quantifying the extent of damage in composite structures. Shearography Speckle (SS) system has been applied in many fields of research, such as aerospace, automotive, power generation, etc. In this chapter, experimental results are presented for the application of SS technique applied to composite specimens with damage in order to localise, but mainly to estimate the damage area. Thus the composite plates (investigated in the previous chapter) with a centre hole ("controlled" damage) and damaged by impact loading ("uncontrolled" damage) are analysed via Shearography. Various excitation methods such as mechanical, thermal, pressure and vibration excitation can be used. And, in this work, method thermal loading is selected. This approach is successful in showing the impact damage area in composite laminate specimens, because delaminations can be observed in the impact damage area. Finally, the potentialities and limitations of this method are discussed. The results show that SS can be used as an excellent alternative to identify and quantify the extent of damage in composite structures.

4.1. Review of Interferometry Methods

The ever-increasing requirements of product quality and reliability demand more efficient measurement and test methods, which should be non-destructive, whole-field and without contact. Optical methods seem to be strong candidates for such purposes. Holography is a highly sensitive, noncontact, coherent-optical measurement and test method, which has been applied in many fields of research under laboratory conditions.

The optical interferometry techniques have been widely investigated in the last four decades. Leendertz and Butters (1974) performed a comparison with results obtained by holographic interferometry and speckle pattern interferometry. Based on this technique, one may measure displacement of the surface normal to itself or, using a different optical arrangement, the components of displacement vector in the plane of the surface. For the measurement of bending moments, it is necessary to obtain the normal displacement function, which must be differentiated twice to yield the curvature. This process can be time consuming and lead to appreciable error in the final result. The first effort to code the variation of the differences in phase of two objects subjected to stresses, in the form of holographic fringes, was developed by Neumann (1980). However, the researcher did not include any experimental evidence to support the proposed method. The method appears to be practically difficult and feasible in double exposure only. Rastogi (1985) presented a comparative holographic interferometry, which addresses a key problem of non-destructive evaluation: comparison of the resistance to strength in real time of two nominally identical specimens. The work reported some new and complementary developments in comparative holographic interferometry.

More recently, the increased power of numerical calculation with the appearance of arrays of CCD (Charge-Coupled Device) and CMOS (Complementary Metal-Oxide-Semiconductor) integrated into camera, with high resolution and small size, allowed a huge development of these optical techniques. Jacquot (2008) presented a review about the nearly 40 years of existence of the Speckle Interferometry (SI). Nokes and Cloud (1993) have investigated a method for increasing the sensitivity of dynamic materials evaluation (DME) to localise damage in fibre reinforced composites. Hertwig *et al.* (1996) reported how the Electronic Speckle Pattern Interferometry (ESPI) is used to detect and to quantify damage in fatigued CFRP laminates via its effect on the surface displacement field. To verify the potentialities and limitations, the results were compared to ultrasonic C-scan data.

Zhang *et al.* (1998) have demonstrated how intensity fringes and phase maps from phase stepped ESPI may be used to evaluate delamination, cracks and other defects in glass-fibre reinforced polyester (GRP) pultruded panels in which the damage was originated from impact tests. The experimental results showed that both intensity fringe patterns and phase maps can be used to detect the internal damage. The intensity fringe approach enables the damage to be examined in real-time, but with the disadvantage of limited visibility and readability. In contrast, the phase map approach is capable of showing the fine features of internal damage with higher visibility and readability, providing post-processing. The damaged areas were calculated and compared to those derived from conventional ultrasonic C-scan and sectioning techniques, showing good correlation.

Gryzagoridis *et al.* (2005) have shown the results from an attempt to detect damage created by impact loading events such as tool drop or bird collisions on composite materials designed for structural applications in the aerospace industry. In addition, the usage of ESPI (Electronic Speckle Pattern Interferometry) for determining the extent of damage on composite panels was demonstrated. Ambu *et al.* (2006) investigated and discussed the feasibility of optical methods to detect impact damage on thin laminates. Specimens impacted by different energy levels were analysed by a holographic procedure and by an electronic speckle pattern interferometry technique. The results obtained by the two techniques were compared to those acquired by a pulse-echo full-volume ultrasonic technique. The investigation showed that both optical methods are able to identify the presence of impact damage, with efficiency dependent on the through-thickness location of the delamination produced by the impact loading.

Lopes *et al.* (2006) studied an experimental/numerical technique for delamination damage detection on thin laminated composite plates. A double pulse TV holography is used for non-contact and accurate measurement of the amplitude mode shapes. The curvature is obtained by applying an improved differentiation/smoothing technique to the experimental data. Thus, the curvatures of each mode were subtracted and the damage was located. Ruzek *et al.* (2006) showed a comparison between the results of visual, ultrasonic C-Scan and laser Shearography impact damage assessment for sandwich panels, which were cut out from sandwich skins of airplane wings. Considering the reliability, simplicity and rapidity of each technique and with the digital indicator measurement as a base, the laser Shearography was evaluated as the most suitable method for that purpose.

Araújo dos Santos *et al.* (2006) have investigated three different methods for the localisation of impact damage in laminated composite plates, based on their vibrational

characteristics. These methods use double pulse TV holography with acoustic excitation for mode shape acquisition and the differences in translations, rotations and curvatures. The rotations and curvatures were obtained via numerical differentiation of mode shapes translations by using a differentiation/smoothing technique. It is shown that the method based on curvatures allows for the localisation of both cases of damage, which can be undetected by visual, X-ray or C-scan inspections. The best localisations are achieved by selecting and applying the method to the most changed mode. Schmidt (2009) investigate the feasibility and applicability of visual defect detection with commercial double-pulse Electronic Speckle Pattern Interferometry (ESPI) system, based on impact-excited elastic waves, on methods with forced vibrations, and methods with thermo-elastic deformations. In the case of forced vibrations, they adopted the methods, which showed an increased potential of damage detection.

Garnier *et al.* (2011) evaluated the efficiency of the NDT methods in the detection of in site defects resulting from Barely Visible Impact Damages (BVID) or in-service damages for complex surfaces, such as wings or rods. A study of three Non Destructive Testing methods (Ultrasonic Testing, InfraRed Thermography and Speckle Shearing Interferometry, known as Shearography) was carried out on different specific types of composite specimens with a variety of defects. Lasik *et al.* (2011) reported a technical development and practical evaluation of a Simple Digital Speckle Pattern Interferometer (DSPI) for the non-invasive, non-contact detection and characterisation of early-stage damage of painted objects of art, like fracturing and layer separation. Lopes *et al.* (2011) presented a structural damage location method, which decreases the number of spatial differentiations required to compute modal curvature fields. The method is numerically and experimentally applied to isotropic and laminated rectangular plates, respectively. A speckle shear interferometer was used to measure the rotation fields of the laminated plate, while the isotropic plate was analysed by FEA (Finite Element Analyses).

Zhu *et al.* (2011) presented a review of the main optical NDT technologies, including fibre optics, electronic speckle, infrared thermography, endoscopic and terahertz technology. The latter refers to the electromagnetic waves with frequency ranging from 0.1 THz to 10 THz. In case of fibre optics features, the integration and embedding in the structure are easy. Electronic speckle focuses on whole-field high precision detection. Endoscopic technology provides images of the internal surface of the object directly. Finally, terahertz technology has created a new way to perform internal NDT, because of its excellent penetration capability to most of non-metallic materials.

Kim *et al.* (2012) investigated the low-velocity impact damage on composite laminates by three different NDE (Non-destructive Evaluation) techniques: Electronic Speckle Pattern Interferometry (ESPI), digital Shearography and ultrasound C-scan. Lopes *et al.* (2012) presented two interferometric techniques and their applications in structural damage identification. Out-of-plane displacement fields of modal response were measured by a pulsed electronic speckle pattern interferometric system (ESPI). The modal rotation fields, defined as the spatial derivative of the displacement field, were measured by a pulsed speckle Shearography system. More recently, Balamurugan and Muruganand (2013) designed a low cost Laser Speckle Interferometer with minor modification of Michelson Interferometer^{TM}. In that work, an electronic laser speckle pattern technique has been adopted to measure small deformation/displacement of a specimen. Therefore, considering the scenario described previously, it is confirmed that it is very strategic to develop an SHM system based on not only vibration-based methods, but also on optical method like speckle Shearography in order to quantify and localise the damage zone.

Since its first demonstration, speckle shearing interferometry, or shearography, has offered the specific advantages of interferometric full-field displacement gradient sensitivity using an optical configuration inherently more resilient to environmental disturbances and vibrations than other interferometric techniques such as electronic speckle pattern interferometry (ESPI). As such it has become an important diagnostic tool, particularly in the field of non-destructive testing where it has been used primarily for qualitative inspection, for example, to reveal delaminations in composite structures. More recently, shearography has been developed to enable quantitative full surface strain measurement (Francis *et al.*, 2010).

The non-contact and full-field measurement allows the calculation of the three dimensional distribution of the displacement and strain/stress of the object under test as a response to a mechanical or thermal loading ESPI has successfully been applied in many fields including automotive, aerospace, electronics and materials research, for the study of material properties, fracture mechanics, fatigue testing, NDT and dynamic behaviour of a variety of components. The full-field nature of the results allows an accurate and easy determination of material parameters and the identification of highly stressed areas. In contrast to conventional methods *e.g.* strain gauge, scanning vibrometer, ESPI systems combine an unsurpassed density of measuring points with very high sensitivity and a dynamic range up to several hundred kHz. Typical applications utilize not just a single measurement but a sequence of measurements, so that the user can follow the evolution of displacement/strain during loading. For operation of

airplanes it is necessary to predict maintenance of aeronautic structures. Thus, as it is known, there are checks of structures during the life of the airplane, which can be performed by shearography speckle on ground. In addition, this technique is well known and certified by the regulatory agencies.

Shearography speckle can perform a quick investigation and brings others common benefits such as non-contact, scalable and full-field measurement. This technique is a really good alternative to estimate damage extension and type in composite structures, because composite materials can have two main kinds of damages such as intralaminar (e.g. fibre and/or matrix failure) and interlaminar (delamination). Therefore, the shearography speckle is a very useful NDE technique, because of its detection capacity for barely visible impact damages, which are not often detected by visual inspection.

4.2. Shearography Speckle

Electronic speckle pattern interferometry (ESPI) is one technique of a family of coherent light interferometry. This family of techniques also includes holographic interferometry, speckle interferometry and speckle shearography. Each of these techniques is capable of measuring either surface displacement or displacement derivatives with practical benefits of being able to make whole-field and non-contact measurements.

Shearography is an optical method, which uses speckle shearing interferometry to measure displacement gradients at the surface of a structure. The speckle patterns produced by a structure in stressed and unstressed states are subtracted, revealing changes in displacement gradient. These are generally more rapid in damaged regions. Laser speckles are produced whenever a surface, whose roughness is of the order of one wavelength of light or greater, is illuminated with highly coherent light. The light scattered from any moderately distant point consists of many coherent wavelets, each arising from a different element of the surface. The optical path differences between these various wavelets may differ by several wavelengths and the interference between these wavelets results in a granular pattern of intensity, which is termed speckle.

4.2.1. Fundamental of Laser Interference

Since the light is viewed as an electromagnetic wave, characterised by a time variation of the electric and magnetic fields, and the propagation of the wave front is described by Maxwell's equations. The spatial and temporal distributions of a harmonic plane wave front propagation direction *k* are represented by Eq. (4-1) (Kreis, 2005).

$$E(\vec{r},t) = A_0 e^{j(kr-\omega t+\phi)} \tag{4.1}$$

where E is the electric field strength, $j = \sqrt{-1}$, A_0 is the wave amplitude, *r* is the wave space vector, *t* is the time, ω is the angular frequency and ϕ is the phase angle of the wave. Figure 2.1 displays two aspects of this wave.

Figure 4.1(a) shows the temporal distribution of the field, and Fig. 4.1(b) gives the spatial distribution of two periods for time instants. A point of constant phase moves with the so called phase velocity, the speed *c*.

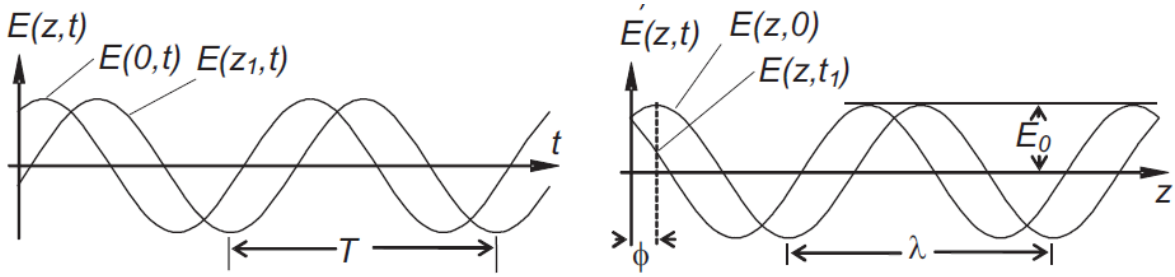

Figure 4-1 – (a) Spatial and (b) temporal distribution of a scalar harmonic wave (Kreis, 2005)

The only parameter of light, which is directly amenable to sensor – eye, photodiode, CCD-target, etc. – is the intensity. The latter is defined by the energy flux through an area per time. From the Maxwell equations,

$$I = \varepsilon_0 c A^2 \tag{4.2}$$

which shows the proportionality of the intensity I to A^2,

$$I \sim A^2 \tag{4.3}$$

It has to be recognised that the intensity has a nonlinear dependence on the complex amplitude. Since there is no sensor, which can follow the frequency of light, it has to integrate

over a measuring time T_m, the momentary intensity is not measurable (Kreis, 2005). So, if $T_m >> T = 2\pi/\omega$, omitting proportionality constants, it can be defined as,

$$I = A_0 A_0^* = |A_0|^2 \tag{4.4}$$

where * denotes the complex conjugate.

The superposition of two or more waves in space is named interference. The resultant intensity at any point depends on whether they reinforced or cancel each other shown in Fig. 4-2. If the beams are in phase, they interfere constructively and their amplitudes add to give a bright speckle. If the beams are out of phase, they interfere destructively and their amplitudes cancel each other out creating a dark speckle (Fig. 4.3).

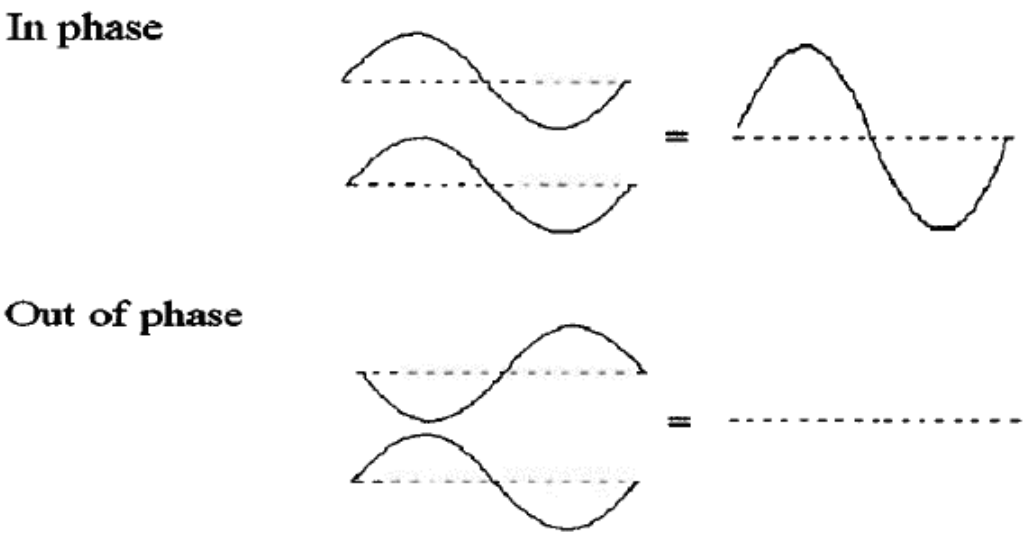

Figure 4-2 – Interference of light wave (An, 2008)

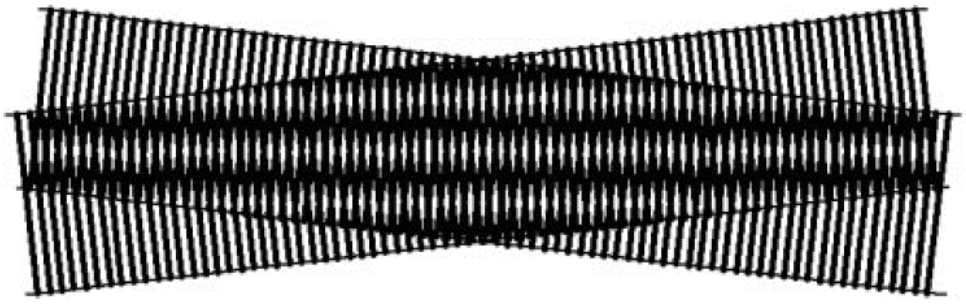

Figure 4-3 – Interference fringes constant in time (Kreis, 2005)

If each single wave described by $E(\vec{r},t)$ is a solution of the wave equation, also the superposition,

$$E(\vec{r},t)=\sum_i E(\vec{r},t) \qquad i=1,2,... \tag{4.5}$$

is a solution, too. This is because the wave equation is a linear differential equation.

The complex amplitude at any point in the interference pattern is the sum of the complex amplitudes of these two waves, it may be written as,

$$A=A_1+A_2 \tag{4.6}$$

where $A_1 = a_1 \exp(-j\phi_1)$ and $A_2 = a_2 \exp(-j\phi_2)$ are the complex amplitudes and ϕ_1, ϕ_2 are the phase angle of the two waves. The resultant intensity is therefore,

$$\begin{aligned} I_1 &= |A_1|^2 \\ I_2 &= |A_2|^2 \\ I &= I_1 + I_2 + 2\sqrt{I_1 I_2}\cos\Delta\phi \end{aligned} \tag{4.7}$$

where I_1 and I_2 are the intensities due to each beam separately and $\Delta\phi = \phi_1 + \phi_2$ is the phase difference between them.

4.2.2. Speckle

The speckle pattern or speckle field (Fig. 4-4) is created by the interference of multiple spherical wavefronts from the reflection points of a rough and diffuse surface, when illuminated by a coherent light. The difference of the path travelled by the wavefront diffused by micro-surfaces leads to interference phenomena and consequently the generation of a standard, called speckle. A speckle pattern develops if the height variations of the rough surface are larger than the wavelength of the light. The speckle has spatially the shape of an ellipsoid (Lopes, 2007), whose length/diameter ratio (L/D) varies depending on the distance to the reflecting surface (Fig. 4-5), where the speckle phase varies linearly. The observation of a speckle pattern is determined by the characteristics of optical systems and image registration. In each case, the average size of the speckle is adjusted to the resolution of the recording system to be observed.

In digital recording systems, the size and number of the pixels determine the resolution of the CCD measurement techniques.

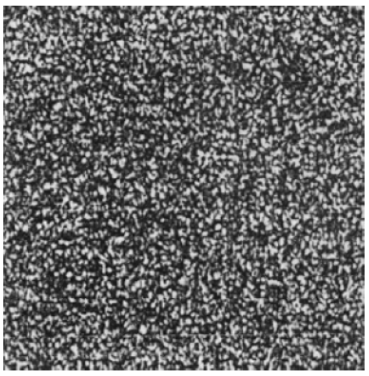

Figure 4-4 – Speckle pattern (Schnars and Jueptner, 2005)

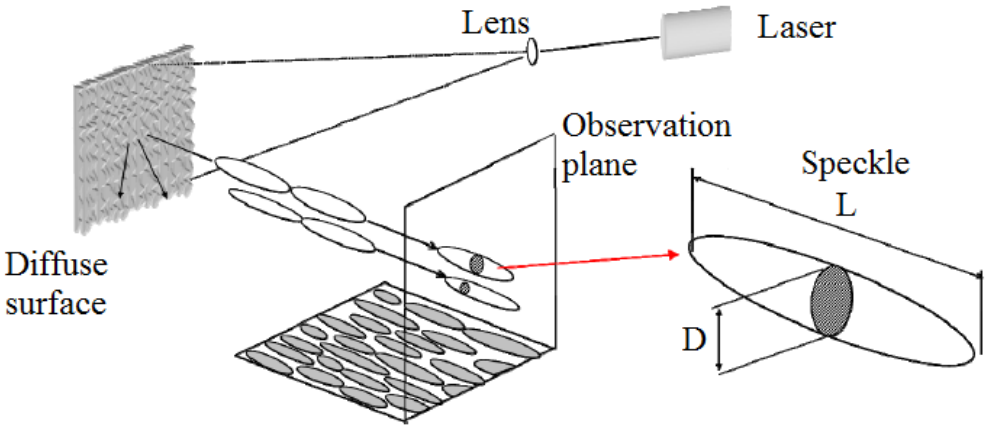

Figure 4-5 – Spatial shape of the speckle (Lopes, 2007)

The technological advances of recent decades transformed interferometry in an experimental tool for studying the behaviour of structures. Moreover, with more powerful CCD and CMOS sensors, as well as the quick processing and recording of large amounts of information have improved the speckle interferometry. It brought some advantages in application on SHM systems:

- ☑ Less recording time (no need to reveal the holograms);
- ☑ Display of result in real time (high rates of image acquisition);
- ☑ Possibility to make quantitative measurements (technical image processing);
- ☑ Increased immunity to external disturbances (vibrations);
- ☑ It made possible the construction of simpler systems, compact and easy to use in industrial environments.

Speckles result from interference of light scattered by the surface points. The phases of the waves scattered by different surface points fluctuate statically due to the height variations. If the waves interfere with each other, a stationary speckle pattern develops. It can be shown that the probability density function for the intensity in speckle pattern obeys negative exponential statistics (Schnars and Jueptner, 2005):

$$P(I)dI = \frac{1}{\langle I \rangle} \exp\left(-\frac{I}{\langle I \rangle} \right) \tag{4.8}$$

where *P(I)dI* is the probability that the intensity at a certain point is lying between *I* and *I* + *dI*. $\langle I \rangle$ is the mean intensity of the entire speckle field. The most probable intensity value of a speckle is, therefore, equal to zero, *i.e.* most speckles are black. The standard deviation σ_I is calculated by

$$\sigma_I = \langle I \rangle \tag{4.9}$$

that means the intensity variations are in the same order as the mean value. A usual definition of the contrast is given by

$$V = \frac{\sigma_I}{\langle I \rangle} \tag{4.10}$$

Based on this relation, it can be concluded that the contrast of a speckle pattern is therefore always unity.

4.2.3. Typical Shearography Speckle System

Two wave fields, object and reference, as in DSPI interfere, but two slightly spatially shifted speckle fields of the rough surface are superposed. The role of the reference wave is taken by one of the two mutually shifted object wave fields, which is called self-reference. The shifting of the speckle fields is performed by a shearing element, i.e. a glass wedge in front of one half of the imaging lens, two tilted glass plates, a Wollaston prism, or a Michelson interferometer-like arrangement with one mirror slightly tilted as shown by Fig. 4-6.

The shear system allows the direct measurement of the displacement gradient. Measurements of static or quasi-static phenomena are performed by using the Michelson type

shear interferometer and the temporal modulation technique of phase via a translation of mirrors by actuation of a piezoelectric actuator for the quantitative determination of the interferogram phase (Fig. 4-6). Indeed, the object wave front is divided by the beam splitter into two wave fronts, and by a slight rotation δ of the one mirror. These are spatially shifted to create the interference phenomenon (*cf.* Fig. 4-7).

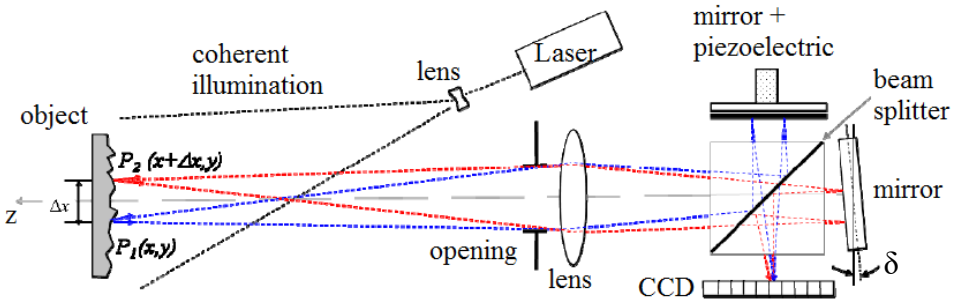

Figure 4-6 – Shear interferometer configuration of Michelson type (Lopes, 2007)

Figure 4-7 – Image of a shearing camera (Schnars and Jueptner, 2005)

The two points on the surface $P_1(x,y)$ and $P_2(x+\Delta x,y)$, laterally separated by Δx due to the mirror rotation δ, are observed by superposition on the image plane. With respect to the wave fronts, they are described by:

$$E_1(x,y) = A_0(x,y)e^{j\phi(x,y)},$$
$$E_2(x,y) = A_0(x,y)e^{j\phi(x+\Delta x,y)}, \tag{4.11}$$

where A_0 is the amplitude, $\phi(x,y)$ is the direct wave phase and $\phi(x+\Delta x,y)$ is the shifted wave phase from Δx in x-axis direction.

The intensities produced by initial interference A, before deformation, and end interference B, after deformation $\Delta\varphi(x,y)$ are given by:

$$\begin{aligned} I_A(x,y) &= \left|E_1(x,y)+E_2(x,y)\right|^2 \\ &= I_1(x,y)+I_2(x,y)+2\sqrt{I_1(x,y)I_2(x,y)}\cos(\psi(x,y)) \end{aligned} \tag{4.12}$$

$$I_B(x,y) = \left|E_1(x,y)+E_2(x,y)\right|^2 = I_1(x,y)+I_2(x,y)+2\sqrt{I_1(x,y)I_2(x,y)}\cos(\psi(x,y)+\Delta\phi(x,y)-\Delta\phi(x+\Delta x,y))$$

The punctual subtraction of the intensities for the two deformation states of the object can be written as:

$$\begin{aligned} (I_A - I_B)(x,y) = 4\sqrt{I_1(x,y)I_2(x,y)}\cdot \\ \sin\left[\psi(x,y)+\frac{\Delta\phi(x,y)-\Delta\phi(x+\Delta x,y)}{2}\right]\cdot \\ \sin\left(\frac{\Delta\phi(x,y)-\Delta\phi(x+\Delta x,y)}{2}\right) \end{aligned} \tag{4.13}$$

The term defined by the square root represents the background intensity, the first sine corresponds to stochastic variation of the speckle noise modelled by the object deformation, the second sine of the expression. In this case, the displacement vector out-of-plane *w(x,y)* and the second sine argument can be related by,

$$\Delta\phi(x,y)-\Delta\phi(x+\Delta x,y) \approx \frac{4\pi\Delta x}{\lambda}\frac{\partial w(x,y)}{\partial x} \tag{4.14}$$

This expression shows that the interference pattern is an approximation of the first spatial derivative of the displacement field in the x-direction of the lateral shift between the wave fronts. Thus, the interferometer is very sensitive to movements of the rigid body with $d(x,y) = \text{Const.}$ and some perturbations, which act equally on the two wave fronts, such as vibration and external interferences to the data acquisition system.

4.2.4. Phase-Shifting Method

The phase maps obtained from the speckle interferometry techniques, by temporal phase with fixed jumps and spatial phase by Fourier transform of a single pattern containing carriers fringe, are usually contaminated by measurement noise of high frequency. The speckle decorrelation partial or total is the main source of this noise. Furthermore, there is the electronic noise in the CCD and CMOS sensors, the quantum nature, which manifests in the form of

random fluctuations in voltage or current. The thermal noise, noise transition and the noise generation-recombination, are in the category of less influential sources. At the end of this range is observed the noise generated by the shock of photons in optical sensors, *i.e.* photon noise.

Regarding the noise filtering techniques, these can be divided into temporal and spatial techniques. The latter are particularly effective in phenomena that present temporal distributions of noise with zero mean. Its influence can be reduced by calculating the record average of a spaced in time sequence. Coming the signal/noise ratio increased in proportion to $\sqrt{n}$, where n is the records number used in the calculation of the arithmetic mean. In the speckle interferometry, spatial distribution of the noise, spatial techniques are particularly useful in reducing the speckle noise in the phase maps by eliminating the high order terms of the spatial frequency or wave number domain.

The phase filtering techniques are the first and main barrier in reducing unwanted noise maps. The application of these techniques have the main objective to improve the signal/noise relation without destroy the phase information. This information is essential for the proper determination of the continuous field measurement. There are several filtering techniques with low-pass filters, among them, the technique commonly used for removing noise in image, have:

- ☑ Average;
- ☑ Gaussian;
- ☑ Median;
- ☑ Wiener;
- ☑ Spline;
- ☑ Fast Fourier Transform (FFT);
- ☑ Windowed Fourier Transform (WFT);
- ☑ Wavelets.

While the fringe pattern describes the surface deformation of the object, its appearance is not unique. The direction of the deformation, towards the optical setup or away, can only be detected with the determination of the phase ϕ. This is commonly done by application of phase shifting techniques (commented above). The optical setup is modified by a phase shifter in one of both beams. This phase-shifter (*e.g.* piezoelectric element behind mirror) allows adding a known phase shift to the random phase ϕ. Several images (*i.e.* ≥ 3) are recorded in a temporal manner, using different known phase shifts. Among these, the most common is the method of the four images offset from one another $\pi/2$. This choice is due to the good compromise between

the number of recordable pictures and the sensitivity to the error produced by deviations in the imposition of the phase shift. Subsequently, the phase angle ϕ can be calculated by

$$\phi(x,y) = \arctan\left[\frac{I_{i,4}(x,y) - I_{i,2}(x,y)}{I_{i,1}(x,y) - I_{i,3}(x,y)}\right], \qquad i = A,B \tag{4.15}$$

In this work, it is considered the phase shift equal π/2, starting of zero and m equal 4. Thus, the phase shift can be calculated as shown in Eq. (4.16) given by Kreis (2005).

$$\Delta\phi = \arctan\left[\frac{I_4 - I_2}{I_1 - I_3}\right], \tag{4.16}$$

The phase difference (after subtraction) is usually displayed in a phase map, which contains still the information of the fringe pattern and, in addition, the directional information of the deformation. It was possible to solve of the phase sampling equations with known and unknown phase shifts (Kreis, 2005). The filtering allows to considerably reduction of the noise in phase maps, making the process of elimination of phase discontinuities (unwrapping) simpler. However, in the presence of high noise level in the maps, these algorithms do not allow remove completely the noise (as shown in Lopes (2007)). In these situations, the perturbations in the maps will be resolved by robust unwrapping methods. The next step of the post-processing consists on analysing the images by using the phase unwrapping methods.

4.2.5. Phase Unwrapping Methods

The phase maps exhibit discontinuous phase distributions defined by the spatial modulation of the measuring field amplitude. For the reconstruction of the continuous field, corresponding to the measurement range, it is necessary to remove properly these discontinuities by applying unwrapping methods. Despite improvements of phase maps introduced by processing, ambiguities still exist in the phase due to the persistence of noise. The high density and/or low contrast of the fringes become the aim of removing the correct discontinuities difficult to achieve.

There are a number of requirements to be fulfilled in order for a reliable demodulation. The first is that continuous phase data are adequately sampled. Each demodulation procedure checks interference phase differences of neighbouring pixels. If due to a violation of the

sampling theorem this difference exceeds π, the demodulation must fail, because of the introduction of unnecessary phase jumps. On the other hand, under sampled high frequency fringe data may result in small phase differences between two pixels, but, in practical, a phase jump between these pixels is missed.

Considering the Eq. (4.16), the phase difference before and after slitting can be calculated separately as:

$$\begin{aligned} \tan\Delta\phi_1 &= \frac{I_4 - I_2}{I_1 - I_3} \\ \tan\Delta\phi_2 &= \frac{I_4 - I_2}{I_1 - I_3} \end{aligned} \tag{4.17}$$

Thus, the phase difference change can be obtained as:

$$\Delta\varphi = \Delta\phi_1 - \Delta\phi_2 \tag{4.18}$$

Therefore, interference phase maps calculated with the arctan function or other inverse trigonometric functions contain 2π jumps at those points, where an extreme value of Δφ (either –π or π) is reached. The interference phase along a line of such a phase image looks like a saw tooth function as shown by Fig 4-8(a). The correction of these modules 2π jumps in order to generate a continuously phase distribution, which is called demodulation, continuation or phase unwrapping. Unwrapping methods can be divided into two categories:

- ☑ Path-following methods:
  - o Goldstein;
  - o Quality-Guided;
  - o Mask Cut;
  - o Flynn.
- ☑ Minimum-norm methods:
  - o FFT/DCT;
  - o PCG;
  - o Multigrid.

In the following, a general description about the unwrapping algorithm is commented. At first, a one-dimensional interference phase distribution is considered. The difference between the phase values of adjacent pixels Δφ(n+1) – Δφ(n) is calculated. If this difference is less than –π, then all phase values from the n+1 pixel onwards are increased by 2π. If this difference is greater than +π, then 2φ is subtracted from all phase values, starting at number

n+1. If none of above mentioned conditions is valid, then the phase value remains unchanged. The practical implementation of this procedure is done by calculating first a step function, which cumulates the 2π jumps for all pixels as shown by Fig 4-8(b). Hence, the continuous phase distribution is calculated by adding this step function to the unwrapped phase distribution as shown by Fig. 4-8(c). Almost every pixel can be used as a starting point for this unwrapping procedure, not necessarily the pixel at the start of the line. If a central pixel is chosen as starting point, then the procedure has to be carried out in both directions from that point.

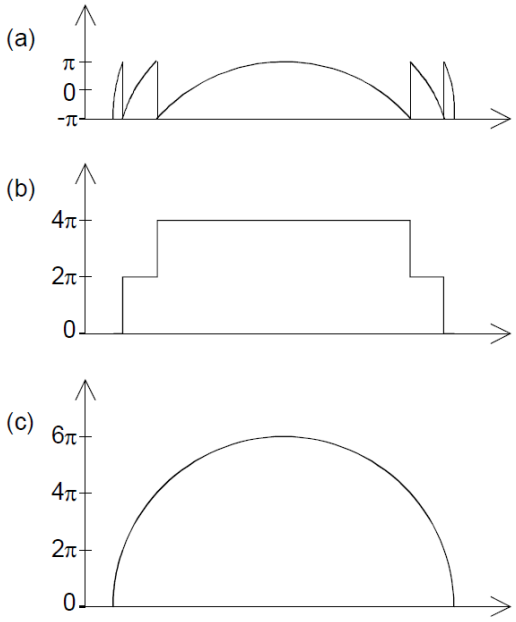

Figure 4-8 – Phase unwrapping (a) Interference phase (b) Step function and (c) Unwrapped interference phase (Schnars and Jueptner, 2005).

4.3. Experimental Setup

The main principle of shearography consists on producing a pair of laterally displaced, or sheared, speckle images. Shearography is an optical method, which uses speckle shearing interferometry to measure displacement gradients at the surface of a structure. The speckle patterns produced by a structure in stressed and unstressed states are subtracted, revealing changes in displacement gradient. These are generally faster in damaged regions. Laser speckles are produced whenever a surface, whose roughness is of the order of one wavelength of light or greater, is illuminated with highly coherent light. The light scattered from any moderately distant point consists of many coherent wavelets, each arising from a different element of the

surface. The optical path differences between these various wavelets may differ by several wavelengths and the interference between these wavelets results in a granular pattern of intensity, which is termed speckle.

The shearography system used in this work is capable to measure the rotation field of a surface with orthogonal movement to the measurement plane. The configuration of this optical transducer is based on the interferometer Michelson and uses the technique of temporal modulation phase (TPM) for extracting the phase map (*cf.*, Fig. 4-6).

The phase maps obtained from the speckle interferometry techniques, by temporal phase with fixed jumps and spatial phase by Fourier transform of a single pattern containing carriers fringe, are usually contaminated by measurement noise of high frequency. The speckle decorrelation partial or total is the main source of this noise. Furthermore, there are the electronic noises in the CCD and CMOS sensors, the quantum nature, which manifests in the form of random fluctuations in voltage or current. The thermal noise, noise transition and the noise generation-recombination, fall into one category less influential sources. At the end of this range is the noise generated by the shock of photons in optical sensors, i.e. photon noise. Regarding the noise filtering techniques, these can be divided into temporal and spatial techniques. The phase filtering techniques are the first and main barrier in reducing unwanted noise maps. The application of these techniques have the main objective to improve the signal/noise relation without destroy the phase information. This information is essential for the proper determination of the continuous field measurement.

The phase maps exhibit discontinuous phase distributions defined by the spatial modulation of the measuring field amplitude. For the reconstruction of the continuous field, corresponding to the measurement range, it is necessary to remove properly these discontinuities by applying unwrapping methods. Despite improvements of phase maps introduced by processing, ambiguities still exist in the phase due to the persistence of noise. The high density and/or low contrast of the fringes become the aim of removing the correct discontinuities difficult to achieve.

Shearography system used in this work is installed at Faculty of Engineering of University of Porto (FEUP - Portugal), and it is capable to measure the rotation field of a surface with orthogonal movement to the measurement plane. The configuration of this optical transducer is based on the interferometer Michelson and uses the technique of temporal modulation phase (TPM) for extracting the phase map. The phase shifting is established by way of the translation of one of the mirrors of the interferometer by a piezoelectric actuator. The

piezoelectric is controlled by a National Instruments PCI-6722™ board via Burleigh PZ-70™ amplifier. A high-resolution Dalsa camera model and image acquisition Matrox Helios XCL™ board model are used for image acquisition. Four images with 4 megapixel (2352x1728) and CMOS sensor were used. A program developed in MATLAB™ 7 runs in order to control the mirror position, offset to acquire the images and to calculate the phase map related to the rotation surface (Fig 4-9).

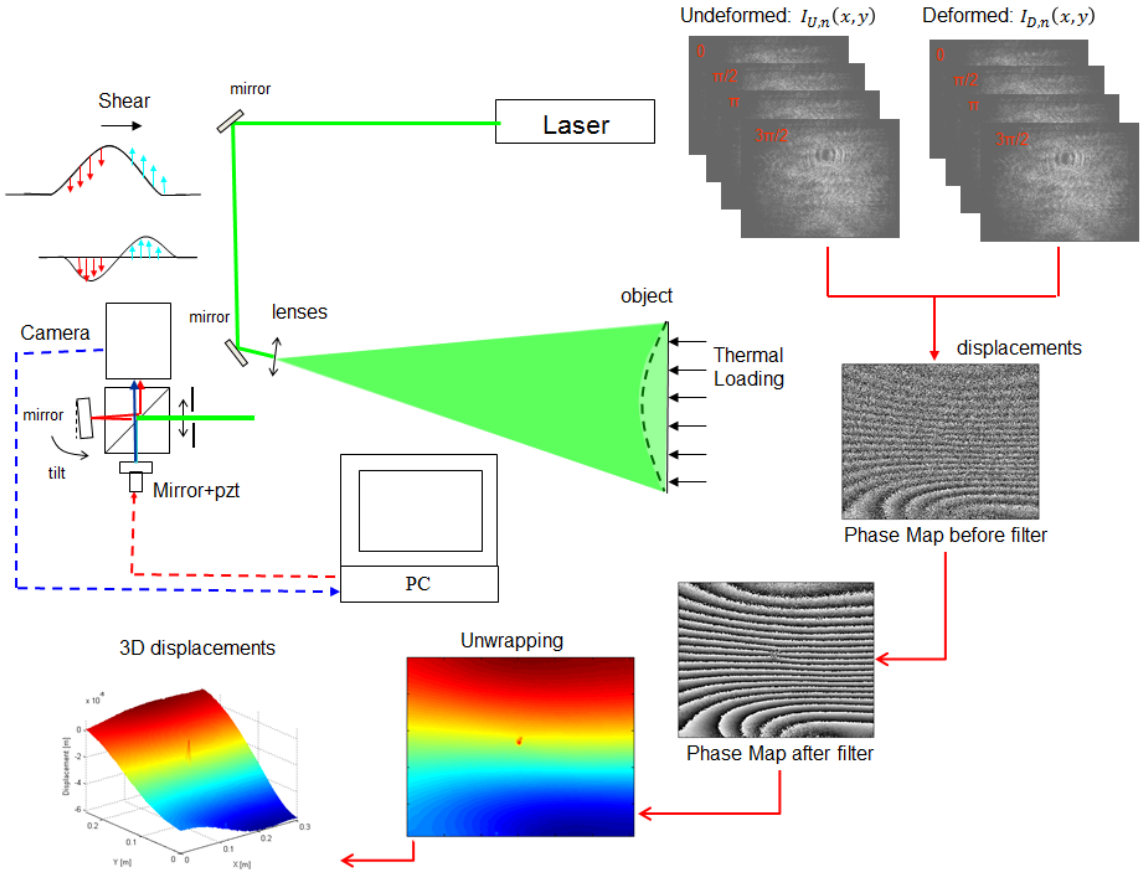

Figure 4-9 – General methodology and steps to measure the displacement.

The experimental setup was mounted on a Newport™ optical table in order to guarantee greater stability to the assembly and experimental measurements (Figure 4-10). The composite specimens were simply supported on this table also. The rotation fields were obtained by the registry before and after the thermal stress, which was measured by the shear system via the technique of temporal phase modulation. The thermal load was applied on one side of the plate by heating the surface for 5 seconds by using a 100W lamp, rising the surface temperature in 2ºC.

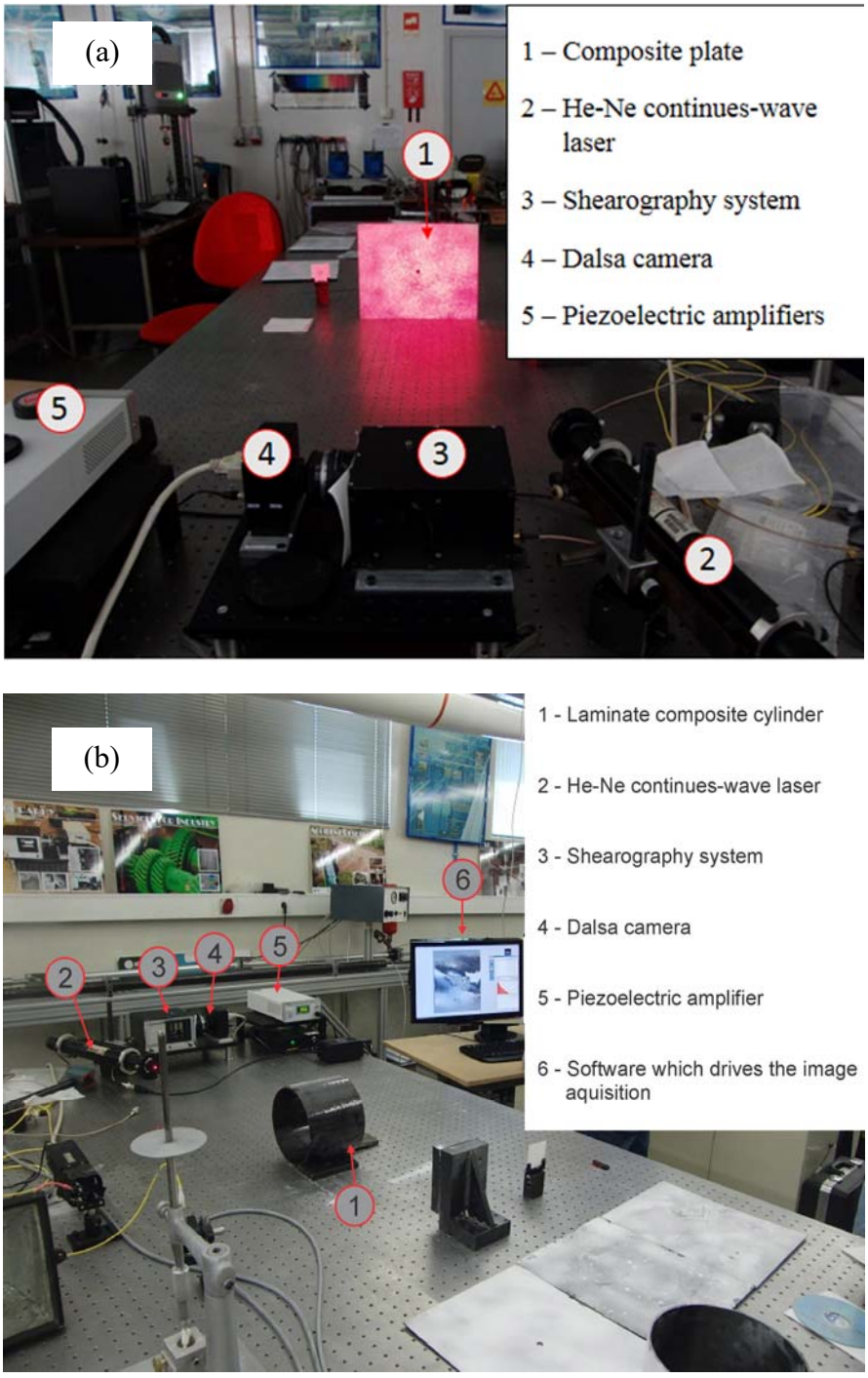

Figure 4-10 – Experimental setup at FEUP (Portugal) (a) Composite plates, and (b) Composite cylinders (Faculty of Engineering of University of Porto – FEUP)

Ultrasonic inspection is considered as the most efficient method used for quality control and materials quality inspection in all major industries. This includes electrical and electronic components manufacturing, production of metallic and composite materials and fabrication of structures such as airframes, piping and pressure vessels, ships, bridges, motor vehicles, machinery and jet engines (Hasiotis *et al.*, 2011).

Ultrasonic NDE uses focused acoustic energies that interact with the micro-structure of the material being analysed Cromer (2010). Water is often used as a coupling media between the wave source and material as it is efficient for transmitting sound energy and creating a distinct and uniform interface with the material. Acoustic waves become reflected when they encounter variations in density such as those at the water/material interface and those caused by internal damage. Since the acoustic properties of air differ significantly than those of the surrounding material, defects within the material (*i.e.* voids, open cracks, delaminations, etc.) reflect different wave characteristics (Cromer, 2010). The resulting feedback includes the variations of wave amplitude and velocity, which are then translated into information regarding the material structure.

In this method, high frequency sound waves, which are generated by a transmitting sensor, travel through the material via a coupling medium. These sound waves are reflected with some attenuation at interfaces, which can be associated to the presence of cracks, voids, inclusions, delamination, or other discontinuities. A transducer receives and converts the signal to a voltage. Once the signals from the transducers are modified, a device displays the output as a time history of the sound waves travelling through the sample.

ASM Handbook (1992) presents the pulse- echo method as the most widely used ultrasonic method; this method is very often used for flaws location and thickness measurements. Ultrasonic data can be presented in different formats, which are A-, B-, and C-scan. A-scans show received ultrasonic energy as a function of time. B-scans display cross-sectional view of a specimen showing the depth or travel time of the sound waves with respect to the linear position of the transducer. C-scan display records echoes from the internal portions of test pieces as a function of the position of each reflecting interface within an area (Hassen *et al.*, 2012). The ultrasonic signal amplitude or the time-of-flight is shown as a shade of gray or a colour for each position, which was scanned. The C-Scan schematic diagram is presented in the Fig. 4-11.

In this work, a C-scan technique at KU Leuven was used to compare the damage extension in the damaged structures with the shearography speckle technique. Figure 4-12 shows the experimental C-Scan test setup used for the composite plates.

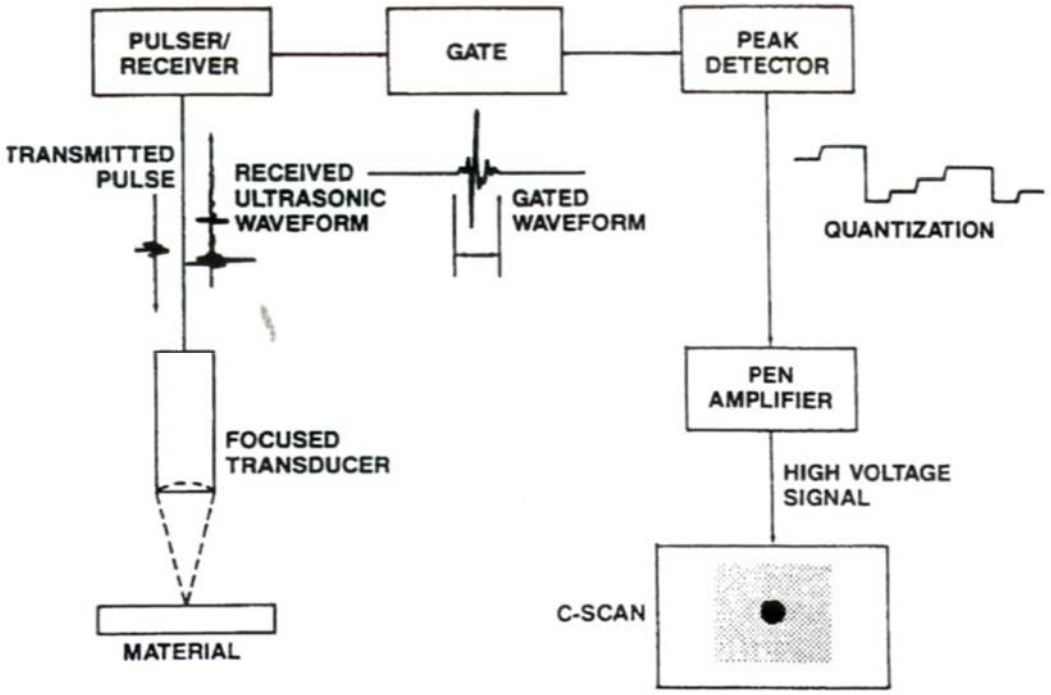

Figure 4-11 – Schematic diagram of pulse-echo C-scan by peak amplitude analysis (Cromer, 2010)

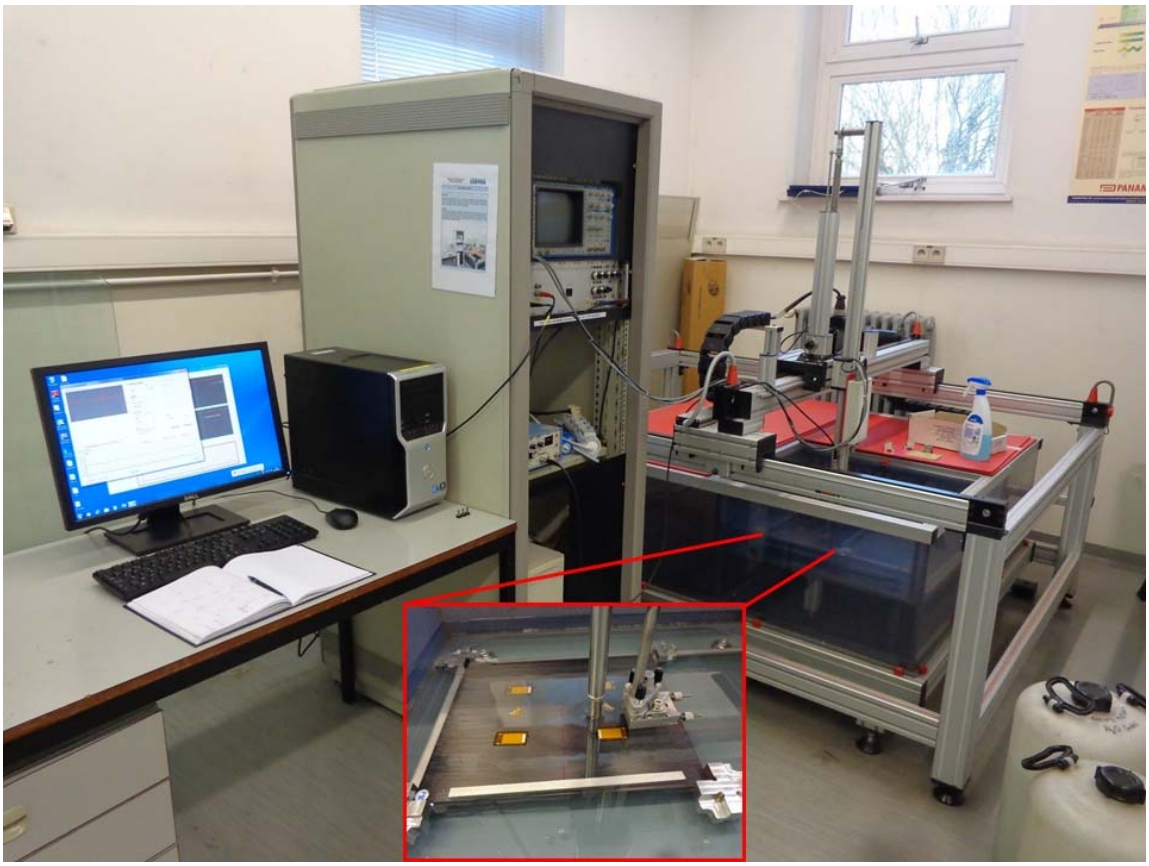

Figure 4-12 – C-Scan test setup used for the composite plates (KU Leuven)

4.4. Results and Discussion

The composite plates and cylinders were analysed via Shearography. In the tests, the composite specimens were simply supported (*cf.*, Fig. 4-10), which is mounted on a Newport^{TM} optical table to guarantee greater stability to the assembly and experimental measurements. The rotation fields are obtained by the registry before and after the thermal stress, which is measured by the SS system via the technique of temporal phase modulation. The thermal load is applied on one side of the plate by heating the surface for 5 seconds with a 100W lamp, rising the surface temperature in 2ºC.

In the experimental procedure for measuring the rotation fields, the first four images of offset $\pi/2$ are acquired with the board in the initial position, whereas the remaining four recorded after heating the surface and stabilized the position. In this process, the evolution of the fringes corresponding to the rotation fields is accompanied by real-time visualization of the interference map, which is obtained by subtraction between the captured image at every moment (distorted image) and the first recorded image (reference image). The set of eight images is processed through the phase calculation techniques, filtering and phase unwrapping, providing the rotation fields.

4.4.1. Carbon Composite Plates

The damage of composite plates under impact loading were predicted via FE model, and after that, the real damaged were inspected by Shearography Speckle. In addition, C-scan analysis was performed in order to compare with the Shearography Speckle system. The SS technique by analysing the disturbances in the rotation field in order to locate and quantify the extension of the damage in the structure was applied. In the Figures from 4-13 to 4-22, it is possible to observe the phase map for all damaged plates after filtration and the corresponding rotation fields obtained for a thermal stress with deviation in horizontal wave fronts of Δx equal to 5mm and vertical wave fronts of Δy equal to 5mm . The damaged areas are depicted by red lines. Also, it is possible to compare this damage with the damage area predicted by the finite element analysis and the C-Scan technique.

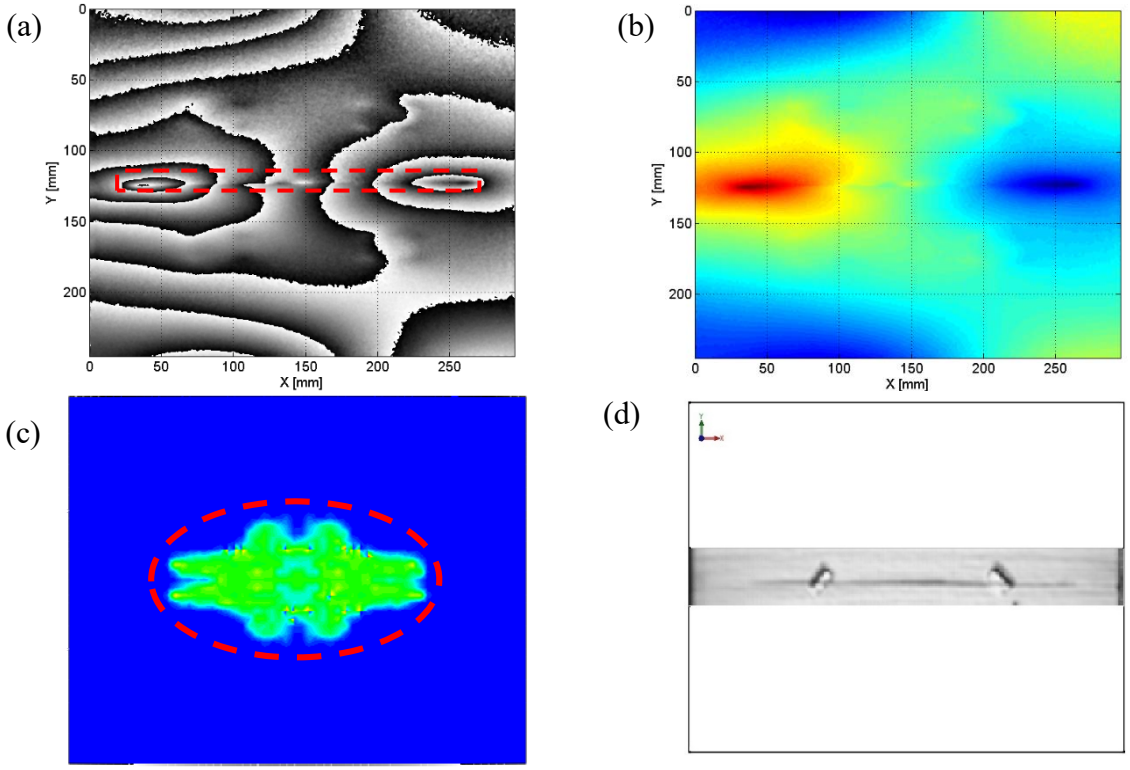

Figure 4-13 – NDT result for a composite plate $P01_{CF}$ (a) filtered phase maps (b) curvature fields (c) computational results and (d) damage area by C-Scan technique.

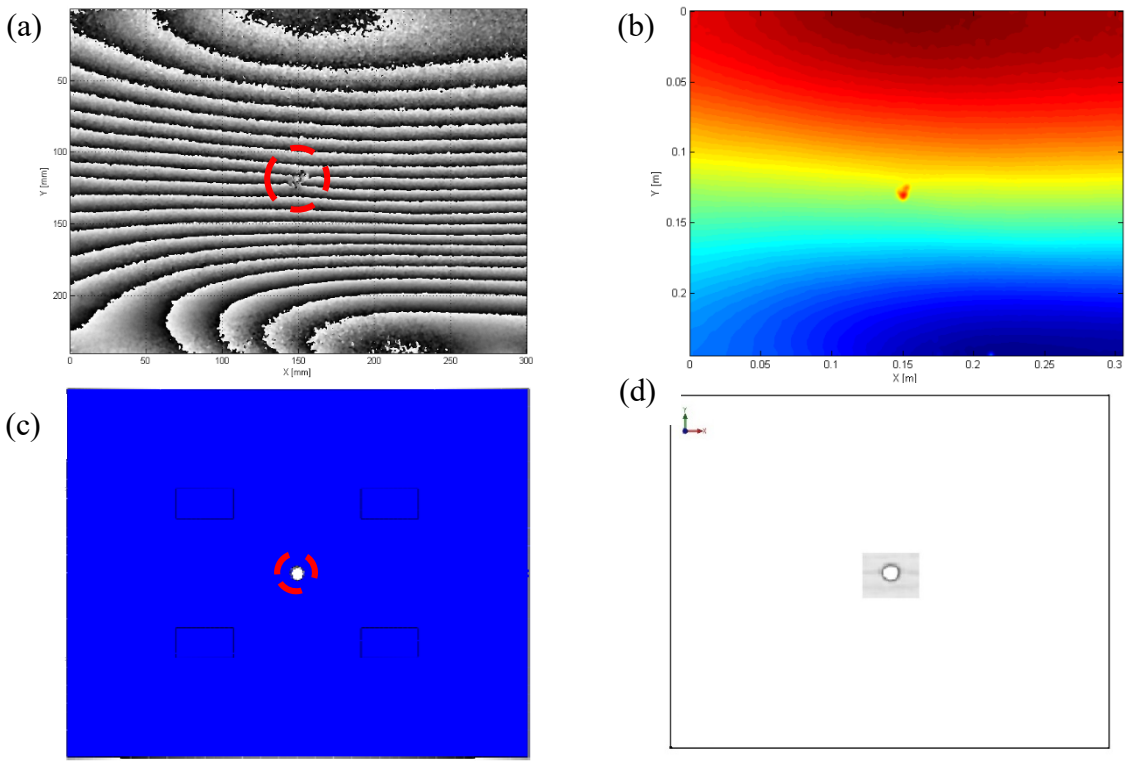

Figure 4-14 – NDT result for a composite plate $P02_{CF}$ (a) filtered phase maps (b) curvature fields (c) computational results and (d) damage area by C-Scan technique.

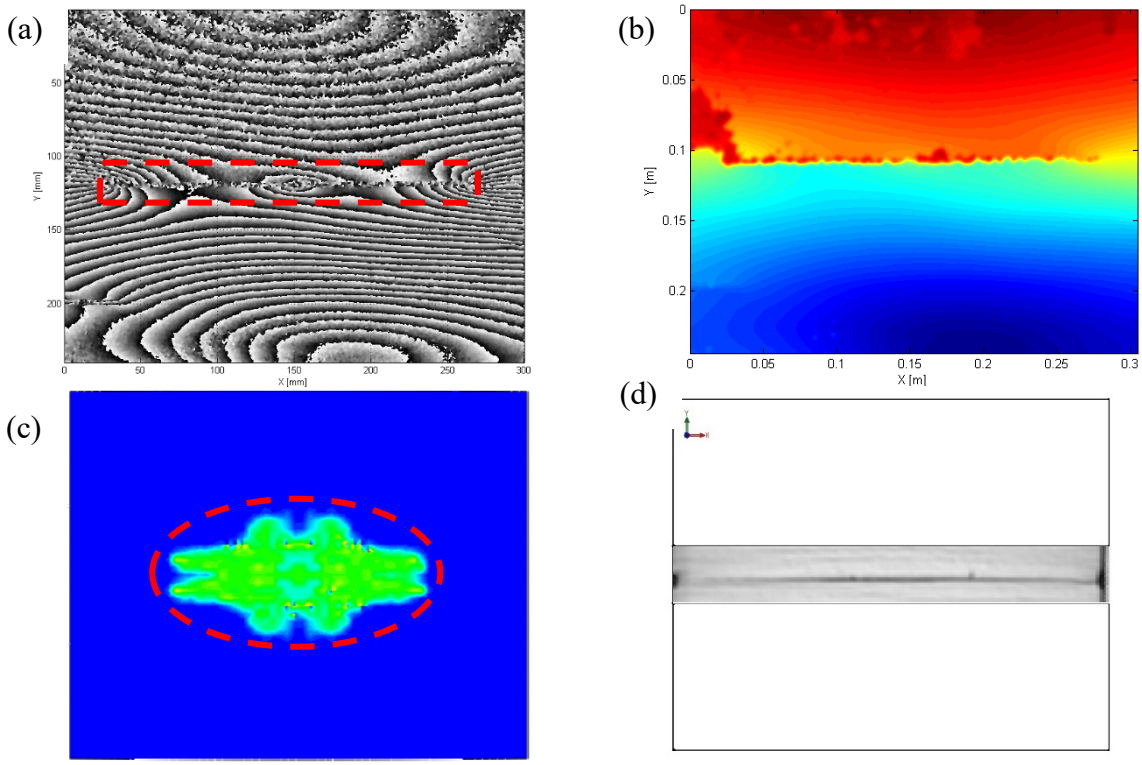

Figure 4-15 – NDT result for a composite plate $P03_{CF}$ (a) filtered phase maps (b) curvature fields (c) computational results and (d) damage area by C-Scan technique.

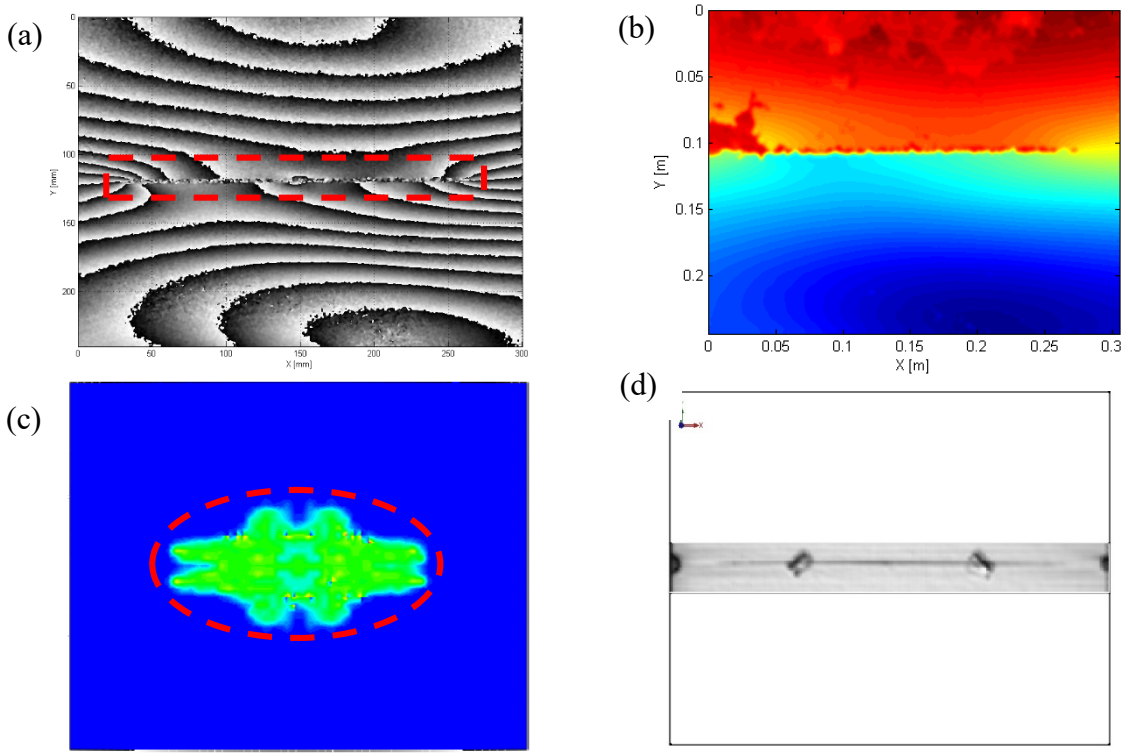

Figure 4-16 – NDT result for a composite plate $P04_{CF}$ (a) filtered phase maps (b) curvature fields (c) computational results and (d) damage area by C-Scan technique.

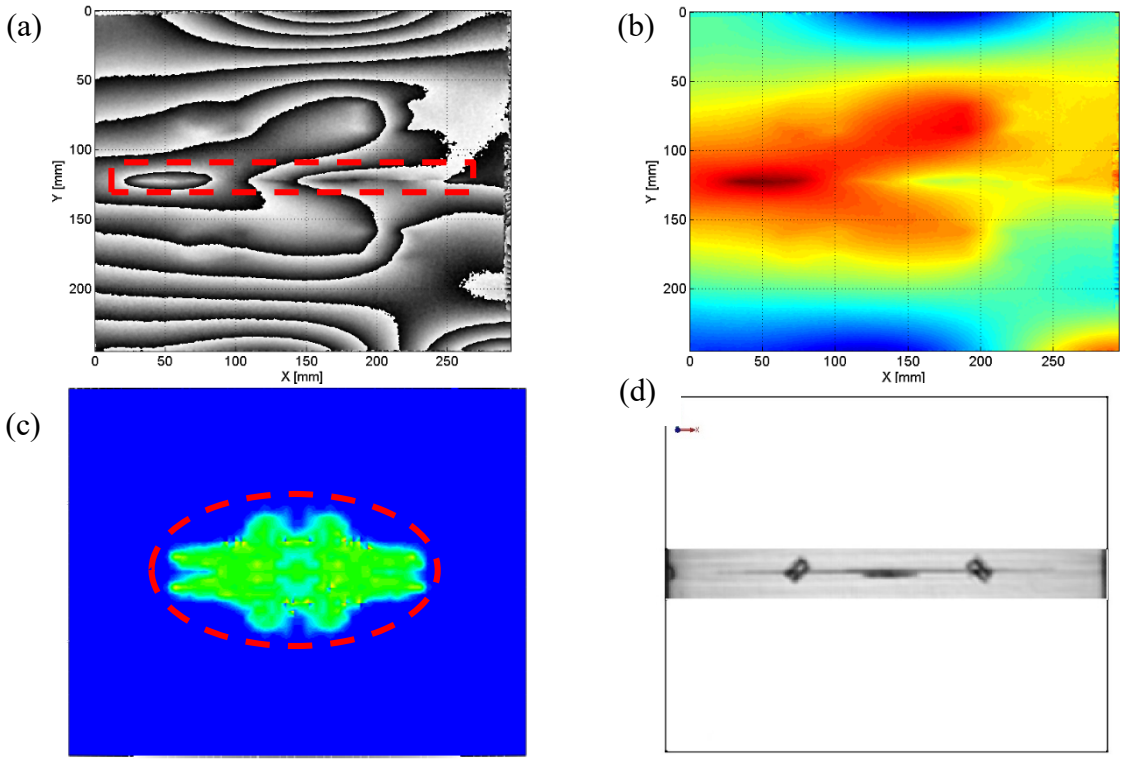

Figure 4-17 – NDT result for a composite plate $P05_{CF}$ (a) filtered phase maps (b) curvature fields (c) computational results and (d) damage area by C-Scan technique.

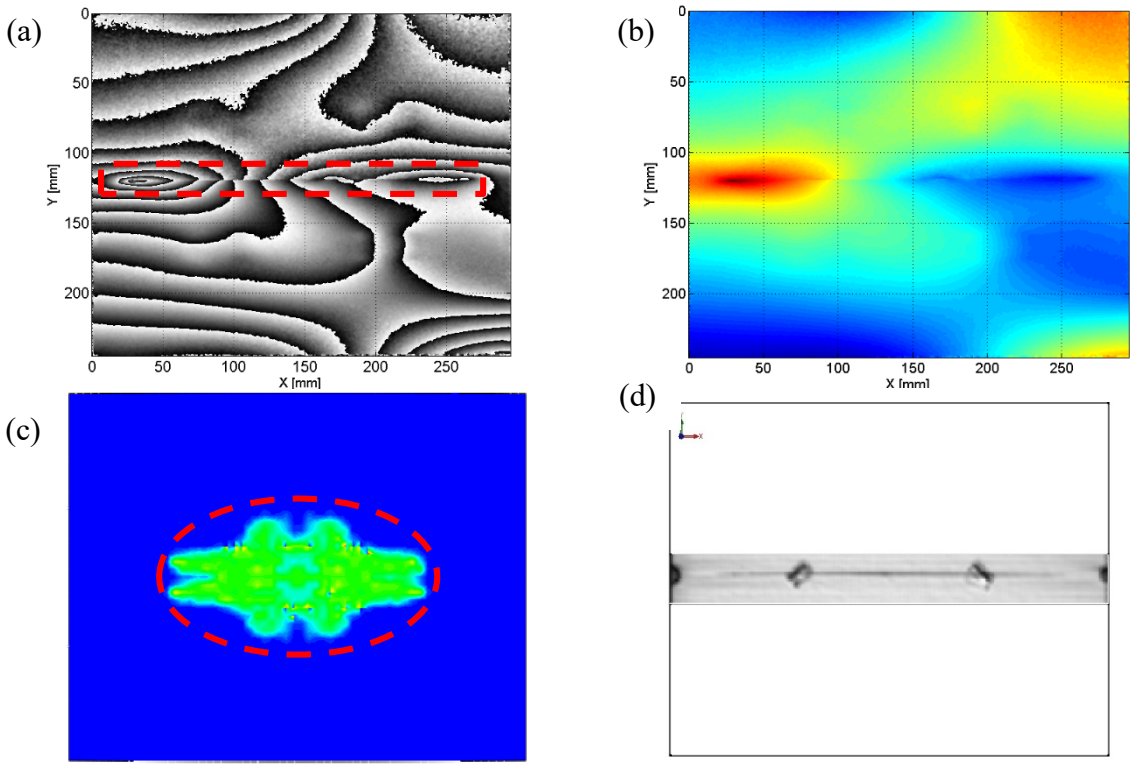

Figure 4-18 – NDT result for a composite plate $P06_{CF}$ (a) filtered phase maps (b) curvature fields (c) computational results and (d) damage area by C-Scan technique.

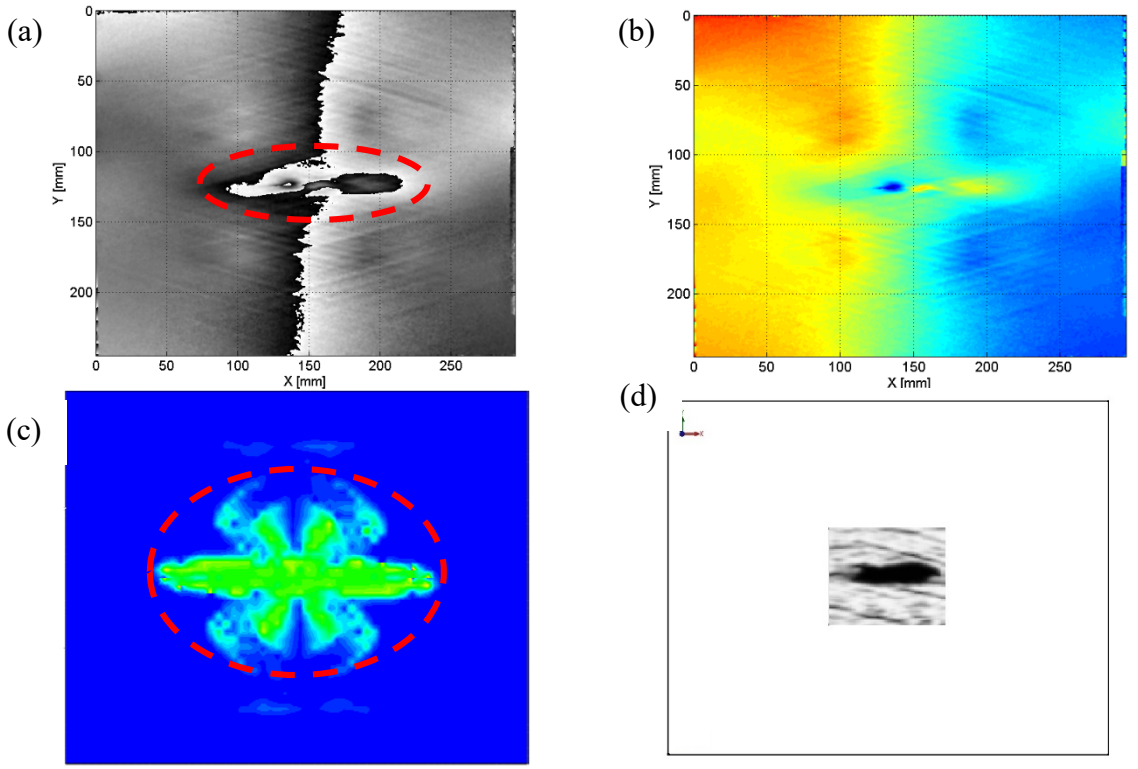

Figure 4-19 – NDT result for a composite plate $P09_{CF}$ (a) filtered phase maps (b) curvature fields (c) computational results and (d) damage area by C-Scan technique.

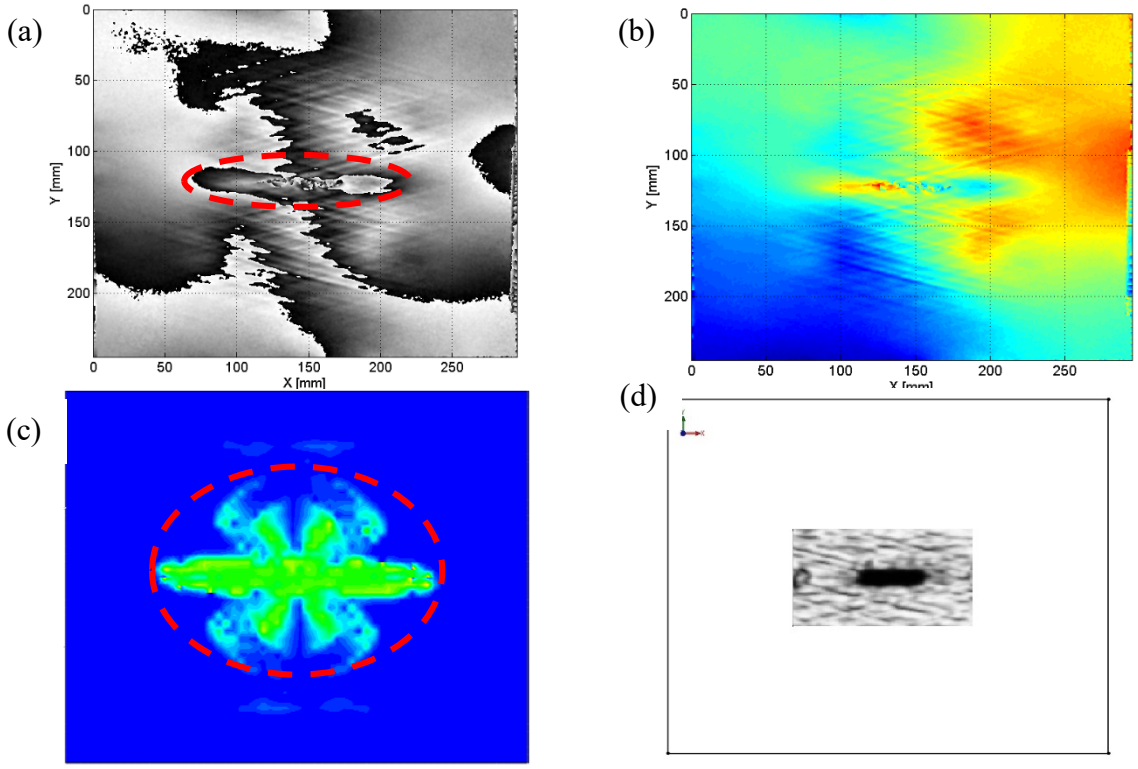

Figure 4-20 – NDT result for a composite plate $P10_{CF}$ (a) filtered phase maps (b) curvature fields (c) computational results and (d) damage area by C-Scan technique.

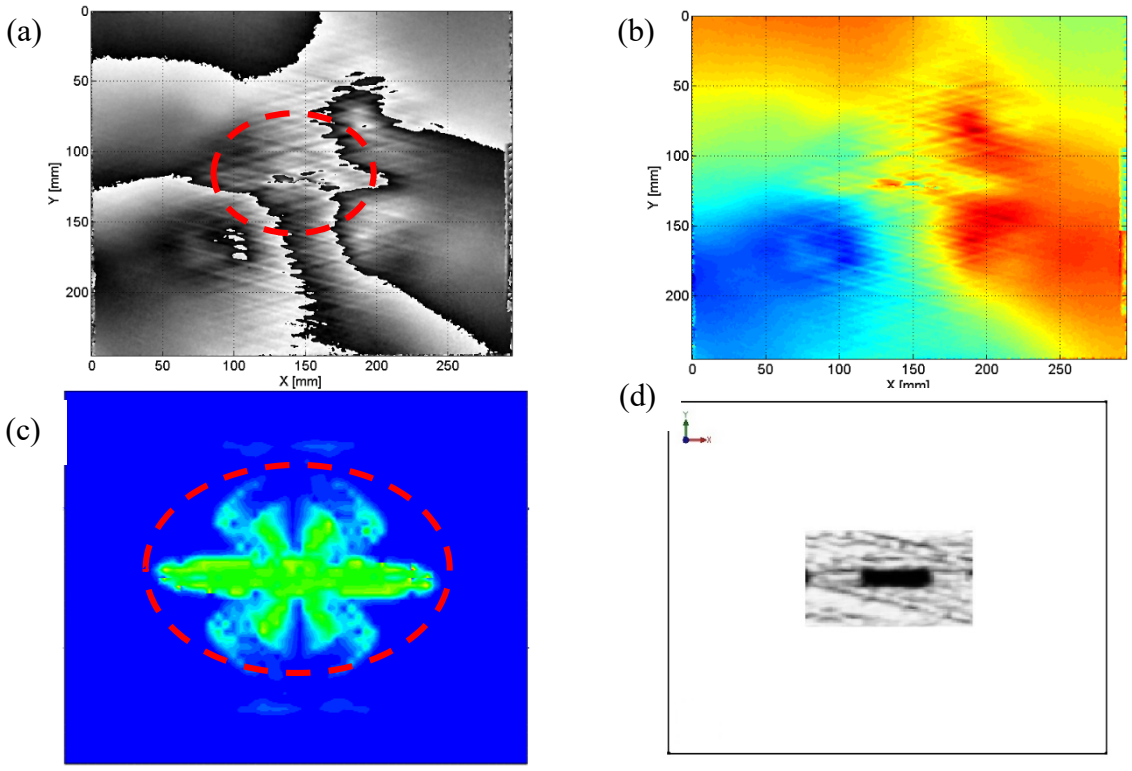

Figure 4-21 – NDT result for a composite plate $P11_{CF}$ (a) filtered phase maps (b) curvature fields (c) computational results and (d) damage area by C-Scan technique.

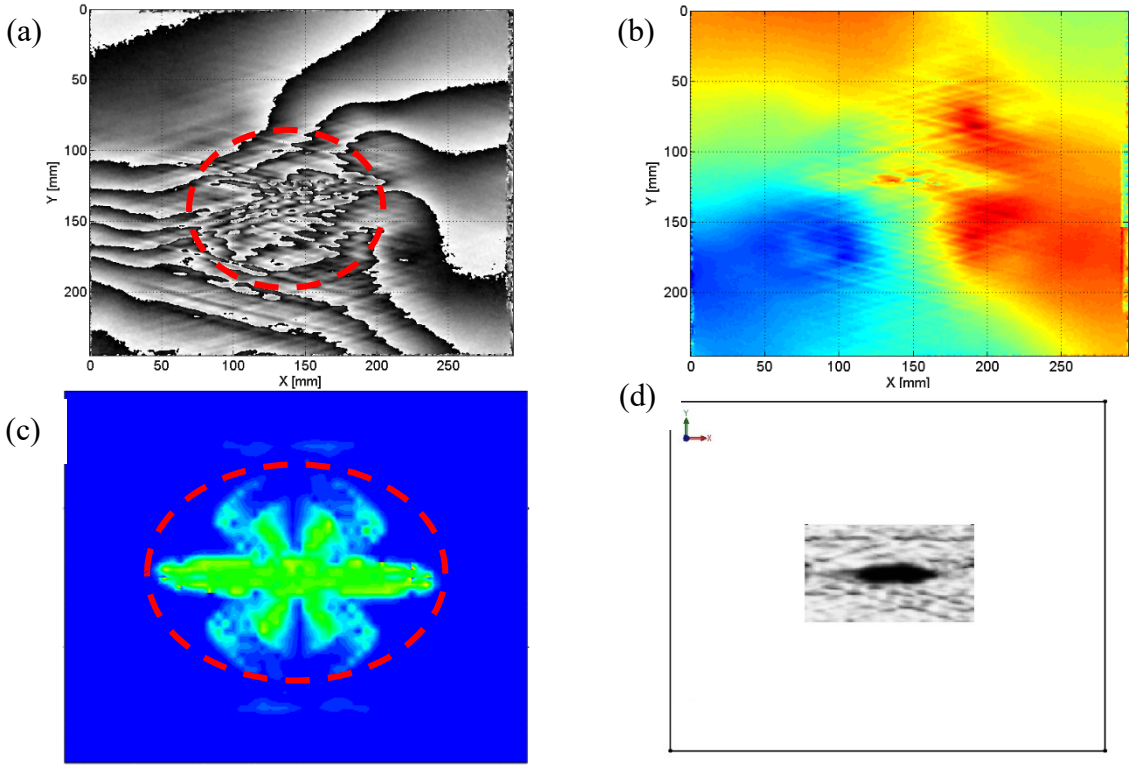

Figure 4-22 – NDT result for a composite plate $P12_{CF}$ (a) filtered phase maps (b) curvature fields (c) computational results and (d) damage area by C-Scan technique.

The phase maps obtained for the thermal loading can be observed in Fig. 4-13 to 4-22, being the shearing value Δx of 10mm. The fringe analyses in the phase map show the presence of damage. It can be seen that because of the stacking sequence, the Plates 01, 03, 04, 05, and 06 show damage in the fibre direction. However, for the Plates 09, 10, 11, and 12, the damage is concentrated on the impact region. In the Plate 02, it is also possible to verify the damage caused by manufacturing process, *i.e.* central hole. The Table 4-1 presents the damage dimensions determined after the use of the optical methodology.

Table 4-1 – Damage dimensions calculated by shearography speckle.

Plate	Damage	Length [mm]	Width [mm]
Plate 01	Longitudinal crack caused by impact	234.90	-
Plate 02	Hole (diameter of 5mm)	6.64	6.32
Plate 03	Longitudinal crack caused by impact	240.65	-
Plate 04	Longitudinal crack caused by impact	224.98	
Plate 05	Longitudinal crack caused by impact	236.11	-
Plate 06	Longitudinal crack caused by impact	243.50	-
Plate 09	Concentrate crack caused by impact	115.54	23.61
Plate 10	Concentrate crack caused by impact	119.51	19.92
Plate 11	Concentrate crack caused by impact	75.94	23.03
Plate 12	Concentrate crack caused by impact	138.19	57.89

The Table 4-2 presents the damage dimensions determined by computational analysis, considering the continuum damage mechanics model.

Table 4-2 – Damage dimensions calculated by computational analysis

Plate	Damage	Length [mm]	Width [mm]
Plate 01	Longitudinal crack caused by impact	174.20	79.39
Plate 02	Hole (diameter of 5mm)	5.00	5.00
Plate 05	Longitudinal crack caused by impact	174.20	79.39
Plate 09	Concentrate crack caused by impact	182.20	110.80
Plate 12	Concentrate crack caused by impact	182.20	110.80

It is possible to observe some differences between the experimental results (Shearography Speckle) and the computational analysis (Continuous Damage Model – UMAT). These differences can be explained, because the uncertainty values in the numerical models such as damping factor, total and each layer thickness and curvature due to the manufacturing process of the plates. Also, due to the continuum damage mechanics formulation that take into account the damage in the fibre and in the matrix, however the damage provided by delamination is neglected and the pre-loading forces during the clamped drop test analysis.

4.4.2. Carbon Composite Cylinders

The damage of composite cylinders under impact loading were predicted via FE model, and after that, the real damaged cylinders were inspected by Shearography Speckle. In the Figures from 4-23 to 4-25, it is possible to observe the numerical and experimental results. The damage zone is calculated dividing the damage area (experimental or computational) by the total area of the cylinder. In the experimental results, it is shown the phase map for all damaged cylinders (Type A, Type B and Type C) after filtration and the corresponding rotation fields obtained for a thermal stress with deviation in horizontal wave fronts of Δx equal to 5mm and vertical wave fronts of Δy equal to 5mm (shearing values). Moreover, the fringes induced by the cylindrical geometry have been smoothed, and the damage has been highlighted with better contrast. The damage zone is indicated by red lines (Figs. 4-23 to 4-25). As a result of the high spatial resolution, a high density of fringes is accomplished in all maps. The analysis of these maps already reveals perturbations in the phase map fringes pattern near the region of the impact. These perturbations in the phase maps of the rotation fields are due to the damage.

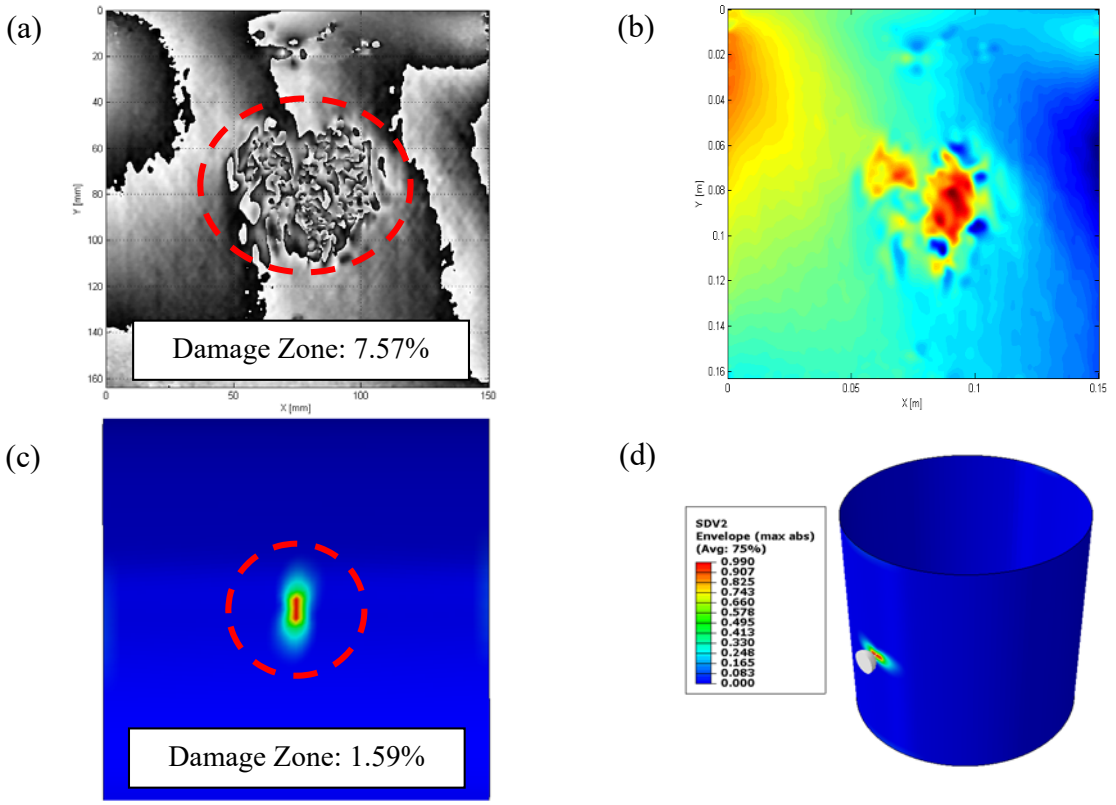

Figure 4-23 – NDT result for a composite cylinder type A (a) filtered phase maps (b) curvature fields (c) computational results and (d) damage area provided by the UMAT code.

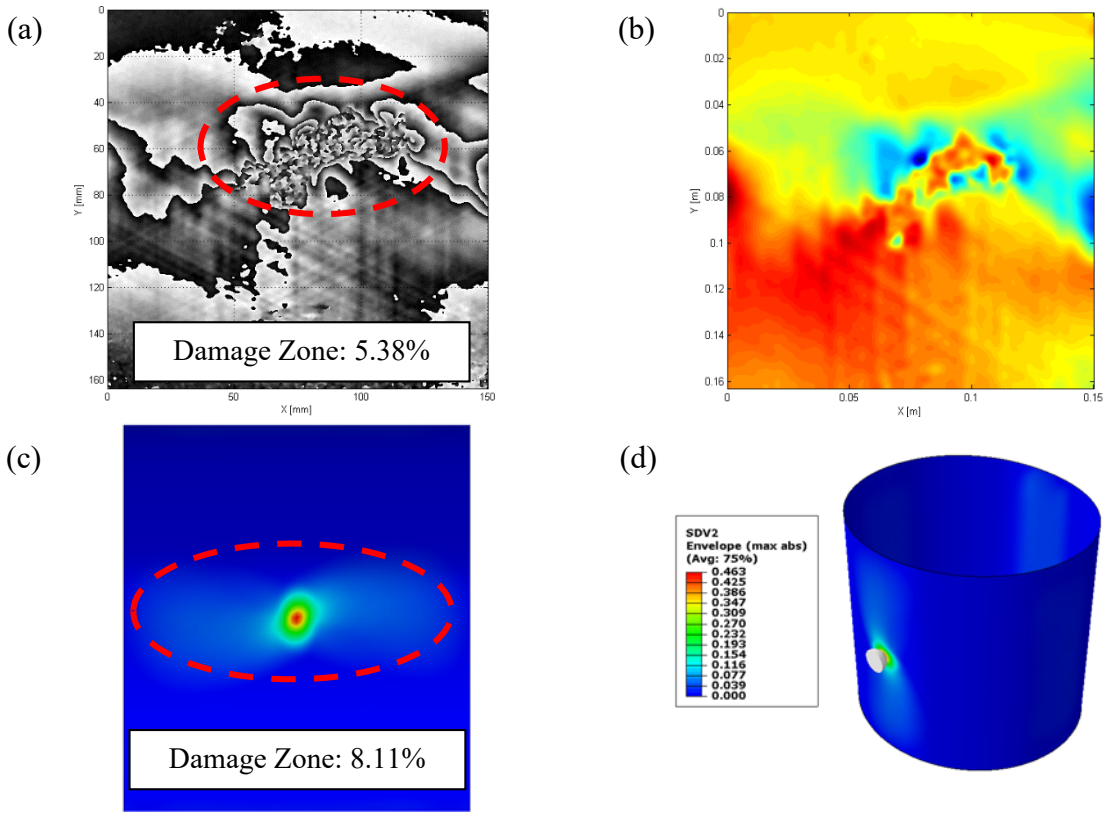

Figure 4-24 – NDT result for a composite cylinder type B (a) filtered phase maps (b) curvature fields (c) computational results and (d) damage area provided by the UMAT code.

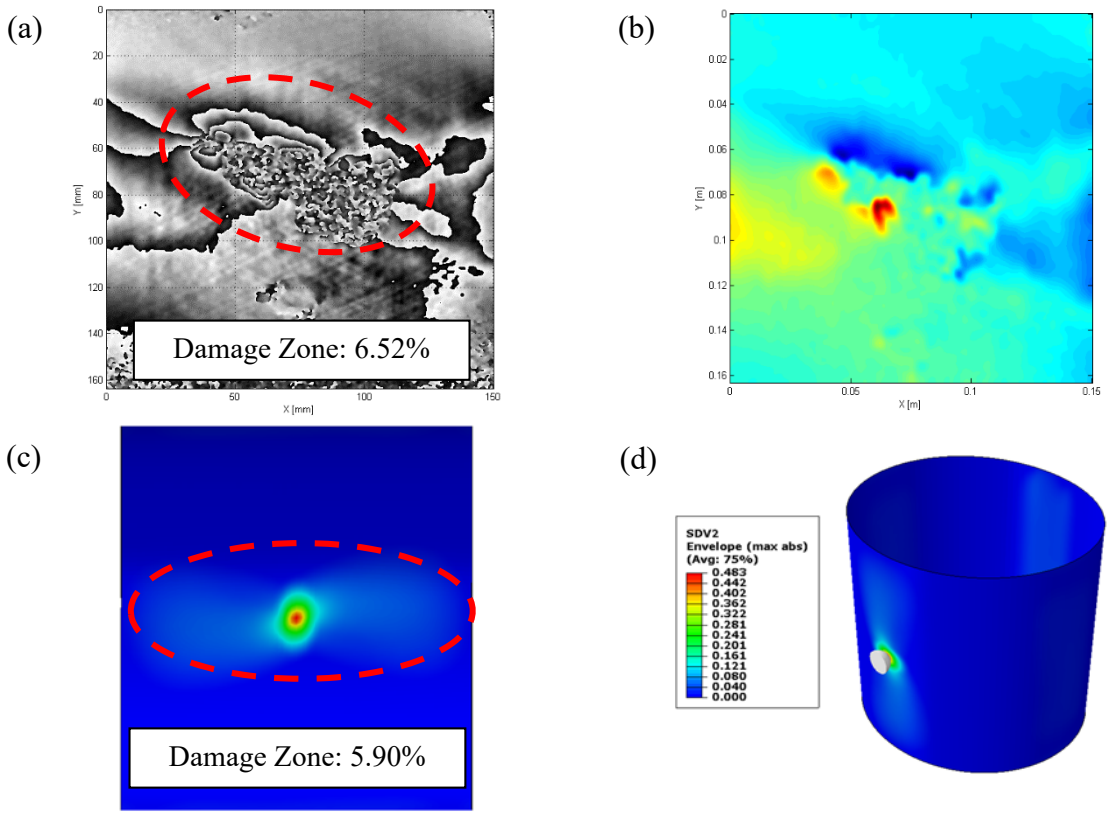

Figure 4-25 – NDT result for a composite cylinder type C (a) filtered phase maps (b) curvature fields (c) computational results and (d) damage area provided by the UMAT code.

Regarding the computational analyses, it is possible to conclude that the FE model has shown a good performance only for cylinder Type C, because it predicted the lamina failure with certain accuracy and low computational cost. For all cylinders type, the classical pine tree shape for damage has not been identified by the numerical analyses, because a delamination model was not implemented. However, it is verified that the damage zones provided by the computational and experimental technique are similar for Type C, as shown in the figures. Therefore, the experimental analyses presented higher damage zone compared to the computational models. Considering the cylinders lay-up, Type A was the most damaged cylinder compared to the type B and C. In fact, this makes sense, because there is a great difference between flexural stiffness of each cylinder type as shown by Ribeiro (2013).

4.5. Partial Conclusions

The damage zone on the carbon fibre/epoxy composite laminates produced by low velocity impact loading was investigated by using computational and experimental techniques. The application of Non Destructive Testing methods to composite specimens was the subject of this study. Shearography speckle was investigated and compared to identify their performance and limitations for impacted and central hole damage in composite laminates. This technique measures the deformation gradient by detecting the phase difference caused by an applied load. Moreover, shearography speckle can perform a quick investigation and brings others common benefits such as non-contact, scalable and full-field measurement. This technique is a really good alternative to estimate damage extension and type in composite structures, because composite materials can have different kinds of damages such as debonds, delamination, matrix cracking and impact, and this estimation is very complicated. Therefore, the experimental results confirm that the shearography speckle is a very useful NDE technique, because of its detection capacity for barely visible impact damages, which are not often detected by visual inspection.

By the other side, the computational results demonstrate the potential and limitations of the material model in order to predict the extension of the damage. Indeed, depends on the stacking sequence of the laminate, it is possible to estimate the extension of the damage with good accuracy or not.

Therefore, shearography technique combined to FE models can be used to detect, to localize and, mainly, to provide extension of the damage in composite structures. In addition, SS could be used as an alternative or complement method in SHM systems. Thus, it will be very useful if the type of damage and/or the location are known a priori. This is the reason that it is very strategy to perform not only a global method like vibration based method, but also Finite Element Analyses, before to carry out a local inspection by using shearography speckle. Therefore, in other words, there is a good perspective for the application of shearography speckle combined to VBM and FE models in SHM systems for composite structures.

CHAPTER 5

Residual Strength Criterion

Composite materials have been utilised for nearly four decades thanks to their beneficial characteristics, such as stability, weight and high stiffness. Particularly in the aerospace industry the use of composites is justified by reducing structural weight with consequent fuel saving and improving performance. Composite laminates are especially sensitive to low velocity impacts since even minor damage can cause considerable reduction in structural integrity. In addition, laminated composite materials are susceptible to damage by out-of-plane impact, often associated to a reduction of mechanical properties. In fact, the impact energy is absorbed through remarkable internal damage mechanisms without exterior signs detectable by visual inspection. Various types of damage, such as delamination, fibre breakage, matrix cracking and fibre–matrix interfacial debonding, can occur, leading to structural failure. To ensure that a damaged structure will not catastrophically fail during service life and will maintain maximum structural efficiency, it is necessary to carry out damage tolerance studies, evaluating the residual properties of the structure after impact. This study presents a new criterion to evaluate the residual strength of laminate composite subject to low velocity impact loading. One of the objectives of this work is the investigation of the feasibility of an elastic flexural test as an effective metric for the residual properties of an impacted composite. For this, a flexure after impact (FAI) test is used alongside the standard CAI (Compression After Impact) to compare its practicality as a damage tolerance technique. Low-velocity impact tests and residual strength tests are performed using an instrumented drop-weight machine and static test machine, respectively. The experiments were carried out for composite specimens, which are flat and rectangular plates. Two different stacking sequences and thicknesses are tested to analyse the influence of these factors on the impact and post-impact response. The residual flexural strength of damaged specimens is evaluated by quasi-static four-point bending test. The results of drop-weight impact tests and FAI tests on carbon/epoxy laminates are presented. A new criterion based on a relationship between damage metric and FAI analysis is proposed. These results are normalised using the maximum load and the metrics for damage analysis, *i.e.* if there is no damage in the structure, then the metric returns zero value. If the structure is partially damaged then the metric returns a number between one and zero. Finally, if the structure is totally damaged (*i.e.* the residual strength is lower than design specification), then the metric returns a value equal to one. In other words, if the structure does not have enough residual strength, considering design requirements, the value is equal to one. Finally, the advantages and limitations of this criterion into the context of SHM system (Structural Health Monitoring System) are discussed.

5.1. Review of Residual Strength

Composite materials have been widely used in aeronautic and aerospace structural components, mainly because of their excellent specific mechanical properties. They may suffer damage during their manufacture, assembly, maintenance or service life, caused by different types of impact, of which low-energy impact is considered the most dangerous. Most composite materials exhibit high sensitivity with respect to loads and effects, but this is not taken into consideration in selecting the structure of the material. Such unfavourable factors include technological defects of different types, local temperature effects, etc. All of these factors decrease the resistance to basic (theoretical) effects, carrying capacity, longevity, and structural integrity. Damage like delamination type can cause a significant decrease in the critical loads on the compressed elements, while surface impacts can reduce the crack resistance (Bolotin and Shchugrev, 1993).

The resistance to impact is an important part in the reliability assessment of composites because the impact loads universally exist in the actual application in aeronautics and astronautics, engineering structure, and other fields (Chenghong *et. al*, 2008). The poor tolerance to accidental low velocity impacts of composite laminates is a limitation to their use in industry (Collombet *et al.*, 1996). Impact damage is considered the primary cause of in-service delamination in composites giving reductions of the compressive residual strength up to 60% (Zheng and Sun, 1998), which is one of the most important aspects that inhibit larger wide-spreading of such structures (Amaro *et al.*, 2006).

Most of the visible damage is a result of high-velocity high-energy impacts, where the impactor perforates into the laminated material. The analysis of such cases is mostly concerned with the estimation of the damage geometry and its influence on the strength of the laminate. On the other hand, most of the invisible damage is the result of low-velocity and/or low-energy impacts. Even though much attention has been devoted recently to the impact problems of composites, the studies are not sufficient especially on the problem caused by invisible damage (Rotem, 1988).

There are at least three dominant failure mechanisms taking place in the composite laminates when subjected to impact loading. These are interlaminar fracture (or delamination), matrix cracking due to transverse shear and translaminar fracture (*i.e.*, fibre fracture/kinking). The first two mechanisms are sensitive to the properties of the matrix material and the last to

the fibre performance, especially the failure strain. Depending on the properties of constituents, choice of fibre and matrix types, the fracture process can be a very complex combination of these energy absorption mechanisms (Kim *et al.*, 1993).

Damage tolerance in laminated composites is usually studied by determining the effect of different impact energies on their residual strength. Normally, the compression after impact (CAI) tests have been performed for the structures damaged by low energy impact. This global testing process has two steps: at first, the specimen is subjected to low-energy transverse impact, which brings about a certain degree of damage inside the laminate; then the damaged specimen is loaded in in-plane compression to determine its residual strength. CAI tests must be carried out in a special device, which avoids global buckling of the impacted specimens; but, sometimes, the failure evolution as the delamination progress gives rise to a local buckling phenomenon on the sublaminates.

The aim of a damage-tolerance study is to evaluate the capacity of a structural element to continue supporting its functions after an impact; for this reason, in a beam designed to bear bending moments, it is necessary to evaluate the residual flexural properties (Santiuste *et al.*, 2010). Several techniques have been used to assess the impact damage tolerance of composite laminates. These can be generally classified into non-destructive tests (NDT) and destructive tests. Among the NDTs, it can highlight methods such as IR Thermography, Ultrasonic Inspection, C-scan, X-Ray Radiography and Mechanical Impedance Analysis. On the other hand, considering the destructive techniques, the compressive strength after impact (CAI) has been the most popular tool (Kim *et al.*, 1993). However, it is possible to find in the literature other post-impact tests conducted by previous investigators include longitudinal and transverse tensile tests (Wu and Springer, 1988; Wyrick and Adams, 1988; Jang *et al.*, 1992), Iosipescu shear test (Wu and Springer, 1988), short beam shear test (Wu and Springer, 1988; Jang *et al.*, 1992), multi-span beam shear test (Williams and Rhodes, 1982), flexural test (Santiuste *et al.*, 2010) and centre-notched flexural test (Maikuma *et al.*, 1990).

The post-impact mechanical properties of composites have been receiving extensive investigation in recent years, most of which devoted to compression properties (CAI). Bolotin and Shchugrev (1993) investigated the sensitivity of three types of composite under low velocity impact. Different mechanical aspects of damaged samples were investigated: residual resistance to interlayer failure as a function of the forms of separation; longitudinal and transverse shear; residual resistance to growth of interlayer fatigue cracks as a function of the forms of shear; residual tensile strength; residual critical buckling force in compression of

damaged samples of different length. The impact energy was used as the principal parameter in the impact event. The results were compared to the mechanical aspects of an undamaged composite. Soutis and Curtis (1996) analysed the results of several selected experimental studies related to impact and post-impact compression damage and failure of continuous carbon-fibre/epoxy composites in order to predict their residual strengths.

Qi and Herszberg (1999) developed a semi-empirical analysis on residual compressive strength (RCS) of carbon/epoxy woven composite laminate, which included the damage effects caused by impact and hygrothermal cycling. The results from the analysis showed a good convergence to the experimental data for the plain-woven fabric laminates. Puhui *et al.* (2002) have presented a new method to determine the compression after impact (CAI) strength of composite laminates. In this method, an impact damage zone was modelled as an equivalent hole. The most outstanding characteristic of the method is the simplification of the impact damage, which was based on the compressive failure mechanisms of impacted laminates. The study provided a very simple and effective approach for CAI strength prediction compared to the previous methods.

Sanchez-Saez *et al.* (2005) examined the damage of various lay-ups of thin carbon/epoxy laminates using compression after impact tests via a new testing device, which adapts to the thicknesses of the specimens and does not require tabs for any modification of the specimen geometry. Based on that device, CAI tests were done for different carbon/epoxy laminate lay-ups (quasi-isotropic, cross-ply and woven) and the values of the residual strength and the normalised residual strength of the laminates were obtained as a function of the impact energy. Nilsson (2005) reported concerns about rapid semi-analytical methods for calculating residual strength of damaged composite structures. First, a modification of a semi-analytical method is presented, which concerns buckling and growth of delaminations in damaged composite structures. Then the characterisation of impact damaged regions in composites as regions with reduced stiffness is discussed. In an attempt to estimate the relative inclusion stiffness, *i.e.* the stiffness reduction coefficient of damaged composite, a comparison between the results from a semi-analytical method, and an alternative method is developed.

An (2008) presented a novel and practical method using crossing-slitting and ESPI in order to obtain reliable and accurate residual stress measurements for uniform and non-uniform stress states. The measurement results show that this procedure plays an important role for the success of residual stress evaluation. Based on the observed displacement data and FE calculated calibration data, an inverse computational method is developed to recover the

residual stresses in a material for both uniform and non-uniform cases. By combining cross-slitting and ESPI, more reliable results for the three in-plane residual stress components can be obtained. Williams *et al.* (2009) considered the development of autonomic self-healing within a carbon fibre-reinforced polymer (CFRP). They demonstrated that a significant strength recovery (>90%) is possible, when a resin filled hollow glass fibre system is distributed at specific interfaces within a laminate, minimising the reduction in mechanical properties whilst maximising the efficiency of the healing event.

Minak *et al.* (2010) have investigated the residual torsional strength of cylindrical T300-carbon/epoxy tubular specimens damaged by low velocity impacts. Results show that, even if the absorbed energy during impacts is the same, the residual torsional strength of the laminates is highly affected by the torsional preload. Wang *et al.* (2010) also investigated low velocity impact characteristics and residual tensile strength of carbon fibre composite laminates by experimental and numerical methods. Two different tensile damage modes after different impact energies were observed. The degradation of residual tensile strengths can be divided into three stages for different impact energies, and amplitudes of degradation were affected by stacking sequences. Rivallant *et al.* (2013) presented a model for the numerical simulation of impact damage, permanent indentation and compression after impact (CAI) in CFRP laminates. The same model was used for the evolution of damage during both low velocity/low energy impact and CAI tests. Moreover, the impact energy effect on the residual strength was evaluated and compared to the experimental data.

The research on residual flexural properties (FAI), especially the influences and mechanisms of the various factors, are still few (Cromer, 2010). Rotem (1988) studied the influence of the material, testing a carbon/epoxy laminate and a less brittle glass/epoxy laminate. Three-point bending tests were conducted in a drop-weight tower to damage the beam. Afterwards, the residual properties were evaluated by static three-point bending tests. Richardson and Wisheart (1996) reviewed the low-velocity impact responses of composite materials. First the term ‘low-velocity impact’ is defined and major impact-induced damage modes are described from onset of damage through to final failure. Then, the effects of the composite’s constituents on impact properties are discussed and post impact performance is assessed in terms of residual strength. Mouritz *et al.* (1997) studied the flexural strength and interlaminar shear strength of stitched and non-stitched glass-reinforced plastic (GRP) laminates under conditions of increasing impact energy and increasing number of repeated

impacts. The three-point flexural strength and short-beam interlaminar shear strength of the GRP before impact loading were reduced by stitching as a result of stitching damage.

Mariatti *et al.* (2001) carried out studies on the flexural damage behaviours of satin and plain continuous-fibre-impregnated thermoplastic (COFIT) prepreg woven composites. Shim and Yang (2005) investigates experimentally and theoretically the mechanism of damage development in composite laminates subjected to low-velocity impact loading; the focus is to describe the effects of impact and laminate parameters on the residual mechanical properties (Young's modulus and failure strength). Amaro *et al.* (2006) presented the results of a study on carbon-fibre-reinforced epoxy composite in which the residual flexural strength was investigated in terms of different stacking sequence and impact energies. After impact, the specimens were analysed by ultrasonic C-Scan inspection to obtain the position and the size of the delaminations in the samples. Zhang and Richardson (2007) investigated the low velocity impact induced non-penetration damage in pultruded glass fibre reinforced polyester (GRP) composite materials using an instrumented falling weight impact test machine with a chisel shaped impactor. The characteristics of the impact event, force/time and force/deflection traces were determined. The post impact structural integrity of impacted specimens was evaluated by three point bending tests.

Reyes and Sharma (2010) investigated the low velocity impact behaviour of three layer thermoplastic laminates consisting of woven glass fibre and polypropylene for two different fibre volume configurations. The impact damaged plates were tested under four point bending (4 PB) loading conditions. Results showed a reduction in flexural strength and modulus as the impact energy increased. Santiuste *et al.* (2010) focused on an experimental study of flexural after impact behaviour of glass/polyester composite beams. The influence of impact energy, beam width, and impactor-nose geometry on the residual flexural strength was evaluated. The residual flexural strength of damaged specimens, evaluated by quasi-static three-point bending tests, was found to depend on the extent of damage, so that the residual flexural strength was lower in the specimens in which the damage reached the edges of the beam. Cromer (2010) presented a series of low-velocity drop-weight impact tests which were conducted on S-2 glass/epoxy samples simply-supported along two edges. The residual compressive strength and flexural properties were measured.

Impacted laminates are typically subjected to compression testing after impact to investigate its residual properties. However, this procedure uses a complex rig, and friction effects between the laminate and guides are often difficult to take into account. During the CAI

test the compression load cannot cause global or total buckling on the tested specimen. The expected result considers only micro-buckling mechanisms followed by fibre breakage, cracks, etc. Also, CAI tests are not very simple to carry out and require more material than the conventional mechanical tests, as tensile, compressive, and flexural.

Several organizations and companies have published recommendations for the CAI test (NASA, Boeing, SACMA, CRAG), but there is no universal standard (ASTM or ISO), which would state the specimen geometry and the test variables. The size of the specimen and the clamping system vary from one study to another, but the devices and the procedures are similar. However, notable differences are found in the subsequent compression tests of the damaged specimens. The large aeronautic and aerospace companies (NASA, Boeing) normally use thick specimens (>3 mm) with their top and bottom edges clamped, and the lateral edges supported, to avoid failure by global buckling of the specimen which is usually narrow. There are, then, problems in testing damaged composite materials in compressive conditions. The test methods of aeronautic companies and other organizations recommend the use of large specimens of thickness above 3 mm. This requires a great deal of material and a high cost, and the test specimens do not always correspond to the actual material of the structure. There is no generally accepted method of testing small specimens with lower than 3 mm thickness; most proposed methods have to use tabs and narrower specimens, and this implies a change in the specimen geometry in some cases and further complexity in the test (Sanchez-Saez *et al.*, 2005).

Residual strength criterion is developed based on Flexure After Impact (FAI) instead of Compression After Impact (CAI) due the problems. Considering the residual strength scenario pointed above, there is a lack of knowledge concerning the flexural residual strength of composite plates. Thus, this work presents a new criterion to evaluate the residual strength of laminate composite subject to low-velocity impact loading using flexural testing. For this, a flexure after impact (FAI) test is used alongside the standard compression after impact (CAI) in order to compare its capability as a damage tolerance technique.

5.2. A New Criterion for Determining Residual Strength

Impact damage may cause significant reductions in stability and strength of composite structures. Low velocity impact damage caused by bird strike, runway debris, dropped tools

during fabrication or maintenance operations may create damages below the "barely visible impact damage" (BVID) limit. This type of damage may not be visible to the naked eye and has to be observed by special techniques, e.g. ultrasonic C-scan. These types of damage could lead to catastrophic failure, unless proper design precautions are taken. Therefore, it is very important to take into consideration the damage caused by impact loading, when designing a composite structure. Since such damage is difficult to detect, especially in-service, structures must be able to function safely with BVID present and/or an efficient SHM system should be used. The complex problem of determining the effects of impact damage may be divided into two sub problems (Nilson, 2005):

- ✓ Impact damage resistance, which deals with the response and damage caused by a certain impact;
- ✓ Impact damage tolerance, which deals with the reduced strength and stability of the structure due to damage.

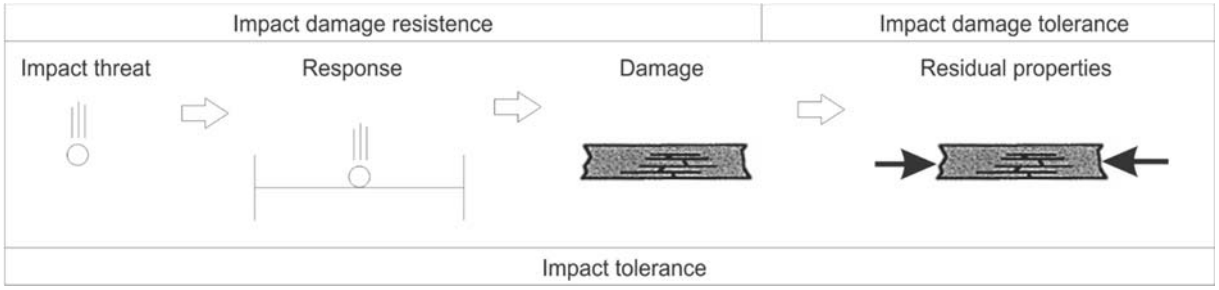

Figure 5-1 – Impact tolerance divided into two sub problems (Nilson, 2005).

In the studies of impact damage on CFRPs, three major damage types are of concern: fibre breakage, matrix cracks and multiple interlaminar delaminations. In fact, the largest effects of impact damage are observed in compression (Nilson, 2005). The reduction of compressive strength due to impact is more significant than the reduction in tensile strength and other strengths. Therefore, there are many works on residual strength, which are focused on delamination buckling, because this type of damage reduces the flexural properties of the laminate and may cause significant reduction in compressive strength. This, it is common to find works about residual strength and compression after impact analysis (CAI) as shown earlier. However, in this work, a new criterion will be proposed. This criterion is based on the prediction of the residual strength of the composite structures under bending loading using 4-

point flexure test. Therefore this criterion will be defined as Flexure After Impact (FAI). Figure 5-2 shows the general steps and Fig. 5-3 the general procedure proposed for this work.

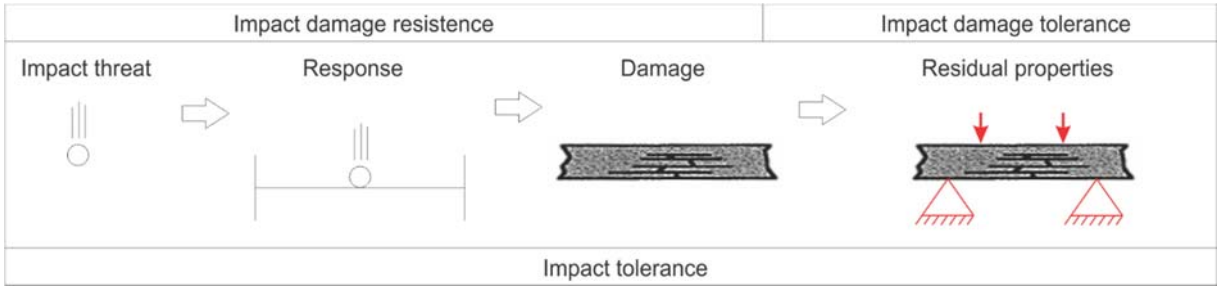

Figure 5-2 – Residual Strength proposed methodology

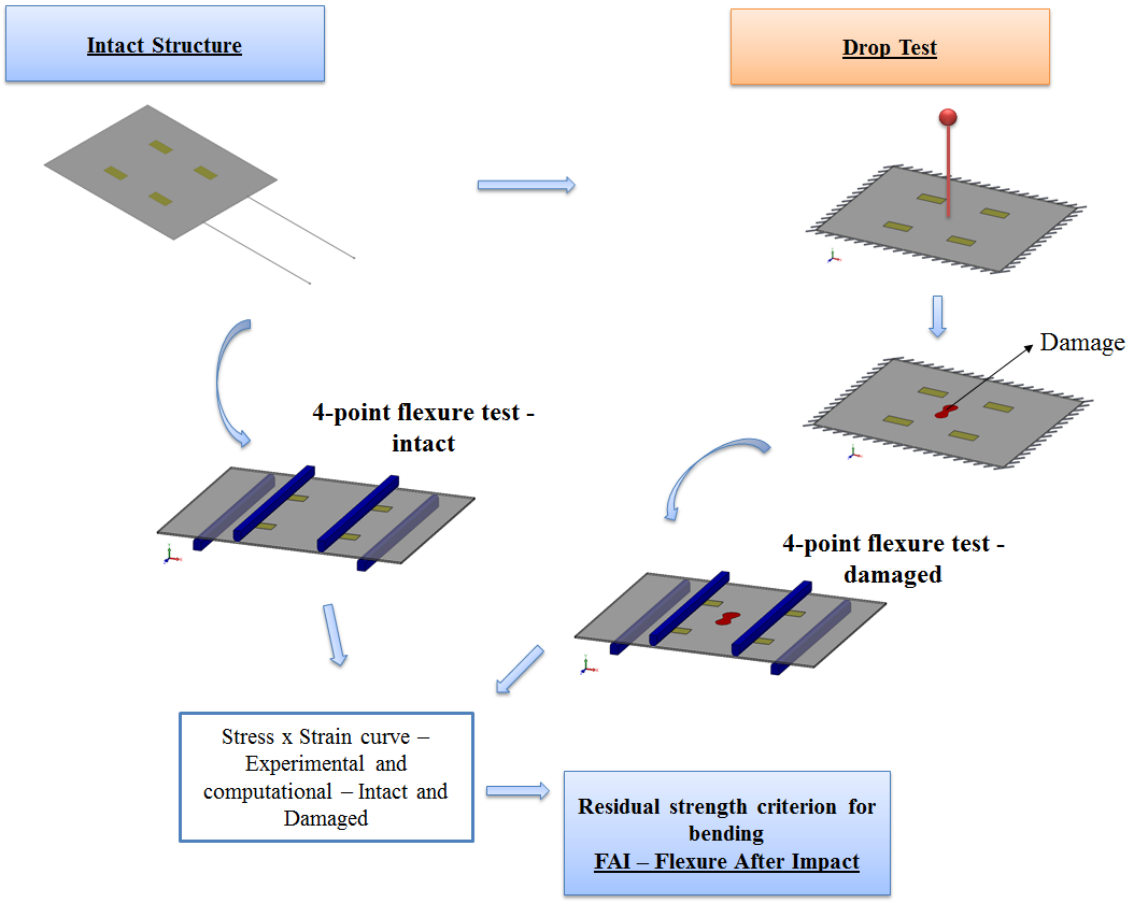

Figure 5-3 – General procedure to determine residual strength by Flexure After Impact (FAI) test.

A flexure after impact (FAI) test is used alongside the standard compression after impact (CAI) to compare its practicality as a damage tolerance technique. Low-velocity impact tests and residual strength tests are performed. A new criterion is based on a relationship between

damage metric and FAI analysis, *i.e.* the moment *versus* curvature graphic. Thus, these results are normalised by using the maximum load for the intact structures and the metrics for damage analyses, *i.e.* if there is no damage in the structure, then the metric returns zero value. If the structure is partially damaged then the metric returns a number between one and zero. Finally, if the structure is totally damaged, then the metric returns a value equal to one. In other words, if the structure does not have enough residual strength, considering design requirements, the metric is equal to one.

5.3. Experimental Setup

The post-impact strength of impacted specimens was evaluated by four-point bending tests under quasi-static conditions. The tests were conducted according to the standard ASTM D6272–10 (ASTM, 2010), since there is no standard to evaluate residual flexural properties. The four-point bending load is applied for a constant cross-head rate of 1.0 mm/min on the specimen impacted side, so that the impacted side is subjected to compressive stress.

The span is ultimately limited by the extent of the fixture, but a larger span also requires a larger deflection to fail the samples. As the bending response tends to be more global with material contributions averaged over a larger area, the increase in support span may also negate the effects of the damage on the mechanical properties. Three span-to-thickness ratios are suggested in the related standard ASTM D6272–10 (ASTM, 2010). Samples are trimmed such that there is sufficient overhang of the support noses should excessive deflection cause the contact line with the material to fall within the span plane and slip from the supports. A four-point condition is used so that the maximum axial fibre stress is uniformly distributed over the area between the loading noses, where the damage sites are situated. This ensures that the stress path must interact with the damaged material. The tests are performed using a universal testing machine, Instron 5985, with a load cell of 250 kN. The equipment is used to measure load and deflection during four-point flexure. In addition, LVDT transducers and digital image correlation are used to get the deflection of the plate and compare to the universal machine cross-head measurements (Fig. 5-4(b) and 5-5(b)).

Regarding the carbon fibre composite plates, the support span *i.e.* the distance between the supporting devices is 180 mm and the load span, *i.e.* the distance between the loading

devices is 90 mm (Fig. 5-4(a)). The span-to-thickness ratio is selected to be 60:1, this large ratio ensures that shear effects are negligible. Regarding the glass fibre composite plates, the support span is 120 mm and the load span is 60 mm (Fig. 5-5(a)). The span-to-thickness ratio is selected to be 70:1. In order to evaluate the residual flexural strength of the impacted specimens, it is necessary to know the properties of undamaged and the damaged specimens (*cf.*, Tab. 2-3 and 2-4). The shorter span in the glass fibre composite plate can be explained by the difference in the dimensions of the specimens (*cf.* Tab. 2.3 and Tab. 2.4).

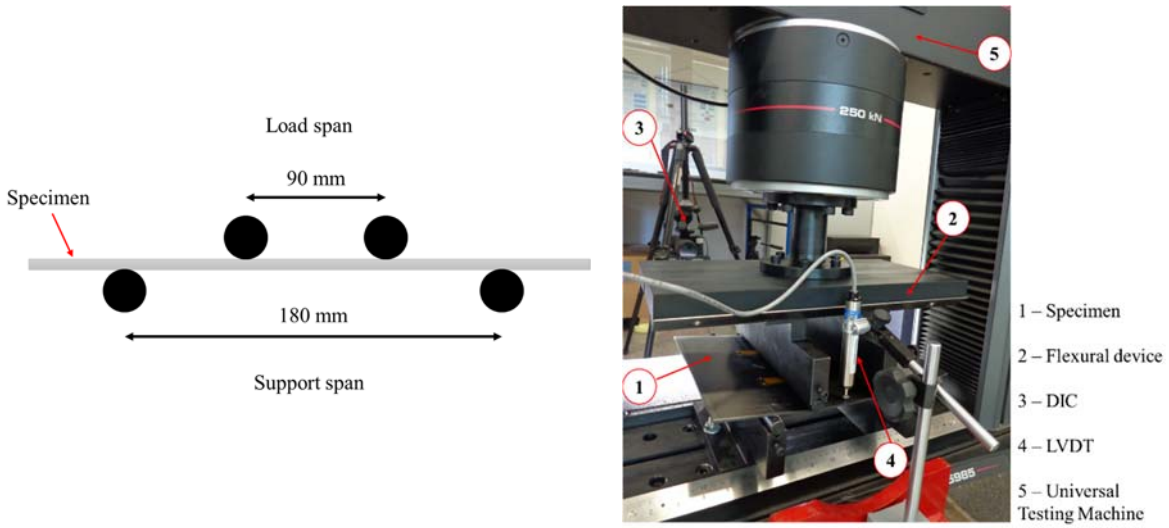

(a) (b)

Figure 5-4 – Experimental test used in the carbon fibre composite plates (a) Fixture setup for four-point FAI testing and (b) Experimental setup for the flexural test.

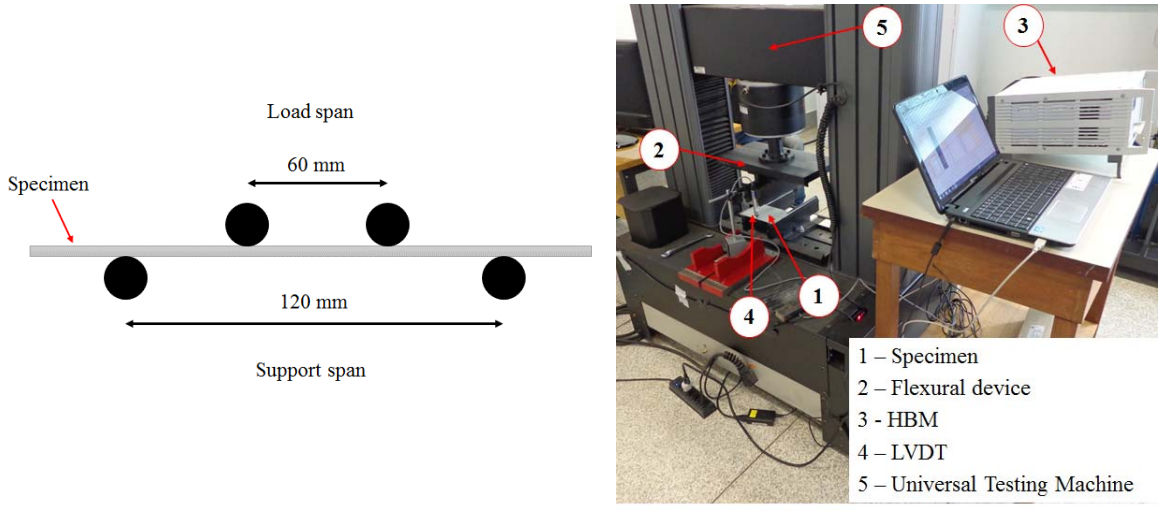

(a) (b)

Figure 5-5 – Experimental test used in the glass fibre composite plates (a) Fixture setup for four-point FAI testing and (b) Experimental setup for the flexural test.

5.4. Computational model

To evaluate the computational material behaviour, it is necessary to perform nonlinear material FE analysis, using ABAQUS™ and the UMAT. A four node reduced integration shell elements with six degrees of freedom (DOF) per node (defined as S8R - ABAQUS™) were used to model the carbon composite plate. The plate was modelled with 2928 quadrilateral elements and 9003 nodes. The material properties are given by Ribeiro *et al.* (2012), similar to Tita (2003). The specimens manufactured and studied by Tita (2003) were made from prepreg M10 from Hexcel™. In fact, they were unidirectional carbon fibres with epoxy resin and the fibre volume ratio was around 63%. The elastic properties and strength values are shown either in Table 2-2 or by Tita (2003) and Tita *et al.* (2008). The FE model for carbon fibre composite plates flexural tests have the same dimensions of the coupons used for experimental tests (Fig. 5-6). As commented in the section 2.3, the carbon fibre composite plates show a curvature along the fibre direction (*cf.* Fig.5-6(a)).

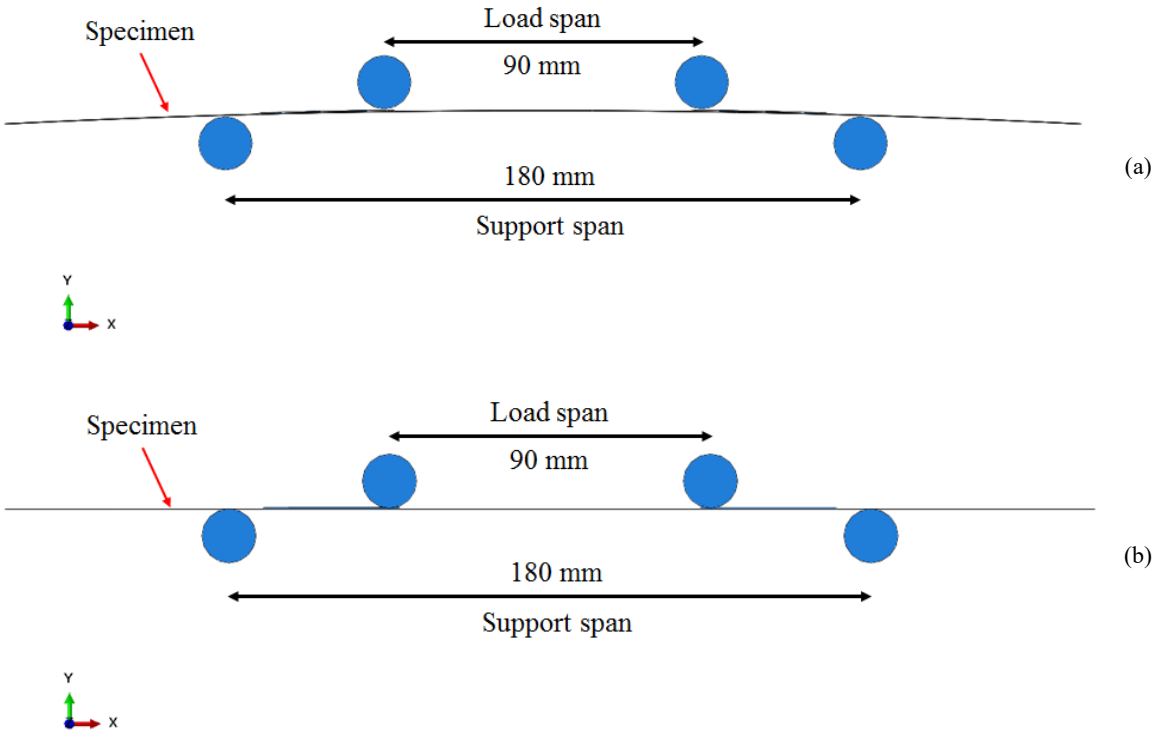

Figure 5-6 – Computational setup for **f**our point bending test (a) $[0]_8$ stacking sequence, and (b) $[0/15/-15/0/15/-15]_s$ stacking sequence.

The bending tests are conducted until coupon failure at a test speed of 1 mm/min and, the test machine provides force vs. displacement data. Figure 5-7 shows the boundary conditions used in this analysis.

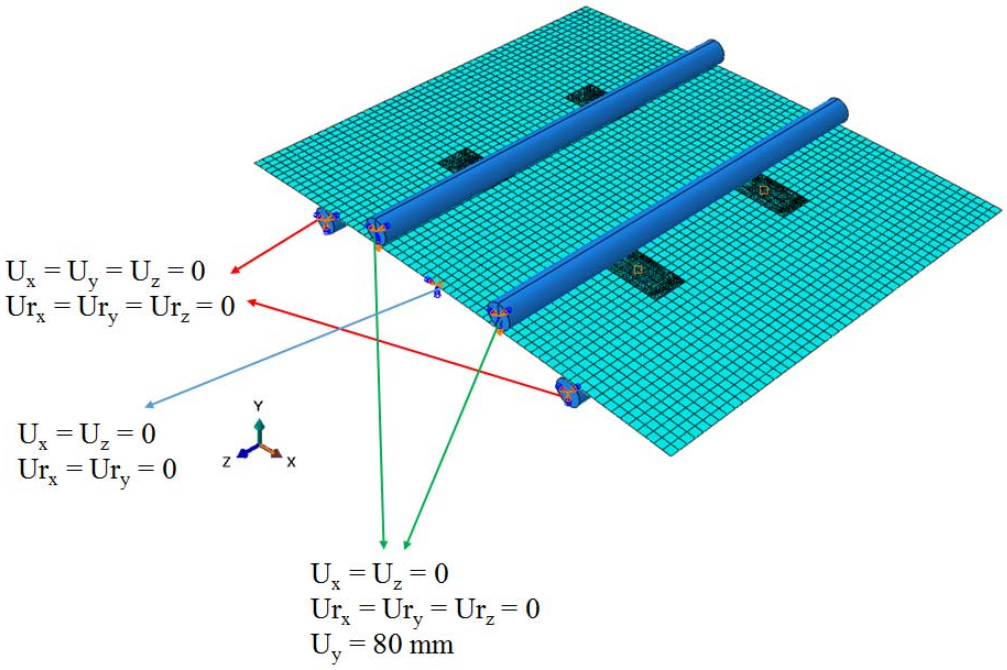

Figure 5-7 – Boundary conditions used in the computational analysis.

5.5. Results and Discussion

Four-point bend tests are more appropriate than three-point bending in the present study, because of several reasons. In three-point bending, the point of load application is at the location of greatest damage and may promote further damage in the specimen. Four-point bending is more suitable for material specimens that experience larger deformation during testing.

Figures 5-8 and 5-9 show the experimental typical force *x* displacement curve for all specimens. The stacking sequence is observed not only in the load force, but also in the behaviour of the curve.

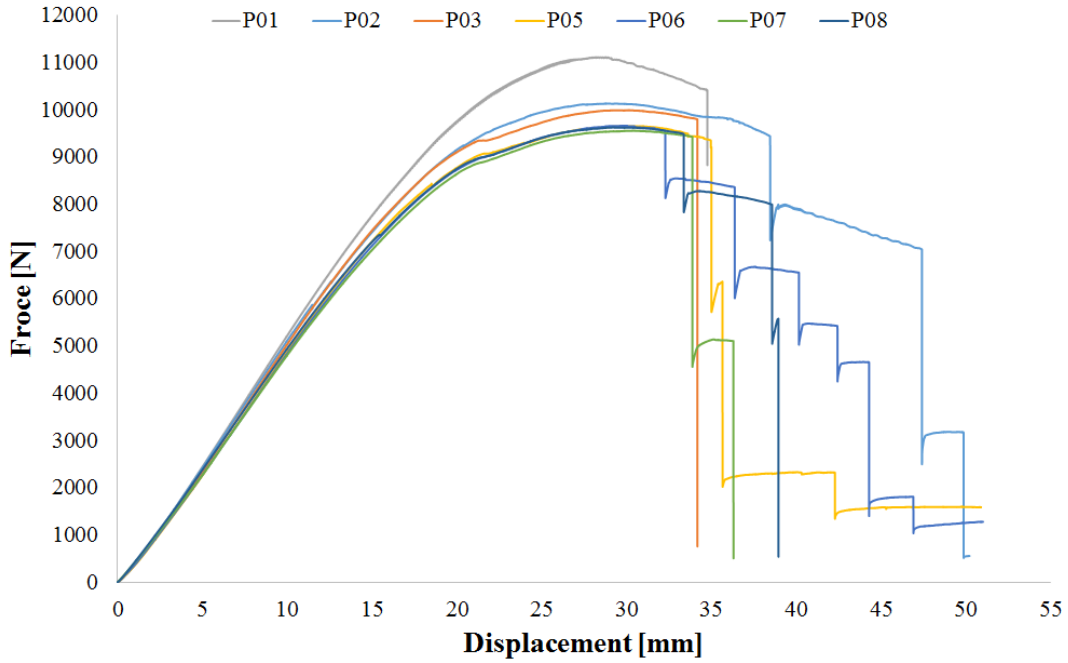

Figure 5-8 – Experimental force *versus* displacement for the carbon fibre composite specimens $[0]_8$

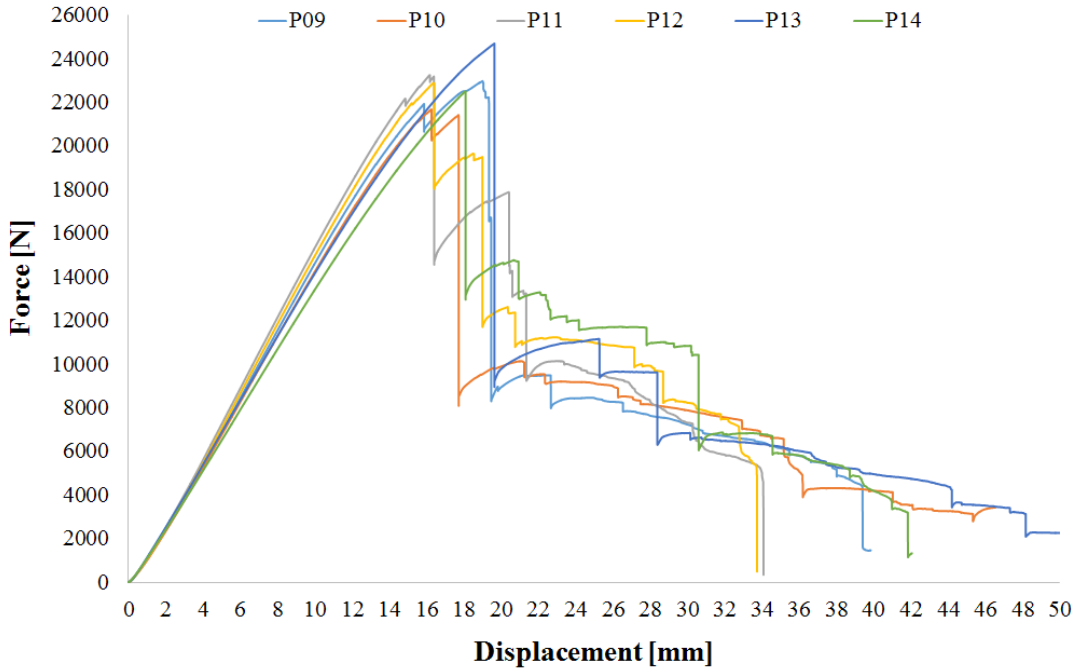

Figure 5-9 – Experimental force *versus* displacement for the carbon fibre composite specimens $[0/15/-15/0/15/-15]_s$

Figures 5-10 and 5-11 show the computational response for $[0]_8$ and $[0/15/-15/0/15/-15]_s$ carbon fibre composite plates, damaged by impact, respectively. The green part represent the fibre damage (SDV1) and the blue one, the intact structure.

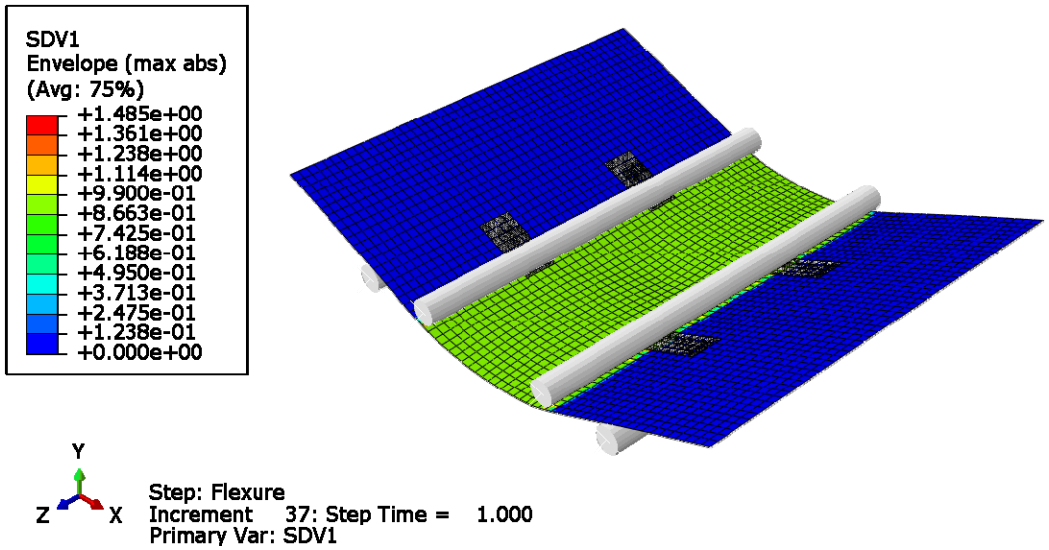

Figure 5-10 – Computational response SDV1 (fibre damage) for the failure analysis composite plates $[0]_8$.

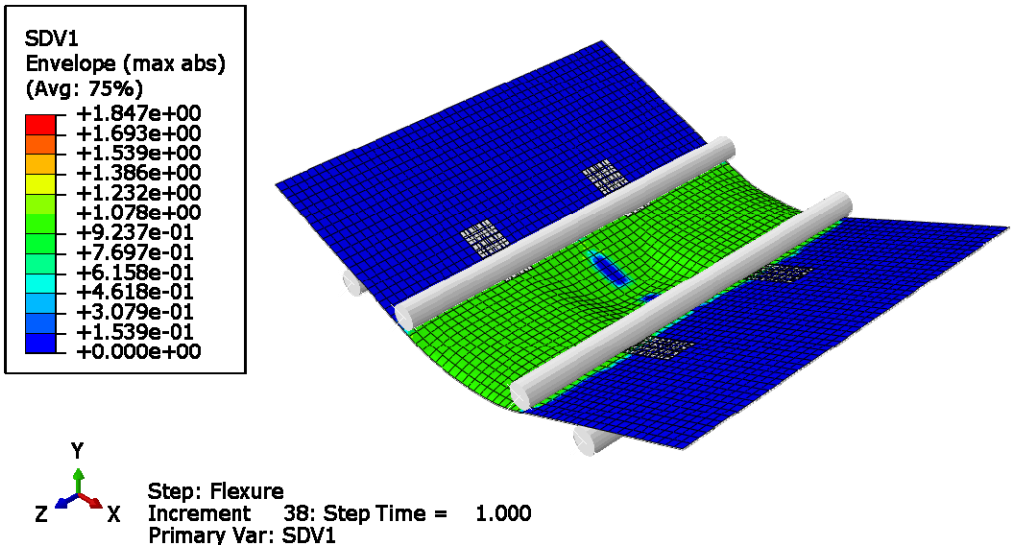

Figure 5-11 – Computational response SDV1 (fibre damage) for the failure analysis composite plate $[0/15/-15/0/15/-15]_s$.

Figures 5-12 and 5-13 show the computational force *vs* displacement curve for $[0]_8$ and $[0/15/-15/0/15/-15]_s$ carbon fibre composite plates, respectively. As in the experimental one, it only small differences are observed between the intact and damaged plates. Also, the difference between the stacking sequences in the load force is shown. The curve behaviour can be explained by the magnitude of the time step in the discretisation during the computational analysis. Hence, a better discretisation is necessary.

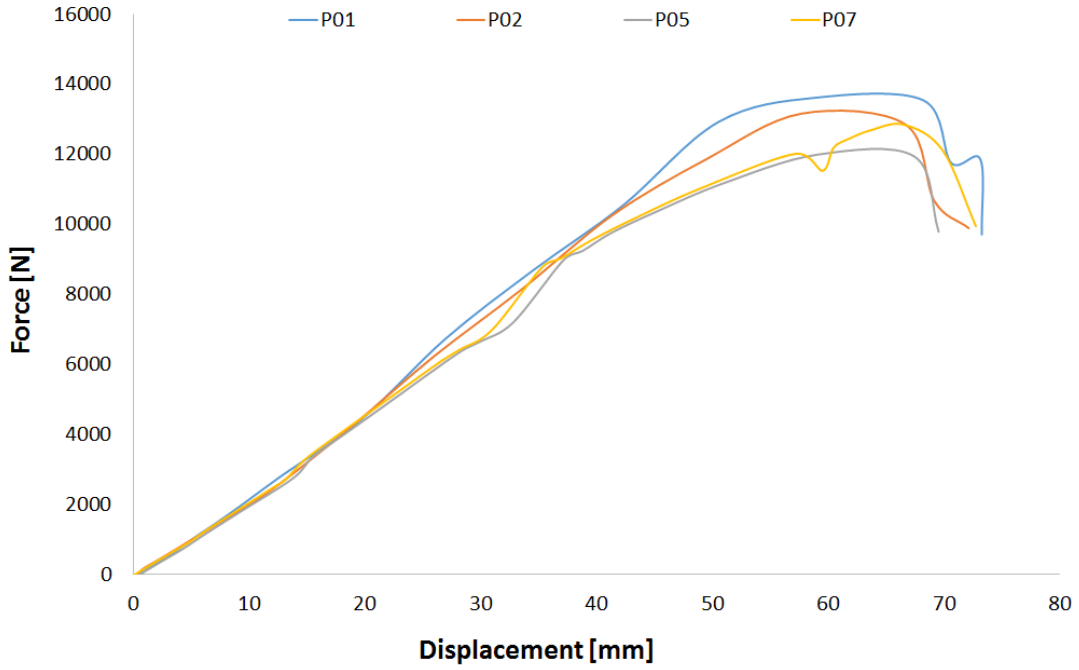

Figure 5-12 – Computational force *versus* displacement for the carbon fibre composite specimens $[0]_{8}$.

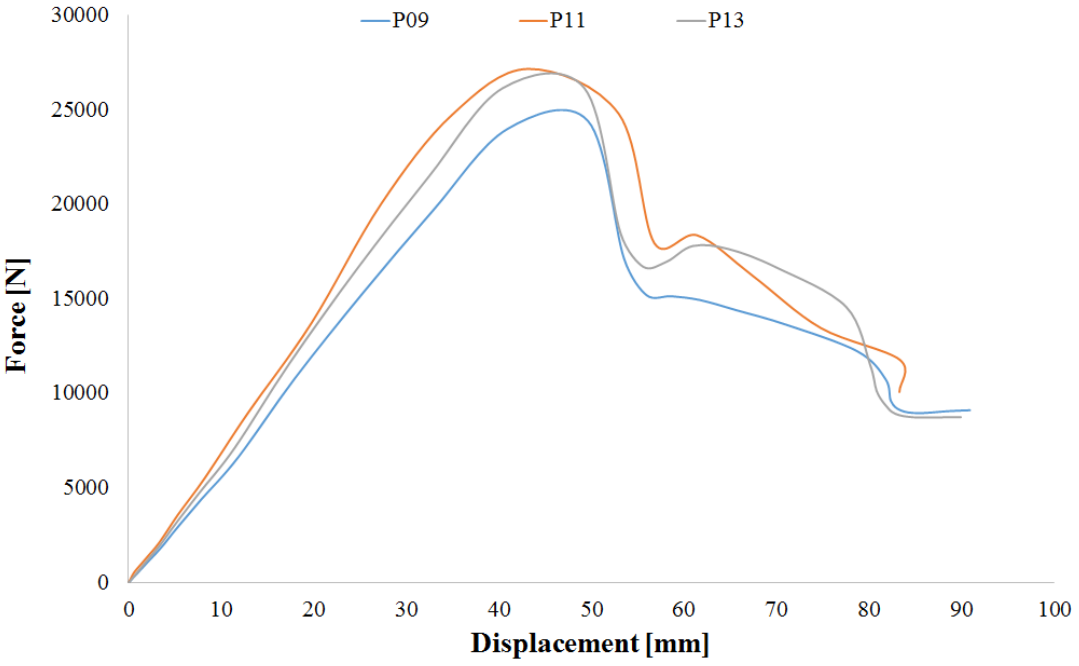

Figure 5-13 – Computational force *versus* displacement for the carbon fibre composite specimens $[0/15/-15/0/15/-15]_{s}$.

Figures 5-14 and 5-15 show the experimental typical force *vs.* displacement curve for unidirectional and bidirectional glass fibre composite plates, respectively. A difference in the load force considering the same stacking sequence is observed. The small jumps can be

explained because the load sensor of the universal test machine. It was used a load cell with 250 kN, and the experiments presented the maximum force of 700 N. Thus, the acquisition time was very fast when compared with the sensitivity of the universal test machine.

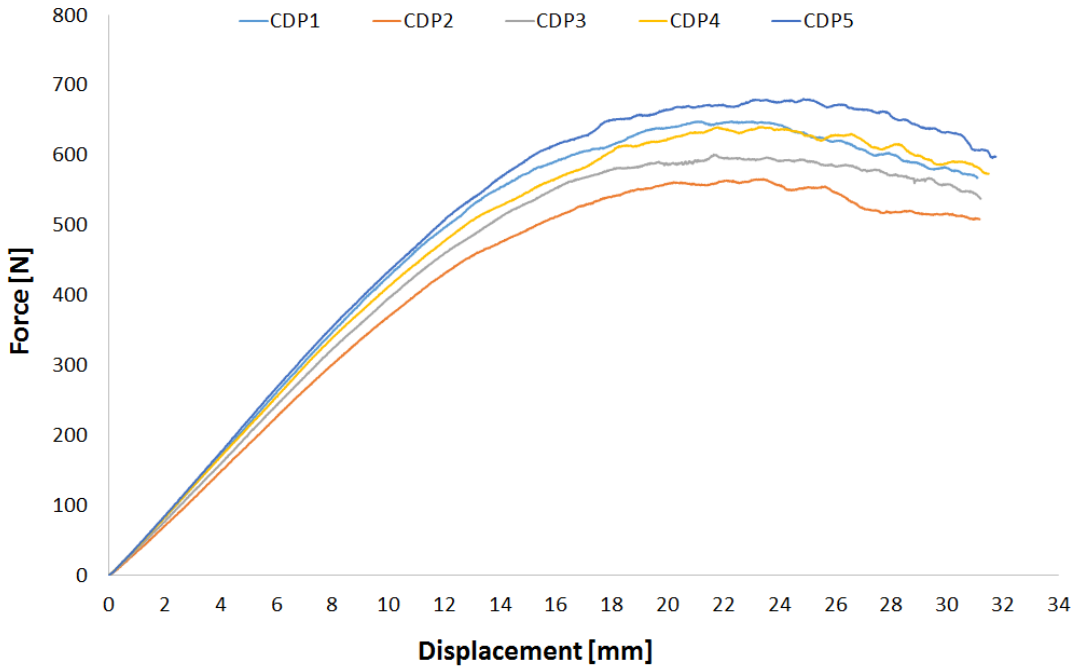

Figure 5-14 – Experimental force *versus* displacement for the unidirectional glass fibre composite plates.

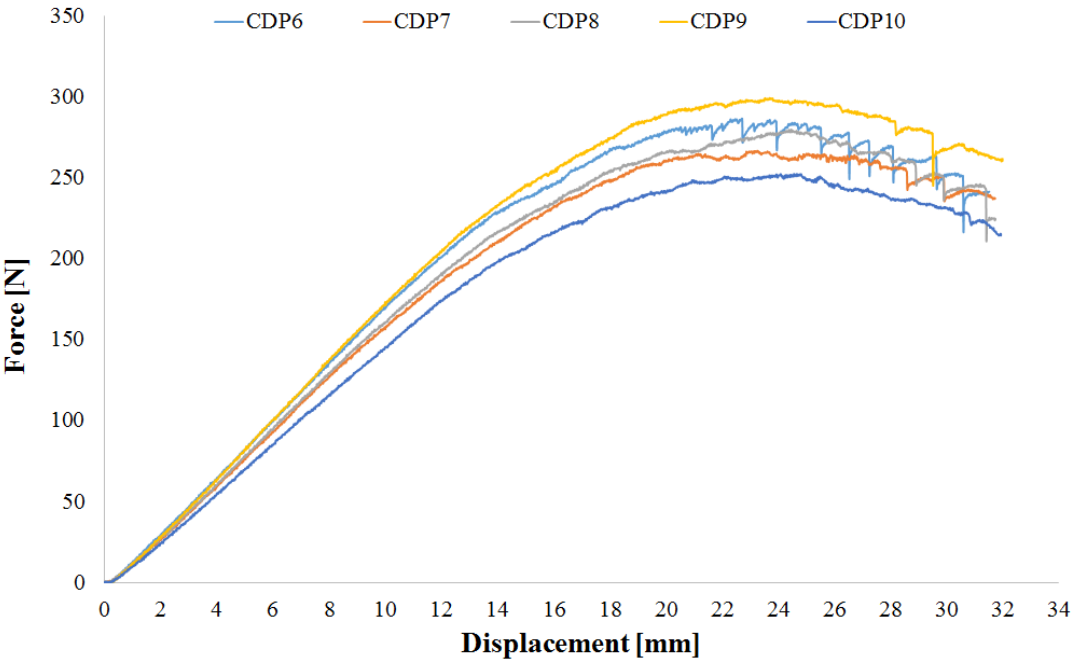

Figure 5-15 – Experimental force *versus* displacement for the bidirectional glass fibre composite plates.

5.5.1. FAI Damage Index

The classical laminate theory (CLT) is applicable to orthotropic continuous fibre laminated composites. The classic theory of laminated composites is based on a series of simplifying hypotheses. Thus, the laminae are considered as very thin, made of a homogeneous, orthotropic, linear elastic material in a plane stress state. Also, perfect adhesion between the laminae and the Kirchhoff hypothesis is assumed. Most of the algorithms and models based on these facts lead to a global stress and strain state analysis without characterization of the mechanical behaviour of these materials. Also, the admissible loads are assumed to be a set of resultants forces and moments, defined at a representative section of the laminate. The ABBD matrix is a 6*x*6 matrix, which relates the applied loads and the associated strains in the laminate. The resultant forces have units of force per unit length of laminate (N/m), and the resultant moments assumed to act on the laminated have units of length times force per unit length of laminate (N.m/m). The loads and moments can be expressed in matrix form, as:

$$\begin{Bmatrix} N_x \\ N_y \\ N_{xy} \\ — \\ M_x \\ M_y \\ M_{xy} \end{Bmatrix} = \begin{bmatrix} A_{11} & A_{12} & A_{16} & | & B_{11} & B_{12} & B_{16} \\ A_{12} & A_{22} & A_{26} & | & B_{12} & B_{22} & B_{26} \\ A_{16} & A_{26} & A_{66} & | & B_{16} & B_{26} & B_{66} \\ — & — & — & — & — & — & — \\ B_{11} & B_{12} & B_{16} & | & D_{11} & D_{12} & D_{16} \\ B_{12} & B_{22} & B_{26} & | & D_{12} & D_{22} & D_{26} \\ B_{16} & B_{26} & B_{66} & | & D_{16} & D_{26} & D_{66} \end{bmatrix} \begin{Bmatrix} \varepsilon_x^0 \\ \varepsilon_y^0 \\ \gamma_{xy}^0 \\ — \\ \kappa_x \\ \kappa_y \\ \kappa_{xy} \end{Bmatrix} \tag{5.1}$$

where, N is the resultant force, M is the resultant moment, ε is the strain, κ is the curvature, the matrix *[A]*, *[B]* and *[D]* are the extensional stiffness matrix, the extensional-bending coupling matrix and the bending stiffness matrix, respectively.

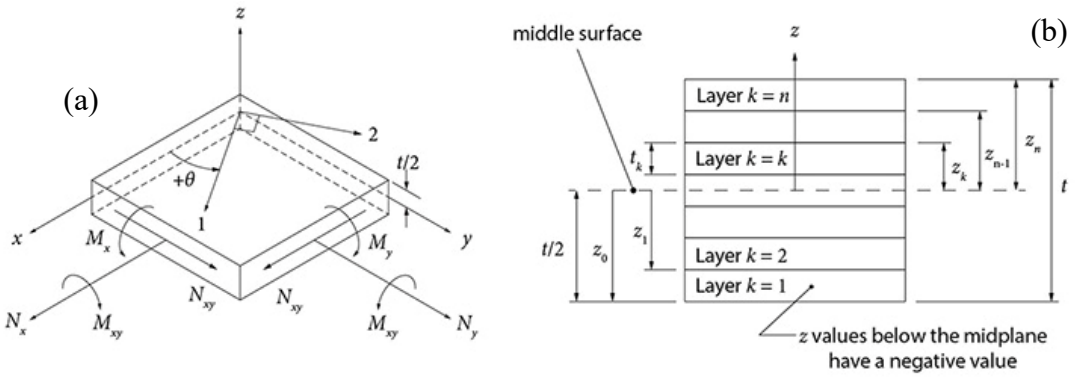

Figure 5-16 – Classical laminate theory (a) loading and (b) Laminated structure (Fonte: http://www.espcomposites.com/software/eLaminate.html).

In the four point bending test, only the moment (M_x) and the curvature (κ_x) are different from zero, thus the matrix can be rewritten as:

$$M_x = D_{11}\kappa_x \tag{5.2}$$

The damage factor is set up as the difference between the maximum moment value for the intact analysis and the damaged value. This criterion is a phenomenological material failure theory, which can be used for composite materials. This criterion assumes that a material fails when 1 minus the division of the active moment by the maximum moment in a material element is greater 0 and less and equal 1, *i.e.* the structure is totally damaged when the failure index in a laminate reaches 1. This failure criterion can be expressed in the form,

$$DI_{FAI} = 1 - \frac{M^{d}_{max}}{M^{i}_{max}} \tag{5.3}$$

where, *d* and *i* are the damaged and intact plates.

These results are normalised using the maximum load and the metrics for damage analysis, *i.e.* if there is no damage in the structure, then the metric returns zero value. If the structure is partially damaged then the metric returns a number between one and zero. For the minimum value ($DI_{FAI} = 1$). The common factor of safety for aerospace structures is 1.5 (for ultimate load), as required in the U.S. by the FAA (Federal Aviation Administration) for loadings from maneuver or gust. The safety factor is defined as FS = material strength/maximum load. According FAA, the maximum load depends on a number of factors, such as failure mode of the structure, material, etc. However, for this study was defined as the maximum bending moment value obtained for the intact structure under 4-point bending test. The safety factor of aircraft is low because a high factor of safety would cause weight to rise to unacceptable levels. That is why the load analysis of the aircraft is so important. Thus, in this work, a safety factor of 1.5 is applied.

$$DI_{FAI} = \frac{M^{i}_{max}}{SF} \tag{5.4}$$

Figures 5-17 to 5-22 show the moment versus curvature graphic for the experimental carbon fibre composite plates (*cf.* Fig. 5-17 and 5-18), computational carbon fibre composite plates (*cf.* Fig. 5-19 and 5-20), and the experimental glass fibre composite plates (*cf.* Fig. 5-21 and 5-22).

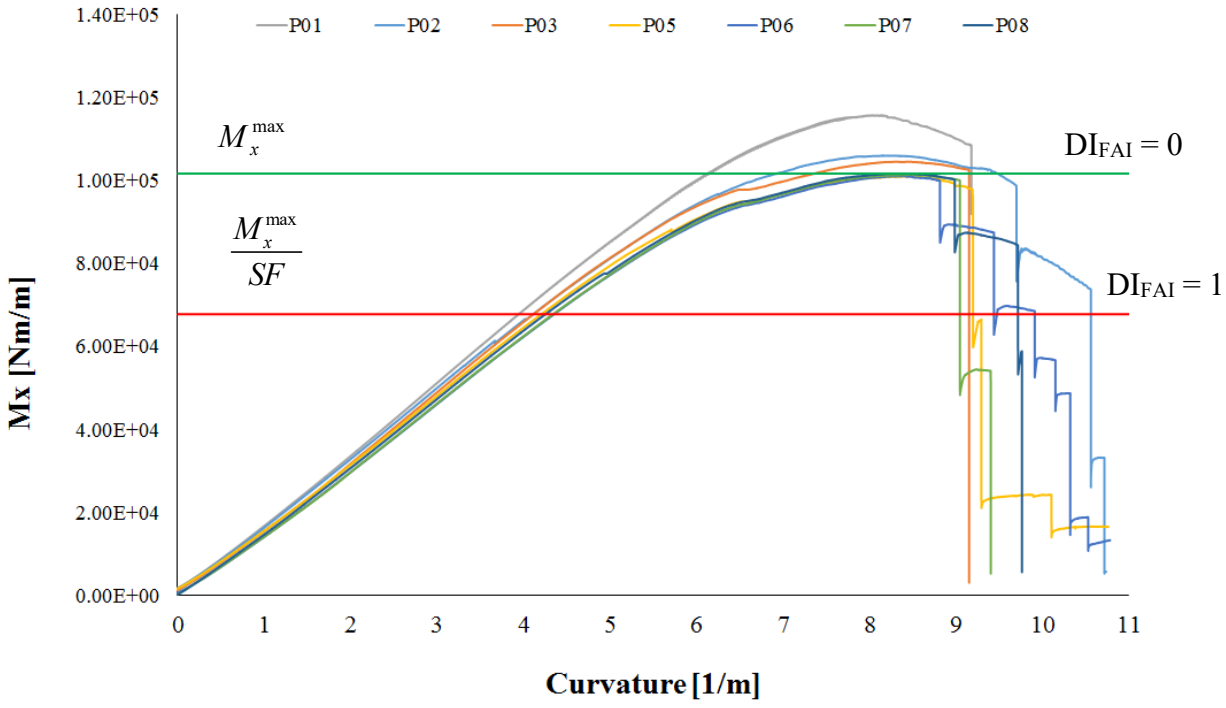

Figure 5-17 – Experimental moment *vs* curvature plot for the carbon composite plates $[0]_8$.

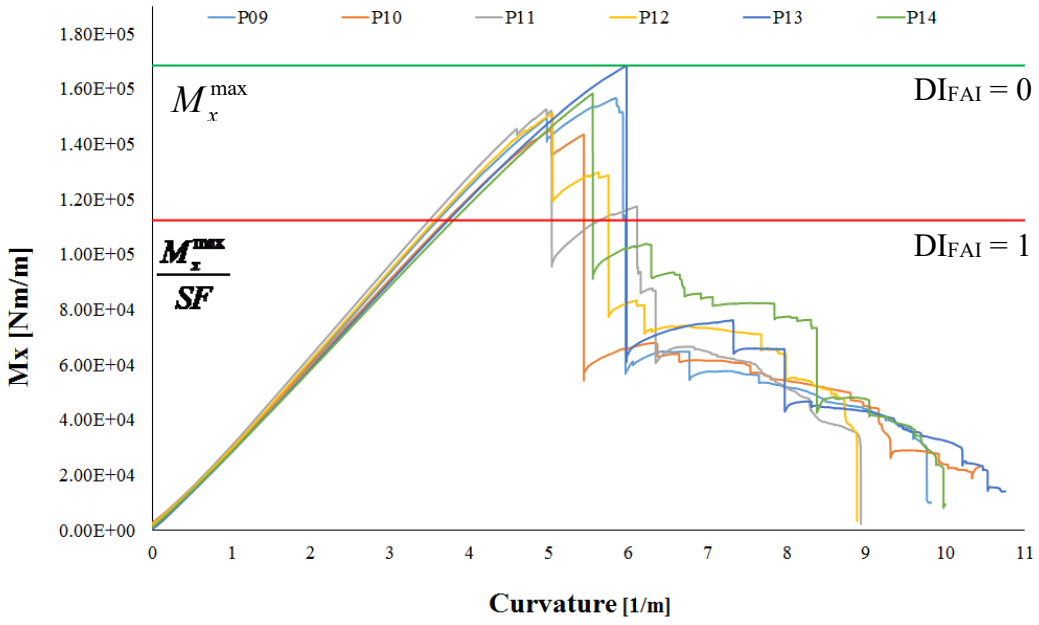

Figure 5-18 – Experimental moment *vs* curvature plot for the carbon composite plates $[0/15/-15/0/15/-15]_s$.

In addition, the two horizontal lines represent the maximum ($DI_{FAI} = 0$) and minimum ($DI_{FAI} = 1$) value allowed. The minimum value was determined dividing the maximum value, for the undamaged plate, by a safe factor (SF) equal to 1.5.

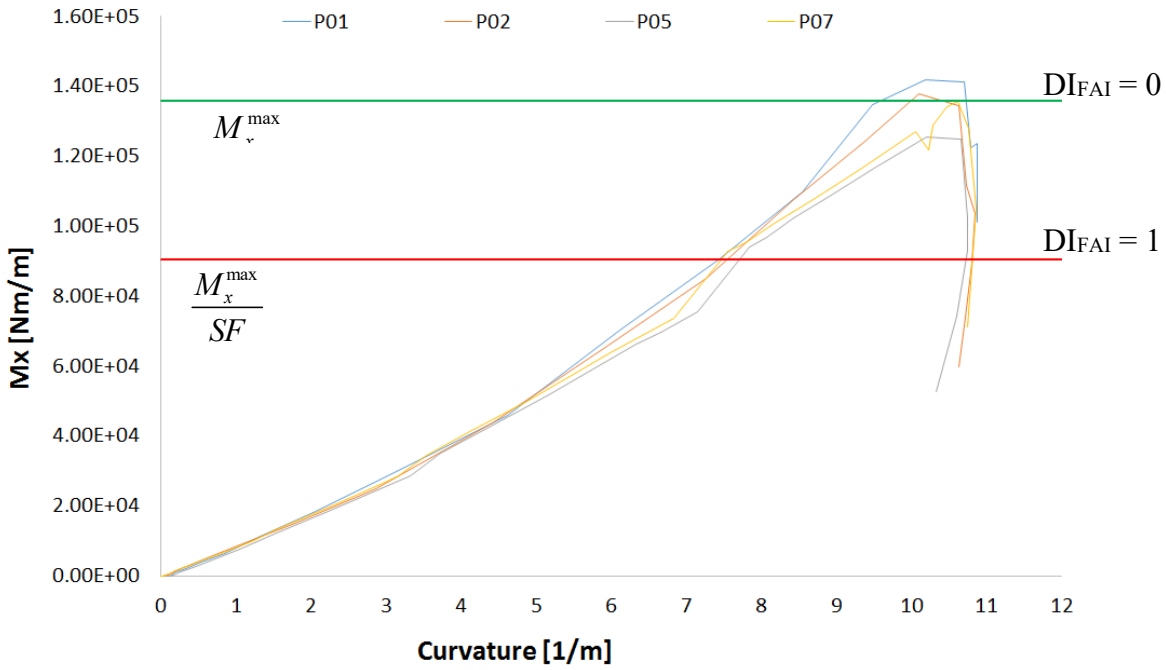

Figure 5-19 – Computational moment *versus* curvature graphic for the carbon fibre composite plates $[0]_8$.

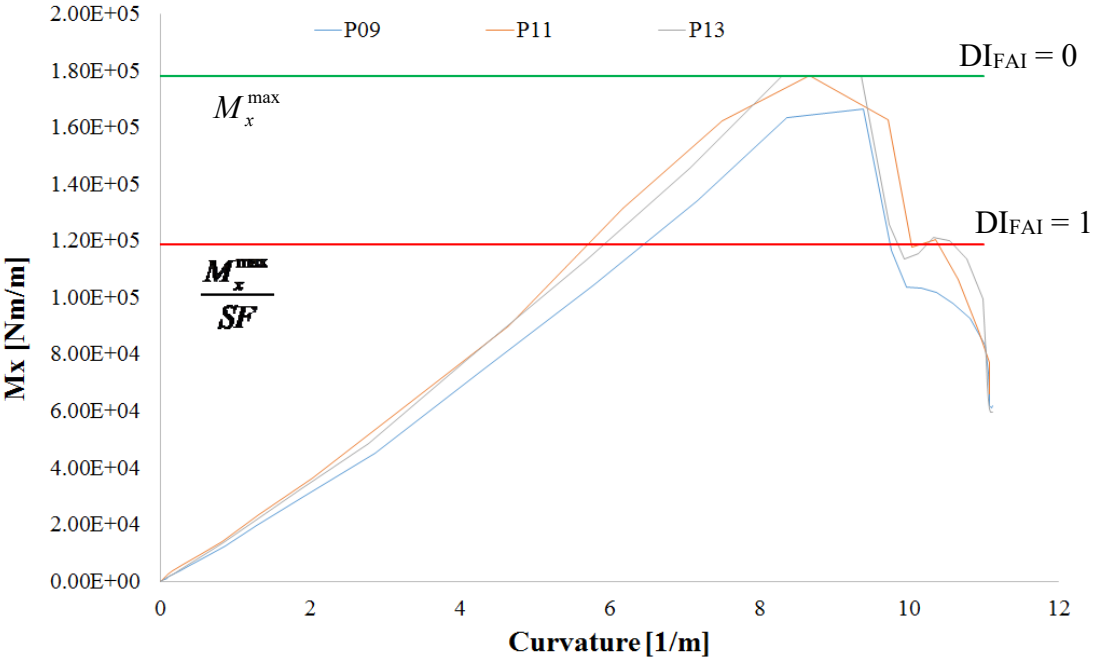

Figure 5-20 – Computational moment *versus* curvature graphic for the carbon fibre composite plates $[0/15/-15/0/15/-15]_s$.

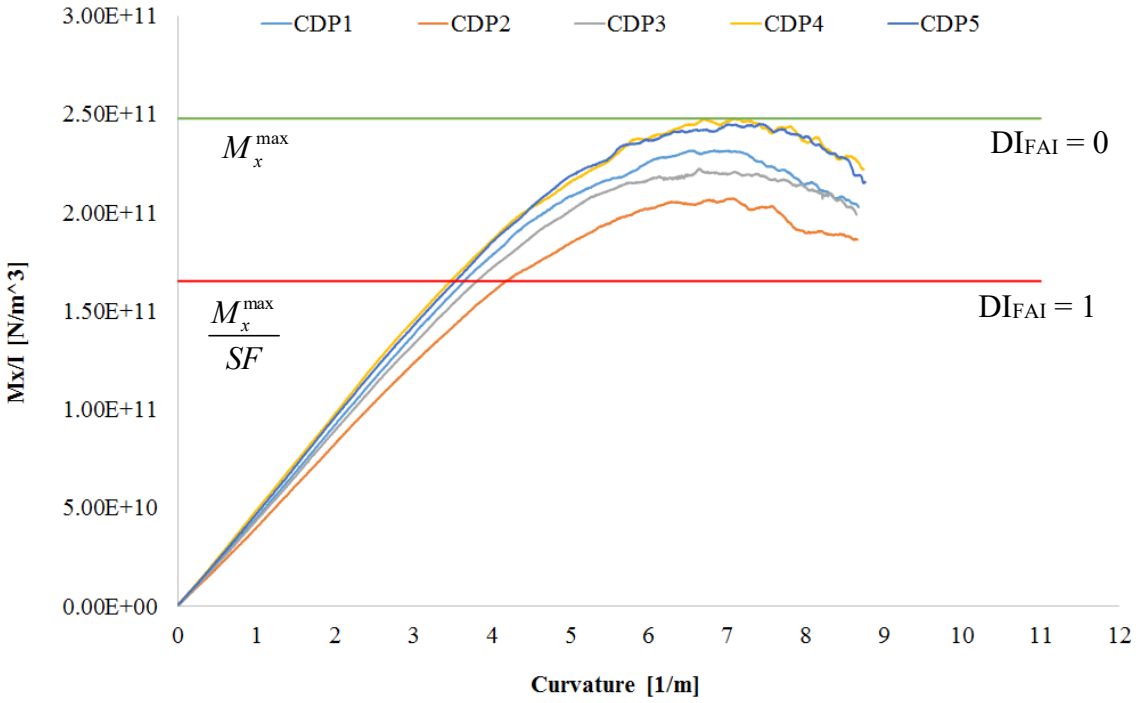

Figure 5-21 – Experimental moment *versus* curvature graphic for the glass fibre composite plates $[0]_8$.

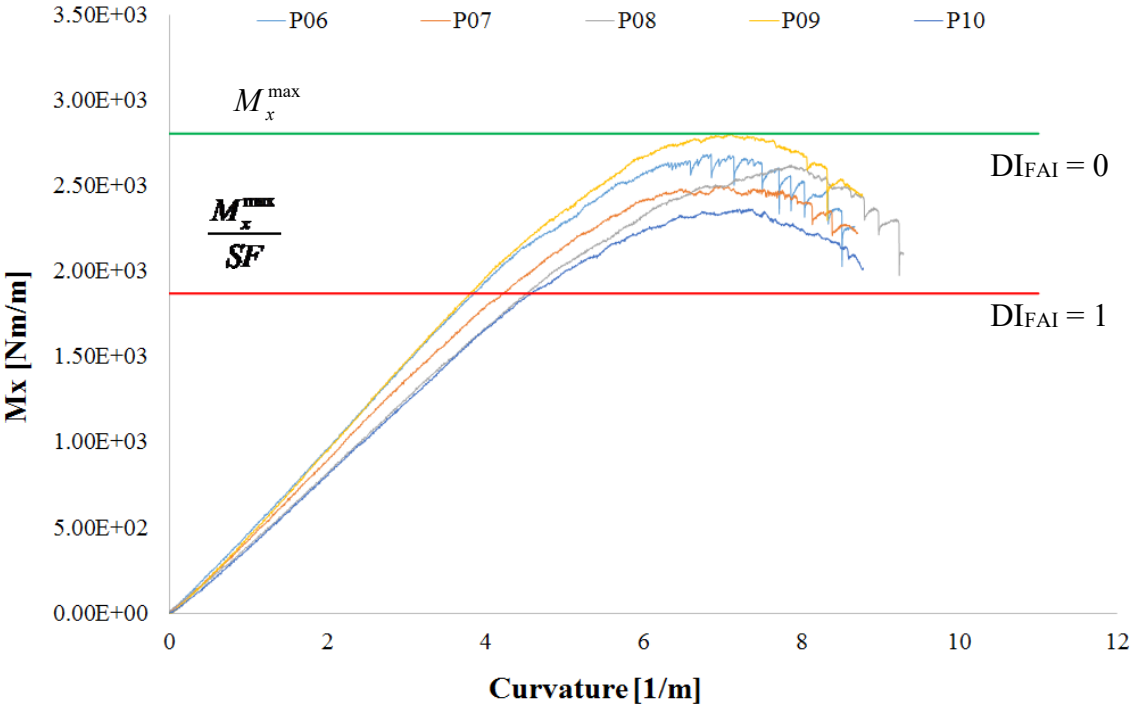

Figure 5-22 – Experimental moment *versus* curvature graphic for the glass fibre composite plates.

Figure 5-17 and Fig. 5-18, show that the plates with stacking sequence equal $[0]_8$ exhibit low influence on the bending test in the fibre direction, this is due to the stacking orientation the crack, for impact test, is parallel the fibre. In addition, the higher value for the damaged

plates ($P01_{CF}$ and $P02_{CF}$) can be explained by the manufacturing $[0/15/-15/0/15/-15]_s$ process, since these plates showed curvature along the fibre direction. However, the plates with stacking sequence $[0/15/-15/0/15/-15]_s$, present some influence of fibre orientation and type of damage. This fact can be supported by the damage index values. Regarding the computational analysis (*cf.* Fig. 5-19 and 5-20), they present the same behaviour of the experimental test. This fact can be seen in the Tab. 5-2. For the plates $[0]_8$, the damage causes almost no influence in the response. However, for the plates $[0/15/-15/0/15/-15]_s$, differences are remarkable.

Regarding the experimental analysis in the glass fibre composite plates (Fig. 5-21 and 5-22), reductions of stiffness and maximum moment are observed, for both unidirectional and bidirectional plates, considering the intact and damaged ones. However, the bidirectional plate (P10_GF-B) showed strange behaviour, this fact can be explained by some defects in the manufacturing process, and it is confirmed in Tab. 5-3.

Table 5-1 to 5-3 show the maximum laminated moment and the damage index values for the experimental carbon fibre composite plates, computational carbon fibre composite plates, and the experimental glass fibre composite plates, respectively.

Table 5-1 – Damage index/metric for the experimental carbon fibre composite plates.

Plate ID	Stack Sequence	Damage Type	M_x^{max} [Nm/m]	DI_{FAI}
$P01\_CF^E$	$[0]_8$	impact	$1.157x10^5$	0.0000
$P02\_CF^E$	$[0]_8$	central hole	$1.060x10^5$	0.0000
$P03\_CF^E$	$[0]_8$	impact	$1.045x10^5$	0.0000
$P05\_CF^E$	$[0]_8$	impact	$1.010x10^5$	0.0067
$P06\_CF^E$	$[0]_8$	impact	$1.011x10^5$	0.0053
$P07\_CF^E$	$[0]_8$	-	$1.014x10^5$	0.0025
$P08\_CF^E$	$[0]_8$	-	$1.017x10^5$	0.0000
$P09\_CF^E$	$[0/15/-15/0/15/-15]_s$	impact	$1.567x10^5$	0.0697
$P10\_CF^E$	$[0/15/-15/0/15/-15]_s$	impact	$1.425x10^5$	0.1380
$P11\_CF^E$	$[0/15/-15/0/15/-15]_s$	impact	$1.525x10^5$	0.0945
$P12\_CF^E$	$[0/15/-15/0/15/-15]_s$	impact	$1.510x10^5$	0.1033
$P13\_CF^E$	$[0/15/-15/0/15/-15]_s$	-	$1.684x10^5$	0.0000
$P14\_CF^E$	$[0/15/-15/0/15/-15]_s$	-	$1.583x10^5$	0.0599

Table 5-2 – Damage index/metric for the computational carbon fibre composite plates.

Plate ID	Stack Sequence	Damage Type	M_x^{max} [Nm/m]	DI_{FAI}
$P01\_CF^E$	$[0]_8$	impact	$1.419x10^5$	0.0000
$P02\_CF^E$	$[0]_8$	central hole	$1.378x10^5$	0.0000
$P05\_CF^E$	$[0]_8$	impact	$1.255x10^5$	0.0754
$P07\_CF^E$	$[0]_8$	-	$1.357x10^5$	0.0000
$P09\_CF^E$	$[0/15/-15/0/15/-15]_s$	impact	$1.664x10^5$	0.0661
$P11\_CF^E$	$[0/15/-15/0/15/-15]_s$	impact	$1.781x10^5$	0.0005
$P13\_CF^E$	$[0/15/-15/0/15/-15]_s$	-	$1.782x10^5$	0.0000

Table 5-3 – Damage index/metric for the experimental glass fibre composite plates

Plate ID	Stack Sequence	Damage Type	M_x^{max} [Nm/m]	DI_{FAI}
P01_GF^E	$[45/-45/0/90/45/-45/0/90]_s$	impact	$5.725x10^3$	0.0469
P02_GF^E	$[45/-45/0/90/45/-45/0/90]_s$	impact	$4.999x10^3$	0.1678
P03_GF^E	$[45/-45/0/90/45/-45/0/90]_s$	impact	$5.308x10^3$	0.1163
P04_GF^E	$[45/-45/0/90/45/-45/0/90]_s$	-	$5.825x10^3$	0.0302
P05_GF^E	$[45/-45/0/90/45/-45/0/90]_s$	-	$6.007x10^3$	0.0000
P06_GF^E	$[45/-45/0/90/45/-45/0/90]_s$	impact	$2.687x10^3$	0.0424
P07_GF^E	$[45/-45/0/90/45/-45/0/90]_s$	impact	$2.500x10^3$	0.1093
P08_GF^E	$[45/-45/0/90/45/-45/0/90]_s$	impact	$2.624x10^3$	0.0651
P09_GF^E	$[45/-45/0/90/45/-45/0/90]_s$	-	$2.807x10^3$	0.0000
P10_GF^E	$[45/-45/0/90/45/-45/0/90]_s$	-	$2.366x10^3$	0.1568

Another method for evaluating the damage index is to observe the evolution over the bending test. For this, not only the damage index is considered, but also the angle (θ) between the moment and the curvature, *i.e.* the tangent line. Figure 5-23 presents the methodology for determination of this damage evolution. The black lines represent the damage evolution, considering the damage index and the angle θ. This evolution is calculated from maximum moment (DI_{FAI} = 0 and $\theta_{initial}$ – green line) until the minimum moment allowed (DI_{FAI} = 1 and θ_{final} – red line).

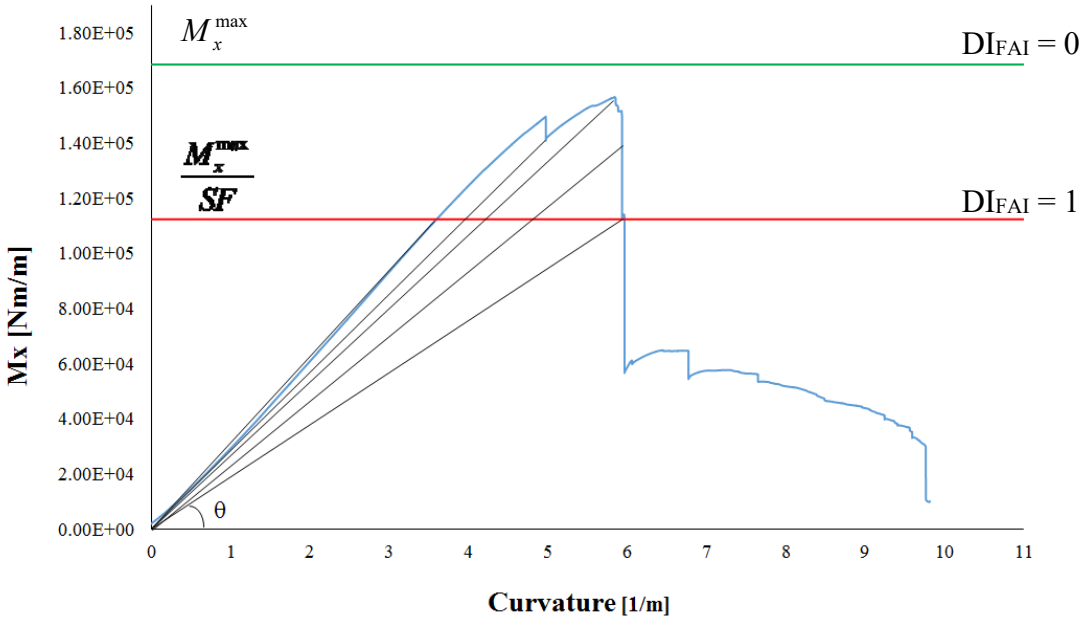

Figure 5-23 – Method for determination the damage evolution index for the bending test

Figures 5-24 and 5-25 show the damage evolution for the experimental carbon fibre composite plates. Due to the fact that the angle θ presented small variation, a mathematical formulation is used to amplify the values,

$$\theta^* = (\theta - \theta_0).10^5 \tag{5.5}$$

where, θ^* is the amplified value of θ, and $\theta_0 = 89.99$.

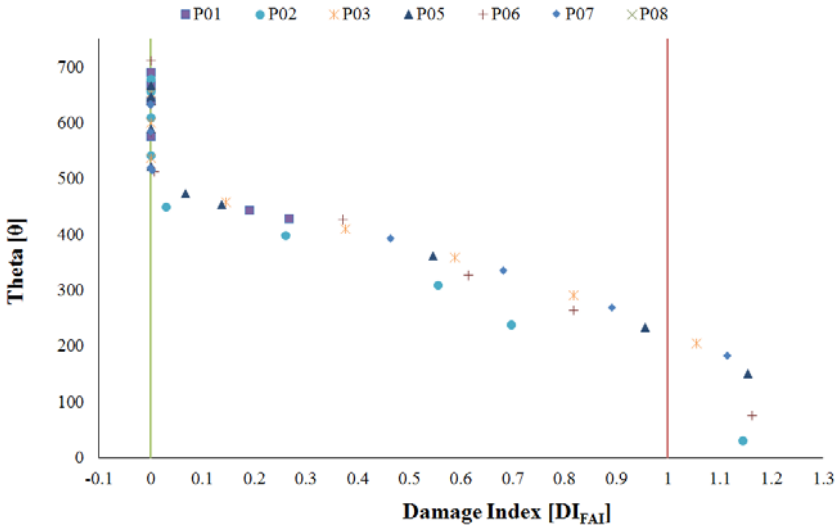

Figure 5-24 – Damage evolution for the carbon fibre composite plates $[0]_8$

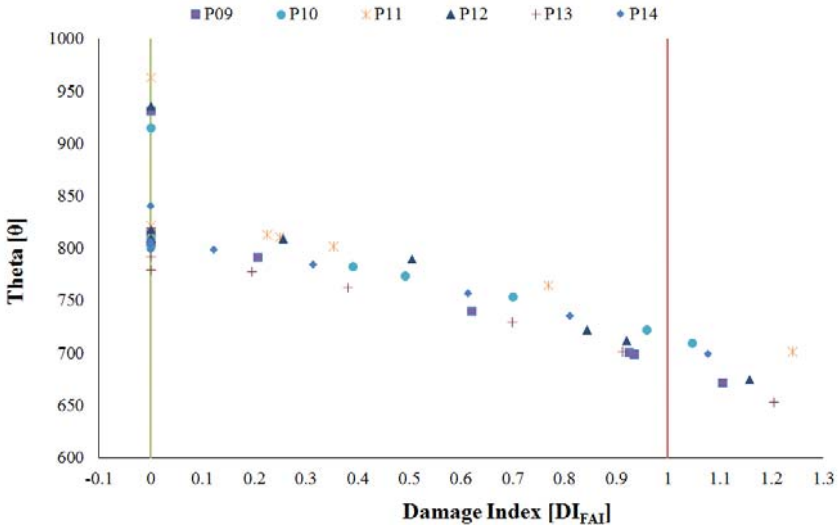

Figure 5-25 – Damage evolution for the carbon fibre composite plates $[0/15/-15/0/15/-15]_s$

In the Fig. 5-24 and 5-25, it is possible to observe that until the θ value reaches the value that corresponds to the maximum moment, the damage index return zero. This represents the elastic part in the graphic. After this value the damage index increases with decreasing θ until it reaches a maximum value of one. This value corresponds to the minimum moment allowed for the structure.

5.6. FAI Damage Index *versus* VBM Damage Index

In order to compare the damage index/metric provided by the vibration-based method and the damage index/metric provided by the flexure after impact, only the 4th vibration mode was considered (flexure in the fibre direction – Fig. 5.26). This is due to the fact that in both analyses the mode shape was equal (Fig. 5.26). To calculate the damage index, the values from 215 to 235 Hz were considered for the plates with stacking sequence $[0]_8$ and from 305 to 330 Hz for the plates with stacking sequence $[0/15/-15/0/15/-15]_s$. Table 5-4 shows the damage index determined by vibration-based method and Tab 5-5 shows the damage index determined by vibration-based method and by flexure test.

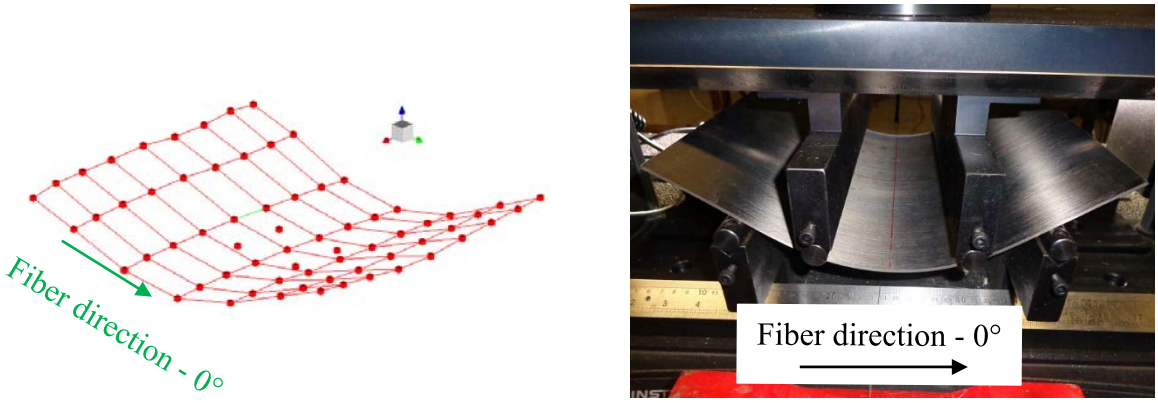

(a) (b)

Figure 5-26 – (a) 4th mode shape considered for DI_{VBM} calculation (b) Flexural After Impact (FAI) analysis.

Table 5-4 – DI provided by vibration based method for all sensors in the carbon fibre composite plates.

Plate ID	Stack Sequence	Damage Type	DI_VBM				
			H_{11}	H_{21}	H_{31}	H_{41}	H_{mean}
P01_CF^E	$[0]_8$	impact	0.1995	0.2381	0.2366	0.3375	0.2529
P02_CF^E	$[0]_8$	central hole	0.1251	0.1049	0.0757	0.0863	0.0980
P03_CF^E	$[0]_8$	impact	0.1464	0.0701	0.0519	0.0464	0.0787
P05_CF^E	$[0]_8$	impact	0.0436	0.1255	0.3988	0.1518	0.1799
P06_CF^E	$[0]_8$	impact	0.1399	0.1118	0.1746	0.2782	0.1761
P09_CF^E	$[0/15/-15/0/15/-15]_s$	impact	0.0257	0.0616	0.1428	0.0957	0.0815
P10_CF^E	$[0/15/-15/0/15/-15]_s$	impact	0.0541	0.0338	0.1580	0.0803	0.0816
P11_CF^E	$[0/15/-15/0/15/-15]_s$	impact	0.0219	0.0190	0.0182	0.1372	0.0491
P12_CF^E	$[0/15/-15/0/15/-15]_s$	impact	0.0530	0.0242	0.0593	0.1936	0.0825

Table 5-5 – DI provided by VBM and FAI for the carbon fibre composite plates.

Plate ID	Stack Sequence	Damage Type	DI_{VBM}	DI_{FAI}
P01_CF^{E}	$[0]_8$	impact	0.2529	0.0000
P02_CF^{E}	$[0]_8$	central hole	0.0980	0.0000
P03_CF^{E}	$[0]_8$	impact	0.0787	0.0000
P05_CF^{E}	$[0]_8$	impact	0.1799	0.0067
P06_CF^{E}	$[0]_8$	impact	0.1761	0.0053
P07_CF^{E}	$[0]_8$	-	-	0.0025
P08_CF^{E}	$[0]_8$	-	-	0.0000
P09_CF^{E}	$[0/15/-15/0/15/-15]_s$	impact	0.0815	0.0697
P10_CF^{E}	$[0/15/-15/0/15/-15]_s$	impact	0.0816	0.1380
P11_CF^{E}	$[0/15/-15/0/15/-15]_s$	impact	0.0491	0.0945
P12_CF^{E}	$[0/15/-15/0/15/-15]_s$	impact	0.0825	0.1033
P13_CF^{E}	$[0/15/-15/0/15/-15]_s$	-	-	0.0000
P14_CF^{E}	$[0/15/-15/0/15/-15]_s$	-	-	0.0599

It is possible to observe that the DI_{VBM} is higher for the carbon fibre composite plates with stacking sequence $[0]_8$, whereas the DI_{FAI} is higher for the carbon fibre composite plates with stacking sequence $[0/15/-15/0/15/-15]_s$. Figure 5-27 shows the correlation between the damage indexmetric DI_{VBM} *versus* DI_{FAI} for the carbon fibre composite plates with stacking sequence $[0]_8$ and $[0/15/-15/0/15/-15]_s$.

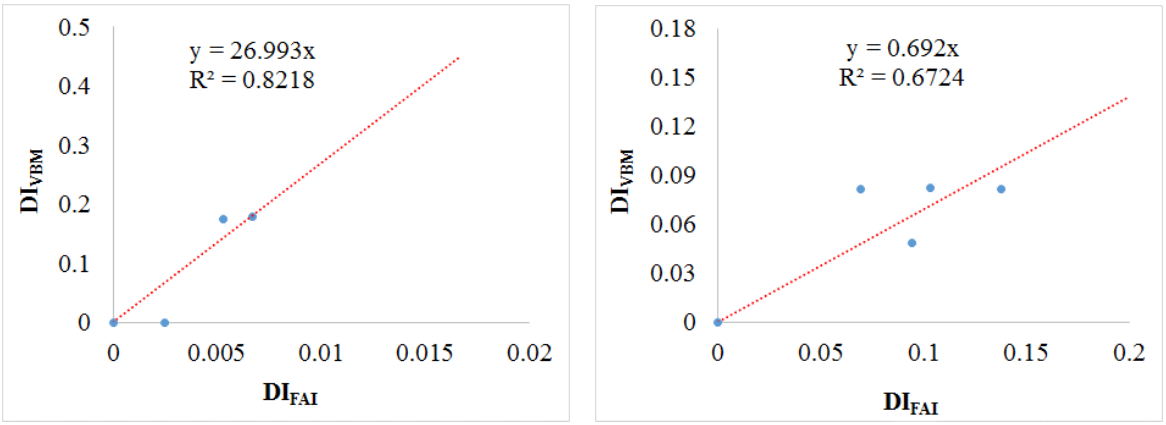

(a) (b)

Figure 5-27 – Damage index correlation for the carbon fibre composite plates (a) stacking sequence $[0]_8$, and (b) staking sequence $[0/15/-15/0/15/-15]_s$

Figure 5-27 shows the regression linear between the damage index/metric provided by vibration-based method and the damage index/metric provided by the flexure after impact test. Considering the maximum DI_{FAI} (equal one), and substituting the DI_{FAI} in the trend line (Fig.

5.27), it is possible to estimate the maximum DI_{VBM}, *i.e.*, 26.993 for $[0]_8$ and 0.692 for $[0/15/-15/0/15/-15]_s$.

5.7. Partial Conclusions

A series of specimens were damaged using an instrumented low velocity impact machine to introduce non-penetration damage and were then subjected to flexural testing. A new flexure after impact criterion was presented. The analysis showed acceptable results, as expected the stacking sequence $[0°]_8$ showed almost no difference between the undamaged and the damaged structure. However, the stacking sequence $[0°/15°/-15°/0°/15°/-15°]_s$ showed some difference between the undamaged and damaged structure. Post impact flexural property testing shows that flexural strength is more sensitive to the presence of localised impact damage than flexural modulus. FAI provides a simple means to test the applicable residual response of a damaged composite structure. Only simple fixtures are required and the nominal test gives both flexural modulus and strength data. It has been shown that the apparent flexural modulus is sensitive to the damage size associated to a particular impact energy level. As a non-destructive test, however, a relationship between the flexural modulus and other residual properties must be established. For this, using linear trend line between damage index provided by the FAI criterion and the damage index provided by the vibration based method was preliminary developed. Therefore, the proposed criterion based on flexure after impact test with the new damage metric combined to damage index provide by vibration based method can be used to identify and estimate the residual strength of the structure. In other words, there is a good perspective for the application of this methodology in SHM systems for composite structures. Therefore, further verification for other cases will be done to improve general conclusions about the SHM system.

CHAPTER 6

Conclusions and Future Works

This thesis focuses on the development of design recommendations and guidelines for detection, localisation and characterisation of damage in composite structures, employing changes in the dynamic behaviour, shearography speckle and flexure after impact. These guidelines contribute to the development of a design tool for research engineers, to assist the implementation of structural health monitoring technology in safety-critical composite structures. The contribution of this PhD to the state of the art should is highlighted. In addition, the conclusions and future works was presented focussing on contribution for the development of SHM systems to be applied in composite structures, which are damaged by impact loading.

6.1. Conclusions

The main objective of this research project consists on contributing for the development of SHM systems to be applied in composite structures, which are damaged by impact loading. Thus, it is necessary to identify and to localise damage, as well as to evaluate the severity of the damage of the composite structures and to propose a new residual strength criterion.

The main contribution was the development of a new computational and experimental SHM system for composite aeronautic structures, proposing the combination of different methods to identify, locate, estimate the extent of damage and provide information about the residual strength of flat plates and curved composite structures. For this, vibration based methods was chosen for damage identification and global localization due to the use of few PZT sensors in order to avoid the increase of weight in the aeronautic structures. A new metric was developed that takes in to account the effects of amplitude and phase of the Frequency Response Function (FRF). Shearography speckle was chosen for local localization and provide the extent of damage. For operation of airplanes it is necessary to predict maintenance of aeronautic structures. Thus, there are checks of structures during the life of the airplane which can be performed by shearography speckle on ground. Also, this technique is well known and certified by the regulatory agencies. Residual strength criterion is developed based on Flexure After Impact (FAI) instead of Compression After Impact (CAI) due the problems related to CAI tests. During the CAI test the compression load cannot cause global or total buckling on the tested specimen. The expected result considers micro-buckling mechanisms followed by fibre breakage, cracks, etc. Also, CAI tests are not very simple to carry out, and require more material than the conventional mechanical tests, as tensile, compressive, and flexural. A new criterion was developed based on the moment versus curvature curves. Finally, a correlation between damage metric from VBM and damage metric from FAI were presented and discussed. This work will show that comparisons between experimental and computational tests can be used to extrapolate the correlation between the damage metrics to obtain the response of the structure for a determined range of interest. Thus, the scientific contribution of the present work can affect the development of smart aircraft structures, which offer significant improvements in the aircraft's life cycle and total weight, as well as in manufacturing and operational/maintenance cost.

Regarding damage identification and location using vibration-based method, it was concluded that there are many advantages in using this technique for an SHM system. Among

these advantages, are the easy implementation and low cost. Also, no requirement for visual inspection, "automation" capability, "global" coverage (in the sense of covering large areas of the structure), and capability of working at a "system level". Furthermore, they tend to be time effective and less expensive than the most alternatives. In addition, aeronautical structure in flight under loads suffer vibrations and this vibrations can be monitored by piezoelectric sensors, *i.e.* the fact that for some of these vibration based damage identification methods no artificial excitation is needed, but only the response at certain degrees of freedom (DOFs) of the structure, is another important advantage because the structure can remain in operation. As a consequence, these methods can be used for permanent health monitoring. The use of few PZT sensor to not interfere with the weight of the aeronautic structures. In some cases, the sensor can be embedded in the laminate structure (*e.g.* piezoelectric sensors) and has the potential for damage detection in flight with appropriate structural modelling. Based on the present work, it can be concluded that by localising dynamic response sensors, damage could be detected and globally located for impact damage. Numerical calculations were used to provide insight into the investigation and the results were compared to experimental data, showing a good agreement. It can also be concluded that SHM systems, which are based on the expected changes in the FRFs obtained from vibration analyses, may be used in real-world situations in which damage detection is required. However, it is necessary to apply suitable metrics (including a new one) in order to identify the damage in the structure.

Regarding damage localisation and quantification via optical method, the measurements of the rotation fields using a Shearography system allowed to successfully localise and quantify the damage areas. In addition, the experimental results showed that Shearography is a very useful NDE technique, because of its detection capacity for barely visible impact damages, which is not detected by visual inspection as well as simple and quick investigation. Moreover, this technique has other benefits such as non-contact, scalable and full-field measurement. These characteristics are very important, because composite materials may exhibit different kinds of damage such as debonds, delamination, matrix cracking and fibre failure. It is very useful if the type of damage and/or the location are known a priori. It is a good strategy to perform first a global analysis based on vibration based and on Finite Element Analyses, before conducting an inspection using SS.

A new criterion was proposed to identify residual strength. In fact, based on the lessons learned about vibration based methods and optical methods, a design of the SHM system can be aided by those techniques. Therefore, by using this SHM system and 4-point flexure test, a

new residual strength criterion was developed. This criterion was named Flexure After Impact (FAI) and it was created in order to overcome the challenges involved in the CAI (Compression After Impact) procedures. The analysis showed acceptable results, as expected the stacking sequence $[0°]_8$ specimens showed almost no difference between the undamaged and the damaged structure. However, the stacking sequence $[0°/15°/-15°/0°/15°/-15°]_s$ specimens showed some difference between the undamaged and damaged structure. Post impact flexural property testing shows that flexural strength is more sensitive to the presence of localised impact damage than flexural modulus. FAI provides a simple means to test the applicable residual response of a damaged composite structure. In addition, it was used the moment *vs.* curvature curves in instead of stress *vs.* strain curve due to the fact that the latter provide a local response. However, the moment *vs.* curvature represent a global response of the structure as well as the vibration based method.

Therefore, the proposed methodology based on frequency response functions with the new damage metric combined to shearography speckle technique and flexure after impact can be used to detect, locate, and mainly, to provide information on the extent of damage and the residual strength in composite structures. It is import to highlight that for each material or stacking orientation, it is necessary a calibration of the SHM system. In other words, there is a good perspective for the application of this methodology in SHM systems for composite structures.

6.2. Future Works

With respect to the work presented in this thesis further research is recommended on the following aspects:

- ✓ Perform sensitive analysis with optimization to select the position of the sensors. The problem of sensor location is crucial for system identification, control, and damage detection which requires accurate measurement of the responses of the system. The measured data are always inaccurate because of the existence of parameter variation or noise. Taking the cost of sensors into account, it is not economical to install sensors in every part of system. In such cases, a practical question that naturally arises is how to select a set with a minimum number of sensor locations from all possibilities, such that

the data collected may provide the greatest opportunities for the detection of failures. Optimal sensor location is a combinatorial problem where one seeks to place N_S sensors out of M potential locations.

- ✓ Insert the damping information in the vibration based damage index. The problem of dissipating energy in structures so as to reduce the amplitudes of the vibrations is an important feature in mechanical design. Generally, the damping in metal structures is low, which results in high amplitudes of the vibrations. For fibre reinforced composite materials, damping is higher and it depends on the constitution of the materials. At the constituent level, the energy dissipation in fibre-reinforced composites is induced by different processes such as the viscoelastic behaviour of matrix, the damping at the fibre-matrix interface, the damping due to damage, etc. At the laminate level, damping is depending on the constituent layer properties as well as layer orientations, interlaminar effects, stacking sequence.
- ✓ Apply the vibration based methods on composite plates with different damage size to determine the robustness of the technique. Piezoelectric ceramic Lead Zirconate Titanate (PZT) based vibration based method (VBM) technique for structural health monitoring (SHM) has been successfully applied to various engineering systems. However, fundamental research work on the sensitivity of the PZT/MFC sensors for damage detection is still in need.
- ✓ Propose new correlation methods between the damage index/metric determined by vibration-based method and the damage index/metric determined by the residual strength of the structure. In this work a linear correlation was present considering lower points of the curve. Computational and experimental analysis can be carried out to obtain other points of the curve and correlate both damage index.
- ✓ Perform uncertainties analysis in the geometric characteristics of the specimens in order to refine the computer models used. Improve the computational models with the real geometrical dimensions of the plates, such as: total thickness, thickness per layer, stacking orientation, and etc.
- ✓ Insert in the methodology a statistical approach to quantify uncertainties of experimental modal parameters. A statistical model consistent with extreme value theory is fitted to the operational data and used to establish control limits. A strategy based on controlling runs is adopted to increase the sensitivity of the detection method.

- ✓ Perform experimental and computational analysis applying the proposed methodology in intact and damage structures, using piezoelectric sensors and the damage models with delamination failure.
- ✓ Apply this SHM system in real situations, *i.e.* real structures;
- ✓ Analyse the information about the extent of damage by other techniques, such as thermography, lamb waves to compare the results and determine the potentiality and limitation of each technique.

CHAPTER 7

References

ABAQUS, 2014, **Documentation**. Pawtucket: Hibbitt, Karlsson & Sorensen.

ABRATE, S. **Impact on Composite Structures**. Cambridge: Cambridge University Press, New York, NY, USA, 1998.

ADAMS, D. **Health monitoring of structural materials and components: Methods with applications**. 1st ed. John Wiley & Sons, New York, 2007.

ADAMS, R.; WALTON, D.; FLITCROFT, J.E.; SHORT, D. **Vibration testing as a nondestructive test tool for composite materials**. ASTM special technical publication, v.580, p.159-175, 1975.

AMARO, A.M.; REIS, P.N.B.; MOURA, M.F.S.F. **Residual strength after low velocity impact in carbon-epoxy laminates**. Materials Science Forum, v.514-516, p.624.628, 2006.

AMBU, R.; AYMERICH, F.; GINESU, F.; PRIOLO, P.; **Assessment of NDT interferometric techniques for impact damage detection in composite laminates**. Composites Science and Technology, v.66, n.2, p.199-205, 2006.

AN, Y. **Residual stress measurement using cross-slitting and ESPI**. Master's thesis, University of British Columbia, Vancouver, Canada, 2008.

ARAÚJO DOS SANTOS, J.V.; LOPES, H.M.R.; VAZ, M.; MOTA SOARES, C.M.; MOTA SOARES, C.A.; DE FREITAS, M.J.M. **Damage localization in laminated composite plates using mode shapes measured by pulsed TV holography**. Composite structures, v.76, n.3, p.272-281, 2006.

ASTM Handbook, **Volume 17: Non- destructive Evaluation and Quality Control**. American Society for Metals, 9th ed., p.516, 1992.

ASTM Standard D6272-10. **Standard test method for flexural properties of unreinforced and reinforced plastics and electrical insulating materials by four point bending**. ASTM International, 2010. <http://www.astm.org>.

ASTM Standard D7136M-15. S**tandard test method for measuring the damage resistance of a fiber-reinforced polymer matrix composite to a drop-weight impact event**. ASTM International, 2015. <http://www.astm.org>.

BALAGEAS, D.; FRITZEN, C. P.; GÜEMES, A. **Structural health monitoring.** 1st ed. ISTE Ltda. 2006.

BALAMURUGAN, R.; MURUGANAND, S. **Digital image processing technique in Laser Speckle Pattern Interferometer for phase evaluation**. International Journal of Engineering and Advanced Technology, v.2, n.3, p.560-562, 2013.

BANDARA, R.P.; CHAN, T.H.; THAMBIRATNAM, D.P. **Structural damage identification with noise polluted frequency response functions (FRFs)**. In Proceedings of the 14th Asia-Pacific Vibration Conference. Hong Kong Polytechnic University, Hong Kong, 2011.

BENZONI, G.; BONESSIO, N.; LOMIENTO, G. Structural Health Monitoring of bridges with seismic response modification devices. **Report No. SSRP-13/02**, Department of Structural Engineering University of California, San Diego La Jolla, California, 2013.

BILGEN, O. **Aerodynamic and electromechanical design, modeling and implementation of piezocomposite airfoils**, Ph.D. Thesis, Faculty of the Virginia Polytechnic Institute and State University, Blacksburg, Virginia, USA, 2010.

BISCANI, F.; NASSER, H.; BELOUETTAR, S.; CARRERA, E. **Equivalent electro-elastic properties of Macro Fiber Composite (MFC) transducers using asymptotic expansion approach**. Composites: Part B, v.42, n.3, p.444-455, 2011.

BOLOTIN, V.V.; SHCHUGOREV, V.N. **Effect of low-velocity impact on the residual strength of composites**. Mechanics of Composite Materials, v.29, n.4, p.357-364, 1994.

BORDEGONI, M.; RIZZI, C. **Innovation in Product Design: From CAD to Virtual Prototyping**. 1st Ed. Springer, 188p. 2011.

CARDEN, E.P.; FANNING, P. **Vibration based condition monitoring: A review**". Structural Health Monitoring, v.3, n.4, p.355-377, 2004.

CHANDRA, S.; BARAI, S.V. **Experimental investigations and critical observations on the use of modal parameters for structural damage detection**. Current Advances in Civil Engineering, v.2, n.1, p.6-15, 2014.

CHENGHONG, H.; YUBIN, L.; ZUOGUANG, Z.; ZHIJIE, S. **Impact damage modes and residual flexural properties of composites beam**. Journal of Reinforced Plastics and Composites, v.27, n.11, p.1163-1175, 2008.

CIANG, C.C.; LEE, J.-R.; BANG, H.-J. **Structural health monitoring for a wind turbine system: a review of damage detection methods**. Measurement Science and Technology, v.19, n.12, p.122001, 2008.

COLLOMBET, F.; BONINI, J.; LATAILLADE, J.L. **A three-dimensional modelling of low velocity impact damage in composite laminates**. International Journal for Numerical Methods in Engineering, v.39, n.9, p.1491-1516, 1996.

CROMER, K.R. **Impact and post-impact response of a composite material to multiple non-coincident impacts**. Master's thesis, Faculty of the University of Delaware, USA, 199p, 2010.

CUC, A.I. **Vibration-based techniques for damage detection and health monitoring of mechanical systems**. Master's thesis, Department of Mechanical Engineering, College of Engineering & Information Technology, University of South, USA, 127p, 2002.

DERAEMAEKER, A.; NASSER, H.; BENJEDDOU A.; PREUMONT, A. **Mixing rules for the piezoelectric properties of macro fiber composites**. Journal of Intelligent Material Systems and Structures, v.20, n.12, p.1475-1482, 2009.

DOEBLING, S.W.; FARRAR, C.R.; PRIME, M.B.; SHEVITZ, D.W. **Damage identification and health monitoring of structural and mechanical systems from changes in their vibration characteristics: A literature review**. Technical report, Los Alamos National Laboratory Report LA-13070-MS, Los Alamos, New Mexico, 1996.

DOEBLING, S.W.; FARRAR, C.R.; PRIME, M.B. **A summary review of vibration-based damage identification methods**. Shock and Vibration Digest, v.30, n.2, p.91-105, 1998.

ELSHAFEY, A.A.; MARZOUK, H.; HADDARA, M.R. **Experimental damage identification using modified mode shape difference**. Journal of Marine Science and Application, v.10, n.2, p.150-155, 2011.

ERTURK, A.; VIERA, W.G.R.; DE MARQUI, C.; INMAN, D.J. **On the energy harvesting potential of piezoaeroelastic systems**. Applied Physics Letters, v.96, n.18, p.184103, 2010.

EWINS, D.J. **Modal testing: Theory, practice and application**. 2nd ed. Research Studies Press LTDA, Baldock, England, 2000.

FAA, FEDERAL AVIATION ADMINISTRATION, **Aviation Maintenance Technician Handbook—Airframe**, Volume 1, U.S. Department of Transportation, FAA-H-8083-31, 2012.

FAN, W.; QIAO, P. **Vibration-based damage identification methods: A review and comparative study**. Structural Health Monitoring, v.10, n.1, p.83-111, 2011.

FARRAR, C.R.; DOEBLING, S.W.; NIX, D.A. **Vibration-based structural damage identification**. Philosophical Transactions of the Royal Society A, v.359, n.1778, p.131-149, 2001.

FARRAR, C.R.; WORDEN, K. **An introduction to structural health monitoring.** Philosophical Transactions of the Royal Society A, v.365, n.1851, p.303-315, 2007.

FASSOIS, S.D.; SAKELLARIOU, J.S. **Time series methods for fault detection and identification in vibrating structures**. In: Structural Health Monitoring 2006: Proceedings of the Third European Workshop, Granada, Spain, 2006.

FERDINAND, P. **The evolution of optical fiber sensors technologies during the 35 last years and their applications in structural health monitoring**. In: 7th European Workshop on Structural Health Monitoring, Nantes, France, 2014.

FLOR, F.R.; MEDEIROS, R.; TITA, V. **Numerical and experimental damage identification in metal-composite bonded joint**. The Journal of Adhesion, v.91, n.10-11, p.863-882, 2015.

FRANCIS, D.; TATAM, R.P.; GROVES, R.M. **Shearography technology and applications: A review**. Measurement Science and Technology, v.21, 102001, 29pp, 2010.

FRITZEN, C.-P. **Vibration-based Structural Health Monitoring – Concepts and applications**. Key Engineering Materials, v.293-294, p.3-20, 2005.

FULLER, C.R.; VON FLOTOW, A.H. **Active control of sound and vibration**. IEEE Control Systems, v.15, n.6, p.9-19, 1995.

FURUKAWA, A.; OTSUKA, H.; KIYONO, J. **Structural damage detection method using uncertain frequency response functions**. Computer-Aided Civil and Infrastructure Engineering, v.21, n.4, p.292-305, 2006.

GARNIER, C.; PASTOR, M.L.; EYMA, F.; LORRAIN, B. **The detection of aeronautical defects in situ on composite structures using Non Destructive Testing**. Composite Structures, v.93, n.5, p.1328-1336, 2011.

GIURGIUTIU, V.; ROGERS, C.A. **Recent Advancements in the Electro-Mechanical (E/M) Impedance Method for Structural Health Monitoring and NDE**. In: 5th Annual International Symposium on Smart Structures and Materials (SPIE), CA, United State, 1998.

GIURGIUTIU, V. **Review of smart-materials actuation solutions for aeroelastic and vibration control**. Journal of Intelligent Material Systems and Structures, v.11, n.7, p.525-544, 2000.

GIURGIUTIU, V.; CUC, A. **Embedded Non-destructive evaluation for structural health monitoring, damage detection, and failure prevention**. The Shock and Vibration Digest, v.37, n.2, p.83-105, 2005.

GIURGIUTIU, V. **Structural Health Monitoring with Piezoelectric Wafer Active Sensors**. Tokyo: Academic Press, 2nd Edition, 2014.

GRYZAGORIDIS, J.; FINDEIS, D.; BOPAPE, W. **Impact damage detection on composites using Electronic Speckle Pattern Interferometry**. Condition monitoring and diagnostic engineering management, Cambridge, 2009.

HAGOOD, N.W.; BENT, A.A. **Development of piezoelectric fiber composites for structural actuation**. AIIA Paper v.1717, p.3625-3638, 1993.

HASIOTIS, T.; Badogiannis, E.; Tsouvalis, N.G. **Application of ultrasonic C-Scan techniques for tracing defects in laminated composite materials**. Journal of Mechanical Engineering, v. 57, n.3, p.192-203, 2011.

HASSEN, A.A.; BOYD, J.; VAIDYA, U.K. **Development of Ultrasonic C-Scan System**. ASTM Journal, 2012.

HERTWIG, M.; FLEMMING, T.; FLOUREUX, T.; AEBISCHER, H.A. **Speckle interferometric damage investigation of fibre-reinforced composites**". Optics and Lasers in Engineering, v.24, n.5, p.485-504, 1996.

HEYLEN, W.; LAMMENS, S.; SAS, P. **Modal analysis theory and testing**. Leuven: Katholieke Universiteit Leuven KUL Press, 1997.

HOUSNER, G.W.; BERGMAN, L.A.; CAUGHEY, T.K.; CHASSIAKOA, A.G.; CLAUS, R.O.; MASRI, S.F.; SKELTON, R.E.; SOONG, T.T.; SPENCER, B.F.; YAO, J.T.P. **Structural Control: Past, Present, and Future**. ASCE Journal of Engineering Mechanics, v.123, n.9, p.897-971, 1997.

ISLAM, A.S.; CRAIG, K.C. **Damage detection in composite structures using piezoelectric materials (and neural net)**. Smart Material and Structure, v.3, n.3, p.318-328, 1994.

JACQUOT, P. **Speckle Interferometry: A Review of the Principal Methods in Use for Experimental Mechanics Applications**. Strain, v.44, n.1, p.57-69, 2008.

JANG, B.P.; KOWBEL, W.; JANG, B.Z. **Impact behaviour and impact fatigue testing of polymer composites**. Composites Science and Technology, v.144, n.2, p.107-118, 1992.

JOHNSON, T.J.; ADAMS, D.E. **Transmissibility as a differential indicator of structural damage**. Journal of Vibration and Acoustics, v.124, n.4, p.634, 2002.

JUNEJA, V.; HAFTKA, R.; CUDNEY, H. **Damage detection and damage detectability analysis and experiments**. Journal of Aerospace Engineering, v.10, n.4, p.135-142, 1997.

KACHANOV, LM. **Introduction to continuum damage mechanics**, Dordrecht: Martinus Nijhoff Publishers, 1986.

KAUFMANN, M. **Cost/Weight Optimization of Aircraft Structures**. KTH, Stockholm, 2008.

KESSLER, S.S.; SPEARING, S.; ATALLA, M.J.; CESNIK, C.E.; SOUTIS, C. **Damage detection in composite materials using frequency response methods**. Composites Part B: Engineering, v.33, n.1, p.87-95, 2002a.

KESSLER, S.S. **Piezoelectric-based in-situ damage detection of composite materials for structural health monitoring systems**, PhD Thesis, Massachusetts Institute of Technology, Cambridge, Massachusetts, USA, 200p, 2002b.

KIM, G.; HONG, S.; JHANG, K.Y.; KIM, G.H.; **NDE of low-velocity impact damages in composite laminates using ESPI, digital shearography and ultrasound C-scan techniques**. International Journal of Precision Engineering and Manufacturing, v.13, n.6, p.869-876, 2012.

KIM, J-K.; MACKAY, D.B.; MAI, Y-W. **Drop-weight impact damage tolerance of CFRP with rubber modified epoxy matrix**. Composites, v.24, n.6, p.485-494, 1993.

KREIS, T. **Handbook of Holographic Interferometry: Optical and Digital Methods**. WILEY-VCH Verlag GmbH & Co. KGaA, Weinheim, 1st edition, 2005.

KURATA, M.; KIM, J.H.; LYNCH, J.P.; LAW, K.H.; SALVINO, L.W. **A probabilistic model updating algorithm for fatigue damage detection in aluminum hull structures**. In Proceedings of the ASME 2010 Conference on Smart Materials, Adaptive Structures and Intelligent Systems SMASIS2010. Philadelphia, Pennsylvania, USA, 2010.

LASYK, L.; LUKOMSKI, M.; BRATASZ, L. **Simple digital speckle pattern interferometer (DSPI) for investigation of art objects**. Optica Applicata, v.41, n.3, p.687-700, 2011.

LEENDERTZ, J.A.; BUTTERS, J.N. **An image-shearing speckle-pattern interferometer for measuring bending moments**. Journal of Physics E: Scientific Instruments, v.6, n.11, p.1107-1110, 1974.

LEHMANN, M.; BÜTER, A.; FRANKENSTEIN, B.; SCHUBERT, F.; BRUNNER, B. **Monitoring System for Delamination Detection – Qualification of Structural Health Monitoring (SHM) Systems**. In: Conference on Damage in Composite Material CDCM 2006, Stuttgart, Germany, 2006.

LIN, T.K.; HUNG, S.L.; HUANG, C.S. **Detection of damage location using novel substructure-based frequency response function approach with a wireless sensing system**. International Journal of Structural Stability and Dynamics, v.12, n.04, p.1250029, 2012.

LIU, Y.; NAYAK, S. **Structural health monitoring: State of the art and perspectives**. Journal of the Minerals, Metals & Materials Society, v.64, n.7, p.789-792, 2012.

LOPES, H.; SANTOS, J.V.A.; GUEDES, R.; VAZ, M. **A hybrid technique for damage detection on laminated plates**. In: Photomechanics. França, 2006.

LOPES, H.M.R. **Desenvolvimento de Técnicas Interferométricas, Contínuas e Pulsadas, Aplicadas à Análise do Dano em Estruturas Compósitas**. PhD. Thesis, Faculdade de Engenharia da Universidade do Porto, Porto, Portugual.2007, (in portuguese).

LOPES, H.M.R.; SANTOS, J.V.A.; SOARES, C.M.M.; GUEDES, R.J.M.; VAZ, M.A.P. **A numerical-experimental method for damage location based on rotation fields spatial differentiation**. Computers and Structures, v.89, n.19–20, p.1754-1770, 2011.

LOPES, H.; RIBEIRO, J.; DOS SANTOS, J.A.; MAIA, N. **Localization of Damage in Beams Using Interferometric Techniques**. In: 6th European Workshop on Structural Health Monitoring, Dresden, Germany, 2012.

MAIA, N.; SILVA, J.; ALMAS, E.; SAMPAIO, R. **Damage detection in structures: from mode shape to frequency response function methods**". Mechanical Systems and Signal Processing, v.17, n.3, p.489-498, 2003.

MAIKUMA, H.; GILLESPIE, J.W.; WILKINS, D.J. **Mode II interlaminar fracture of the centre notched flexural specimen under impact loading**. Journal of Composite Materials, v.24, n.2, p.124-149, 1990.

MAIN, J.A.; GARCIA, E.; NEWTON, D.V. **Precision position-control of piezoelectric actuators using charge feedback**. Proceedings of SPIE 2441, p.243-254, 1995.

MAIO, C.E.B.; TRINDADE, M.A. **Evaluation of metrics and techniques for the detection of delamination in composite structures using piezoelectric sensors**. In: 21nd International Congress of Mechanical Engineering (COBEM2011), Natal, Rio Grande do Norte, Brazil, 2011.

MAL, A.; RICCI, F.; BANERJEE, S.; SHIH, F. **A conceptual structural health monitoring system based on vibration and wave propagation**. Structural health monitoring, v.4, n.3, p.283-293, 2005.

MARIATTI, M.; NASIR, M.; ISMAIL, H. **The flexural behavior of woven prepreg thermoplastic composites**. Journal of Thermoplastic Composite Materials, v.14, n.4., p.290-305, 2001.

MATZENMILLER, A.; LUBLINER, J.; TAYLOR, RL. **A constitutive model for anisotropic damage in fiber-composites**. Mechanics of Materials, v.20, n.2, p.125-152, 1995.

MCCONNELL, K.G.; VAROTO, P.S. **Vibration testing: Theory and practice**. 2nd ed. John Wiley & Sons, New York, 1995.

MEDEIROS, R.; SARTORATO, M.; RIBEIRO, M.L.; VANDEPITTE, D.; TITA, V. **Numerical and experimental analyses about SHM metrics using piezoelectric materials**. In Proceedings of ISMA2012-USD2012. Leuven, Belgium, 2012.

MEDEIROS, R.; BORGES, E.N.; RIBEIRO, M.L.; CARVALHO, F.G.; TITA, V. **Vibration-based structural monitoring applied on hybrid bonded joints**. In: 22nd International Congress of Mechanical Engineering (COBEM2013), Ribeirão Preto, São Paulo, Brazil, p.319-330, 2013.

MEDEIROS, R.; RIBEIRO, M.L.; TITA, V. **Computational methodology of damage detection on composite cylinders: Structural health monitoring for automotive components**. International Journal of Automotive Composites, v.1, p.112-128, 2014a.

MEDEIROS, R.; FLOR, F.R.; RIBEIRO, M.L.; TITA, V. **Debonding identification in metal-composite bonded joint using vibration testing**. In: VIII National Congress of Mechanical Engineering (CONEM2014), Uberlândia, Minas Gerais, Brazil, 2014b.

MEDEIROS, R.; LOPEZ, H.M.R.; GUEDES, R.M.; VAZ, M.A.P.; VANDEPITTE, D.; TITA, V. **A new approach for SHM system: combination of vibration based method and shearography speckle**. In: 5th International Symposium on Solid Mechanics (MecSol2015), Belo Horizonte, Brazil, 2015a.

MEDEIROS, R.; LOPEZ, H.M.R.; GUEDES, R.M.; VAZ, M.A.P.; VANDEPITTE, D.; TITA, V. **A new methodology for Structural Health Monitoring applications**. Procedia Engineering, v.114, p.54-61, 2015b.

MICKENS, T.; SCHULZ, M.; SUNDARESAN, M.; GHOSHAL, A.; NASER, A.; REICHMEIDER, R. **Structural health monitoring of an aircraft joint**. Mechanical Systems and Signal Processing, v.17, n.2, p.285-303, 2003.

MINAK, G.; ABRATE, S.; GHELLI, D.; PANCIROLI, R.; ZUCCHELLI, A. **Residual torsional strength after impact of CFRP tubes**. Composites Part B: Engineering, v.41, n.8, p.637-645, 2010.

MOAVENI, B.; HE, X.; CONTE, J.P.; DE CALLAFON, R.A. **Damage identification of a composite beam using finite element model updating**. Computer-Aided Civil and Infrastructure Engineering, v.23, n.5, p.339-359, 2008.

MODENA, C.; SONDA, D.; ZONTA, D. **Damage localization in reinforced concrete structures by using damping measurements**. In: Proceedings of the International Conference on Damage Assessment of Structures, Dublin, Ireland, p.132–141, 1999.

MONACO, E.; FRANCO, F.; LECCE, L. **Experimental and numerical activities on damage detection using magnetostrictive actuators and statistical analysis**. Journal of Intelligent Material Systems and Structures, v.11, n.7, p.567-578, 2000.

MONTALVÃO, D.; MAIA, N.; RIBEIRO, A. **A review of vibration-based structural health monitoring with special emphasis on composite materials**. Shock and Vibration Digest, v.38, n.4, p.295-324, 2006.

MOURITZ, A.P.; GALLAGHER, J.; GOODWIN, A.A. **Flexural strength and interlaminar shear strength of stitched GRP laminates following repeated impacts**. Composites Science and Technology, v.57, n.5, p.509-522, 1997.

NEUMANN, D.B. **Comparative Holography**. In: OSA Technical Digest, Topical Meeting on Hologram Interferometry and Speckle Metrology, Paper MB2-1, 1980.

NILSSON, E. **Residual Strength Prediction of Composite Laminates Containing Impact Damage** Master Thesis in Solid Mechanics, Linköping University, 2005.

NOKES, J.P; CLOUD, G.L. **The application of interferometric techniques to the nondestructive inspection of fiber-reinforced materials**. Experimental Mechanics, v.33, n.4, p.314-319, 1993.

OOIJEVAAR, T.; LOENDERSLOOT, R.; WARNET, L.; DE BOER, A.; AKKERMAN, R. **Vibration based structural health monitoring of a composite t-beam**. Composite Structures, v.92, n.9, p.2007-2015, 2010.

OOIJEVAAR, T. **Vibration based structural health monitoring of composite skin-stiffener structures**. PhD thesis, University of Twente, Enschede, Netherlands, 194p, 2014.

PAIVA, J.M.F.; MAYER, S.; REZENDE, M.C. **Evaluation of compression after impact strength of carbon/epoxy composites used in aeronautical area**. In: 18th International Congress of Mechanical Engineering (COBEM2005), Ouro Preto, MG, Brazil, 2005.

PANDEY, A.; BISWAS, M.; SAMMAN, M. **Damage detection from changes in curvature mode shapes**. Journal of Sound and Vibration, v.145, n.2, p.321-332, 1991.

PARDOEN, G.C. **Effect of delamination on the natural frequencies of composite laminates**. Journal of Composite Materials, v.23, n.12, p.1200-1215, 1989.

PEETERS, B.; DER AUWERAER, H.V.; GUILLAUME, P.; LEURIDAN, J. **The polymax frequency-domain method: a new standard for modal parameter estimation?.** Shock and Vibration, v.11, n.3-4, p.395-409, 2004.

PUHUI, C.; ZHEN, S.; JUNYANG, W.; **A new method for Compression After Impact strength prediction of composite laminates**. Journal of Composite Materials, v.36, n.5, p.589-610, 2002.

QI, B.; HERSZBERG, I. **An engineering approach for predicting residual strength of carbon/epoxy laminates after impact and hygrothermal cycling**. Composite Structures, v.47, n.1-4, p.483-490, 1999.

RAGHAVAN, A.; CESNIK, C.E.S. **Review of guided-wave structural health monitoring**. The Shock and Vibration Digest, v.39, n.2, p.91-114, 2007.

RASTOGI, P.K. **Comparative holographic interferometry: a nondestructive inspection system for detection of flaws**. Experimental Mechanics, v.25, n.4, p.325-337, 1985.

RASTOGI, P.K.; HACK, E. **Optical Methods for Solid Mechanics: A Full-Field Approach**. 1st Edition. John Wiley & Sons, 2013.

REDDY, D.M.; SWARNAMANI, S. **Application of the FRF curvature energy damage detection method to plate like structures**. World Journal of Modelling and Simulation, v.8, n.2, p.147-153, 2012.

REYES, G.; SHARMA, U. **Modeling and damage repair of woven thermoplastic composites subjected to low velocity impact**. Composite Structures, v.92, n.2, p.523-531, 2010.

RIBEIRO, M.L.; TITA, V.; VANDEPITTE, D. **A new damage model for composite laminates**. Composite Structures, v.94, n.2, p.635-642, 2012a.

RIBEIRO, M.L.; MEDEIROS, R.; SARTORATO, M.; TITA, V. **Detecção de dano em cilindros de compósito empregando material piezelétrico**. In Proceedings of the VII Congresso Nacional de Engenharia Mecânica CONEM2012. São Luís, Maranhão, Brasil, 2012b.

RIBEIRO, M.L. **Damage and progressive failure analysis for aeronautic composite structures with curvature**. PhD Thesis – São Carlos School of Engineering – University of São Paulo, São Carlos, 2013a.

RIBEIRO, M.L.; VANDEPITTE, D.; TITA, V. **Damage model and progressive failure analyses for filament wound composite laminates**. Applied Composite Materials, v.20, n.5, p.975-992, 2013b.

RIBEIRO, M.L.; VANDEPITTE, D.; TITA, V. **Experimental analysis of transverse impact loading on composite cylinders**. Composite Structures, v.133, p.547-563, 2015.

RICHARDSON, M.O.W.; WISHEART M.J. **Review of low-velocity impact properties of composite materials**. Composites Part A: Applied Science and Manufacturing, v.27, n.12, p.1123-1131, 1996.

RIVALLANT, S.; BOUVET, C.; HONGKARNJANAKUL, N. **Failure analysis of CFRP laminates subjected to compression after impact: FE simulation using discrete interface elements**. Composites Part A: Applied Science and Manufacturing, v.55, p.83-93, 2013.

ROTEM, A. **The strength of laminated composite materials under repeated impact loading**. Journal of Composites Technology & Research, v.10, n.2, p.74-79, 1988.

RUZEK, R.; LOHONKA, R.; JIRONC, J. **Ultrasonic C-Scan and shearography NDI techniques evaluation of impact defects identification**. NDT & E International, v.39, n.2, p.132-142, 2006.

RYTTER, A. **Vibration based inspection of civil engineering structures**", Ph.D. Thesis, Aalborg University, Denmark, 1993.

SALAWU, O. **Detection of structural damage through changes in frequency: a review**. Engineering Structures, v.19, n.9, p.718-723, 1997.

SALEHI, M.; ZIAEI-RAD, S.; GHAYOUR, M.; VAZIRI-ZANJANI, M.A. **A structural damage detection technique based on measured frequency response functions**. Contemporary Engineering Sciences, v.3, n.5, p.215-226, 2010.

SAMPAIO, R.; MAIA, N.; SILVA, J. **Damage detection using the frequency-response-function curvature method**. Journal of Sound and Vibration, v.226, n.5, p.1029-1042, 1999.

SANCHEZ-SAEZ, S.; BARBERO, E.; ZAERA, R.; NAVARRO, C. **Compression after impact of thin composite laminates**. Composites Science and Technology, v.65, n.13, p.1911-1919, 2005.

SANTIUSTE, C.; SANCHEZ-SAEZ, S.; BARBERO, E. **Residual flexural strength after low-velocity impact in glass/polyester composite beams**. Composite Structures, v.92, n.1, p.25-30, 2010.

SCHMIDT, A. **Experimental Investigations on Nondestructive Testing Methods for Defect Detection with Double-pulse Electronic Speckle Pattern Interferometry**, Ph.D. Thesis, Faculty of Mechanical Engineering, Helmut-Schmidt-University / University of the Federal Armed Forces Hamburg, Hamburg, Germany, 2009.

SCHNARS, U.; JUEPTNER, W. **Digital holography: digital hologram recording, numerical reconstruction and related techniques**. Springer – Verlag Berlin Heidelberg, 1st edition, 2005.

SHAHDIN, A.; MORLIER, J.; GOURINAT, Y. **Correlating low-energy impact damage with changes in modal parameters: A preliminary study on composite beams**. Structural Health Monitoring, v.8, n.6, p.523-536, 2009.

SHIM, V.P.W.; YANG, L.M. **Characterization of the residual mechanical properties of woven fabric reinforced composites after low-velocity impact**. International Journal of Mechanical Sciences, v.47, n.4-5, p.647-665, 2005.

SILVA, S.; DIAS JÚNIOR, M.; LOPES JUNIOR, V. **Structural health monitoring in smart structures through time series analysis**. Structural Health Monitoring, v.7, n.3, p.231-244, 2008.

SINOU, J.-J. **A review of damage detection and health monitoring of mechanical systems from changes in the measurement of linear and non-linear vibrations**. Mechanical Vibrations: Measurement, Effects and Control, p.643-702, 2009.

SLÄTTE, F.; JOVANOV, K. Structural health monitoring for aerospace composite structures-an investigation of the potential using the finite element method. Master's Thesis in Applied Mechanics, Chalmers University of Technology, Gothenburg, Sweden 2012.

SOUTIS, C.; CURTIS, P.T. **Prediction of the post-impact compressive strength of CFRP laminated composites**. Composites Science and Technology, v.56, n.6, p.677-684, 1996.

STASZEWSKI, W.J.; MAHZAN, S.; TRAYNOR, R. **Health monitoring of aerospace composite structures – Active and passive approach**. Composites Science and Technology, v.69, n.11, p.1678-1685, 2009.

SU, Z.; Ye, L.; Lu, Y. **Guided Lamb waves for identification of damage in composite structures: A review**. Journal of Sound and Vibration, v.295, n.3-5, p.753-780, 2006.

SUBRAMANIAN, A. Damage detection and characterization of fiber reinforced composites using ultrasonics. Master of Science, Iowa State University, Ames, Iowa, 2013.

SUNDARAM, R.; KAMATH, G.M.; GUPTA, N. **Structural health monitoring of composite structures - Issues and Challenges**. International Journal of Vehicle Structures & Systems, v.4, n.3, p. 74-85, 2012.

THYAGARAJAN, S.; SCHULZ, M.; PAI, P.; CHUNG, J. **Detecting structural damage using frequency response functions**". Journal of Sound and Vibration, v.210, n.1, p. 162-170, 1998.

TRENDAFILOVA, I.; PALAZZETTI, R.; ZUCCHELLI, A. **Damage assessment based on general signal correlation. Application for delamination diagnosis in composite structures**. European Journal of Mechanics-A/Solids, v.49, p.197-204, 2015.

TITA, V. **Contribution to the study of damage and progressive failure on composite structures**. PhD Thesis – Escola de Engenharia de São Carlos, Universidade de São Paulo, São Carlos, 2003.

TITA, V.; DE CARVALHO, J.; VANDEPITTE, D. **Failure analysis of low velocity impact on thin composite laminates: Experimental and numerical approaches**. Composite Structures, v.83, n.4, p.413-428, 2008.

ULLAH, I.; SINHA, J.K.; PINKERTON, A. **Vibration-based delamination detection in a composite plate**. Mechanics of Advanced Materials and Structures, v.20, n.7, p.536-551, 2013.

VANDIVER, J. **Detection of structural failure on fixed platforms by measurement of dynamic response**. Journal of Petroleum Technology, v.3, n.3, p.305-310, 1977.

WANG, K. **Vibration analysis of cracked composite bending-torsion beams for damage diagnosis**. PhD Thesis, Virginia Polytechnic Institute and State University, Blacksburg, Virginia, USA, 183p, 2004.

WANG, S.-X.; WU, L.-Z.; MA, L. **Low-velocity impact and residual tensile strength analysis to carbon fiber composite laminates**. Materials & Design, v.31, n.1, p.118-125, 2010.

WANG, Z.; LIN, R.; LIM, M. **Structural damage detection using measured FRF data**. Computer Methods in Applied Mechanics and Engineering, v.147, n.1-2, p.187-197, 1997.

WILKIE, W.K.; BRYANT, R.G.; HIGH, W.J.; FOX, R.L.; HELLBAUM, R.F.; JALINK JR, A.; LITTLE, B.D.; MIRICK, P.H. **Low-cost piezocomposite actuator for structural control applications**. In: SPIE's 7th annual international symposium on smart structures and materials, Newport Beach, CA, USA, 2000.

WILLIAMS, G.J.; BOND, I.P.; TRASK, R.S. **Compression after impact assessment of self-healing CFRP**. Composites Part A: Applied Science and Manufacturing, v.40, n.9, p.1399-1406, 2009.

WILLIAMS, J.G.; RHODES, M.D. **Effect of resin on impact damage tolerance of graphite/epoxy laminates**. In: Proceedings of the 6th Conference on Composite Materials: Testing and Design, ASTM STP 787 edited by I.M. Daniel, American Society for Testing and Materials, p.450-480, 1982.

WORDEN, K.; FARRAR, C.R.; HAYWOOD, J.; TODD, M. **A review of nonlinear dynamics applications to structural health monitoring**. Structural Control and Health Monitoring, v.15, n.4, p.540-567, 2008.

WU, H.T.; SPRINGER, G.S. **Measurements of matrix cracking and delamination caused by impact on composite plates**. Journal of Composite Materials, v.22, n.6, p.518-532, 1988.

WYRICK, D.A.; ADAMS, D.F. **Residual strength of a carbon/epoxy composites material subjected to repeated impact**. Journal of Composite Materials, v.22, n.8, p749-765, 1988.

YAM, L.H.; WEI, Z.; CHENG, L. **Nondestructive detection of internal delamination by vibration-based method for composite plates**. Journal of Composite Materials, v.38, n.24, p.2183-2198, 2004.

ZABARAS, N.; PERVEZ, T. **Viscous damping approximation of laminated anisotropic composite plates using the finite element method**. Computer Methods in Applied Mechanics and Engineering, v.81 n.3, p.291-316, 1990.

ZANG, C.; FRISWELL, M.I.; IMREGUN, M. **Structural health monitoring and damage assessment using measured FRFs from multiples sensors, part I: The indicator of correlation criteria**. Key Engineering Materials, v.245-246, p.131-140, 2003.

ZHANG, Z.Y.; RICHARDSON, M.O.W.; WISHEART, M.; TYRER, J.R.; PETZING, J. **ESPI non-destructive testing of GRP composite materials containing impact damage**. Composites Part A: Applied science and manufacturing, v.29, n.7, p.721-729, 1998.

ZHANG, Z.Y.; RICHARDSON, M.O.W. **Low velocity impact induced damage evaluation and its effect on the residual flexural properties of pultruded GRP composites**. Composite Structures, v.81, n.2, p.195-201, 2007.

ZHENG, S.; SUN, C.T. **Delamination interaction in laminated structures**. Engineering Fracture Mechanics, v.59, n.2, p.225-240, 1998.

ZHONG, Y.; YUAN, S.; QIU, L. **Multi-impact source localisation on aircraft composite structure using uniform linear PZT sensors array**. Structure and Infrastructure Engineering, v.11, n.3, p.310-320, 2015.

ZHU, Y.-K.; TIAN, G.-Y.; LU, R.-S.; ZHANG, H. **A review of optical NDT technologies**. Sensors, v.11, n.8, p.7773-7798, 2011.

ZHU, K.; CHEN, M.; LU, Q.; WANG, B.; FANG, D. **Debonding detection of honeycomb sandwich structures using frequency response functions**. Journal of Sound and Vibration, v.333, n.21, p. 5299-5311, 2014.

ZOU, Y.; TONG, L.; STEVEN, G. **Vibration-based model-dependent damage (delamination) identification and health monitoring for composite structures a review**. Journal of Sound and Vibration, v.230, n.2, p.357-378, 2000.

APPENDIX A

Damage Indentification Methods

A structural health monitoring technique typically consists of the selection of suitable damage sensitive feature and the subsequent condensation and classification of the information with the help of a damage metric. A summary of the literature pertaining to the various methods for damage identification and health monitoring of structures based on changes in their measured dynamic properties is presented by Ooijevaar (2014) and complemented in this section.

A.1. Time domain

Statistical time series analysis

COR	Correlation functions (non-parametric)	Fassois and Sakellariou, 2007
AR	Autoregressive models (parametric)	Fassois and Sakellariou, 2007
VFP	Vector-dependent functionally pooled	Kopsaftopoulos and Fassois, 2006

Time-frequency analysis

WA	Wavelet transform based methods	Rucka and Wilde, 2006
HT	Hilbert transform based methods	Huang *et al.*, 1998
HHT	Hilbert-Huang transform based methods	Huang *et al.*, 1998
EMD	Empirical mode decomposition	Huang *et al.*, 1998
CPD	Conjugate-pair decomposition	Pai, 2011

A.2. Frequency domain

Frequency response function / operational deflection shapes

FRFCH	Frequency response function change	Kessler *et al.*, 2002
FRFDI	Frequency response function damage index	Mickens *et al.*, 2003
FRFSHP	Frequency response function shape method	Liu *et al.*, 2009
DRQ	Detection and relative damage quantification indicator	Maia *et al.*, 2007
FRAC	Frequency response assurance criterion	Heylen and Lammens, 1996
CORTHOG	Coordinate orthogonality check	Avitabile and Pechinsky, 1994
CCF	Complex correlation coefficient	Der Auweraer, 1998
MFAC	Modal FRF assurance criterion	Fotsch and Ewins, 2001
FDAC	Frequency domain assurance criterion	Pascual *et al.*, 1997
RVAC	Response vector assurance criterion	Sampaio *et al.*, 2003
ODSC	Operational deflection shape change	Pascual *et al.*, 1999
GSC	Global shape correlation	Zang and Imregun, 2007
GAC	Global amplitude correlation	Zang and Imregun, 2007

Frequency response function curvature

FRFC	Frequency response function curvature	Sampaio *et al.*, 1999
SFRFDI	Strain frequency response damage index	Maia *et al.*, 2003

Mechanical impedance (Z)

RMSD	Root mean square deviation	Park *et al.*, 2003
MAPD	Mean absolute percentage deviation	Giurgiutiu and Zagrai, 2005
CCD	Correlation coefficient deviation	Giurgiutiu and Zagrai, 2005

Transmissibility function (T)

TDI	Transmissibility damage index	Johnson and Adams, 2002

Antiresonances

AFN	Antiresonance shift	Wahl *et al.*, 1996

Higher harmonics (nonlinear effect)

HH	Higher harmonic imaging	Krohn *et al.*, 2002

Modulations (nonlinear effect)

AFN	Vibro-acoustic modulations	Donskoy and Sutin, 1998

A.3. Modal domain

Natural frequencies

CAC	Cawley-Adams criterion	Cawley and Adams, 1979
NNF	Normalized Natural Frequencies	Davini et al., 1995
%C	Percentage changes in the natural frequencies	Narkis, 1994
% Ψ	Changes in the ratio of frequencies	Sinou, 2007
DLAC	Damage location assurance criterion	Messina *et al.*, 1998
MDLAC	Multiple damage location assurance criterion	Messina *et al.*, 1998
SDI	Single damage indicator	Kim and Stubbs, 2003
FMAC	Frequency scaled modal assurance criterion	Fotsch and Ewins, 2001

Mode shape

MS	Mode shape amplitude change	Gladwell and Morassi, 1999
MSS	Mode shape slope	Ho and Ewins, 2000
MSAC	Mode shape amplitude comparison	Ho and Ewins, 2000
MAC	Modal assurance criteria	West, 1984
IMAC	Inverse modal assurance criterion	Mitchell, 2001
COMAC	Coordinate modal assurance criterion	Lieven and Ewins, 1988
ECOMAC	Enhanced coordinate modal assurance criterion	Hunt, 1992
PMAC	Partial modal assurance criterion	Heylen, 1990
MACSR	Modal assurance criterion square root	O'Callahan, 1998
SMAC	Scaled modal assurance criterion	Brechlin *et al.*, 1998
MACRV	modal assurance criterion using reciprocal modal vectors	Wei *et al.*, 1990
MCC	Mutual correspondence criterion	Milecek, 1994
MCC	Modal correlation coefficient	Samman, 1996
FD	Fractal dimension method	Hadjileontiadis *et al.*, 2005
GFD	Generalized fractal dimension	Wang and Qiao, 2007
AWCD	Approximate waveform capacity dimension	Qiao and Cao, 2008
MSRC	Mode shape rotation change	Abdo and Hori, 2002
WTM	Wavelet transform method	Liew and Wang, 1998
CWT	Continuous wavelet transform	Hong *et al.*, 2002
SWT	Stationary wavelet transform	Zhong and Oyadiji, 2007

Mode shape curvature

MSC	Mode shape curvature method	Pandey *et al.*,1991
MSCS	Mode shape curvature squared method	Ho and Ewins, 2000
CDF	Curvature damage factor method	Abdel Wahab and De Roeck, 1999
GSM	Gapped smoothing method	Ratcliffe, 1997

Modal Strain Energy

MSE	Modal strain energy method	Stubbs *et al.*, 1992
MSECR	Modal strain energy change ratio	Shi and Law, 1998

Modal damping

SDC	Specific damping capacity	Kyriazoglou et al., 2004

Dynamic stiffness (combination of modal parameters)

ESC	Effective stiffness change	Khoo *et al.*, 2004

Dynamic flexibility (combination of modal parameters)

MFL	Modal flexibility method	Pandey and Biswas, 1994
FI	Flexibility index	Ho and Ewins, 2000
MFLC	Modal flexibility curvature method	Lu *et al.*, 2002
ULS	Uniform load surface method	Zhang and Aktan, 1995
ULSC	Uniform load surface curvature	Wu and Law, 2004
MCI	Modal compliance index method	Choi *et al.*, 2005
DFCC	Dynamic flexibility curvature change	Zhang and Aktan, 1995

Updating methods

OMU	Optimal Matrix Updating	Baruch, 1982
EA	Eigenstructure Assignment Methods	Mottershead and Friswell, 1993
SBU	Sensitivity-Based Updating Methods	Farhat and Hemez, 1993
SMU	Stochastic Model Updating Methods	Mares *et al.*, 2006

Other methods

MF	Modal filters	Meirovitch and Baruh, 1985
MD	Modal peak density	Chrysochoidis and Saravanos, 2004
SCCM	Spectral center correction method	Zhong *et al.*, 2008
GA	Genetic algorithm	Maity and Tripathy, 2005
ANN	Artificial Neural Network	Ritter and Kirkegaard (1997)

A.4. References

ABDEL WAHAB, M.M.; DE ROECK, G. **Damage detection in bridges using modal curvatures: application to a real damage scenario**. Journal of Sound and Vibration, v.226, n.2, p.217-235, 1999.

ABDO, M.A.-B.; HORI, M. **A numerical study of structural damage detection using changes in the rotation of mode shapes**. Journal of Sound and vibration, v.251, n.2, p.227-239, 2002.

AVITABILE, P.; PECHINSKY, F. **Coordinate orthogonality check (CORTHOG)**. In: Proceedings, International Modal Analysis Conference, p.753-760, 1994.

BARUCH, M. **Optimal correction of mass and stiffness matrices using measured modes**. AIAA Journal, v.20, n.11, p.1623-1626, 1982.

BRECHLIN, E.; BENDEL, K.; KEIPER, W. **A new scaled modal assurance criterion for eigenmodes containing rotational degrees of freedom**. In: Proceedings, International Seminar on Modal Analysis, ISMA23, 7 pp., 1998.

CAWLEY, P.; ADAMS, R.D. **The location of defects in structures from measurements of natural frequencies**. Journal of Strain Analysis, v.14, n.2, p.49-57, 1979.

CHOI, S.; PARK, S.; YOON, S.; STUBBS, N. **Nondestructive damage identification in plate structures using changes in modal compliance**. NDT & E Internacional, v.38, n.7, p.529-540, 2005.

CHRYSOCHOIDIS, N.A.; SARAVANOS, D.A. **Assessing the effects of delamination on the damped dynamic response of composite beams with piezoelectric actuators and sensors**. Smart Materials and Structures, v.13, p.733-742, 2004.

DER AUWERAER, V.; IADEVAIA, M.; EMBORG, U.; GUSTAVSSON, M.; TENGZELIUS, U.; HORLIN, N. **Linking test and analysis results in the medium frequency range using principal field shapes**. In: Proceedings, International Seminar on Modal Analysis, ISMA23, 8 pp., 1998.

DAVINI, C.; MORASSI, A.; ROVERE, N. **Modal analysis of notched bars: tests and comments on the sensitivity of an identification technique**. Journal of Sound and Vibration, v.179, n.3, p.402-416, 1995.

DONSKOY, D.M.; SUTIN, A.M. **Vibro-acoustic modulation nondestructive evaluation technique**. Journal of Intelligent Material Systems and Structures, v.9, n.9, p.765-771, 1998.

FARHAT, C.; HEMEZ, F.M. **Updating finite element dynamic models using an element-by-element sensitivity methodology**. AIAA Journal, v.31, n.9, p.1702-1711, 1993.

FASSOIS, S.D.; SAKELLARIOU, J.S. **Time-series methods for fault detection and identification in vibrating structures**. Philosophical Transactions of the Royal Society A: Mathematical, Physical and Engineering Sciences, v.365, n.1851, p.411-48, 2007.

FOTSCH, D.; EWINS, D.J. **Further applications of the FMAC**. In: Proceedings, International Modal Analysis Conference, p.635-639, 2001.

GIURGIUTIU, V.; ZAGRAI, A. **Damage detection in thin plates and aerospace structures with the electro-mechanical impedance method**. Structural Health Monitoring, v.4, n.2, p.99-118, 2005.

GLADWELL, G.M.L.; MORASSI, A. **Estimating damage in a rod from changes in node positions**. Inverse Problems in Engineering, v.7, p.215-233, 1999.

HADJILEONTIADIS, L.J.; DOUKA, E.; TROCHIDIS, A. **Fractal dimension analysis for crack identification in beam structures**. Mechanical Systems and Signal Processing, v.19, n.3, p.659-674, 2005.

HEYLEN, W. **Extensions of the Modal Assurance Criterion**. Journal of Vibrations and Acoustics, v.112, p.468-472, 1990.

HEYLEN, W.; LAMMENS, S. **FRAC: A Consistent way of Comparing Frequency Response Functions**. In: Proceedings, International Conference on Identification in Engineering, Swansea, p.48-57, 1996.

HO, Y.; EWINS, D. **On the structural damage identification with mode shapes**. In: Proceedings of the European COST F3 Conference on System Identification and Structural Health Monitoring Madrid, Spain, 1, p.677–686, 2000.

HONG, J.-C.; KIM, Y.Y.; LEE, H.C.; LEE, Y.W. **Damage detection using the Lipschitz exponent estimated by the wavelet transform: applications to vibration modes of a beam**. International Journal of Solids and Structures, v.39, n.7, p.1803-1816, 2002.

HUANG, N.E.; SHEN, Z.; LONG, S.R.; WU, M.C.; SHIH, H.H.; ZHENG, Q.; YEN, N.-C.; TUNG, C.C.; LIU, H.H. **The empirical mode decomposition and the Hilbert spectrum for nonlinear and non-stationary time series analysis**. Proceedings of the Royal Society A, v.454, p.903-995, 1998.

HUNT, D.L. **Application of an enhanced coordinate modal assurance criterion**, Proceedings of the 10th International Modal Analysis Conference, San Diego, CA, p.66–71, 1992.

JOHNSON, T.J.; ADAMS, D.E. **Transmissibility as a differential indicator of structural damage**. Journal of Vibration and Acoustics, v.124, n.4, p.634, 2002.

KESSLER, S.S.; SPEARING, S.M.; ATALLA, M.J.; CESNIK, C.E.S.; SOUTIS, C. **Damage detection in composite materials using frequency response methods**. Composites Part B: Engineering, v.33, n.1, p.87-95, 2002.

KHOO, L.M.; MANTENA, P.R.; JADHAV, P. **Structural damage assessment using vibration modal analysis**. Structural Health Monitoring, v.3, n.2, p.177-194, 2004.

KIM, J.T.; STUBBS, N. **Crack detection in beam-type structures using frequency data**. Journal of Sound and Vibration, v.259, n.1, p.145-160, 2003.

KOPSAFTOPOULOS, F.P.; FASSOIS, S.D. **Identification of stochastic systems under multiple operating conditions: The vector dependent FP-ARX parametrization**. In: Proceedings of 14th Mediterranean Conference on Control and Automation, Ancona, Italy, 2006.

KROHN, N.; STOESSEL, R.; BUSSE, G. **Acoustic non-linearity for defect selective imaging**. Ultrasonics, v.40, n.1-8, p.633-639, 2002.

KYRIAZOGLOU, C.; PAGE, B.L.; GUILD, F. **Vibration damping for crack detection in composite laminates**. Composites Part A: Applied Science and Manufacturing, v.35, n.7-8, p.945–953, 2004.

LIEVEN, N.A.J.; EWINS, D. J. **Spatial correlation of mode shapes: the coordinate modal assurance criterion (COMAC**). In: Proceedings of the 6th International Modal Analysis Conference, Bethel, 1988.

LIEW, K.M.; WANG, Q. **Application of wavelet theory for crack identification in structures**. Journal of Engineering Mechanics-ASCE, v.124, p.152-157, 1998.

LIU, X.; LIEVEN, N.A.J.; ESCAMILLA-AMBROSIO, P.J. **Frequency response function shape-based methods for structural damage localization**. Mechanical Systems and Signal Processing, v.23, n.4, p.1243-1259, 2009.

LU, Q.; REN, G.; ZHAO, Y. **Multiple damage location with flexibility curvature and relative frequency change for beam structures**. Journal of Sound and Vibration, v.253, n.5, p.1101-1114, 2002.

MAIA, N.; SILVA, J.M.M.; ALMAS, E.A.M.; SAMPAIO, R.P.C. **Damage detection in structures: from mode shape to frequency response function methods**. Mechanical Systems and Signal Processing, v.17, n.3, p.489-498, 2003.

MAIA, N.M.M.; RIBEIRO, A.M.R.; FONTUL, M.; MONTALVÃO, D.; SAMPAIO, R.P.C. **Using the detection and relative damage quantification indicator (DRQ) with transmissibility**. Key Engineering Materials, v.347, p.455-460, 2007.

MAITY, D.; TRIPATHY, R.R. **Damage assessment of structures from changes in natural frequencies using genetic algorithm**. Structural Engineering and Mechanics, v.19, p.21-42, 2005.

MARES, C.; MOTTERSHEAD, J.E.; FRISWELL, M.I. **Stochastic model updating: Part 1—theory and simulated example**. Mechanical Systems and Signal Processing, v.20, n.7, p.1674-1695, 2006.

MEDEIROS, R.; MORENO, M.E.; MARQUES, F.D.; TITA, V. **Effective properties evaluation for smart composite materials**. Journal of the Brazilian Society of Mechanical Sciences and Engineering, v.34, p.362-370, 2012.

MEDEIROS, R.; RODRIGUEZ-RAMOS, R.; GUINOVART-DIAZ, R.; BRAVO-CASTILLERO, J.; OTERO, J.A.; TITA, V. **Numerical and analytical analyses for active fiber composite piezoelectric composite materials**. Journal of Intelligent Material Systems and Structures, v.26, n.1 p.101-118, 2015.

MEIROVITCH, L.; BARUH, H. **The implementation of modal filters for control of structures**. Journal of Guidance, Control, and Dynamics, v.8, n.6, p.707-716, 1985.

MESSINA, A.; WILLIAMS, E.J.; CONTURSI, T. **Structural damage detection by a sensitivity and statistical-based method**. Journal of Sound and Vibration, v.216, n.5, p.791-808, 1998.

MICKENS, T.; SCHULZ, M.; SUNDARESAN, M.; GHOSHAL, A.; NASER, A.S.; REICHMEIDER, R. **Structural health monitoring of an aircraft joint**. Mechanical Systems and Signal Processing, v.17, n.2, p.285-303, 2003.

MILECEK, S. **The use of modal assurance criterion extended**. In: Proceedings, International Modal Analysis Conference, p.363-369, 1994.

MITCHELL, L.D. **Increasing the sensitivity of the modal assurance criteria to small mode shape changes: The IMAC**. In: Proceedings, International Modal Analysis Conference, p.64-69, 2001.

MOTTERSHEAD, J.E.; FRISWELL, M.I. **Model updating in structural dynamics: A survey**. Journal of Sound and Vibration, v.167, n.2, p.347-375, 1993.

NARKIS, Y. **Identification of crack location in vibrating simply supported beams**. Journal of Sound and Vibration, v.172, n.4, p.549-558, 1994.

O'CALLAHAN, J. **Correlation Considerations – Part 4 (Modal Vector Correlation Techniques)**. In: Proceedings, International Modal Analysis Conference, p.197-206, 1998.

PAI, P.F. **Time–frequency characterization of nonlinear normal modes and challenges in nonlinearity identification of dynamical systems**. Mechanical Systems and Signal Processing, v.25, n.7, p.2358-2374, 2011.

PANDEY, A.K.; BISWAS, M.; SAMMAN, M.M. **Damage detection from changes in curvature mode shapes**. Journal of Sound and Vibration, v.145, n.2, p.321-332, 1991.

PANDEY, A.K.; BISWAS, M. **Damage detection in structures using changes in flexibility**. Journal of Sound and Vibration, v.169, n.1, p.3-17, 1994.

PARK, G.; SOHN, H.; FARRAR, C.R.; INMAN, D.J. **Overview of piezoelectric impedance-based health monitoring and path forward**. The Shock and Vibration Digest, v.35, n.6, p.451-463, 2003.

PASCUAL, R.; GOLINVAL, J.C.; RAZETO, M. **A frequency domain correlation technique for model correlation and updating**. In Proceedings of the 15th International Modal Analysis Conference (IMAC XV), p.587–592, 1997.

PASCUAL, R.; GOLINVAL, J.C.; RAZETO, M. **On-line damage assessment using operating deflection shapes**. In Proceedings of the 17th International Modal Analysis Conference (IMAC XVII), p.238–243, 1999.

QIAO, P.; CAO, M. **Waveform fractal dimension for mode shape-based damage identification of beam-type structures**. International Journal of Solids and Structures, v.45, n.22-23, p.5946-5961, 2008.

RATCLIFFE, C. **Damage detection using a modified laplacian operator on mode shape data**. Journal of Sound and Vibration, v.204, n.3, p.505-517, 1997.

RITTER A.; KIRKEGAARD, P. **Vibration based inspection using neural networks**. In: Proceeding of 2nd international conference on structural damage assessment using advanced signal processing procedures, 1997.

RODRIGUEZ-RAMOS, R.; MEDEIROS, R.; GUINOVART-DIAZ, R.; BRAVO-CASTILLERO, J.; OTERO, J.A.; TITA, V. **Different approaches for calculating the effective elastic properties in composite materials under imperfect contact adherence**. Composite Structures, v.99, p.264-275, 2013.

RUCKA, M.; WILDE, K. **Application of continuous wavelet transform in vibration based damage detection method for beams and plates**. Journal of Sound and Vibration, v.297, n.3-5, p.536-550, 2006.

SAMMAN, M.M. **A modal correlation coefficient (MCC) for detection of kinks in mode shapes**. In: ASME Journal of Vibration and Acoustics, v.118, n.2, p.271-271, 1996.

SAMPAIO, R.P.C.; MAIA, N.M.M.; SILVA, J.M.M. **Damage detection using the frequency-response-function curvature method**. Journal of Sound and Vibration, v.226, n.5, p.1029-1042, 1999.

SAMPAIO, R.; MAIA, N.; SILVA, J. **The frequency domain assurance criterion as a tool for damage identification**. In: Proceedings of the 5th International Conference on Damage Assessment of Structures, Southampton, England, UK, 1, p.69-76, 2003.

SHI, Z.; LAW, S.S. **Structural damage localization from modal strain energy change**. Journal of Sound and Vibration, v.218, n.5, p.825-844, 1998.

SINOU, J.-J. **Numerical investigations of a robust identification of crack location and size in beams using only changes in ratio pulsations of the cracked beams**. Structural Engineering Mechanics, v.25, n.6, p.691-716, 2007.

STUBBS, N.; KIM J.T.; TOPOLE, K. **An efficient and robust algorithm for damage location in offshore platforms**. In: Proceedings of the ASCE 10th Structures Congress, 1992.

TITA, V.; MEDEIROS, R.; MARQUES, F.D.; MORENO, M.E. **Effective properties evaluation for smart composite materials with imperfect fiber-matrix adhesion**. Journal of Composite Materials, on line, p.1-19, 2015.

WAHL, F.; SCHMIDT, G.; FORRAI, L. **On the significance of antiresonance frequencies in experimental structural analysis**. Journal of Sound and Vibration, v.219, n.3, p.379-394, 1996.

WANG, J.; QIAO, P. **Improved damage detection for beam-type structures using a uniform load surface**. Structural Health Monitoring, v.6, n.2, p.99-110, 2007.

WEI, J.C.; WANG, W.; ALLEMANG, R.J. **Model correlation and orthogonality criteria based on reciprocal modal vectors**. In: Proceedings, SAE Noise and Vibration Conference. p.607-616, 1990.

WEST, W.M. **Illustration of the use of modal assurance criterion to detect structural changes in an orbiter test specimen**. In: Proceedings of the Air Force Conference on Aircraft Structural Integrity, Los Angles, 1984.

WU, D.; LAW, S.S. **Damage localization in plate structures from uniform load surface curvature**. Journal of Sound and Vibration, v.276, n.1-2, p.227-244, 2004.

ZANG, C.; IMREGUN, M. **Structural damage detection using artificial neural networks and measured FRF data reduced via principal component projection**. Journal of Sound and Vibration, v.242, n.5, p.813-827, 2001.

ZHANG, Z.; AKTAN, A.E. **The damage indices for constructed facilities**. In: Proceedings of the 13th International Modal Analysis Conference, v.1, p.1520-1529, 1995.

ZHONG, S.; OYADIJI, S.O. **Crack detection in simply supported beams without baseline modal parameters by stationary wavelet transform**. Mechanical Systems and Signal Processing, v.21, n.4, p.1853-1884, 2007.

ZHONG, S.; YADIJI, S.O.; DING, K. **Response-only method for damage detection of beam-like structures using high accuracy frequencies with auxiliary mass spatial probing**. Journal of Sound and Vibration, v.311, n.3-5, p.1075-1099, 2008.

APPENDIX B

Scientific Publications

This appendix presented the scientific contributions related directly or indirectly to this PhD thesis.

B.1. Article in Scientific Journals

[1] **MEDEIROS, R.**; SARTORATO, M.; VANDEPITTE, D.; TITA, V. A frequency based damage detection in unidirectional composite plates using MFC sensors. *Journal of Sound and Vibration*, (under review).

[2] SARTORATO, M.; **MEDEIROS, R.**; VANDEPITTE, D.; TITA, V. Computational model for supporting SHM systems design: Damage identification via numerical analyses. *Mechanical Systems and Signal Processing*, (under review).

[3] COSTA, R.R.C.; **DE MEDEIROS, RICARDO**; RIBEIRO, M.L.; TITA, V. Experimental and numerical analysis of single lap bonded joints: epoxy and castor oil PU-glass fiber composites. *The Journal of Adhesion* (under review).

[4] SANTANA, H.B.; **DE MEDEIROS, R.**; RODRÍGUEZ-RAMOS, R.; TITA, V. Different interface models for calculating the effective properties in piezoelectric composite materials with imperfect fiber-matrix adhesion. *Composite Structures*, (under review).

[5] **DE MEDEIROS, R.**; RIBEIRO, M.L.; TITA, V. Experimental methodology for testing metal-composite bolted joints. *Journal of Mineral Metal and Material Engineering*, v. 2, p. 11-22, 2016.

[6] **MEDEIROS, R.**; LOPES, H.M.R.; GUEDES, R.M.; VAZ, M.A.P.; VANDEPITTE, D.; TITA, V. A new methodology for structural health monitoring applications. *Procedia Engineering*, v.114, p.54-61, 2015.

[7] RIBEIRO, M.L.; **MEDEIROS, R.**; Computational parametric study of low-velocity impact response of composite cylinder for automotive components. *International Journal of Automotive Composites*, v.1, n.2-3, p.131-157, 2015.

[8] TITA, V.; **MEDEIROS, R.**; MARQUES, F.D.; MORENO, M.E. Effective properties evaluation for smart composite materials with imperfect fiber–matrix adhesion. *Journal of Composite Materials*, v.49, n.29, 2015.

[9] SARTORATO, M.; **MEDEIROS, R.**; TITA, V. A finite element formulation for smart piezoelectric composite shells: Mathematical formulation, computational analysis and experimental evaluation. *Composite Structures*, v.127, p.185-198, 2015.

[10] FLOR, F.R.; **MEDEIROS, R.**; TITA, V. Numerical and experimental damage identification in metal-composite bonded joint. The Journal of Adhesion, v.91, n.10-11, p.863-882, 2015.

[11] **MEDEIROS, R.**; RODRIGUEZ-RAMOS, R.; GUINOVART-DIAZ, R.; BRAVO-CASTILLERO, J.; OTERO, J.A.; TITA, V. Numerical and analytical analyses for active fiber composite piezoelectric composite materials. *Journal of Intelligent Material Systems and Structures*, v.26, n.1, p.101-118, 2015.

[12] **MEDEIROS, R.**; BORGES, E.N.; TITA, V. Experimental analyses of metal-composite bonded joints: damage identification. *Applied Adhesion Science*, v.2, p.13, 2014.

[13] **MEDEIROS, R.**; RIBEIRO, M.L.; TITA, V. Computational methodology of damage detection on composite cylinders: Structural health monitoring for automotive components. *International Journal of Automotive Composites*, v.1, n.1, p.112-128, 2014.

[14] RODRIGUEZ-RAMOS, R.; **MEDEIROS, R.**; GUINOVART-DIAZ, R.; BRAVO-CASTILLERO, J.; OTERO, J.A.; TITA, V. Different approaches for calculating the effective elastic properties in composite materials under imperfect contact adherence. *Composite Structures*, v.99, p.264-275, 2013.

[15] RIBEIRO, M.L.; ANGELICO, R.A.; **MEDEIROS, R.**; TITA, V. Finite element analyses of low velocity impact on thin composite disks. *International Journal of Composite Materials*, v.3, p.59-70, 2013.

[16] **MEDEIROS, R.**; MORENO, M.E.; MARQUES, F.D.; TITA, V. Effective properties evaluation for smart composite materials. *Journal of the Brazilian Society of Mechanical Sciences and Engineering*, v.34, p.362-370, 2012.

[17] **MEDEIROS, R.**; RIBEIRO, M.L.; FERREIRA, G.F.O.; MARQUES, F.D.; TITA, V. Numerical and experimental dynamic analyses via smart composites. *International Journal of Vehicle Structures & Systems*, v.4, p.141-147, 2012.

[18] SARTORATO, M.; **DE MEDEIROS, R.**; RIBEIRO, M.L.; TITA, V. Representative volume element based transverse shear characterisation of laminated composites. International Journal of Vehicle Structures & Systems, v. 4, p. 136-140, 2012.

B.2. Full Papers at Scientific Conferences

[1] **MEDEIROS, R.**; SARTORATO, M.; TITA, S.P.S.; VANDEPITTE, D.; RIBEIRO, M.L.; TITA, V. Residual strength criterion based on damage metric and flexural after impact (FAI) test for composite materials. In: *23nd International Congress of Mechanical Engineering (COBEM2015)*, Rio de Janeiro, Brazil, 2015.

[2] **MEDEIROS, R.**; DANIEL, G.S.; RIBEIRO, M.L.; TITA, V. Computational tool for fatigue analysis in composite material. In: *23nd International Congress of Mechanical Engineering (COBEM2015)*, Rio de Janeiro, Brazil, 2015.

[3] **MEDEIROS, R.**; TITA, S.P.S.; VANDEPITTE, D.; TITA, V. A new structural health monitoring system for composite materials based on the combination of different methods. In: *Meeting on Aeronautical Composite Materials and Structures (MACMS2015)*, São Carlos, São Paulo, Brazil, 2015.

[4] **MEDEIROS, R.**; TITA, S.P.S.; VANDEPITTE, D.; TITA, V. Residual flexural strength criterion for composite plates subjected to low velocity impact. In: *Meeting on Aeronautical Composite Materials and Structures (MACMS2015)*, São Carlos, São Paulo, Brazil, 2015.

[5] ELOY, F.S.; COSTA, R.R.C.; **MEDEIROS, R.**; RIBEIRO, M.L.; TITA, V. Comparison between mechanical properties of bio and synthetic composites for use in aircraft interior structures. In: *Meeting on Aeronautical Composite Materials and Structures (MACMS2015)*, São Carlos, São Paulo, Brazil, 2015.

[6] COSTA, R.R.C.; ELOY, F.S.; **MEDEIROS, R.**; RIBEIRO, M.L.; TITA, V. Experimental dynamic investigations of bio and synthetic composites for use in aircraft interior structures. In: *Meeting on Aeronautical Composite Materials and Structures (MACMS2015)*, São Carlos, São Paulo, Brazil, 2015.

[7] **MEDEIROS, R.** LOPES, H.M.R.; GUEDES, R.M.; VAZ, M.A.P.; TITA, V. A new approach for SHM system: combination of vibration based method and shearography speckle. In: *Fifth International Symposium on Solid Mechanics (MECSOL2015),* Belo Horizonte, Minas Gerais, Brazil, 2015.

[8] SARTORATO, M.; **MEDEIROS, R.**; TITA, V.; TALREJA, R. A multiscale based continuum model: influence of crack sliding mode on composite materials damage evolution. In: *Fifth International Symposium on Solid Mechanics (MECSOL2015),* Belo Horizonte, Minas Gerais, Brazil, 2015.

[9] FERREIRA, G.F.O; **MEDEIROS, R.**; OGEA, J.L.; TITA, V. Damage simulation in composite structures under tensile load considering friction and sliding effect. In: *Fifth International Symposium on Solid Mechanics (MECSOL2015),* Belo Horizonte, Minas Gerais, Brazil, 2015.

[10] **MEDEIROS, R.**; LOPES, H.M.R.; GUEDES, R.M.; VAZ, M.A.P.; TITA, V. Identificação do dano em laminados compósito através da combinação de diferentes técnicas. In: *3ª Conferência Nacional em Ensaios Não Destrutivos (3CNEND)*, Amadora, Portugal, 2014.

[11] **MEDEIROS, R.**; SARTORATO, M.; VANDEPITTE, D.; TITA, V. SHM of composite plates: Vibration based method by using PZT sensors. In: *International Conference on Noise and Vibration Engineering (ISMA2014)*, Leuven, Belgium, p.3811-3826, 2014.

[12] **MEDEIROS, R.**; SARTORATO, M.; VANDEPITTE, D.; TITA, V. Experimental damage identification for unidirectional carbon reinforced plates. In: *2nd Brazilian Conference on Composite Materials (BCCM2)*, São José dos Campos, São Paulo, Brazil, 2014.

[13] **MEDEIROS**, R.; FLOR, F.R.; RIBEIRO, M.L.; TITA, V. Impact damage quantification in composite cylinders using computational and experimental techniques. In: *VIII National Congress of Mechanical Engineering (CONEM2014)*, Uberlândia, Minas Gerais, Brazil, 2014.

[14] **MEDEIROS, R.**; FLOR, F.R.; RIBEIRO, M.L.; TITA, V. Debonding identification in metal-composite bonded joint using vibration testing. In: *VIII National Congress of Mechanical Engineering (CONEM2014)*, Uberlândia, Minas Gerais, Brazil, 2014.

[15] **MEDEIROS, R.**; SARTORATO, M.; MARQUES, F.D.; VANDEPITTE, D.; TITA, V. Vibration-based damage identification applied for composite plate: Experimental analyses. In: *22nd International Congress of Mechanical Engineering (COBEM2013)*, Ribeirão Preto, São Paulo, Brazil, p.331-342, 2013.

[16] SARTORATO, M.; **MEDEIROS, R.**; MARQUES, F.D.; VANDEPITTE, D.; TITA, V. Vibration-based damage identification applied for composite plate: Numerical analyses. In: *22nd International Congress of Mechanical Engineering (COBEM2013)*, Ribeirão Preto, São Paulo, Brazil, p.952-962, 2013.

[17] **MEDEIROS, R.**; BORGES, E.N.; RIBEIRO, M.L.; CARVALHO, F.G.; TITA, V. Vibration-based structural monitoring applied on hybrid bonded joints. In: *22nd International Congress of Mechanical Engineering (COBEM2013)*, Ribeirão Preto, São Paulo, Brazil, p.319-330, 2013.

[18] **MEDEIROS, R.**; RIBEIRO, M.L.; SARTORATO, M.; MARINUCCI, G.; TITA, V. Computational simulation using PZT as sensor elements for damage detection on impacted composite cylinders. In: *4th International Symposium on Solid Mechanics (MECSOL2013)*, Porto Alegre, Rio Grande do Sul, Brazil, 2013.

[19] RIBEIRO, M.L.; ANGELICO, R.A.; **MEDEIROS, R.**; MARINUCCI, G.; TITA, V. Numerical and experimental analyses of low velocity impact on thin composite. In: *4th International Symposium on Solid Mechanics (MECSOL2013)*, Porto Alegre, Rio Grande do Sul, Brazil, 2013.

[20] **MEDEIROS, R.**; SARTORATO, M.; RIBEIRO, M.L.; VANDEPITTE, D.; TITA, V. Numerical and experimental analyses about SHM metrics using piezoelectric materials. In: *International Conference on Noise and Vibration Engineering (ISMA2012)*, Leuven, Belgium, 2012.

[21] RIBEIRO, M.L.; **MEDEIROS, R.**; SARTORATO, M.; TITA, V. Damage detection in carbon fiber filament winding cylinders using smart piezoceramic materials. In: *VII National Congress of Mechanical Engineering (CONEM2012)*, São Luis, Maranhão, Brazil, 2012.

[22] SARTORATO, M.; RIBEIRO, M. L.; **MEDEIROS, R.**; TITA, V. A finite element for active composite plates with piezoelectric layers applied to composite cylinders. In: *VII Congresso Nacional de Engenharia Mecânica (CONEM2012)*, 2012, São Luis - Maranhão. Proceedings of CONEM, 2012.

[23] **MEDEIROS, R**.; RIBEIRO, M.L.; FERREIRA, G.F.O.; MARQUES, F.D.; TITA, V. Numerical and experimental dynamic analyses in smart composites. In: *1st Brazilian Conference on Composite Materials (BCCM1)*, 2012, Natal-RN. Proceedings of the Brazilian Conference on Composite Materials, 2012. v. 1.

[24] SARTORATO, M.; **MEDEIROS, R.**; RIBEIRO, M.L. ; TITA, V. Transversal shear characterization of thick laminated composite using a representative volume element (RVE). In: *1st Brazilian Conference on Composite Materials (BCCM1)*, 2012, Natal-RN. Proceedings of the Brazilian Conference on Composite Materials, 2012. v. 1.

[25] SARTORATO, M.; **MEDEIROS, R.**; TITA, V. A finite element for active composite plates with piezoelectric layers and experimental validation. In: 10th World Congress on Computational Mechanics (WCCM2012), 2012, São Paulo. Proceedings of WCCM, 2012.

[26] ALMEIDA, A.S.; **MEDEIROS, R.**; RIBEIRO, M.L.; TITA, V.; MARQUES, F.D. Piezo-fiber composite sensor tailoring using genetic algorithm. In: *10th World Congress on Computational Mechanics (WCCM2012)*, 2012, São Paulo - SP. Proceedings of WCCM, 2012.

B.3. Abstracts at Scientific Conferences

[1] COSTA, R.R.C.; **DE MEDEIROS, RICARDO**; RIBEIRO, M.L.; TITA, V. Experimental and numerical analysis of single lap bonded joints: epoxy and castor oil PU-glass fiber composites. In: 3ª Conferência Luso-Brasileira de Adesão e Adesivos (CLBA2016), 2016, Rio de Janeiro. Proceedings of CLBA2016, 2016.

[2] **MEDEIROS, R.** LOPES, H.M.R.; GUEDES, R.M.; VAZ, M.A.P.; VANDEPITTE, D.; TITA, V. A new methodology for structural health monitoring applications. In: International Conference on Structural Integrity (ISCI2015), Funchal, Portugal, 2015.

[3] **DE MEDEIROS, R.;** SARTORATO, M.; VANDEPITTE, D.; TITA, V. Flexural After Impact (FAI): A new criterion to evaluate the residual strength of composite materials. In: *18th International Conference on Composite Structures (ICCS18)*, Lisbon. Portugal, 2015.

[4] **MEDEIROS, R.**; FLOR, F.R.; RIBEIRO, M.L.; TITA, V. Numerical and experimental damage identification in metal-composite bonded joints. In: *2ª Conferência Luso-Brasileira de Adesão e Adesivos (CLBA2014)*, Porto, Portugal, 2014.

[5] **MEDEIROS, R.**; LOPES, H.M.R.; GUEDES, R.M.; VAZ, M.A.P.; TITA, V. Damage quantification of composite structures using Speckle Shear Interferometer. In: *1st International Conference on Mechanics of Composites (MECHCOMP2014*), Long Island, New York, USA, 2014.

[6] **MEDEIROS, R.**; RIBEIRO, M.L.; BORGES, E.N.; TITA, V. Computational and experimental dynamic analyses of hybrid bonded joints monitored through smart composites. In: *17th International Conference on Composite Structures (ICCS17)*, Porto, Portugal, 2013.

[7] SARTORATO, M.; **MEDEIROS, R.**; RIBEIRO, M.L.; TITA, V. A non-linear finite element for curved active composites with embedded piezoelectric layers. In: *17th International Conference on Composite Structures (ICCS17)*, 2013, Porto. Proceedings of ICCS17, 2013.

[8] RIBEIRO, M.L.; **MEDEIROS, R.**; VERA, R.V.; TITA, V. Structural and flammability analyses of aeronautical interior structures made of natural fiber composite. In: *17th International Conference on Composite Structures (ICCS17)*, 2013, Porto. Proceedings of ICCS17, 2013.

[9] RODRIGUEZ-RAMOS, R.; **MEDEIROS, R.**; GUINOVART-DIAZ, R.; BRAVO-CASTILLERO, J.; OTERO, J. A.; TITA, V. Numerical and analytical approaches for computing effective elastic properties in composite materials under imperfect contact adherence. In: *10th World Congress on Computational Mechanics (WCCM2012)*, São Paulo, Brazil, 2012.